Atomistic Modelling and Dynamic Analysis of Single Walled Boron Nitride Nanotubes (SW-BNNTs) in Presence of Defects

THESIS

Submitted in partial fulfillment of the requirements for the degree of

DOCTOR OF PHILOSOPHY

by

HARSH SHARMA

2018PHXF0415P

Under the Supervision of

Prof. Sharad Shrivastava

&

Co- Supervision of

Prof. Jitendra S. Rathore

BITS Pilani
Pilani Campus

BIRLA INSTITUTE OF TECHNOLOGY & SCIENCE, PILANI

PILANI-333031, RAJASTHAN, INDIA

2023

Dedicate this to my parents and wife, who never once to my knowledge tried to kill my thoughts and desire.

BIRLA INSTITUTE OF TECHNOLOGY AND SCIENCE, PILANI

CERTIFICATE

This is to certify that the thesis titled **"Atomistic Modelling and Dynamic Analysis of Single Walled Boron Nitride Nanotubes (SW-BNNTs) in Presence of Defects"** submitted by **Harsh Sharma** ID No **2018PHXF0415P** for award of Ph.D. of the institute embodies original work done by him under our supervision.

Signature of Co-Supervisor
Prof. Jitendra S. Rathore
Associate Professor,
Mechanical Engineering Department,
Birla Institute of Technology and Science, Pilani,
Rajasthan-333031, India

Date:

Signature of Supervisor
Prof. Sharad Shrivastava
Associate Professor,
Mechanical Engineering Department,
Birla Institute of Technology and Science, Pilani,
Rajasthan-333031, India

Date:

Declaration of Authorship

I, **HARSH SHARMA**, declare that this Doctoral Thesis titled, ‘‘Atomistic Modelling and Dynamic Analysis of Single Walled Boron Nitride Nanotubes (SW-BNNTs) in Presence of Defects’’ and the work presented in it are my own. I confirm that:

- This work was done wholly or mainly while in candidature for a research degree at this University.
- Where any part of this thesis has previously been submitted for a degree or any other qualification at this University or any other institution, this has been clearly stated.
- Where I have consulted the published work of others, this is always clearly attributed.
- Where I have quoted from the work of others, the source is always given. With the exception of such quotations, this thesis is entirely my own work.
- I have acknowledged all main sources of help.
- Where the thesis is based on work done by myself jointly with others, I have made clearexactly what was done by others and what I have contributed myself.

Signed: _____

Date: _____

Acknowledgement

My heartfelt and foremost gratitude is expressed to my supervisor **Prof. Sharad Shrivastava** and co-supervisor **Prof. Jitendra S. Rathore**, for welcoming me onboard on this stimulating research and for being the best supervisors I could ever wish for. I express my sincere thanks to **Prof. Sharad Shrivastava** for introducing me to this fascinating research on metal and alloy matrix nanocomposites. I offer my respectful obeisance unto the lotus feet of my both supervisors for all his valuable guidance, excellent direction, everlasting encouragement, and inspiration given to me without which the present work would not have been possible. It was indeed my privilege to work under the supervision of the supervision of both. Their expertise in presenting the scientific work added scientific value in my thesis.

I am immensely thankful to **Prof. V Ramgopal Rao**, Vice-Chancellor and **Prof. Sovik Bhattacharyya** former Vice-Chancellor, BITS Pilani, and **Prof. Sudhir Kumar Barai**, Director, BITS Pilani, Pilani Campus for their support and blessings. I express my gratitude to **Prof. S. K. Verma** (Dean, Administration, BITS Pilani, Pilani Campus) for his kind support. I also express my sincere thanks to **Prof. Shamik Chakraborty**, Associate Dean, Academic-Graduate Studies & Research Division (AGSRD) for his motivation, constant support and encouragement. I thank **Prof. Srikanta Routroy**, Head of the Department of Mechanical Engineering for his valuable support and guidance. I am highly indebted to **Prof. Navin Singh**, Associate Dean, Student Welfare Division, for his encouragement and suggestions.

I express sincere thanks to **Prof. Arun Jalan**, DRC convener, Department of Mechanical Engineering. I pay my heartfelt gratitude to my DAC members **Prof. Arun Jalan** and **Prof. Sachin U. Belgamwar** for their valuable suggestions and for sparing their valuable time for departmental evaluation of this thesis. I would also like to acknowledge all faculty members as well as non-academic staff of Department of Mechanical Engineering for their support, encouragement, and cooperation. It is my pleasure to acknowledge the individuals who have contributed to the evolution of this work.

I would like to extend my deepest gratitude to my mentor **Prof. Sandesh Trivedi**, for their guidance, support, and invaluable contributions throughout my academic journey. Their expert knowledge, thoughtful advice, and unwavering encouragement have been instrumental

in the completion of this thesis. Their dedication to my success has been a constant source of inspiration, and I am forever grateful for their mentorship and friendship. This thesis would not have been possible without their invaluable contributions.

I owe my gratitude to fellow research scholars of Mechanical Engineering Department for their constant support. I would like to thank and appreciate my dearest friends Ayush Owhal, Diplesh Gautam, Dhruv Deshwal, Pradeep Shukla, Pradnya Chabbi, Ashish Khare, Naveen P.T, for their support.

Words cannot do justice to the support, love and affection I have received during this research work from my parents **Shri Ashok Kumar Sharma** and **Smt. Mala Sharma**, I am deeply indebted for their endless love, support, and guidance throughout my life. Their unwavering encouragement and belief in me have been the driving force behind my success. I am grateful for the sacrifices they have made to give me the best opportunities, for the lessons they have taught me, and for the love they have shown me.

I would like to express my sincerest gratitude to my wife **Mrs. Krati Sharma**, for her unwavering love, support, and encouragement throughout my academic journey. Her understanding, patience, and sacrifices have been invaluable to me, and have made this accomplishment possible. Thank you for being my partner in every step of the way.

My heartfelt gratitude to my brother **Mr. Vaibhav Sharma**, sister-in-law **Mrs. Divya Sharma**, and my nephew **Mr. Shivay Sharma** for their love, support, and encouragement throughout my academic journey. Their constant presence in my life has been a source of inspiration and motivation. I am grateful to acknowledge my beloved pet **Doodoo**, who has been my constant companion and source of joy throughout my academic journey. Their unwavering loyalty and love have been a source of comfort and inspiration. Their presence in my life has been a reminder to take a break and find joy in the little things. I am grateful for the companionship and love they have provided me. Thank you for being my furry friend. I pray and thank the Almighty for showering HIS divine blessings and giving me an inner strength and patience. In last thank you all for your love, support, and unwavering belief in me. Without you, I would not be the person I am today.

Harsh Sharma

BIRLA INSTITUTE OF TECHNOLOGY AND SCIENCE, PILANI CAMPUS

Abstract

Doctor of Philosophy

Atomistic Modelling and Dynamic Analysis of Single Walled Boron Nitride Nanotubes (SW-BNNTs) in Presence of Defects

by Harsh Sharma

Boron nitride nanotubes (BNNTs) were hypothetically predicted in the year 1994 by Rubio et al. and Blasé et al, the same were experimentally realised by Chopra and co-workers in 1995 and laid foundation for the scientific community to conduct further research. As boron nitride nanotube possesses many remarkable properties, research in this field advanced at a breath-taking pace, ever since with many unexpected discoveries. The real progress in nanotechnology in the last two decades, has been due to a series of advances in a variety of complementary areas, such as: the discoveries of atomically precise materials like nanotubes associated with development of manipulation techniques to image and manipulate atomic and molecular configurations in real materials. Simultaneously, the conceptualization and demonstration of individual electronic and logic devices with materials at an atomic or molecular level and the advances in computational nanotechnology, i.e., modelling and simulation based on actual physics and chemistry of possible nanomaterials, devices, and applications, also complemented the progress in above field. It turns out that at nanoscale, devices and system sizes are sufficiently small, so that, it is possible to describe their behaviour in a more accurate manner.

The modelling and simulation techniques have also become predictive in nature and many novel concepts and designs were initially proposed followed by their realization or verification through experiments. Further, the advances in nanotechnology encouraged many researchers to believe that the incorporation of BNNTs in a matrix makes them the ultimate reinforcing material The primary objective of the present work is to study the dynamic behaviour of BNNTs with focus on their mass sensing ability. The computational methods

employed in this work include continuum mechanics, finite element method and hybrid modelling approach. The analytical formulation is based on energy approach and 4" order Runga-Kutta method and Galerkin approach have been employed for obtaining solution of the equations. Continuum mechanics approach is employed to study the effect of mass variations on the single walled and multi walled boron nitride nanotube as well as nanocomposites reinforeced with single walled boron nitride nanotubes SW-BNNT, the effects of different boundary conditions, viz., cantilever and bridged, on the computed frequencies are investigated for possible applications in vibrating mass sensors or nanoresonators of the femtogram scale mass. Euler-Bernoulli's principle is utilized for modelling of a straight and wavy BNNT based mass sensor. The excitations are due to the previously conducted experimental studies.

The analytical formulation considers the cubic nonlinearity induced in the system due to stretching of the mid-plane for doubly clamped boundary condition and quadratic nonlinearity due to the curvature (waviness) of the It is observed that the mass sensitivity of SW-BNNT reaches up to 10^{-26} kg. The effect of variation in length on frequency is found to be more significant as compared to that of nanotube, thereby suggesting the suitability of smaller BNNTs in mass sensing applications due to enhanced sensitiveness The excitations induced in the BNNT system due to presence of defects are also analysed.

A hybrid modelling approach is used for development of 3D atomistic FE model consisting of a beam element that represents a B-N bond and the point masses at the ends correspond to the atomic mass of boron and nitrogen, the effect of various atomic vacancy defects and their positions is analysed. It is observed that the effect of atomic vacancy is maximum when it is nearer to the fixed end. Further, movement of the vacancy towards the free end results in negative frequency shift. This indicates that the exciting frequency of defective nanotube is larger than that of pristine one A finite element-based continuum mechanics approach is employed for modelling of waviness and pinholes in BNNT. The vibration responses of wavy doubly clamped BNNT for varying waviness factor and length are analysed using techniques such as time series, phase space, Poincaré maps and fast Fourier transforms. Regions of periodic sub-harmonic, quasi- periodic and chaotic response for wavy SW-BNNT based mass sensing system are observed. the effects of different temperatures on

the structural and elastic properties of atomistic model of monovacancy defected SW-BNNTs were investigated by using MD simulation.

An advance extended Tersoff potential was successfully used to describe the interactions between the boron and nitrogen atoms of SW-BNNTs. The mean square displacement revealed the structural stability of monovacancy defected SW-BNNT structures during equilibration up to 2400 K temperature. At higher temperature, the shape of monovacancy defected site converted into new polygenic defected sites to maintain the stability of structure. The monovacancy defected SW-BNNTs showed reduction in thermal stability and mechanical performance at high temperature. For uniaxial tensile straining, the pristine SW-BNNTs showed 39.02% and 46.15% decrease in axial stress and strain on increasing the temperature from 300 K to 2400 K, which further decreased with the monovacancy defects. Similarly, for torsional straining, the pristine SW-BNNTs showed 70.72 % and 54.99% decrease in change in stored PE and twisting angle on increasing the temperature from 300 K to 2400 K, whereas further reduction in change in PE was observed in the monovacancy defected SW-BNNTs. The Young's modulus, Poisson's ratio, and shear modulus of monovacancy defected SW-BNNTs were decreased on increasing the monovacancy concentration and temperature under the uniaxial tensile and torsional quasi-static strain environment.

TABLE OF CONTENTS

LIST OF FIGURES

LIST OF TABLES

LIST OF NOMENCLATURE

ν = Poisson's ratio

$\phi - \phi_0$ = change in angle due to bond twisting

θ_0 = regular bond angle

a = side of hexagonal RVE

a_{B-N} = length of B-N bond

C_i = coefficients of van der Waal interaction

d = diameter of beam element representing BN bond

E_{at} = associated energy with angle torsion

E_{av} = associated energy with angle variation

E_{nb} = non-bonded interaction energy consisting of electrostatics

E_{bs} = associated energy with bond stretching

E_c = Young's modulus of composite

E_{inv} = associated energy for inversion terms

E_{matrix} = Young's modulus of matrix

E_{bnnt} = Young's modulus of BNNT

E_{vdW} = non bonded van der Walls interaction

E_z = effective Young's modulus

f_{o_reso} = resonance frequency without attached mass

f_{reso} = resonance frequency

G = shear modulus of beam element

h = degree of curvature associated with BNNT

J = polar moment of Inertia

k_1 = bond stretching stiffness

k_2 = bond angle bending stiffness

k_3 = torsional stiffness

$k_{equiv.}$ = equivalent stiffness of SW-BNNT

L = length of beam element

L_{center} = length of middle portion of discontinuous BNNT in composite

$m_{equiv.}$ = equivalent mass of SW-BNNT

Q = quality factor

r_i = inner radius of BNNT

r_o = outer radius of BNNT

$r - r_0$ = increment in bond stretching

t = thickness of BNNT

T = kinetic Energy of SW-BNNT

U = potential Energy of SW-BNNT

$u(x,t)$ = transverse displacement of SW-BNNT

$V(r)$ = Leanord-Jones potential

V_{BNNT} = volume fraction of BNNT

α = change in semi-bond rotation angle

Δa = change in the cross section

ΔL = axial stretching of the beam element, i.e., BN bond

$\Delta\Omega$ = relative rotation between ends of beam element

$\varepsilon_{bending}$ = strain energy of a uniform beam subjected to bending moment

$\varepsilon_{tension}$ = strain energy of a uniform beam subjected to axial force

$\varepsilon_{torsion}$ = strain energy of a uniform beam under pure torsion

ε_{vdW} = van der Waals interaction

ε_w = coefficient due to mid-plane stretching of doubly clamped wavy BNNT

$\theta - \theta_0$ = change in bond angle

λL = Eigen value

ξ = damping coefficient

ρ_{BNNT} = density of BNNT

ABBREVIATIONS

AFM	= atomic force microscopy
AMBER	= Assisted model building with energy refinement
BNNT	= boron nitride nanotube
CNT	= carbon nanotube
DFT	= density functional theory
DWBNNT	= double walled boron nitride nanotube
FEM	= finite element method
FFT	= fast Fourier transform
fg	= femtogram
HA	= hydroxyapatite
HRTEM	= high resolution transmission electron microscopy
MD	= Molecular Dynamics
MEMS	= Micro Electro Mechanical System
MWNT	= Multi Walled Nanotube
NEMS	= Nano Electro Mechanical System
PLA	= Polylactide
PMMA	= Poly methyl-methacrylate
ROM	= Rules of Mixtures
RVE	= Representative Volume Element
SEM	= Scanning Electron Microscopy
SPM	= Scanning Probe Microscopy
S-W	= Stone Wales
SW-BNNT	= Single Walled Boron Nitride Nanotube
TW-BNNT	= Tripple Walled Boron Nitride Nanotube
SWCNT	= Single Walled Carbon Nanotube
TBMD	= Tight Binding Molecular Dynamics
TEM	= Transmission Electron Microscopy
UFF	= Universal force field
zg	= Zeptogram

"Nanotechnology is the key to unlocking a new world of possibilities. It will revolutionize the way we build, create, and interact with the world around us."

- David D. Cole

Chapter 1

Introduction

The structural properties of any material have a great impact and are important for a particular application. For example, a material with high strength and stiffness is desirable for a structural application, while a material with high thermal conductivity is desirable for a heat dissipation application. Similarly, materials with high electrical and magnetic conductivity are important for electronic and magnetic applications, respectively. Understanding the structural properties of a material also helps in developing new materials with specific properties for advanced applications. Enhancements of such properties like better strength and stiffness have been the topic of interest in the past few decades. Most of the existing industrial materials do not possess outstanding mechanical properties and various systems need to become self-sensing, better responsive and intelligent enough to provide real-time safety for users by retaining their reliability and optimizing performance. Presently used smart materials like piezoelectric ceramics and shape memory alloy and their structures essentially have certain limitations with regard to their sensitiveness, size and costs associated with them and are bulky too.

Researchers and scientists are nowadays exploring nanotechnology, which can provide the path to develop perfect materials from the atomic scale. Biologically stimulated nanotechnology, which refers to bio-nanotechnology, is also a topic of interest to generate new smart materials and systems intelligent enough to sense and respond to environmental changes. Presently used biological sensors based on principles of optical detection are fundamentally complex because of the number of steps involved and larger sample size requirement. These sensors are sensitive enough, but the cost associated with them is more and their miniaturisation is too difficult, thus, providing bulky system. Conventional bio-sensing is achieved through relatively micro-sized sensors and the size of the sensor is adversely affected by temperature, light, electrical noise etc. when these are exposed to the environment.

Recently, researchers have been investigating nanoscale sensors based on gold particles, nanotube based sensors, nanotube reinforced polymeric sensors and nanotube arrays. In this chapter, a brief description about history of nanotechnology, concept of nanomechanics,

introduction of boron nitride nanotubes(BNNTs) and its properties are presented. The various applications of BNNTs in different areas and types of defects normally present in BNNTs are also discussed. Various modelling techniques presently employed for modelling and simulation for nanotubes, source of vibraton in BNNTs are discussed in this chapter.

1.1. History of nanotechnology

The first journey of nanoscale science begun with the estimation of diameter of sugar molecule by Albert Einstein in the year 1905, followed by the development of electron microscopes for imaging sub-nanometer objects in 1931. Later in the year 1959, Richard Feynman forecast the novel period of nanoscience as the lightning rod for innovative thinking milestones in his talk titled "*There is plenty of room at the bottom*." Then, development of scanning tunnelling microscope took place in 1981 for capturing images of individual atoms.

In the demanding field of nanotechnology, nowadays, researchers and scientists are trying to control atoms and molecules separately to arrange them for specific purposes by manipulating them with a high degree of accuracy. An enormous research attention has been dedicated for studying nanomaterials in the research community in the past few decades. Nanotubes are the best example that puts great impact of nanotechnology to the well-being of humans. At the same time, it is also possible to manipulate individual atoms with the help of atomic force microscope.

The properties of a substance depend mainly on the arrangement of its atoms. Nano-scale refers to the size at atomic or molecular levels of approximately 1-100 nm range on length scale, providing novel properties and functionalities to nanomaterial.

There are possibly two main reasons for visualizing properties of nanomaterials in different manner as number of scientific principles are becoming dominant at the nanoscale:

- Comparatively larger surface area of nanomaterials makes them more chemically reactive thereby enhancing their strength and other properties like lightness, high electrical conductivity, high porosity, good thermal insulation etc. when compared to the same mass of material produced in a bulk.
- Behaviour of matter at the nanoscale level is dominated by quantum effects thus affecting the electrical, magnetic and optical performance of nanomaterials.

Nano-electromechanical systems (NEMS) based on nanoscale materials like nanowires and nanotubes offer a potential for new applications. Such applications, in turn, enable us to probe the fundamental mechanical properties of these materials in new ways. The very low mass and high stiffness of BNNTs are particularly advantageous for nano-electromechanical resonator devices.

Carbon nanotubes (CNTs), a well-known one-dimensional nanomaterial have been gaining more interest in research from the time, since they were first discovered by Ijima in the year 1991[1]. Soon after the discovery of CNT, another metastable state boron nitride nanotubes (BNNTs) were hypothetically predicted in the year 1994 [2,3], Later on, BNNT was experimentally realized in 1995 [4] and group using arc discharge method. This method involves passing an electric current through a mixture of boron and nitrogen gases, which results in the formation of BNNTs through a process of carbonization.

The BNNTs that were produced by this method were found to have unique properties, such as high thermal stability and electrical insulation, which made them attractive for a wide range of potential applications. The successful synthesis of BNNTs by the arc discharge method marked the beginning of a new field of research in the study of these unique materials and their potential uses.

BNNTs are considered to be structurally similar to their counterpart CNTs, which possess extraordinary mechanical as well as structural properties. However, partially ionic bonding nature of BNNT makes them different from CNT as far as electronic properties are concerned. BNNTs are always semiconducting with wide band gap of approximately 5.5eV which can be tuned theoretically by doping and treated as an electrical insulator at room temperature. Apart from this, its electronic band gap is not dependent on the diameter of tube, helicity, or number of tubular walls in the case of multi-walled BNNTs [5]. Thus, BNNTs are having constant electronic properties making them acceptable in many areas like high-temperatures, high-power electronics, and deep-ultraviolet photo electronic devices.

In addition, BNNTs display other extraordinary properties like superb thermal conductivity [6-8], ability to remain stable (chemically) at high temperatures, greater resistance to oxidation than their counterpart CNTs [9-11] and other remarkable mechanical properties such as Young's modulus clarified [12]. The comparison of various properties of BNNT and CNT are presented in a comparative manner in Table 1.1.

Table 1.1**:** Comparison between properties of BNNTs and CNTs

Property	**BNNTs**	**CNTs**
Colour	White	Black
Electrical Properties	Almost constant wide band gap (~5.0 eV) [13].	Semi metallic or semi conducting, depending on the chirality, diameter, and no. of tubular walls [6]
Mechanical Properties (Young's modulus)	~1.18 TPa [12].	~1.25 TPa [8]
Thermal Conductivity	~350 W/mK (for outer diameter of 30-40 nm tube) [15]	~ 300 W/mK (diameter of 30-40 nm) and >3000 W/mK (diameter of ~14nm) [15]
Optical Properties	Applicable in the deep-UV regime [13].	Applicable in the near-IR regime [17]
Chemical Stability as per [9].	Stable up to 1100^{o}C in air	Stable up to ~500^{o}C in air

1.2. Concept of nano mechanisms

High resonance frequencies of the order of gigahertz as well as low damping and resonance peak at higher frequency of nanostructures makes them sensitive enough, particularly for measuring physical quantities requiring very small perturbations like mass. These outstanding properties of nanoresonator make them suitable for many mass sensing applications. For better understanding of their dynamic behaviour, damped simple harmonic oscillator can be used for describing motion of nanoresonator in the linear region. This can be well explained by considering one-degree of freedom system consisting of mass (m), viscous damper (c), and spring (k) and system is assumed to be driven by a harmonic force resulting in following equation of motion.

$$m\ddot{x} + c\dot{x} + kx = F\cos(\omega t) \tag{1.1}$$

and its steady-state solution is given as:

$$x(t) = \frac{F_0 / m}{\sqrt{\left(\omega_0^2 - \omega^2\right)^2 + \left(2\zeta\omega_0\omega\right)^2}} \cos\left(\omega t - \phi\right) \tag{1.2}$$

$$\tan\left(\phi\right) = \frac{\left(\omega_0^2 - \omega^2\right)}{2\zeta\omega_0\omega} \tag{1.3}$$

The dynamic motion of the above system is thus, characterised by following two parameters:

- Resonance frequency $(\omega_0) = \sqrt{k/m}$, and
- Damping coefficient $\zeta = 1/2(Q) = c/2(\omega_0 m)$.

where, $Q = \omega_0 / \Delta\omega$ representing the quality factor.

In order to detect any variation in physical quantity accurate monitoring of resonance frequency is required, which mainly depends on the system mass and spring constant. Based on this fact, mass of any object can be detected, when it is attached to the system. When the system is allowed to interact with any force, its spring constant changes and causes a shift in resonance frequency thus enabling force measurement. Therefore, for a nanomechanical resonator used as a mass sensor, its mass sensitivity (minimum detectable mass) can be evaluated as:

$$\delta m = \frac{\partial m_{effective}}{\partial \omega_0} . \delta\omega = \frac{\delta\omega}{R} \tag{1.4}$$

where, '*R*' is the mass responsivity. The above relation is valid only for situations where, attached mass is maintained much less than effective mass of resonator in order to nullify the effect of quality factor as well as the spring constant for linear dynamics. Thus, for obtaining better sensitivity of resonator, smaller mass with high resonance frequency is desirable.

1.3. Boron nitride nanotube structure

A boron nitride nanotube (BNNT) comprises of equal proportions of boron and nitrogen atoms and is structurally like carbon nanotube (CNT). Different forms of BNNT can be visualized by rolling up a hexagonal boron nitride sheet into a cylindrical form along different directions as depicted in Fig. 1.1. There may be one or more layers of boron nitride sheet along its radial

direction, and accordingly they are categorized as single-wall boron nitride nanotubes (SW-BNNTs) and multi-wall boron nitride nanotubes (MW-BNNT), respectively.

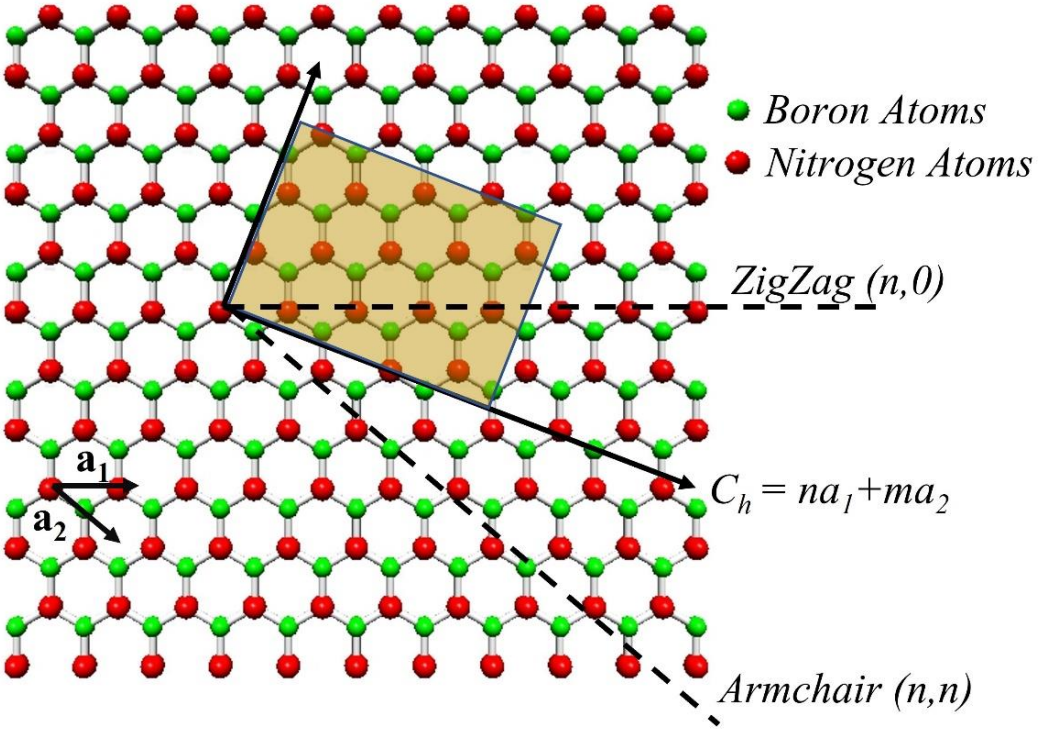

Fig. 1.1. Structure of BNNT obtained from rolling up of h-BN sheet [18].

Based on primary symmetry, a BNNT can be classified as achiral or chiral. In an achiral type, mirror image of nanotube has a structure identical to the original one. The different forms of an achiral BNNT depending on shape of cross-sectional ring are armchair BNNT and zigzag BNNT as shown in Fig. 1.2 (a) and (b).

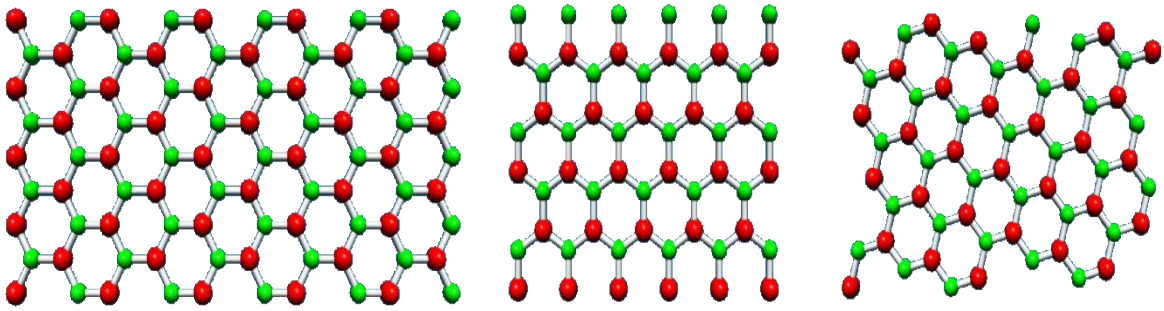

(a) (b) (c)

Fig. 1.2. Different structural forms of BNNT (a) Armchair (b) Zigzag and (c) Chiral.

Chiral nanotubes display a spiral symmetry in which mirror image is not identical to the original one. The chiral nanotube is also called axially chiral in the chemical nomenclature. Both these types of nanotubes are designated by chiral indices *n* and *m* and their values classify nanotube in three different cases as:

Case 1: when $m = n$ the nanotube is called "Armchair nanotube" ($\theta = 30^{\circ}$).

Case 2: when $m = 0$ the nanotube is called "Zigzag nanotube" ($\theta = 0^{\circ}$).

Case 3: when $m \neq n$ the nanotube is called "Chiral nanotube" ($0^0 < \theta < 30^{\circ}$).

BNNTs of various structural forms (zigzag, chiral, and armchair) can be generated by rolling up of hexagonal boron nitride sheet in different orientations as described in Fig. 1.1. Two lattice vectors (a_1 and a_2), chiral vector (also known as roll up vector, C_h) and chiral angle (θ) are used to define the structure of a nanotube. The chirality vector is perpendicular to the nanotube axis, and it can be represented by:

$$C_h = n.a_1 + m.a_2 = (n, m) \tag{1.5}$$

where *n* and *m* are integers 0<=|*m*|<=*n*. The values of chirality angle (θ) lie in the range 0<=|θ|<= 30^0 because of hexagonal symmetry of the honeycomb lattice. The chiral angle determines the angle of hexagons with respect to the direction of the nanotube axis and spiral symmetry of nanotube can be specified by this angle. The chirality angle can be expressed by:

$$\theta = \cos^{-1}\left[\frac{(C_h.a_1)}{|C_h|.|a_1|}\right] = \cos^{-1}\left[\frac{2n+m}{2\sqrt{n^2+m^2+nm}}\right] \tag{1.6}$$

Chiral angle along with the diameter of nanotube are important parameters for defining properties of nanotubes. The diameter of nanotube in terms of chiral indices can be expressed as:

$$d_{nanotube} = \frac{1}{\pi} a_{B-N} \sqrt{3\left(n^2+m^2+nm\right)} \tag{1.7}$$

where $a_{B\text{-}N}$ = 0.145 nm represents the B-N bond length.

1.4. Properties of boron nitride nanotube

1.4.1. electrical properties

BNNTs are considered to be wide band gap nanomaterials because of their ionic bonding nature and their constant electronic properties which cannot be altered by their diameters, chirality and number of walls in the case of multi-walled BNNTs [3]. BNNTs provide better electric insulation at room temperature because of their wide band gap of ~5 eV [13]. The band gap of BNNT can be tuned by carbon doping [14], radial deformation [15], or by giant Stark effect [16-20].

1.4.2. Mechanical properties

The axial Young's modulus of individual MW-BNNTs has been experimentally measured in using thermal vibration technique and found to be 1.18 TPa [12], which is highest amongst all other well-known insulating nanomaterials. This is consistent with the values obtained theoretically based on the tight binding technique [21]. However, due to polygonal cross-sectional morphology of MW-BNNTs, lower value of modulus (0.5-0.6 TPa) was observed [22]. This observation was based on in-situ bending test performed on MW-BNNTs under transmission electron microscopy (TEM).

On the basis of their exceptional stiffness value [23], BNNTs are promising candidates for reinforcement in polymeric composites as well as ceramics [24-26]. This leads to applications requiring lighter, but strong structures such as in automobiles and in airplanes.

1.4.3. Thermal properties

It is known that high density nano-electromechanical system (NEMS) generate great amount of heat radiations and this demands nanomaterials having high thermal conductivity. Thermal properties of BNNTs have been studied using a number of techniques like tight binding approach and density functional theory [27-28]. It was found that BNNTs have higher thermal conductivity at room temperature as compared to CNTs.

Golberg and Chen systematically studied another remarkable thermal property of BNNTs and found that BNNTs have high resistance to thermal oxidation[29-30]. Later on, Zhi observed that BNNTs are stable at 1100^0 C in air[31]. The main reason for high resistance to oxidation is

due to the fact that h-BN network remains for the nano-crystalline structures in BNNT at higher temperatures.

1.5. Applications of boron nitride nanotube

1.5.1. BNNT based composites for mechanical applications

The polymer matrix may be strengthened by mixing BNNTs in polymer as BNNTs have outstanding mechanical properties. Non-covalent interaction can be used to functionalize the BNNTs, and this can be achieved by wrapping of BNNTs with polymer. The π-π interactions between most of the long chain polymers (benzene rings) and side wall of BNNTs can be easily achieved due to sp^2 hybridized h-BN network. Functionalized BNNTs can be perfectly dissolved in most of the organic solvents[32-34]. further clarified that such interaction helps in purifying the BNNTs.

Thus, the strength of any structural material can be enhanced by reinforcing it with some volume percentage of BNNT. At the same time, polymeric material reinforced with BNNT can be used as a mass sensor which is not influenced by environmental factors unlike conventional sensor.

1.5.2. Bio-medical applications

It has been observed that BNNTs have the ability to interact with biological entities like proteins or DNA through π-stacking[35,36]. The DNA can be removed by annealing at 700^{o}C for 30 minutes in air to obtain a clean BNNT surface. This kind of functionalization of BNNTs with biological materials makes BNNTs suitable for sensing and biomedical applications. It has been experimentally shown that BNNTs could be non-cytotoxic as well as bio-compatible and most appropriate material for therapeutic or diagnostic purposes in biomedical applications[37-39].

Furthermore, reinforcement of BNNTs into biodegradable polymers like polycaprolactone (PLC) and polylactic acid (PLA), with biocompatibility and enhanced mechanical properties, was proved to display increased osteoblast cell viability and its possible application in orthopaedic scaffolds[25].

It has also been proposed that BNNTs may be used in boron neutron capture therapy (BNCT) to carry boron[40]. In such a case, when BNNT is delivered into cancerous cells, it may

absorb neutrons from an external source of neutron beam and due to which generation of localized alpha radiation can help in killing the tumours.

1.5.3. Nanoresonator

Nano-electromechanical systems (NEMS) hold promise for a number of scientific and technological applications. High frequency nanoresonators are one of the critical components used in many NEMS like devices for detecting charge, oscillators, etc[41,42]. Based on the principle of electrical actuation, nanoelectromechanical oscillator was developed and detection of oscillation mode of guitar string type in doubly-clamped nanotube was achieved[43]. Similarly, on the basis of oscillation of innermost tube in the case of multi walled nanotube with respect to outer most tube, an oscillator design having frequencies in the range of GHz[44,45].

The fundamental frequency of nanotube can be predicted by employing an approach based on molecular structural mechanics. This approach was successfully implemented for single wall carbon nanotube (SW-CNT) based nanomechanical resonators of cantilevered as well as bridged configurations. The frequency of such nanomechanical resonator lies in the range of several gigahertz and maximum up to 1.5 THz[46]. Similarly, it has been studied ropes made of hundreds of SWNTs have bending frequencies in the range of MHz[47]. Another parallel study conducted for cantilevered SWNTs alone having aspect ratios of approximately L/D = 100 also clarified that fundamental resonance frequencies lie in the range of MHz[48].

1.5.4. Nanotube as sensors and probes

Nanotubes are used in sensor applications because of better sensing capability with high sensitivity. It has been studied that electron transport as well as thermal power of nanotube is so sensitive that it is even capable of sensing the substances affecting the actual charge injected on nanotube[49]. This is because of the smaller size of nanotube supported with features like low density and enough stiffness. At the same time smaller diameter of nanotube facilitate narrow imaging with better resolution as compared to conventional nanoprobes[50]. Through covalent functionalization of tip of nanotube with ligands capable to respond biologically, it is possible to map biological and chemical functions[51]. Nanoscopic tweezers can be used as nanoprobes[52]. Mass sensors based on resonance frequency can be successfully employed for applications requiring sensing of small mass of the order of zeptogram level like monitoring of chemical

reaction and metal deposition, mass detectors and sensors for bio-medical applications[53-55]. All such applications rely on principle of resonance frequency shift due to added mass on sensor.

At the same time, micromechanical resonators have been explored and are gaining more attention. The advantage of micromechanical resonators is that their mass sensitivity can be improved by miniaturization of their dimensions[56]. It has been testified that the mass of the order of femtogram level can be detected with the help of micro-sized silicon/ silicon nitride cantilevers. Even higher mass sensitivity can be achieved through scaling down the micro-sized resonator to nanosize results in better sensitive nanoresonators suitable for detection of various gas molecules, bacteria/viruses[57-58].All the above applications of nanotubes have motivated for current work to study the dynamics of BNNT based nanoresonator used as mass sensor.

1.6. Existing modelling and simulation techniques

Most of the present analyses for investigating the mechanical behaviour of boron nitride nanotubes are carried out with atomistic. However, for bulky systems such as NEMS and nanotube reinforced composites that comprise of a number of BNNTs restrict the use of such atomistic simulation techniques because of their limitations both on the time scale as well as on the length scale. A continuum mechanics-based approach is thus, suitable for the design and analysis of such large scale systems. There have been limited studies of BNNTs with continuum approaches and in all such studies; BNNTs are modelled as thin shells. Though results based on continuum mechanics approach are reasonably agreeable compared to atomistic simulations, the shell model further requires fitting atomistic simulation results to determine the elastic parameters such as flexural rigidity. Moreover, the shell model confined to infinitesimal strain and linear elasticity[59-61].

1.7. Sources of vibrations

1.7.1. Parametric excitations

Parametric excitation refers to the process of generating vibrations in a system by applying a periodic external force or by changing certain parameters of the system. In the case of BNNTs (Boron Nitride Nanotubes), parametric excitation can be used to generate vibrations in the nanotube structure. The exact method of parametric excitation will depend on the specific BNNT system being studied and the type of vibrations that are being generated. One way to generate

parametric excitation in BNNTs is through the application of a time-varying external force, such as a mechanical load or an electromagnetic field. This can cause the BNNT to vibrate at a specific frequency, known as the natural frequency of the system. The boundary conditions, length and diameter of nanotubes are among the main parameter that influences the excitation frequency of nanotube. Two different boundary conditions namely cantilevered and doubly clamped are employed in the present work. The general expression for fundamental frequency of pristine BNNT is given by:

$$f_n = \frac{1}{2\pi}\sqrt{\frac{K_{eq}}{M_{eq}}} \tag{1.8}$$

Where, K_{eq} is equivalent to stiffness and its value depends on type of boundary condition. Because of their different values, system would excite at different frequencies. M_{eq} represent the equivalent mass of system and its value for cantilevered boundary condition is:

$$M_{eq} = \rho_{bnnt} A_{bnnt} L_{bnnt} + 4\left(M_{added}\right) \tag{1.9}$$

And for doubly-clamped configuration, it is given by:

$$M_{eq} = \rho_{bnnt} A_{bnnt} L_{bnnt} + 2.52\left(M_{added}\right) \tag{1.10}$$

Thus, it can be seen that excitation frequency depends on amount of added mass (M_{added}) on BNNT. Also, for a particular boundary condition it can be seen that change in length causes a change in the stiffness of the nanotube. It has been shown that shorter BNNTs are better candidates for mass sensing due to higher mass sensitivity. The different sources of vibration in nanotube are illustrated in Fig. 1.3.

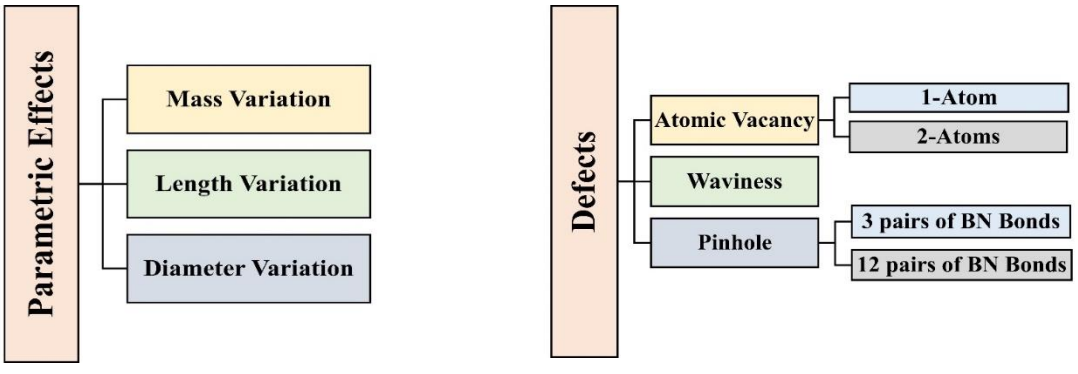

(a) (b)

Fig. 1.3. Sources of vibration in nanotube due to (a) parametric effect and (b) defects.

As compared to the achiral nanotubes, it is seen that chiral nanotubes behave differently. The reason can be attributed to the orientation of the bonds existing between the boron and nitrogen atoms in the crystal lattice. As the orientation of the bonds is different in chiral nanotubes as compared to zigzag or armchair forms, the deflection of the bonds due to the addition of the mass would be different. Due to the difference in the deflection, the stiffness is also different which would change the frequency at which the system excites. Hence, chirality can also be considered as an important parameter leading to the parametric excitations.

1.7.2. Defects in boron nitride nanotubes

BNNTs have superior properties comparable to the traditional engineering materials. However, these properties hold only for the ideal case of BNNTs, where these are made of perfect hexagonal graphite honeycomb lattice of mono-atomic layer thickness. However, in actual practice BNNTs are found to have certain defects associated with it. The advantages or disadvantages of the presence of defects in BNNT depend on their applications. Structural defects may increase the adhesion of other atoms and molecules to BNNT. Moreover, it has also been found that the defects in BNNT can change its resonant frequency as compared to that of a pristine BNNT. The defects that have been considered for the purpose of analysis in this research include the following:

A. Waviness

BNNTs are assumed to behave as perfectly straight beams or straight cylindrical shells similar to CNTs. However, these small structures are not usually straight, but rather have certain degree of surface deviation in the form of curvature or waviness along the nanotube's length. The curved morphology is due to process-induced waviness during manufacturing processes, in addition to mechanical properties such as low bending stiffness and large aspect ratio.

B. Missing boron/nitrogen atoms in the lattice structure (Vacancy defect)

BNNTs are widely used in the design of nanosensors and actuators. Any defect in the manufactured nanotube plays an important role in the natural frequencies of these structures. The nanotubes act as basic elements of these nanostructures; therefore, vibrations of BNNTs get considerable importance. Most of the previous work as found in literature have focused on the

simulation and estimation of the mechanical properties of perfect BNNTs and have ignored the effect of initial defects. Whereas experimental observations have reported the presence of topological defects, such as the Stone Wales (SW) defect and vacancy defects in BNNT.

C. Pinhole defect

Various defects on the BNNT wall have been reported, which are formed during the synthesizing process. Some of them are reported to be large enough for C_{60} molecule or metal molecules to pass through. In applying the BNNT to nano-probes or nano-cantilever beams, the defects would affect the mechanical characteristics such as yield strength and a resonant frequency. Two types of pinhole defects (i) 3 pairs of missing B-N bonds and (ii) 12 pairs of missing B-N bonds have been considered in the present analysis.

1.8. Organization of the thesis

The present research work is organized in following manner:

Chapter 1 provides a brief description about history of nanotechnology and the concept of nanomechanics followed by the discovery of boron nitride nanotube, its structure and associated properties. The various applications of BNNT in different areas and types of defects normally present in BNNT are also discussed. Various modelling techniques presently employed for modelling and simulation of nanotubes by various researchers are studied. The sources of vibration generation in BNNTs and objectives of the present research are also discussed, followed by organization of the thesis chapters.

Chapter 2 deals with critical review of the published literature on various studies and methodologies suitable for BNNTs and its composites. The literature on applications of BNNTs, mass sensing and defects that include waviness, atomic vacancies and pinhole defects in nanotube is discussed.

Chapter 3 presents the dynamic analysis of single-walled as well as multi-walled BNNT based mass sensor. The applicability of the continuum mechanics approach for nanoscale modelling is discussed and same is employed for modelling of BNNT. In order to take into account the effect of chirality, hybrid modelling approach which is a blend of structural mechanics and molecular mechanics is used for analysing achiral BNNT based mass sensor. For

modelling of a straight clamp-free and doubly clamped SW-BNNT, continuum mechanics approach (Euler Bernoulli principle) is used for calculating the resonant frequency. A molecular structural mechanics based 3D-atomistic finite element model consisting of beam elements and point masses is utilized for modelling of BNNTs of different forms, viz., armchair and zigzag. The excitations generated here are due to the change in mass as well as parametric variations. The results obtained are validated with the previously published experimental results.

The vibration excitations induced in the BNNT system due to the presence of defects have been presented. A molecular structural mechanics based atomistic finite element model consisting of beam elements and point masses is implemented for analysing vibrational behaviour of defective SW-BNNT. Influence of defects like atomic vacancies, pin hole defect etc. on dynamics of nanotubes is investigated and discussed.

Chapter 4, A continuum mechanics based finite element model has been utilized for modelling of waviness in BNNT. The vibration responses of wavy doubly clamped BNNT subjected to different length and waviness are analysed. The vibration excitation frequencies resulting from the interaction of defect like waviness existing in SW-BNNT is explored. The non-linearity in nanotube arises due to mid-plane stretching in case of doubly-clamped BNNT system and surface deviation due to waviness is also discussed. The non-linear dynamic analysis of a wavy BNNT behaving as mass sensors is also done. A nonlinear mathematical model for wavy SW-BNNT is developed using energy approach with the Galerkin method and analysed using 4^{th} order Runga-Kutta method. The dynamic responses are obtained using various response tools like time series, phase space, Poincaré section and Fast Fourier Transforms.

Chapter 5 deals with the structural and thermal stability of single-walled boron nitride nanotubes (SW-BNNTs) under strained conditions are essential in pursuit of their applications that are subjected to high temperature processing and/or working environment. However, there are dearth of high temperature (> 1000 K) studies on SW-BNNTs and other forms of hexagonal boron nitride (h-BN) structures, either with or without defects, due to experimental difficulties. an atomistic approach is adopted to perform uniaxial tensile and torsional quasi-static straining of pristine and monovacancy defected SW-BNNTs at different temperatures while the thermal stability of monovacancy defected SW-BNNT structures were predicted from its mean square displacement during equilibration up to 2400 K temperature.

Chapter 6 provides a comprehensive discussion and conclusions arising out of the present work. The scope for future work is also presented in this chapter.

1.9. Motivation

Boron nitride nanotubes (BNNTs) exhibit exceptional thermal, mechanical, optical, and electrical characteristics, making them a potential nanomaterial. Recent research shown that BNNTs are superior to carbon nanotubes for most energy-environment applications. BNNTs are a wide-bandgap insulator with thermal oxidation resistance, piezoelectric characteristics, high hydrogen adsorption, UV luminescence, cytocompatibility, and stability. Unique qualities of BNNT make it a great material for membranes. These features can help water filtration, gas separation, sensing, and battery separator membranes. Recent research shows defects present in boron nitride nanotube BNNTs influence their characteristics and properties. These defects change their topological, geometrical, and dynamic properties. It also been proven that no nanotube can perfect there is higher chance of defects presence in BNNT during synthesis, characterization and purification. To improve the properties like flow, rejection, anti-fouling, sensing, structural, thermal, electrical, mechanical, and optical characteristics proper independent defect is required. Which can be explored using molecular simulation. This viewpoint essay analyses advanced BNNT features.

REFERENCES

[1.] Iijima, S. Helical microtubules of graphitic carbon, Nature, vol. 354, 1991, pp. 56-58.

[2.] Rubio, A., Corkill, J.L. and Cohen, M.L., Theory of graphitic boron nitride nanotubes. Physical Review B, vol. 49(7), 1994, pp. 5081.

[3.] Blase, X., Rubio, A. Louie. S. and Cohen, M.L., Stability and Band Gap Constancy of Boron Nitride Nanotubes, Europhysics Letters, vol. 28, 1994, pp. 335.

[4.] Chopra, N.G., Luyken, R.J., Cherrey, K., Crespi, V.H., Cohen, M.L., Louie, S.G. and Zettl A. Boron Nitride Nanotubes, Science, vol. 269, 1995, pp. 966-967.

[5.] Blasé, X., Charlier, J.C., Vita, A.D. and Car, R., Theory of composite B[sub x]C[sub y]N[sub z] nanotube heterojunctions, Applied Physics Letters, vol. 70(2), 1997, pp. 197-199.

[6.] Han, W.Q., Mickelson, W., Cumings, J. and Zettl, A., Transformation of BxCyNz nanotubes to pure BN nanotubes, Applied Physics Letters, vol. 81 (6), 2002, pp. 1110-1112.

[7.] Xiao, Y., Yan, X.H., Cao, J.X., Ding, J.W., Mao, Y.L. and Xiang, J., Specific heat and quantized thermal conductance of single-walled boron nitride nanotubes. Physical Review B, vol. 69, 2004, pp. 205415.

[8.] Chang, C.W., Han, W.Q. and Zettl, A., Thermal conductivity of B-C-N and BN nanotubes, Applied Physics Letters, vol. 86 (17), 2005, pp. 173102.

[9.] Golberg, D., Bando, Y., Kurashima, K. and Sato, T., Synthesis and characterization of ropes made of BN multiwalled nanotubes, Scripta Materialia, vol. 44, 2001, pp. 1561-1565.

[10.] Golberg, D., Bando, Y., Tang, C. and Zhi, C., Boron nitride nanotubes. Advanced Materials, vol. 19, 2007a, pp. 2413.

[11.] Tang, C. and Bando, Y., Effect of BN coatings on oxidation resistance and field emission of SiC nanowires, Applied Physics Letters, vol. 83, 2003, pp. 659-661.

[12.] Chopra, N.G. and Zettl, A., Measurement of the elastic modulus of a multi wall boron nitride nanotube, Solid State Communications, vol. 105, 1998, pp. 297–300.

[13.] Lee, C.H., Xie, M., Kayastha, V., Wang, J. and Yap, Y.K., Patterned Growth of Boron Nitride Nanotubes by Catalytic Chemical Vapour Deposition, Chemistry of Materials, vol. 22, 2010, pp. 1782-1787.

[14.] Miyamoto, Y., Rubio, A., Cohen, M.L. and Louie, S.G., Chiral tubules of hexagonal BC2N, Physical Review B, vol. 50, 1994, pp. 4976.

[15.] Kim, Y.H., Chang, K.J. and Louie, S.G., Electronic structure of radially deformed BN and BC3 nanotubes. Physical Review B, vol. 63, 2001b, pp. 205408.

[16.] Khoo, K.H., Mazzoni, M.S.C. and Louie, S.G., Tuning the electronic properties of boron nitride nanotubes with transverse electric fields: A giant dc Stark effect, Phys. Rev. B, vol. 69, 2004, pp. 201401.

[17.] Chen, C.W., Lee, M.H. and Clark, S.J., Band gap modification of single-walled carbon nanotube and boron nitride nanotube under a transverse electric field, Nanotechnology, vol. 15, 2004, pp. 1837-1843.

[18.] S. Trivedi, S. C. Sharma, and S. P. Harsha, "Single walled-boron nitride nanotubes based nanoresonator for sensing of acetone molecules," Nano, vol. 9, no. 8, p. 1450086, Dec. 2014, doi: 10.1142/S1793292014500866.

[18.] Ishigami, M., Sau, J.D., Aloni, S., Cohen, M.L. and Zettl, A., Observation of the Giant Stark Effect in Boron-Nitride Nanotubes, Physical Review Letters, vol. 94, 2005, pp. 056804.

[19.] Ishigami, M., Sau, J.D., Aloni, S., Cohen, M.L. and Zettl, A., Symmetry Breaking in Boron Nitride Nanotubes, Physical Review Letters, vol. 97, 2006, pp. 176804.

[20.] Cohen, M.L. and Zettl, A., The physics of boron nitride nanotubes. Physics Today, vol. 63, 2010, pp. 34-38.

[21.] Sánchez-Portal, D. and Hernández, E., Vibrational properties of single-wall nanotubes and monolayers of hexagonal BN, Physical Review B, vol. 66, 2002, pp. 235415.

[22.] Golberg, D., Costa, P.M.F.J., Lourie, O., Mitome, M., Bai, X., Kurashima, K., Zhi, C., Tang, C. and Bando, Y., Direct Force Measurements and Kinking under Elastic Deformation of Individual Multi walled Boron Nitride Nanotubes, Nano Letters, vol. 7, 2007b, pp. 2146-2151.

[23.] Chopra, N.G. and Zettl, A., Measurement of the elastic modulus of a multi wall boron nitride nanotube, Solid State Communications, vol. 105, 1998, pp. 297–300.

[24.] Hernández, E., Goze, C., Bernier, P. and Rubio, A., Elastic Properties of C and BxCyNz Composite Nanotubes, Physical Review Letters, vol. 80, 1998, pp. 4502.

[25.] Bakshi, S.R., Lahiri, D. and Agarwal, A., Carbon nanotube reinforced metal matrix composites-a review, International Material Review, vol. 55, 2010, pp. 41-64.

[26.] Huang, Q., Bando, Y., Xu, X., Nishimura, T., Zhi, C., Tang, C., Xu, F., Gao, L. and Golberg, D., Enhancing super-plasticity of engineering ceramics by introducing BN nanotubes, Nanotechnology, vol. 18, 2007, pp. 485706.

[27.] Wirtz, L., Rubio, A., Concha R.A. de la and Loiseau, A., Ab initio calculations of the lattice dynamics of boron nitride nanotubes, Physical Review B, vol. 68, 2003, pp. 045425.

[28.] Xiao, Y., Yan, X.H., Cao, J.X., Ding, J.W., Mao, Y.L. and Xiang, J., Specific heat and quantized thermal conductance of single-walled boron nitride nanotubes. Physical Review B, vol. 69, 2004, pp. 205415.

[29.] Golberg, D., Bando, Y., Kurashima, K. and Sato, T., Synthesis and characterization of ropes made of BN multiwalled nanotubes, Scripta Materialia, vol. 44, 2001, pp. 1561-1565.

[30.] Chen, C.W., Lee, M.H. and Clark, S.J., Band gap modification of single-walled carbon nanotube and boron nitride nanotube under a transverse electric field, Nanotechnology, vol. 15, 2004, pp. 1837-1843.

[31.] Zhi, C., Bando, Y., Tang, C., Honda, S., Sato, K., Kuwahara, H. and Golberg, D., Characteristics of Boron Nitride Nanotube–Polyaniline Composites, Angewandte Chemie International Edition, vol. 44, 2005b, pp. 7929.

[32.] Zhi, C., Bando, Y., Tang, C., Xie, R., Sekiguchi, T. and Golberg, D., Perfectly Dissolved Boron Nitride Nanotubes Due to Polymer Wrapping, Journal of American Chemical Society, vol. 127, 2005c, pp. 15996-15997.

[33.] Xie, S.Y., Wang, W., Fernando, K.A.S., Wang, X., Lin, Y. and Sun, Y.P., Solubilization of boron nitride nanotubes, Chemical Communications, vol. 29, 2005, pp. 3670-3672.

[34.] Zhi, C., Bando, Y., Tang, C., Honda, S., Sato, K., Kuwahara, H. and Golberg, D., Purification of Boron Nitride Nanotubes through Polymer Wrapping, Journal of Physical Chemistry B, vol. 110, 2006b, pp. 1525-1528.

[35.] Zhi, C., Bando, Y., Tang, C. and Golberg, D., Immobilization of Proteins on Boron Nitride Nanotubes, Journal of American Chemical Society, vol. 127, 2005a, pp. 17144-17145.

[36.] Zhi, C., Bando, Y., Wang, W., Tang, C., Kuwahara, H. and Golberg, D., DNA-Mediated Assembly of Boron Nitride Nanotubes, Chemistry - An Asian Journal, vol. 2, 2007, pp. 1581-1585.

[37.] Ciofani, G., Raffa, V., Menciassi, A. and Cuschieri, A., Boron nitride nanotubes: an innovative tool for nanomedicine, Nano Today, vol. 4, 2009a, pp. 8–10.

[38.] Chen, X., Wu, P., Rousseas, M., Okawa, D., Gartner, Z., Zettl, A. and Bertozzi, C.R., Boron nitride nanotubes are non-cytotoxic and can be functionalized for Interaction with Proteins and cells, Journal of the American Chemical Society, vol. 131, 2009, pp. 890-891.

[39.] Ciofani, G., Danti, S., D'Alessandro, D., Moscato, S. and Menciassi, A., Assessing cytotoxicity of boron nitride nanotubes: Interference with the MTT assay, Biochemistry and Biophysics Research Communication, vol. 394, 2010, pp. 405-411.

[40.] Ciofani, G., Raffa, V., Yu, J., Chen, Y., Obata, Y., Takeoka, S., Menciassi, A. and Cuschieri, A., Boron Nitride Nanotubes: A Novel Vector for Targeted Magnetic Drug Delivery, Current Nanoscience, vol. 5, 2009c, pp. 33-38.

[41.] Kwon, Y.W., Manthena, C., Oh, J.J., and Srivastva, D., Vibrational characteristics of carbon nanotubes as nanomechanical resonators, Journal of Nanoscience and Nanotechnology, vol. 5, 2005, pp. 703–712.

[42.] Pelesko, J.A., and Bernstein, D.H., Modeling MEMS and NEMS, Boca Raton (FL): Chapman & Hall/ CRC, 2003.

[43.] Sazonova, V., Yaish, Y., Ustenel, H., Roundy, D., Arias T.A. and McEuen, P., A tunable carbon nanotube electromechanical oscillator, Nature, vol. 431, 2004, pp. 284–287.

[44.] Zheng, Q, and Jiang, Q., Multiwalled carbon nanotubes as gigahertz oscillators, Physical Review Letters, vol. 88, 2002, pp. 45503/1–3.

[45.] Zheng, Q, Liu, J.Z., and Jiang, Q., Excess van der Waals interaction energy of a multiwalled carbon nanotube with an extruded core and the induced core oscillation. Physical Review B, vol. 65, 2002, pp. 245409/1–6.

[46.] Li, C. and Chou, T.W., Single walled carbon nanotubes as ultrahigh frequency nanomechanical resonators, Physical Review B, vol. 68, 2003c, pp. 73405/1-3.

[47.] Reulet, B., Kasumov, A.Y., Kociak, M., Deblock, R., Khodos, I.I., Gorbatov, Y.B., V., Volkov, T., Journet, C. and Bouchiat, H., Acoustoelectric effects in carbon nanotubes, Physical Review Letters, vol. 85, 2000, pp. 2829–2832.

[48.] Gao, R, Wang, Z.L., Bai, Z., de Heer, W., Dai, L., and Gao, M., Nanomechanics of individual carbon nanotubes from pyrolytically grown arrays, Physical Review Letters, vol. 85, 2000, pp. 622–625.

[49.] Dai, H. J., Hafner, J. H., Rinzler A. G., Colbert D. T., and Smalley, R. E., Nanotubes as nanoprobes in scanning probe microscopy, Nature, vol. 384, 1996, pp. 147-150.

[50.] Wong, S.S., Joselevich, E., Woolley, A.T., Cheung, C.L., and Lieber, C.M., Covalently functionalized nanotubes as nanometre- sized probes in chemistry and biology, Nature, vol. 394, 1998, pp. 52-55.

[51.] Kim, P. and Lieber, C. M., Nanotube Nanotweezers, Science, vol. 286, 1999, pp. 2148-2150.

[52.] Cassell, A.M., Raymakers, J.A., Kong, J. and Dai, H.J., Large scale CVD synthesis of single-walled carbon nanotubes, The Journal of Physical Chemistry B, vol. 103, 1999, pp. 6484-6492.

[53.] Benes, E., Groschl, M., Burger, W., and Schmid, M., Sensors based on piezoelectric resonators, Sensors & Actuators A: Physical, vol. 48, 1995, pp. 1-21.

[54.] Hauptmann P., Lucklum, R., Puttmer, A., and Henning, B., Ultrasonic sensors for process monitoring and chemical analysis: state-of-the-art and trends, Sensors and Actuators A, vol. 67, 1998, pp. 32- 48.

[55.] Lu, C. and Czanderna W., Applications of Piezoelectric Quartz Crystal, 1984, Elsevier, New York.

[56.] Lavrik, N. V. and Datskos, P. G., Femtogram mass detection using photothermally actuated nanomechanical resonators, Applied Physics Letters, vol. 82, 2003, pp. 2697-2699.

[57.] Baughman, R. H., Cui, C., Zakhidov, A.A., Iqbal, Z., Barisci, J.N., Spinks, G. M., Wallace, G.G., Mazzoldi, A., De Rossi, D., Rinzler, A.G., Jaschinski, O., Roth, S. and Kertesz, M., Carbon Nanotube Actuators, Science, vol. 284, 1999, pp. 1340-1344.

[58.] Kim, P. and Lieber, C. M., Nanotube Nanotweezers, Science, vol. 286, 1999, pp. 2148-2150.

[59.] Hernández, E., Goze, C., Bernier, P. and Rubio, A., Elastic Properties of C and BxCyNz Composite Nanotubes, Physical Review Letters, vol. 80, 1998, pp. 4502.

[60.] Bettinger, H.F., Dumitrica, T., Scuseria, G.E. and Yakobson, B.I., Mechanically induced defects and strength of BN nanotubes, Physical Review B, vol. 65, 2002, pp. 041406–041410.

[61.] Moon, W. and Hwang, H., Molecular mechanics of structural properties of boron nitride nanotubes, Physica E: Low-Dimensional Systems and Nanostructures, vol. 23, 2004, pp. 26-30.

CHAPTER 2

Literature Review

2.1. Introduction

It is found that nanotubes (both CNT and BNNT) have superior properties compared to the traditional engineering materials because of the different behaviour at nanolevel. However, these properties hold only for the ideal case of nanotubes where they are made of perfect hexagonal graphite/ boron nitride honeycomb lattice of mono-atomic layer thickness. However, in actual practice the nanotube contains certain topological and other defects which arise during synthesis processes. Boron nitride nanotubes (BNNTs) have been progressively studied for their suitability in various applications due to their exceptional physicochemical properties including large hydrophobicity, electrical and thermal insulation, good hydrogen storage capability and better resistance to oxidation. BNNTs are also appreciated for probable biomedical applications comprising drug delivery, boron neutron capture therapy (BNCT).

Since the present work concerns with dynamic analysis of both pristine and defective BNNTs to sense mass as small as of the order of femtogram level, thus, the current literature review is mainly concerned with various computational nanomechanics tools, employed for analysing behaviour of nanotubes and its composites. The biocompatibility and toxicity of BNNT are also reviewed for their possible applications in biomedical engineering. At the same time, present work also deals with BNNT based composites behaving as mass sensors, the same are critically reviewed from theoretical aspects.

An extensive literature review has been done covering analytical as well as experimental aspects in regards to nanotube based materials and their applications as sensors.

2.2. Review of analytical work

Computational nanomechanics approach can be applied successfully for the development of nanosensor. Analysis and design of nanomaterial is possible through modelling and simulation in

an effective manner. As a matter of fact, it is very cumbersome to establish analytical models at the nanoscale dimensions and at the same time conducting experiments on such nanoscale material is expensive too. On the contrary, modelling and simulation of nanosensor not only provide useful guidelines to the experimentalists for conducting experiments, but also helps in optimizing the cost and time required for analysis of nanomaterials.

The exactness of simulation results depends on accuracy of mathematical models of nanomaterials under investigation. Mainly, three different modelling techniques, viz., continuum mechanics, atomistic approach and hybrid (i.e., molecular structural mechanics) approach have been employed for obtaining analytical solutions for nanomaterials. Each of these have their own merits and de-merits. Atomistic modelling approach is most preferable for performing simulation at molecular/atomic level, but their use is limited only for smaller number of molecules or atoms, because of more cost as well as time associated with them. In order to obtain an analytical solution of a large-sized atomic system, other powerful and effective models are required. Unlike classical molecular dynamics a kind of atomistic modelling approach, continuum mechanics-based modelling technique is useful for analysing static and dynamic mechanical properties of comparatively larger systems of nanotubes. Though, the continuum approach ignores the effect of chirality and forces acting on the individual atoms of nanotubes. Hybrid modelling approach, popularly known as molecular structural mechanics approach, which is a blend of both the approaches discussed above.

Yakobson, et al. [1], performed MD simulation on single and double walled carbon nanotubes with the consideration of chirality at different temperatures and observed that rise in temperatures causes reduction in the breaking strain of CNTs. Subsequently, Hernandez, et al., carried out molecular dynamics simulation for comparing elastic properties of various nanotubes employing tight binding molecular dynamics (TBMD). It was observed that Young's modulus of carbon nanotube is highest. They recommended that for calculating deformation the continuum shell model be made equivalent with the atomistic model while considering representative thickness of the continuum shell as 0.066 nm. This results in Young's modulus of the continuum shell to be as large as 5.5 TPa. Later on, use of Young's modulus per unit thickness was proposed by Hernandez, et al., [2].

In case of uniaxial loading, quantum molecular dynamic simulations were used by Nardelli et al. [3], for investigating the static as well as dynamic properties of CNT. Although results revealed outstanding properties, but some topological defects were observed for deformation greater than 5%. They emphasised on careful consideration of assumptions, like cross-section for using continuum mechanics approach for achieving optimum results.

Baumeier et al. [4], presented the comparative results based on ab-initio study of single-walled silicon carbide, boron nitride and barium oxide nanotubes of armchair and zigzag forms. They used pseudo potentials for obtaining structural and electronic properties. On the basis of such potential the dependency of various properties on diameter and iconicity of nanotube were investigated. The importance of band gap for various device applications and its progression with diameter of nanotube was discussed and analysed. Dwivedy and Kar[5,6] investigated the non-linear behaviour of a slender beam with an attached mass at an arbitrary position under vertical base excitation for combined parametric and internal resonances. Later on, They established second order temporal differential equation for a slender beam with an attached mass at an arbitrary position under vertical base excitation which retained cubic non-linearity. The equations helped in determining the nature of various responses like periodic, quasi-periodic and chaotic responses of the system for various bifurcating parameters, namely, damping, amplitude and frequency of base motion, attached mass and its location.

Ru[7] studied the elastic buckling behaviour of SW-CNT ropes subjected to high pressure using continuum mechanic's model. Concerns about inconvenience in application of parameters as proposed by Yakobson, et al., while studying properties of MW-CNT were also expressed by Ru. Later, while modelling a SW-CNT, Ru emphasised on use of independent material properties for obtaining bending rigidity of equivalent continuum shell against the equivalent thickness of wall[8-10]. Qian et al. [11], further demonstrated the significant impact of waviness on the mechanical behaviour of CNT. Ralich et al., explained modelling of thermal variations at nanoscale. Chakraborty et al. [12-13], provided theoretical insight of electronic and transport characteristics of CNTs.

A concept of molecular structural mechanics-based modelling approach for nanotube were explained by Li and Chou and found that the structure of nanotube at molecular level behaved in

similar pattern as that of space frame like structure. Based on this approach in combination with stiffness matrix method, the possibility of CNT as a nanoresonator was explored by Li and Chou for calculating the fundamental frequencies of CNTs for two most common configurations. Further, the dependency of frequency on length and diameter of nanotube was discussed. In case of DW-CNTs, the onset of non-coaxial vibration from the third resonant frequency was also observed by Li and Chou, and thus suggested their suitability as high frequency nanoresonator[14-17].

A truss model based on molecular mechanics approach for different forms of SW-CNT was developed by Bodily and Sun[18] using interatomic potential energy and derived various rigidities and static properties. The dynamic behaviour of a planar circular curved beam was analysed by Kang et al. [19], using wave propagation approach.

Li and Chou[20] established mass-resonance frequency relationship for CNT based nanoresonators and observed that the mass sensitivity of the order of 10^{-21} gm can be achieved. For a mass value higher than 10^{-20} gm a logarithmic linear relationship was observed between them.

Chakraborty et al. [21], explained the possible requirement for further exploration of graphite in regard to quantum properties of single graphite layer known as grapheme. In metallised CNT, bond rotation defects like Stone-Waals, enhanced one-dimensional effects as compared to pristine CNT of conducting nature as clarified by Gayathri and Geetha[22].

Use of atomistic and continuum mechanics-based modelling approaches were explained by Wilber et al. [23], for interaction between various layers of graphene. Later on, the buckling instability in such layers was observed and explained the reasons of such phenomenon by identifying the existence of nonlinearities.

Based on atomic mass resolution, Jensen et al. [24,25], developed a CNT based nanomechanical resonator to behave fundamentally as a mass spectrometer with mass sensitivity of 1.32×10^{-25} kg/Hz. A reduction in frequency was observed due to landing of gold atom on CNT and based on such reduction the mass of gold atom was identified.

Chandra et al. [26], conducted micromechanical study for composites consisting of two different phases. The analysis of piezoelectric power generators were discussed thoroughly for MEMS applications.

Theoretical aspect of various properties of graphene were comprehensively discussed by Abergel et al., Bakshi et al. [27,28], highlighted the use of carbon nanotubes and its composites in structural applications in their extensive review based on CNT reinforced composites. Various processing techniques, dispersion of nanotube in matrix, interface zone between nanotube and matrix material and mechanical properties of composite were critically review by them.

The enhancement in mechanical properties due to CNT in matrix of different materials was explained. The utility of interface zone between CNT and metal matrix was demonstrated. Also the use of CNT embedded aluminium composite in micro-electromechanical systems (MEMS) was thoroughly reviewed and suggested for use in high frequency nanoresonators requiring higher modulus of elasticity[28].

Geetha and Gayathri[29] studied CNT and BNNT for gas adsorption application and related advantages, disadvantages were discussed. A spring based finite element formulation to predict the vibrational behaviour of single and multi-walled carbon nanotubes to investigate their mass sensing when a nanoparticle is attached to them is studied by Georgantzinos and Anifantis[30,31].

Boldrin et al. [32], explained the mechanics of h-BN and equivalent thickness and in-plane mechanical properties of h-BN sheet using principles of energy equivalence that were extracted analytically and highlighted the mechanism of deformation in h-BN sheet. Further, they clarified that a mechanical model of single BN bond of equivalent thickness and mechanical properties is capable of describing in-plane elastic properties of h-BN sheet.

Panchal et al. [33,34], used FEM based molecular structural mechanics for evaluating dynamics behaviour of SW-BNNT as a potential resonant nanomechanical sensor for different types of armchair layups with cantilevered and bridged end constraints. A mass sensitivity up to 10^{-1} zg was observed.

2.3. Review of experimental work

Nanotubes being at nanoscale render great difficulty while using conventional methods for characterising them, hence novel approach is required for characterisation of individual entities like BNNT. At the same time, performing experiment on such small size nanotube is quite cumbersome for analysing its mechanical behaviour. Researchers are finding it quite challenging to measure the deformation and difficulties are experienced while handling the nanotube.

Various characterisation techniques for such nanomaterials have been studied by (Treacy et al. [35],), (Krishnan et al. [36],), (Poncharal et al. [37],), (Gao et al. [38],) and (Wang et al. [39],) and are:

- SPM (Scanning Probe Microscopy),
- TEM (Transmission Electron Microscopy),
- SEM (Scanning Electron Microscopy), and
- AFM (Atomic Force Microscopy),
- FFM (Friction Force Microscopy),
- MFM (Magnetic Force Microscopy),

Methods like TEM were used to directly observe various patterns of vibration. Bending modulus of individual MW-CNT was measured by Wong, et al., using AFM. Young's modulus of boron nitride (BN) nanotubes was measured by Chopra and Zettl on similar grounds. Later on, Krishnan, et al., also estimated the modulus of elasticity for SW-CNT (1.25 TPa) by capturing micrographic images of different carbon nanotubes[40,41].

Poncharal and Wang[43,44] used the TEM technique for capturing the vibration patterns of the carbon nanotube. Although, the effect of waviness or curvature of CNT on the vibration behaviour was not considered, but the images captured by them clearly indicates surface deviation of wavy nature. The flexural modulus of cantilevered MW-CNTs was evaluated by Poncharal, et al., for investigating mechanical resonance behaviour using an electric field

excitation method. Increase in diameter of nanotube resulted in sharp decrease in elastic bending modulus. A similar excitation technique was also explored by Gao et al., to calculate bending modulus of CNT using TEM.

Suryawanshi et al. [43], used a transmission electron microscope to measure the effective elastic modulus of BNNTs using the electric-field-induced resonance method and found the value of Young's modulus to be 722 GPa which was close to theoretical value of about 850 GPa. Wu et al. [44],reported Raman and time-resolved photoluminescence spectroscopic studies of multiwalled BN and BxCyNz nanotubes. A comparison of the photoluminescence of BN nanotubes to that of hexagonal BN was found consistent with the existence of a spatially indirect band gap in multiwalled BN nanotubes.

Atomic-resolution scanning tunnelling microscopy (STM) is a powerful technique for identifying SWNT defects as explained by Ishigami et al. [44], Pant et al. [45], reported electrical conductivity and dielectric studies on the composites of conducting polyaniline (PANI) with crystalline semiconducting ZnS powder. An unusual behaviour of dc conductivity of composite was observed at room temperature for volume fraction of PANI > 0·65. Conductivity values of the composites were found to be increased as compared to the PANI itself for small volume fraction of 0·85. Bai et al. [46], observed transformation of an electrically insulated MW-BNNT into a semiconductor under controlled conditions for elastic bending deformation. Piezoelectrical behaviour of deformed BNNT was observed during experimentations. A smooth tuning was thus observed from insulating to semiconducting via bending deformation[47].

Zhi et al. [48,49], used a chemical-vapour-deposition method to fabricate BNNT/polystyrene composite films. Transmission electron microscopy was used for investigating the interactions between two phases. An increase of 21% in elastic modulus due to addition of 1% wt. of BNNT in polystyrene was observed.

Wang et al. [50], proposed an elastic beam theory to study the buckling of single-walled carbon nanotubes with one atomic vacancy for strain prediction and compared the same using molecular dynamics approach. Results revealed effectiveness of continuum mechanics theory for longer CNTs. Pokropivny et al. [51], calculated Raman spectra of SW-BNNT using the ab-initio

Hartree–Fock (RHF) methods and proposed a technique for obtaining BNNT stable dispersions suitable for biological applications, based on polyethyleneimine (PEI) water solutions.

Gil-Santos et al. [52], illustrated that addition of mass of an analyte at different locations provide different and complementary information on theoretical and experimental basis for stochastic and deterministic responses of a pair of coupled nanocantilevers.

Jiang[54] investigated the electrochemical performance of cupric oxide nanoparticles-modified multi-walled carbon nanotubes (MWCNTs) array electrode using cyclic voltammetry and chronoamperometry for sensitive nonenzymatic glucose detection[53]. Samanta et al characterized multiwalled boron nitride nanotubes (BNNTs) and functionalized BNNTs by Lewis bases such as trioctylamine (TOA), tributylamine (TBA), and triphenylphosphine (TPP), etc., in organogels formed by triphenylenevinylene (TPV)-based low molecular weight gelator (LMWG) in toluene.

Ghassemi et al. [56], critically reviewed the mechanical properties of BN nanotubes from both experimental and simulation perspectives. The stress-strain curve was used to evaluate the values of Young's modulus and Poisson's ratio for nanotubules[55]. Terao et al., fabricated BNNT/polyvinyl alcohol (PVA) composite fibres (< 5 vol % BNNTs) using electro-spinning for investigating thermal behaviour of composite. Results reveal that an increase in volume fraction caused significant improvement in thermal conductivities which were found to be suitable for various applications.

Rajput et al. [57], proposed a method for the preparation of magnetic nanocomposites consisting of magnetic nanoparticles (MNPs), polybenzoxazine (PB), linear low-density polyethylene (LLDPE) and LLDPE-g-Maleic anhydride (LgM). X-Ray diffraction, thermo gravimetric analysis and differential scanning calorimeter, scanning electron microscopy, universal testing machine and vibrating sample magnetometer were used for characterizing the developed composites. Mechanical flexibility as well as magnetic properties were observed in the developed composite.

2.4. Nanotube based mass and bio-sensors

Ever since its inception, researchers have explored the feasibility of nanotubes for variety of applications requiring mass sensing.

Ruoff and Lorents discussed various mechanical and thermal properties of carbon nanotubes. The natural resonance (fundamental vibrational frequency) of a cantilevered single-wall nanotube of length 1 micron was observed to be about 12 MHz. The thermal expansion of carbon nanotubes was isotropic. The thermal conductivity was highly anisotropic (along the long axis) and most probably higher than any other material[58].

Previous studies related with CNTs (Dai et al. [59],), (Kim and Lieber[60]) suggest that CNTs have good electrical properties and high mechanical strength so they can be used as nanosensors in nanoelectronics, nanodevices, and nanocomposites. Mass sensing with a resonator is based on the fact that the resonant frequency is sensitive to the attached mass and its position. The attached mass results in resonant frequency shift of the resonator.

Dat Thun T. et al explained variation in resonance frequency, deflection, amplitude, and Q-factor of a micro-cantilever-based resonators due to external factors like mass loading, surface stress, or damping in their review. Halicioglu calculated atomic stresses under axial strain conditions for graphitic tubules with different radii and structures for long tubules using Brenner's function. Results showed the stress to be tensile in radial direction and compressive in the tangential direction. Gao et al presented an extensive molecular mechanics and molecular dynamics studies on the energy, structure, mechanical and vibrational properties of single-wall carbon nanotubes to explore the stability domains for varying structures of CNT[61-63].

Chandra et al. [64], reviewed the status of research on damping in fibre-reinforced composite materials and structures with emphasis on polymer composites. Liu et al.[65], used fast multipole boundary element method for modelling of CNT reinforced composites. The CNTs were treated as rigid fibres due to their exceptionally high stiffness compared with commonly used polymer matrix materials. Liu et al modelled interphases in unidirectional fibre-reinforced composites under transverse loading using an advanced boundary element method based on the elasticity theory for two different RVEs. Results showed that for higher fibre volume fractions, the

interphase properties had significant effect on the micromechanical behaviours of the composites.

Macucci et al. [66], outlined the major challenges such as the integration of nonequilibrium phenomena and molecular-scale properties for nanoscale device modelling. Srivastava et al. [67], presented a review on computational techniques and their role in nanotube-based computer simulation for developing the next generation of multifunctional materials and molecular-scale electronic and computing devices, sensors, actuators, and machines. A review of advances in carbon nanotubes and their composites based on structural and synthesis methods along with their characterisation was presented by Thostenson et al., [68].

Chen[69] applied an advanced boundary element method (BEM) with thin-body capabilities to model multiple cells of fibre-reinforced composites considering the interphases. A comparison of BEM with FEM approach to the multiple-cell modelling was done. Results showed that BEM to be accurate and efficient enough for analysing fibre-reinforced composites. Kang and Hwang[70,71] investigated the mechanical deformations of Cu{100} nanowires using the steepest-descent method. Simulations for cases like elongation, shearing, rotation and rotated elongation was carried out. For rotational deformation, the torque was found to be inversely proportional to the tension force. The effect of rotation on free vibration of flexible cantilever beam with mass attached at tip was observed by Kumar et al. [72].

It was also observed that defective sites in nanotube are found to be advantageous because of enhancement in hydrogen uptake. Effect of various types of defects on the dynamics of CNT was examined by Hirai and Nishimaki[73], employing molecular mechanics method. Results revealed that the bending rigidity was significantly affected by incorporation of pinhole defect in nanotube. The continuum mechanics approaches that have modelled the exact atomic lattice of CNTs was considered to be structural mechanics approach.

Li and Chou[14-17] applied their molecular structural mechanics approach to study the frequency shifts in cantilevered and bridged SWNTs with attached particles. It was predicted that mass sensitivity of such CNT nano balances can reach 10^{-21} g, and that a logarithmically linear relationship exists between the resonant frequency and the attached mass when the mass is larger than 10^{-20} g.

Since molecular dynamic simulations are restricted to small scale systems and for short time duration, continuum mechanics-based models are generally preferred to investigate the elastic response of CNTs and same was elaborated by [(Ru et al. [74],), (Yoon et al. [75],), (Wang and Varadan [76],), and (Wang et al. [77],]. Dynamic behaviour of CNTs was studied using continuum mechanics approach with Euler–Bernoulli beam theory as well as Timoshenko beam concept by [(Ru et al.,), (Yoon et al.,)]. The wave propagation behaviour was also studied by Wang and Varadan for analysing vibrational characteristics of CNT.

Arroyo et al. [78], used generalized local quasi continuum method to investigate the effect of diameter on bending stiffness of multiwalled carbon nanotubes (MWCNTs). A reduction in the effective bending stiffness was observed with increasing diameter.

Xu et al. [79], explained various significant properties of BNNT like high stiffness and better flexibility with high resistance to fracture. Wang and Wang (2004) used fem package ABAQUS to investigate the bending deformation of CNTs and rippling behaviour (wave like distortion) was simulated. A significant decrease in tangential stiffness due to rippling was attributed to non-linear relationship between bending moment and curvature.

Researchers investigated reasons for difference in the vibration behaviour between considered single- and double-walled carbon nanotubes using molecular-structural-mechanics method. A drop of 10% was observed for fundamental frequencies of double-walled carbon nanotubes as compared to those of single-walled carbon nanotubes for the same outer diameter. Chen et al. [81], studied thermal stability of BNNT and found that BNNT are stable at 700 °C in air. Onset of oxidation in BNNT occurred at 800 °C as compared with their counterpart CNTs at 400 °C under the same environmental conditions. This suggests the pronounced resistance of BNNT to oxidation.

Kireitse et al. [82], presented a review on development of the next generation of vibration damping systems having direct relevance to industry in areas of transportation (aerospace, automotive, rail), electronics and civil infrastructure development. Arroyo et al. [83], reviewed mechanics of carbon nanotube with more emphasis on Cauchy-Born rule and used multiple-elastic shell model to study the effect of pressure on radial breathing modes (RBMs) of multiwall carbon nanotubes (MWNTs) while considering van der Waals interaction. An increase in van der

Waals interaction coefficients between the outermost few layers of MWNTs was observed due to high external pressure. A significant increase was observed in RBM frequencies of MWNTs with increasing external pressure.

Allen reviewed changes in SWNT conductivity to study the interaction of biomolecules with SWNTs in regards to field-effect transistors (FETs) and use of FET devices based on nanotubes for detecting biomolecules like proteins, DNA hybridization and enzymatic reactions involving glucose were explained. Verma et al., used Tersoff–Brenner potential to evaluate the effect of tube diameter on elastic properties of BNNT[84,85].

Kwon et al. [86], observed the kinetics of bio molecular interactions such as antigen-antibody interactions and/or DNA hybridization based on a resonant frequency shift to gain insights into the kinetics of various molecular interactions. Yuan and Liew[87] investigated the effect of boron nitride (BN) impurities on the elastic properties of armchair (5, 5) (10, 10) and zigzag (9, 0) (18, 0) SW-CNTs using molecular dynamics method. Due to BN doping a decrease in Young's modulus of CNT was observed and also reported that both forms of CNT behave in a different manner.

Zhi et al. [88], explained the novelty of BNNT because of their various outstanding properties like wide band gap, mechanical properties, high thermal conductivity and robustness to oxidation. They further clarified that all such extraordinary properties make BNNT suitable candidate for next generation nano composites. Song et al. [89], proposed an analytic approach for determining the tensile and bending stiffness of a hexagonal boron-nitride (h-BN) monolayer and single- and multi-wall boron-nitride nanotubes (BNNTs) based on the interatomic potential. For single- and multi-wall BNNTs, the stiffness was found to be dependent on the (inner most or outer most) wall radius and the number of the walls.

Georgantzinos et al. [90], computed vibrational behaviour of SW-CNTs using a linear spring-based element formulation. Results revealed existence of new natural frequencies and mode shapes for different boundary conditions and defects. Jeon and Mahan[91] constructed a model to describe the lattice dynamics of a single-wall boron nitride nanotube. Flexure modes in BNNT, consisting of polar atoms, were identified. The frequency of the radial breathing mode was found to be inversely proportional to the tube radius.

Santosh et al. [92], studied the elastic properties of BNNTs for varying partial atomic charges on boron and nitrogen in the absence of specific partial atomic charge information for boron and nitrogen. It was observed that Young's modulus of BNNTs was greater than CNTs of same radius. The higher value of Young's modulus was due to increase in magnitude of the partial atomic charge on B and N. Nanotube based sensors were modelled and explained theoretically by Chowdhury et al. [93-95], using continuum mechanics approach employing Euler–Bernoulli theorem.

The dynamic characteristics of SW and MWCNT were examined for detecting nano mass employing a spring-based FE methodology by Georgantzinos and Anifantis[96]. Lee et al. [97], used nonlocal elasticity theory to calculate the frequency shift of cantilever CNT when mass is attached on it. Simultaneously, the mass of silver nano particles were detected experimentally using CNT based mass sensor. It was observed that the amount of mass as well as its position along the length of CNT affects its resonance frequency.

The dynamic stiffness of MWCNTs was enhanced leading to rise in frequency up to 50%. Tooski[98] established Vlasov and Maxwell's equations for obtaining numerical solutions to describe the effects of toxin/pollutant gas pressure and functionalized single wall carbon nanotube-based sensor in a perturbed microwave resonant cavity. A shift in resonance frequency was observed for small variation in gas pressure.

Adhikari and Chowdhary [99] derived calibration constants for CNT based mass sensors for two different boundary conditions in terms of added mass. Based on UFF potential a molecular mechanics model was used to validate their results. In order to predict the effective Young's modulus of CNT reinforced nanocomposites, The modified rule of mixtures by taking into account the interfacial effects. A semi-continuum finite element model was employed for cylindrical RVE to simulate molecular mechanics behaviour. Special joint elements of variable stiffness which interconnect the two materials were used. The results yielded a novel modified rule of mixtures.

Anand et al. [100], in their study, investigated the impact of waviness on a nanomechanical resonator's mass sensitivity. They applied a finite element model to examine the vibration signature of a single walled carbon nano tube (SW-CNT) with waviness along its axis that

was doubly clamped at a source and a drain which was also used to represent a single mode resonator. Analysis of vibration responses of carbon nanotubes with waviness treated as thin shells was done in this research work. The findings demonstrated the SW-CNT's sensitivity as its waviness changes on varying lengths and masses which were attached at the centre of a doubly clamped SW-CNT. It was shown that the sensitivity of resonance frequency shifts to tube length and waviness.

In order to simulate a single mode resonator, Anand Y. Joshi et al. [101], performed a dynamic study on a single-walled carbon nanotube with surface deviation along its axis that is doubly clamped at a source and a drain. Investigations were made into the resonant frequency of doubly clamped single walled carbon nanotubes (SW-CNT) with deviation. The findings demonstrated the sensitivity of single-walled carbon nanotubes with varying degrees of waviness to various masses (connected in the centre of a doubly clamped SW-CNT) and lengths. It was established that resonant frequency shifts are sensitive to tube length and waviness. It was discovered that as length increases, the influence of waviness increases. With varying levels of mass, the vibration signature displayed superharmonic and subharmonic responses. The study was useful in discovering that the peak excitation appeared in the vibration signature in chaotic nature with decreased vibration amplitude as the mass coupled to CNT increases.

Arlett et al. [102], also presented an extensive review about micro- and nanoscale biosensors, from mechanical bio sensing point of view. For improving the device performance, fabrication reproducibility and system integration general issues critical to the success of next-generation mechanical biosensor were explained. The need for a greater understanding of analyte–sensor interactions on the nanoscale and of stochastic processes in the sensing environment was also discussed.

Kirtania and Chakraborty[103] considered a three dimensional (3D) square RVE with one CNT fibre surrounded by matrix to explain the debonding between the broken carbon nanotube (CNT) and the matrix in CNT-based composites using multiscale modelling. Kasar et al., carried out 3-D non-linear finite element analysis of three typical interior beam column joint sub-assemblages to study inelastic behaviour of such joints with different column to beam strength ratio.

Parametric analysis of moment connection was also discussed and utility of beam to column strength ratio was discussed.

Panchal et al. [104], illustrated the suitability of BNNTs to be used as a nano resonator, using continuum mechanics based approach and finite element method (FEM) for two different types of end constraints. A mass sensitivity of 10-26 kg was observed. Computational mechanism has been discussed for large deformable bodies. They presented reviews on work involving fabricating and characterizing carbon- nanotube-based metal matrix and polymer composites.

Anand Y. Joshi et al. [105], conducted research on the nonlinear vibration analysis of a mass sensor based on wavy single-walled carbon nanotubes that is doubly clamped at a source and a drain. The nonlinear vibration response caused by changing attached mass was determined in the current experiment using an analytical model of a bridge CNT with waviness on the surface. The connected mass and the geometrical distortion of the CNT were the major causes of the system's excitation. According to the study's findings, the vibrations caused by connected mass on wavy CNT reach their maximum peaks at their natural frequencies, whereas other excitations exhibited at their higher harmonics. When mass was increased, system excitations and vibrational amplitude rose but excitation frequency decreases. Through the research it was discovered that the periodic, subharmonic, and chaotic behaviour largely depends on carbon nanotube mass and geometric flaws.

Using a 3-D representative volume element containing long and short wavy carbon nanotubes, Unnati A. Joshi et al. [106], investigated the impact of wavy carbon nanotubes on mechanical characteristics such as elasticity and strength aspects for nanocomposites. It was implicated that waviness greatly lowers the effective reinforcement of the nanocomposites. Although the composites have an unusually high modulus, it was demonstrated that the waviness can greatly impair the stiffening effect of the nanotubes. This limits the total effective modulus of the composites. According to the simulation results, long CNTs had different stiffness and superior reinforcing trends than short, wavy CNTs. Strength prediction was done utilising all three representative volume elements (RVEs) with both long and short CNTs, and the results showed that increasing the values of the waviness indices causes the tensile strength of nanocomposites to drop. An examination of the relative strengths of composites based on long and short CNTs shows that the long CNT had a greater reinforcing strength.

Anand Y. Joshi et al. [107], studied the nonlinear vibrational behaviour of mass sensors based on single-walled carbon nanotubes and examined an analytical model of a bridged CNT with surface variations. The connected mass and the geometrical distortion of the CNT are the major causes of the system's excitation. Instability and chaos in the dynamic reaction were found. It was evident that the surface deviations and attached mass affect the regions of periodic, subharmonic, and chaotic behaviour. Frequency spectra and Poincare maps were used to explain and illustrate the variety of system behaviour. From the acquired data, it can be inferred that he largest peaks in the vibration signature caused by attached mass on wavy CNT were seen at its natural frequency whereas additional excitations occur at higher harmonics. Surface deviation increased system excitations and vibration amplitude, while excitation frequency decreased as surface deviation increased. The responses may be divided into two types based on the dynamic properties of the system as a result of the attached mass on the wavy CNT. First of all, this system matched periodic responses when surface deviations were 0.1, 0.4, and 0.5 for a length of 10 nm and 0.1 and 0.5 for a length of 15 nm. Secondly, it was found that the responses were hard to define as they might be erratic or chaotic and very sensitive when the deviations on the CNT are 0.2 and 0.3 for a length of 10nm and 0.2, 0.3 and 0.4 for a length of 15 nm. Compared to quadratic nonlinearity, which is primarily influenced by the geometry of the CNT, cubic nonlinearity, which resulted from midplane stretching, was less sensitive to changes in geometry as concluded by the research. The waviness factor caused the quadratic nonlinearity to follow a parabolic profile, which grew with the waviness factor, whereas the waviness factor caused the cubic nonlinearity to decrease.

Saurabh Kumar et al. [108], examined the vibrational properties of single-walled boron nitride nanotubes (SWBNNT) with surface deviation as waviness along its axis and confirmed their viability as nanomechanical sensors. Analysis of SWBNNTs with waviness as mass resonators was done employing the continuum solid modelling based finite element method approach. The bridged and cantilevered configurations were taken into consideration and their resonant frequencies were calculated. It was discovered that the resonant frequency shift is rather strong for both the configuration with the rise in mass attached and with a significant increase in lengths of wavy SWBNNT, but it gradually decreases with further increase in length. Additionally, the resonant frequency rose as the attached mass was increased.

S. Trivedi et al. [109], investigated the viability of biosensors made of multi-walled boron nitride nanotubes (MW-BNNTs) with a virus or bacteria attached at the free end of a cantilever. In order to get the resonant frequencies of the cantilevered triple-walled boron nitridenanotube (TW-BNNT) using an analytical method based on continuum mechanics, several viruses and bacteria with mass on the order of the zeptogram level are taken into consideration. The simulation is run for varying lengths with different viruses and bacteria adhered to the cantilevered TW-BNNT tip. By taking into consideration the effective wall thickness of tubes and van der Waals interaction between different BNNTs, the simulated resonance frequency values from the finite element approach are compared with the outcomes from the analytical method. The findings from the two techniques are seen to be closely related, further demonstrating the viability of the suggested paradigm. According to the results, TW-BNNT of shorter length is more sensitive to identifying viruses and bacteria with zeptogram-ordered mass.

J. H. Kang et al. [110], suggested that sensors and gadgets for space exploration must work in extreme circumstances such high temperature fluctuation, atomic oxygen, and high-energy ionising radiation. However, traditional or cutting-edge electroactive materials like lead zirconate titanate, poly(vinylidene fluoride), and CNT-doped polyimides have limits in extreme applications. Theoretical investigations have revealed that boron nitride nanotubes (BNNTs) exhibit strength-to-weight ratios equivalent to CNTs, outstanding high-temperature stability (to 800 °C in air), significant electroactive properties, and strong neutron radiation shielding. We exhibited BNNT electroactivity in innovative multifunctional electroactive nanocomposites in this work. The 2 wt % BNNT/polyimide composite showed electroactive strain with linear piezoelectric and nonlinear electrostrictive components in an external electric field. Stretching the 2 wt % BNNT/polyimide composite aligned the BNNTs, increasing electroactive properties by 460%. An all-nanotube actuator with a BNNT buckypaper layer between two single-walled carbon nanotube electrode layers has greater electroactive characteristics. BNNT composites are ideal for space missions because to their neutron radiation shielding and ultraviolet/visible/near-infrared optical characteristics.

N. Li. et al. [111], studied that chemical vapour deposition 2D materials often include nanoscale cracks. Nano-cracks may reduce 2D material mechanical performance. Molecular dynamics was used to study the mechanical performance and failure behaviour of h-BN sheets with nano-cracks. h-BN sheet mechanical characteristics and fracture type or size were examined.

Temperature and strain rate affect h-BN sheet mechanical properties. When the fracture size exceeded the threshold value, h-BN sheets' Young's modulus fell linearly. The zigzag h-BN sheet's Young's modulus decreased quicker than the armchair's as fracture size increased. As crack size increased, fracture strength dropped quickly. After a crucial crack size, fracture strength changed little. Temperature and strain rate affected h-BN sheet mechanical characteristics with fractures. This work will help to estimate h-BN sheet mechanical performance and failure mechanism.

T. Li. et al. [112], showed that CNTs are semimetallic and BNNTs are large band gap insulators. Despite their electrical differences, CNTs and BNNTs' mechanical and thermal characteristics are useful for study into their prospective uses. This study examines CNT and BNNT mechanical and thermal characteristics using molecular dynamics simulations. Under axial compressions, CNTs' Young's modulus is 1.1 TPa and BNNTs' 0.72 TPa.

CNTs are axially stiffer than BNNTs and have a critical bucking strain and maximum stress inversely related to diameter and length-diameter ratio. Thermal conductivities of (10, 0) CNTs and (10, 0) BNNTs decrease with length and temperature and are lower than those of their two-dimensional equivalents, graphene nanoribbons (GNRs) and BNNRs, respectively. BNNTs (BNNRs) have better thermal conductivity than CNTs (GNRs) at temperatures below 200 K (130 K) but lower at higher temperatures. Thermal conductivities of a (10, 0) CNT and BNNT under various axial compressive loads are also examined. Low-frequency phonons from flexure modes dominate CNT and BNNT thermal conductivity.

J. H. Los. et al. [113], studied that large-scale atomistic simulations use an extended Tersoff potential for boron nitride (BN-ExTeP). BN-ExTeP properly depicts the key low-energy B, N, and BN structures and quantitatively correct bonding patterns as a function of coordination. The suggested expansion of the bond order to increase bonding reliance on the chemical environment accurately describes point defects in hexagonal and cubic BN. They utilised the molecular dynamics LAMMPS programme to establish the fundamental parameters of pristine 2D (h-BN) and the elastic properties of defective (h-BN) as a function of defect density at zero temperature. We found a considerable link between the amount of the static corrugation generated by defects and the weakening of in-plane elastic moduli.

J. H. Kim et al. [114], showed that Boron nitride nanotube (BNNT) comprises a hexagonal network of boron and nitrogen atoms like carbon nanotube (CNT). BNNT's unusual atomic structure gives it great mechanical strength, high thermal conductivity, electrical insulation, piezoelectricity, neutron shielding, and oxidation resistance. Since 1995, BNNT has had low yield and quality compared to CNT, restricting its practical usage. However, recent BNNT synthesis achievements have made this material accessible and opened the door to intriguing uses. We reviewed current boron nitride nanotube manufacturing methods in this study. BNNT uses included polymer composite reinforcement, heat management packages, piezo actuators, and neutron shielding nanomaterial.

Jiger et al. [115], conducted a study in which Continuum modelling based analytical and finite element method (FEM) simulation approaches were used to estimate the natural frequencies of various modes of vibration of SWBNNTs with different types of wavy curvatures including sinusoidal, elliptical, and parabolic waviness. The observed results implied that regardless of the kind of waviness, natural frequencies rise as the degree of curvature (e/l) increases. It was discovered that the sinusoidal waviness had a greater natural frequency for a specific e/l value and nanotube length. The influence on natural frequencies due to the existence of parabolic waviness in the atomic structure, was found to be significant as the length of the nanotube rises. The study also suggested that influence on natural frequency caused by the presence of parabolic and elliptical waviness in the atomic structure of the nanotubes are similar as the length increases.

V. Choyal et al. [116-120], examined the influence of aspect ratio (L/D) on Boron nitride nanotubes (BNNTs) Young's modulus using molecular dynamics simulations with a Tersoff force field. BNNT length may affect elastic characteristics, hence L/D values were 5, 10, 15, 20, and 25. Young's modulus of a BNNT grows with aspect ratio and stabilises around L/D ~15. This foundational work shows that BNNT aspect ratio affects their mechanical properties as fillers in multifunctional nanocomposites.

They studied that MD simulations using a three-body Tersoff potential force field predicted the transversely isotropic elastic characteristics of pristine and defective BNNTs. BNNTs are subjected to uniaxial tension, twisting moment, in-plane shear, and biaxial tension. BNNT chirality, diameter, vacancy concentration, and vacancy pore dispersion throughout the length and circumference were rigorously investigated. We found that BNNT elastic coefficients

decrease with diameter, except axial Young's modulus. Young's modulus of BNNT rises with tube diameter and peaks at 14 Å before falling. BNNTs' axial Young's modulus increases with aspect ratio and stabilises at L/D < 15. BNNTs' elastic characteristics are strongly affected by vacancies. A 2% vacancy concentration in (10, 10) BNNT reduces its axial Young's, shear, plane strain bulk, and in-plane shear moduli by 14%, 25%, 14%, and 18%, respectively. Using the strain effective approach, we examined the electrical characteristics of pristine and damaged BNNTs under four transversely isotropic loading situations. Loading circumstances, diameter, and vacancy concentration can change BNNTs' electronic characteristics. Our fundamental work shows that vacancy defective BNNTs determine their elastic and electronic characteristics and are widely employed in nano-electronic devices and multifunctional nanocomposites.

They also showed that molecular dynamics simulations using a three-body Tersoff potential force field established the temperature-dependent transversely isotropic elastic characteristics of multi-walled boron nitride nanotubes (MWBNNTs). MWBNNTs were loaded in uniaxial tension, torsional moment, in-plane biaxial tension, and shear to compute these elastic characteristics. Chirality, layers, and aspect ratio (AR) were considered. MWBNNTs with more layers have lower elastic constants. MWBNNT elastic moduli are chirality-dependent, not AR-dependent. Temperature also affected MWBNNT transversely isotropic elastic constants. MWBNNT mechanical characteristics change significantly with temperature. MWBNNTs' axial Young's, longitudinal shear, plane-strain bulk, and in-plane shear moduli decreased by 10% as temperature increased. MWBNNT mechanical characteristics and failure behaviour vary on layer count, chirality, and temperature. This study may be used to construct MWBNNT-based advanced nanocomposite structures for thermal applications.

N.A. Sakharova et al. [121], investigated the elastic characteristics of chiral and non-chiral single-walled boron nitride nanotubes throughout a broad spectrum of the materials' chiral indices and diameters. In order to accomplish this goal, a three-dimensional finite element model was utilised to evaluate the rigidities of the structures, and then, after that, the elastic moduli and Poisson's ratio of the structures. An exhaustive investigation was carried out in order to have a better comprehension of the influence that the input parameters had on the outcomes of the numerical simulation. The elastic characteristics of single-walled boron nitride nanotubes are displayed alongside those found for single-walled carbon nanotubes for the purpose of comparison.

X. Liu. [122] examined how CNT-unit defects affect the mechanical characteristics of a honeycomb CNT-based network, super carbon nanotube (SCNT) using molecular dynamics simulations. Defect number, distribution continuity, and orientation effect faulty SCNT tensile strengths. Single-fault tensile strength decreases by 0–25% depending on defect position, while three defects reduce it by nearly 50%. SCNTs with the same defect number have 20% tensile strength variances due to distribution continuity. Tensile strength increases with a smaller fault arranging angle. Defective SCNTs have multiple modes of stress concentration with variable concentration degrees according to defect quantity, arranging direction, and continuity. The effective crack length of fracture mechanics explains the mechanism.

Boron nitride nanotubes (BNNTs) have attracted significant attention due to their unique properties and potential applications in various fields. Understanding the mechanical behavior and properties of BNNTs is crucial for their effective utilization. Computational modeling techniques, such as molecular mechanics (MM), molecular dynamics (MD), and quantum mechanics (QM), play a vital role in providing insights into the structural, mechanical, and electronic properties of BNNTs. This literature review aims to provide a comparative study on various multiscale methods employed for investigating BNNTs.

Molecular Mechanics (MM) Approach:

MM is a widely used method to study the mechanical behavior of BNNTs due to its computational efficiency. MM employs simplified force fields to describe the interatomic interactions within the system. Several studies have utilized MM to investigate the mechanical properties of BNNTs, including elastic modulus, tensile strength, and fracture behavior. For instance, Zhang et al. (2018) employed MM simulations to examine the tensile properties of BNNTs with various chirality and diameter.

Molecular Dynamics (MD) Simulations:

MD simulations offer a more detailed description of BNNTs by considering atomic motions and thermal effects. MD captures the dynamics and time evolution of the system by numerically solving Newton's equations of motion. MD has been extensively utilized to investigate the mechanical behavior, thermal conductivity, and phonon properties of BNNTs. Liu et al. (2019)

employed MD simulations to study the thermal transport properties of BNNTs and revealed the impact of tube diameter and temperature on thermal conductivity [123].

Quantum Mechanics (QM) Methods:

QM methods provide a more accurate description of electronic structure and chemical bonding within BNNTs. Density functional theory (DFT), a widely used QM method, has been employed to study the electronic and optical properties of BNNTs. QM calculations have been used to investigate band structures, optical absorption, and electronic transport properties of BNNTs. Chen et al. (2021) employed DFT calculations to explore the electronic properties and band gaps of BNNTs with different chiralities [123].

Multiscale Methods:

Multiscale approaches combine the strengths of MM, MD, and QM methods to study BNNTs. These methods bridge the atomistic scale of MD simulations with the accuracy of QM calculations, allowing for a more comprehensive understanding of BNNT properties. Coarse-grained MD models coupled with QM calculations have been employed to investigate the mechanical properties and deformation mechanisms of BNNTs. For example, Guo et al. (2020) developed a multiscale approach combining MD and QM calculations to study the mechanical response and failure modes of BNNTs under different loading conditions.

A comparative study of various computational methods for investigating BNNTs reveals that MM, MD, and QM methods each offer distinct advantages and limitations. MM provides a computationally efficient means to study mechanical properties, while MD captures the dynamics and thermal effects. QM methods offer accurate electronic structure information. Multiscale approaches, combining these methods, enable a comprehensive understanding of BNNT properties.

Boron nitride nanotubes (BNNTs) are attracting increasing attention due to their unique properties and potential applications in various fields. Functionalizing the surface of BNNTs with different chemical groups allows for tailoring their properties and expanding their range of applications. In this literature review, main aim to provide an overview of the functional groups that have been introduced onto BNNTs and their implications [124].

Amine (-NH2) Functionalization:

Amine functionalization involves the attachment of amino groups to the surface of BNNTs. This modification can be achieved through various methods, such as amine coupling reactions. Amine-functionalized BNNTs have shown promise in applications such as drug delivery, bioimaging, and sensing. For instance, Hu et al. (2016) demonstrated the successful functionalization of BNNTs with amino groups and their application in pH-responsive drug delivery [125].

Hydroxyl (-OH) Functionalization:

Hydroxyl functional groups can be introduced onto BNNTs through oxidation or chemical treatments. Hydroxyl-functionalized BNNTs have been utilized in various fields, including energy storage, catalysis, and nanocomposites. Liu et al. (2017) reported the successful hydroxylation of BNNTs and their application in enhancing the thermal stability and flame retardancy of polymeric nanocomposites [126].

Carboxyl (-COOH) Functionalization:

Carboxyl groups can be attached to the surface of BNNTs through oxidation or chemical reactions. Carboxyl-functionalized BNNTs have shown potential in applications such as bioconjugation, sensing, and composite materials. Wang et al. (2019) functionalized BNNTs with carboxyl groups and demonstrated their application in the fabrication of high-performance polymer composites [127].

Epoxy (-O-) Functionalization:

Epoxy groups can be introduced onto BNNTs through reactions with oxygen-containing compounds. Epoxy-functionalized BNNTs have been utilized in applications such as nanocomposites, reinforcement materials, and electronic devices. Tang et al. (2020) reported the successful epoxy functionalization of BNNTs and their application in enhancing the mechanical properties of epoxy-based nanocomposites.

Functionalization of BNNTs with various chemical groups offers opportunities for tailoring their properties and expanding their applications. Amine, hydroxyl, carboxyl, and epoxy functional

groups are commonly introduced onto the surface of BNNTs, enabling enhanced properties such as bioactivity, improved thermal stability, chemical reactivity, and mechanical reinforcement. The choice of functional group depends on the specific application requirements. Further research and development in functionalization techniques and characterization methods will contribute to the exploration of new functional groups and their applications in BNNT-based materials and devices [128].

2.5 Gap in existing research

From the literature in the field of boron nitride nanotube-based mass sensors; the gaps in the published literature are pointed out as follows:

1. In the majority of the research work being reported in this field, mathematical models of boron nitride nanotubes are developed using different methods as suggested in the literature. Very little information is available regarding the mathematical modeling of SW-BNNT based nano-resonators for fixed- free and fixed-fixed boundary conditions.
2. Effect of defects on the vibrational behavior and dynamic properties of SW-BNNT based mass sensors/nano-resonator has not been done so far.
3. The effect of surface waviness, chirality, and defects (single and multiple atomic vacancies, pinholes) in SW-BNNT when used as mass sensors/nano-resonator have not been considered yet.
4. Dynamic analysis of monovacancy-defected SW-BNNT for different temperatures range is not been considered till now.

2.6 Objectives of the study

The suitability of nanotube as a nanoresonator and a mass detector for detecting small mass of the order of femtogram level has motivated to further explore their dynamic characteristics. In the recent years, CNTs have been explored and widely used in the design of mass sensors and actuators. At the same time other inorganic nanotubes like BNNTs having structural properties comparable to that of CNTs need to be explored.

Although experimental works are in progress for nanomaterial, but due to certain limitations, many researchers still believe in computational nanomechanics because of the fact that computer simulation is totally based on actual physical models of nanomaterials and predict

correct results which may be useful for experimental interpretation. Continuum mechanics and other computational nanomechanics tools like ABAQUS, ANSYS, and LAMMPS have to be explored for simulating the dynamic behaviour of BNNTs. Based on the above following are the objectives of current thesis:

1. To study the various defects such as single and multiple atomic vacancy, pinhole, surface deviation like waviness and its effect in SW-BNNTs.
2. To study the dynamic analysis of SW-BNNTs based nano-resonators for fixed- free and fixed-fixed boundary conditions under the influence of single and multiple vacancy defects using hybrid approach.
3. To understand the effect of different nonlinearity sources vibrational on the behavior of SW-BNNTs based mass sensors/nano-resonator.
4. To study the structural and thermal stability of (SW-BNNTs) under strained conditions.

REFERENCES

[1] Yakobson, B.I., Brabec, C.J. and Bernholc, J., Nanomechanics of Carbon Tubes: Instabilities beyond Linear Response, Physical Review Letters, vol. 76, 1996, pp. 2511.

[2] Hernández, E., Goze, C., Bernier, P. and Rubio, A., Elastic Properties of C and BxCyNz Composite Nanotubes, Physical Review Letters, vol. 80, 1998, pp. 4502.

[3] Nardelli, M.B., Yakobson, B.I. and Bemholc, J., Brittle and Ductile Behavior in Carbon Nanotubes, Physical Review Letters, vol. 81, 1998, pp. 4656-4659.

[4] Baughman, R. H., Cui, C., Zakhidov, A.A., Iqbal, Z., Barisci, J.N., Spinks, G. M., Wallace, G.G., Mazzoldi, A., De Rossi, D., Rinzler, A.G., Jaschinski, O., Roth, S. and Kertesz, M., Carbon Nanotube Actuators, Science, vol. 284, 1999, pp. 1340-1344.

[5] Dwivedy, S.K. and Kar, R.C., Dynamics of a slender beam with an attached mass under combination of parametric and internal resonances, Part I: steady state response, Journal of Sound and Vibration, vol. 221, 1999, pp. 823-848.

[6] Dwivedy, S.K. and Kar, R.C., Dynamics of a slender beam with an attached mass under combination of parametric and internal resonances, Part II: Periodic and Chaotic response, Journal of Sound and Vibration, vol. 222, 1999, pp. 281-305.

[7] Ru, C.Q., Effect of van der Waals forces on axial buckling of a double-walled carbon nanotube, Journal of Applied Physics, vol. 87, 2000a, pp. 7227-7231.

[8] Ru, C.Q., Effective bending stiffness of carbon nanotubes, Physical Review B, vol. 62, 2000b, pp. 9973-9976.

[9] Yakobson, B.I., Brabec, C.J. and Bernholc, J., Nanomechanics of Carbon Tubes: Instabilities beyond Linear Response, Physical Review Letters, vol. 76, 1996, pp. 2511.

[10] Ru, C.Q., Elastic buckling of single-walled carbon nanotube ropes under high pressure, Physical Review B, vol. 62, 2000c, pp.10405-10408.

[11] Qian, D., Dickey, E.C., Andrews, R. and Rantell, T., Load transfer and deformation mechanisms in carbon nanotube-polystyrene composites, Applied Physics Letters, vol. 76, 2000, pp. 2868.

[12] Ralich, R. M., Ramsier, R. D., Quinn, D. D., Clemons, C. B. and Young, G. W., Measuring and Modeling Thermal Fluctuations at Nanometer Length Scales, Physical Review E, vol. 65, 2002, pp. 57601/1-57601/4.

[13] Chakraborty, T., Peters, F. and Sivan, U., Nano-Physics and Bio electronics: A New Odyssey, Elsevier Publishers, Amsterdam, 2002.

[14] Li, C. and Chou, T.W., A structural mechanics approach for the analysis of carbon nanotubes. International Journal of Solids and Structures, vol. 40, 2003a, pp. 2487–2499.

[15] Li, C. and Chou, T.W., Elastic moduli of multi-walled carbon nanotubes and the effect of van der Waals forces, Composites Science and Technology, vol. 63, 2003, pp. 1517–1524.

[16] Li, C. and Chou, T.W., Single walled carbon nanotubes as ultrahigh frequency nanomechanical resonators, Physical Review B, vol. 68, 2003b, pp. 73405/1-3.

[17] Li, C. and Chou, T.W., Vibrational behaviors of multiwalled-carbon nanotube based nanomechanical resonators, Applied Physics Letters, vol. 84, 2003c, pp. 121-123.

[18] Bodily, B. H. and Sun, C.T., Structural and equivalent continuum properties of single-walled carbon nanotubes, International Journal of Materials and Product Technology, vol. 18, 2003, pp. 381-397.

[19] Kang, J.W. and Hwang, H.J., Mechanical deformation study of copper nanowire using atomistic simulation, Nanotechnology, vol. 12, 2001, pp. 295.

[20] Li, C., and Chou, T. W., Mass detection using carbon nanotube based nanomechanical resonators, Applied Physics Letters, vol. 48 (25), 2004, pp. 5246-5248.

[21] Chakraborty, T., Graphene: A nanoscale quantum playing field, Physics in Canada, vol. 62, 2006, pp. 351-354.

[22] Gayathri, V. and Geetha, R., Carbon nanotube as NEMS sensor – effect of chirality and stone-wales defect intend, Journal of Physics, vol. 34, 2006, pp. 824-828.

[23] Quinn, D.D., Wilber, J.P., Clemons, C.B., Young, G.W. and Buldum, A., Buckling Instabilities in Coupled Nano-Layers, International Journal of Non-Linear Mechanics, vol. 42, 2007, pp. 681-689.

[24] Jensen, K., Kim, K. and Zettl, A., An atomic-resolution nanomechanical mass sensor, Nature Nanotechnology, vol. 3, 2008, pp. 533-537.

[25] Jensen, K., Kim, K. and Zettl, A., An atomic-resolution nanomechanical mass sensor, Nature Nanotechnology, vol. 3, 2008, pp. 533-537.

[26] Chandra R., Kumar P. and Singh S.P., Micromechanical Study of Two Phase Composite, World Journal of Engineering, vol.6, 2009, pp. 119-120.

[27] Abergel D.S.L., Apalkov V., Berashevich J., Ziegler K. and Chakraborty T., Properties of graphene: a theoretical perspective, Advances in Physics, vol. 59, (4), 2010, pp. 261 – 482.

[28] Bakshi, S.R., Lahiri, D. and Agarwal, A., Carbon nanotube reinforced metal matrix composites-a review, International Material Review, vol. 55, 2010, pp. 41-64.

[29] Geetha, R. and Gayathri, V., Comparative Study on Gas Adsorption in Defected Carbon and Boron Nitride Nanotube, Current NanoScience, vol. 6, (2), 2010, pp. 131-136.

[30] Georgantzinos, S.K. and Anifantis N.K., Carbon nanotube-based resonant nanomechanical sensors: A computational investigation of their behavior, Physica E: Low Dimensional Systems and Nanostructures, vol. 42, 2010, pp. 1795–1801.

[31] Georgantzinos, S.K., Giannopoulos, G.I. and Anifantis, N.K., Effective Young's Modulus of Carbon Nanotube Composites: From Multi-Scale Finite Element Predictions to an Analytical Rule, Journal of Computational and Theoretical Nanoscience, vol. 7, 2010, pp. 1436.

[32] Boldrin, L., Scarpa, F., Chowdhury, R. and Adhikari, S., Effective mechanical properties of hexagonal boron nitride nanosheets, Nanotechnology, vol. 22, 2011, pp. 505702.

[33] Panchal, M. B., Upadhyay, S. H. and Harsha, S. P., An efficient finite element model for analysis of Single Walled Boron Nitride Nanotube-based resonant nanomechanical sensors, Nano, vol. 08, 2013, pp. 1350011.

[34] Panchal, M. B., Upadhyay, S. H. and Harsha, S. P., Mass detection using Single Walled Boron Nitride Nanotube as a nanomechanical resonator," Nano, vol. 07, 2012, pp. 1250029.

[35] Treacy, M.M.J., Ebbesen, T.W. and Gibson, J.M., Exceptionally high Young's modulus observed for individual carbon nanotubes, Nature, vol. 381, 1996, pp. 678.

[36] Krishnan, A., Dujardin, E., Ebbesen, T.W., Yianilos, P.N. and Treacy, M.M.J., Young's modulus of single-walled nanotubes, Physical Review B, vol. 58, 1998, pp. 14013.

[37] Poncharal, P., Wang, Z. L., Ugarte, D. and de Heer, W.A., Electrostatic deflections and electromechanical resonances of carbon nanotubes. Science, vol. 283, 1999, pp. 1513-1516.

[38] Gao, R, Wang, Z.L., Bai, Z., de Heer, W., Dai, L., and Gao, M., Nanomechanics of individual carbon nanotubes from pyrolytically grown arrays, Physical Review Letters, vol. 85, 2000, pp. 622–625.

[39] Wang, Z.L., Gao, R.P., Pan, Z.W. and Dai, Z.R., Nano-Scale Mechanics of Nanotubes, Nanowires, and Nanobelts, Advanced Engineering Materials, vol. 3, 2001, pp. 657-661.

[40] Wong, E.W., Sheehan, P.E. and Lieber, C.M., Nanobeam mechanics: elasticity, strength, and toughness of nanorods and nanotubes, Science, vol. 277, 1997, pp. 1971-1975.

[41] Chopra, N.G. and Zettl, A., Measurement of the elastic modulus of a multi wall boron nitride nanotube, Solid State Communications, vol. 105, 1998, pp. 297–300.

[42] Krishnan, A., Dujardin, E., Ebbesen, T.W., Yianilos, P.N. and Treacy, M.M.J., Young's modulus of single-walled nanotubes, Physical Review B, vol. 58, 1998, pp. 14013.

[43] Poncharal, P., Wang, Z. L., Ugarte, D. and de Heer, W.A., Electrostatic deflections and electromechanical resonances of carbon nanotubes. Science, vol. 283, 1999, pp. 1513-1516.

[44] Wu, J., Han, W.Q., Walukiewicz, W., Ager, J.W., Shan, W., Haller, E.E. and Zett, A., Raman Spectroscopy and Time-Resolved Photoluminescence of BN and $B_xC_yN_z$ Nanotubes, Nano Letters, vol. 4, 2004, pp. 647.

[45] Ishigami, M., Sau, J.D., Aloni, S., Cohen, M.L. and Zettl, A., Observation of the Giant Stark Effect in Boron-Nitride Nanotubes, Physical Review Letters, vol. 94, 2005, pp. 056804.

[46] Pant, H.C, Patra, M.K., Negi, S.C., Bhatia, A., Vadera, S.R. and Kumar, N., Studies on conductivity and dielectric properties of polyaniline–zinc sulphide composites, Bulletin of Materials Science, vol. 29, 2006, pp. 379–384.

[47] Bai, X., Golberg, D., Bando, Y., Zhi, C., Tang, C., Mitome, M. and Kurashima, K., Deformation-Driven Electrical Transport of Individual Boron Nitride Nanotubes, Nano Letters, vol. 7, 2007, pp. 632-637.

[48] Zhi, C., Bando, Y., Tang, C., Honda, S., Sato, K., Kuwahara, H. and Golberg, D., Purification of Boron Nitride Nanotubes through Polymer Wrapping, Journal of Physical Chemistry B, vol. 110, 2006, pp. 1525-1528.

[49] Zhi, C., Bando, Y., Tang, C., Honda, S., Kuwahara, H. and Golberg, D., Boron nitride nanotubes/polystyrene composites, Journal of Materials Research, vol. 21, 2006, pp. 2794-2800.

[50] Wang, Q., Varadan, V.K., Xiang, Y., Han, Q.K. and Wen, B.C., On instability of single-walled carbon nanotubes with a vacancy defect, International Journal of Structural Stability and Dynamics, vol. 8, 2008, 357–366

[51] Pokropivny, V., Kovrygin, S., Gubanov, V., Lohmus, R., Lohmus, A. and Vesi, U., Ab-initio calculation of Raman spectra of single-walled BN nanotubes, Physica E: Low-Dimensional Systems and Nanostructures, vol. 40, pp. 2339-2342.

[52] Gil-Santos, E., Ramos, D., Jana, A., Calleja, M., Raman, A. and Tamayo, Mass Sensing Based on Deterministic and Stochastic Responses of Elastically Coupled Nanocantilevers, Nano Letters, vol. 9, 2009, pp. 4122.

[53] Jiang, L and Guo, W., A molecular mechanics study on size-dependent elastic properties of single-walled boron nitride nanotubes, Journal of the Mechanics and Physics of Solids, vol. 59, 2011, pp. 1204–1213.

[54] Samanta, S.K., Gomathi, A., Bhattacharya, S. and Rao, C.N.R., Novel Nanocomposites made of Boron Nitride Nanotubes and a Physical Gel, Langmuir, American Chemical Society, vol. 26, 2010, pp. 12230.

[55] Ghassemi, H.M. and Yassar, R.S., On the Mechanical Behavior of Boron Nitride Nanotubes, Applied Mechanics Reviews, vol. 63, 2010, pp. 020804.

[56] Terao, T., Zhi, C., Bando, Y., Mitome, M., Tang, C. and Golberg, D. Alignment of Boron Nitride Nanotubes in Polymeric Composite Films for Thermal Conductivity Improvement. Journal of Physical Chemistry C, vol. 114, 2010, pp. 4340.

[57] Rajput, A.B. Sharifi, M., Pol, H.V., Patra, M.K., Vadera, S.R., Singrue, P.M. and Ghosha, N.N., Preparation of flexible magnetic nanocomposites of linear low-density polyethylene-polybenzoxazine-magnetic nanoparticles and their mechanical and magnetic properties, Journal of Nanoscience Letters, vol. 3, 2013, pp. 26.

[58] Ruoff, R.S. and Lorents, D.C. Mechanical and thermal properties of carbon nanotubes, Carbon, vol. 33, 1995, pp. 925.

[59] Dai, H. J., Hafner, J. H., Rinzler A. G., Colbert D. T., and Smalley, R. E., Nanotubes as nanoprobes in scanning probe microscopy, Nature, vol. 384, 1996, pp. 147-150.

[60] Kim, P. and Lieber, C. M., Nanotube Nanotweezers, Science, vol. 286, 1999, pp. 2148-2150.

[61] Dat, T.T, Oden, P.I and Warmack, R.J., Microcantilever Sensors, Microscale Thermophysical Engineering, vol. 1, 1997, pp. 185.

[62] Halicioglu, T., Stress calculation for carbon nanotubes, Thin Solid Films, vol. 312, 1998, pp. 11-14.

[63] Gao, G.H., Cagin, T. and Goddard, W.A., Energetics, structure, mechanical and vibrational properties of single-walled carbon nanotubes, Nanotechnology, vol. 9, 1998, pp. 184.

[64] Chandra R., Singh S.P. and Gupta K., Damping studies in fibre-reinforced composites - a review, Composite Structures, vol. 46, 1999, pp. 41-51.

[65] Liu, Y.J., Xu, N. and Luo, J.F., Modeling of Interphases in Fiber-Reinforced Composites Under Transverse Loading Using the Boundary Element Method, Journal of Applied Mechanics, vol. 67, 2000, pp. 41.

[66] Macucci, M., Iannaccone, G., Greer, J. and Martorell, Status and perspectives of nanoscale device modelling, Journal of Nanotechnology, vol. 12, 2001, pp. 136.

[67] Srivastava, D., Menon, M. and Cho, K., Computational nanotechnology with carbon nanotubes and fullerenes, Computing in Science and Engineering, vol. 3, 2001, pp. 42.

[68] Thostenson, E.T., Ren, Z.F. and Chou, T.W., Advances in the science and technology of carbon nanotubes and their composites, Composites Science and Technology, vol. 61, 2001, pp. 1899.

[69] Chen, X.L. and Liu, Y.J., Multiple-cell modeling of fiber-reinforced composites with the presence of interphases using the boundary element method, Computational Materials Science, vol. 21, 2001, pp. 86-94.

[70] Kang, J.W. and Hwang, H.J., Mechanical deformation study of copper nanowire using atomistic simulation, Nanotechnology, vol. 12, 2001, pp. 295.

[71] Ma, R., Bando, Y., Zhu, H., Sato, T., Xu, C. and Wu, D., Hydrogen Uptake in Boron Nitride Nanotubes at Room Temperature, Journal of the American Chemical Society, vol. 124, 2002, pp. 7672.

[72] Kumar, R., Dwivedy, S.K. and Dixit, U.S., Effect of rotation on free vibration of flexible cantilever beam with tip mass, International Conference on Theoretical Applied Computational and Experimental Mechanics, 2004, Kharagpur.

[73] Hirai Y. and Nishimaki S., Molecular Dynamics Studies on Mechanical Properties of Carbon Nano Tubes with Pinhole Defects, Japanese Journal of Applied Physics, 42, 2003, pp. 4120 - 4123.

[74] Yoon, J., Ru, C.Q. and Mioduchowski, A., Noncoaxial resonance of an isolated multiwall carbon nanotube, Physical Review B, vol. 66, 2002, pp. 233402.

[75] Yoon, J., Ru, C.Q., and Mioduchowski, A., Terahertz vibration of short carbon nano tubes modeled as Timoshenko beams. Journal of Applied Mechanics, vol. 72, 2005a. pp. 10-17.

[76] Yoon, J., Ru, C.Q., and Mioduchowski, A., Vibration and instability of carbon nanotubes conveying fluid, Composites Science and Technology, 2005b. vol. 65, pp.1326-1336.

[77] Wang, Q., Varadan, V.K., Xiang, Y., Han, Q.K. and Wen, B.C., On instability of single-walled carbon nanotubes with a vacancy defect, International Journal of Structural Stability and Dynamics, vol. 8, 2008, 357–366.

[78] Arroyo, M., and Belytschko, T., Nonlinear Mechanical Response and Rippling of Thick Multiwalled Carbon Nanotubes, Physical Review Letters, vol. 91, 2003, pp. 215505.

[79] Xu, F., Bando, Y., Golberg, D., Ma, R., Li, Y. and Tang, C., Elastic deformation of helical-conical boron nitride nanotubes, Journal of Chemical Physics, vol. 119, 2003, pp. 3436.

[80] Wang, X.Y. and Wang, X., Numerical simulation for bending modulus of carbon nanotubes and some explanations for experiment. Composites: Part B, vol. 35, 2004, pp. 79.

[81] Chen, Y., Zou, J., Campbell, S.J. and Caer, G.L., Boron nitride nanotubes: Pronounced resistance to oxidation, Applied Physics Letters, vol. 84, 2004, pp. 2430-2432.

[82] Kireitse, M.V., Tomlinson, G.R., Lu, J, Altenbach, H., Rongong, G., Bochkareva, L.V. and Hui, D. Preliminary Results on Vibration Damping Properties of Nanoscale-Reinforced Materials. In: Proceeding of ENS 05 Conference, Paris, France, 2005, pp. 159.

[83] Arroyo, M. and Belytschko, T., Continuum mechanics modeling and simulation of carbon nanotubes, Meccanica, vol. 40, 2005, pp. 455-469.

[84] Allen, B.L., Kichambare, P.D. and Star, A., Carbon Nanotube Field-Effect-Transistor-Based Biosensors, Advanced Materials, vol. 19, 2007, pp. 1439-1451.

[85] Verma, V., Jindal, V.K. and Dharamvir, K., Elastic moduli of a boron nitride nanotube, Nanotechnology, vol. 18, 2007, pp. 435711 (6 pages).

[86] Kwon, T., Eom, K., Park, J., Yoon, D.S. and Lee, H.L., Micromechanical observation of the kinetics of biomolecular interactions, Applied Physics Letters, vol. 93, 2008, pp. 173901

[87] Yuan, J. and Liew, K.M, Effects of boron nitride impurities on the elastic properties of carbon nanotubes, Nanotechnology, vol. 19, 2008, pp. 445703 (8pages).

[88] Zhi, C.Y., Bando, Y., Tang, C.C., Huang, Q. and Golberg, D., Boron nitride nanotubes: functionalization and composites, Journal of Materials Chemistry, vol. 18, 2008, pp. 3900.

[89] Song, J., Wu, J., Huang, Y., Hwang, K.C. and Jiang, H., Stiffness and Thickness of Boron-Nitride Nanotubes, Journal of Nanoscience and Nanotechnology, vol. 8, 2008, pp. 3774-3780.

[90] Georgantzinos, S. K., Giannopoulos, G. I. and Anifantis, N. K., An efficient numerical model for vibration analysis of single-walled carbon nanotubes, Computational Mechanics, vol. 43, 2009, pp. 731-741.

[91] Jeon, G.S., and Mahan, G.D., Lattice vibrations of a single-wall boron nitride nanotube, Physical Review B, vol. 79, 2009, pp. 085424.

[92] Santosh, M., Maiti, P.K., and Sood, A. K., Elastic Properties of Boron Nitride Nanotubes and Their Comparison with Carbon Nanotubes, Journal of Nanoscience and Nanotechnology, vol. 9, 2009, pp. 5425-5430.

[93] Chowdhury R., Adhikari S. and Mitchell J., Vibrating carbon nanotube based bio-sensors, Physica E: Low-dimensional Systems and Nanostructures, vol. 42, (2), 2009, pp. 104-109.

[94] Chowdhury, R., Wang, C.Y. and Adhikari, S., Low frequency vibration of multiwall carbon nanotubes with heterogeneous boundaries, Journal of Physics D: Applied Physics, vol. 43, 2010, pp. 085405 (8 pages).

[95] Chowdhury, R., Wang, C.Y., Adhikari, S. and Scarpa, F., Vibration and symmetry-breaking of boron nitride nanotubes, Nanotechnology, vol. 21, 2010, pp. 365702.

[96] Georgantzinos, S.K. and Anifantis N.K., Carbon nanotube-based resonant nanomechanical sensors: A computational investigation of their behavior, Physica E: Low Dimensional Systems and Nanostructures, vol. 42, 2010, pp. 1795–1801.

[97] Georgantzinos, S.K., Giannopoulos, G.I. and Anifantis, N.K., Effective Young's Modulus of Carbon Nanotube Composites: From Multi-Scale Finite Element Predictions to an Analytical Rule, Journal of Computational and Theoretical Nanoscience, vol. 7, 2010, pp. 1436.

[98] Tooski, S. B., Functionalized single wall carbon nanotube sensor in a perturbed microwave resonant cavity based toxin/pollutant gas pressure sensor, Journal of Applied Physics, vol. 107, 2010, pp. 034315.

[99] Adhikari, S. and Chowdhury, R., The calibration of carbon nanotube based bionanosensors, Journal of Applied Physics, vol. 107, 2010, pp. 124322.

[100] Joshi, A.Y., Harsha, S.P. and Sharma, S.C., Vibration signature analysis of single walled carbon nanotube based nanomechanical sensors, Physica E, vol. 42, 2010, pp. 2115–2123.

[101] Joshi, A.Y., Sharma, S.C. and Harsha, S.P., The Effect of Pinhole Defect on Dynamic Characteristics of Single Walled Carbon Nanotube Based Mass Sensors, Journal of Computational and Theoretical Nanoscience, vol. 8, 2011, pp. 776.

[102] Arlett, J.L., Myers, E.B. and Roukes, M.L., Comparative advantages of mechanical biosensors, Nature Nanotechnology, vol. 6, 2011, pp. 203.

[103] Kirtania, S. and Chakraborty, D., Fracture Behavior of Carbon Nanotube-Based Composites with a Broken Fiber Using Multi-Scale Finite Element Modeling, Journal of Computational and Theoretical Nanoscience, vol. 11, 2014, pp. 676.

[104] Panchal, M. B., Upadhyay, S. H. and Harsha, S. P., Mass detection using Single Walled Boron Nitride Nanotube as a nanomechanical resonator," Nano, vol. 07, 2012, pp. 1250029.

[105] Gupta, A., Joshi, A.Y., Sharma, S.C. and Harsha, S.P., Dynamic analysis of fixed-free single walled carbon nanotube based biosensors because of various viruses, IET Nanobiotechnology, vol. 6, 2012, pp. 115–121.

[106] U. A. Joshi, S. C. Sharma, and S. P. Harsha, “Effect of waviness on the mechanical properties of carbon nanotube based composites,” Phys. E Low-Dimensional Syst. Nanostructures, vol. 43, no. 8, pp. 1453–1460, 2011.

[107] A. Y. Joshi, S. C. Sharma, and S. P. Harsha, “Chaotic response analysis of single-walled carbon nanotube due to surface deviations,” Nano, vol. 7, no. 2, pp. 1–10, 2012.

[108] S. Kumar, S. H. Upadhyay, and A. Kumar, “Continuum Solid Modeling Based Finite Element Method Simulation Approach for Wavy Single Walled Boron Nitride Nanotube Based Resonant Nano Mechanical Sensors,” J. Comput. Theor. Nanosci., vol. 12, no. 8, pp. 1841–1846, Aug. 2015, doi: 10.1166/jctn.2015.3967.

[109] S. Trivedi, S. Kumar, S.C. Sharma, S.P. Harsha, Biosensing application of multiwall boron nitride nanotube-based nanoresonator for detecting various viruses, IET Nanobiotechnology. 9 (2015) 259–263.

[110] J.H. Kang, G. Sauti, C. Park, V.I. Yamakov, K.E. Wise, S.E. Lowther, C.C. Fay, S.A. Thibeault, R.G. Bryant, Multifunctional Electroactive Nanocomposites Based on Piezoelectric Boron Nitride Nanotubes, ACS Nano. 9 (2015) 11942–11950.

[111] N. Li, N. Ding, S. Qu, L. Liu, W. Guo, C.-M.L. Wu, Mechanical properties and failure behavior of hexagonal boron nitride sheets with nano-cracks, Comput. Mater. Sci. 140 (2017) 356–366.

[112] T. Li, Z. Tang, Z. Huang, J. Yu, A comparison between the mechanical and thermal properties of single-walled carbon nanotubes and boron nitride nanotubes, Phys. E Low-Dimensional Syst. Nanostructures. 85 (2017) 137–142.

[113] J.H. Los, J.M.H. Kroes, K. Albe, R.M. Gordillo, M.I. Katsnelson, A. Fasolino, Extended Tersoff potential for boron nitride: Energetics and elastic properties of pristine and defective h-BN, Phys. Rev. B. 96 (2017) 184108.

[114] J.H. Kim, T.V. Pham, J.H. Hwang, C.S. Kim, M.J. Kim, Boron nitride nanotubes: synthesis and applications, Nano Converg. 5 (2018) 17.

[115] R. Article, J. A. Desai, and M. B. Panchal, “Vibrational characterization of wavy atomic structures of single walled boron nitride nanotubes,” 2019, doi: 10.1140/epjp/i2019-12516-3.

[116] V.K. Choyal, V. Choyal, S. Nevhal, A. Bergaley, S.I. Kundalwal, Effect of aspects ratio on Young’s modulus of boron nitride nanotubes: A molecular dynamics study, Mater.

Today Proc. 26 (2020) 1–4.

[117] V. Choyal, V.K. Choyal, S.I. Kundalwal, Effect of atom vacancies on elastic and electronic properties of transversely isotropic boron nitride nanotubes: A comprehensive computational study, Comput. Mater. Sci. 156 (2019) 332–345.

[118] V. Choyal, S.I. Kundalwal, Transversely isotropic elastic properties of multi-walled boron nitride nanotubes under a thermal environment, Nanotechnology. 31 (2020) 395707.

[119] V.K. Choyal, V. Choyal, S. Nevhal, A. Bergaley, S.I. Kundalwal, Effect of aspects ratio on Young's modulus of boron nitride nanotubes: A molecular dynamics study, Mater. Today Proc. 26 (2020) 1–4.

[120] N.A. Sakharova, J.M. Antunes, A.F.G. Pereira, B.M. Chaparro, J. V. Fernandes, On the Determination of Elastic Properties of Single-Walled Boron Nitride Nanotubes by Numerical Simulation, Materials (Basel). 14 (2021) 3183.

[121] X. Liu, C. Li, J. Eckert, K.G. Prashanth, O. Renk, L. Teng, Y. Liu, R. Bao, J. Tao, T. Shen, J. Yi, Microstructure evolution and mechanical properties of carbon nanotubes reinforced Al matrix composites, Mater. Charact. 133 (2022) 122–132.

[122] Liu, B., et al. Molecular dynamics study on thermal transport properties of boron nitride nanotubes. Journal of Applied Physics, 125(20) (2019), 204305.

[123] Chen, G., et al. First-principles study on the electronic and optical properties of single-walled boron nitride nanotubes. Journal of Applied Physics, 129(2) (2021), 025301.

[124] Guo, Y., et al. Multiscale modeling of mechanical properties of boron nitride nanotubes under uniaxial tension. Nanotechnology, 31(5) (2020), 055705.

[125] Hu, Z., et al. Amine-functionalized boron nitride nanotubes for pH-responsive drug delivery. Nanotechnology, 27(18) (2016), 185101.

[126] Liu, Y., et al. Hydroxylation of boron nitride nanotubes and their application in enhancing thermal stability and flame retardancy of polymeric nanocomposites. ACS Applied Materials & Interfaces, 9(10) (2017), 8776-8783.

[127] Wang, C., et al. Functionalization of boron nitride nanotubes with carboxyl groups for improved polymer nanocomposites. RSC Advances, 9(15) (2019), 8316-8323.

[128] Tang, Z., et al. Epoxy functionalization of boron nitride nanotubes for high-performance epoxy-based nanocomposites. Nanotechnology, 31(28) (2020), 285701.

CHAPTER 3

Dynamic Analysis of Single-Walled Boron Nitride Nanotube in Presence of Defects

3.1. Introduction

Vibrations induced in nanotubes are having substantial significance in many application areas mainly based on nano mechanical devices such as charge detectors, oscillators and various sensors. Vibrations in nanotubes can be observed during manufacturing processes, for example in processing of nano-composites by ultra-sonication as well as during non-destructive evaluation processes like Raman spectroscopy. The vibrational behaviour of CNTs has been observed by electron microscope and used to calculate effective elastic moduli along with other mechanical characteristics of CNTs in a non-destructive manner. Above findings have motivated for analysing vibrational behaviour of nanotubes comprising of bio-conjugate material like boron nitride in order to explore their sensing features.

It has been observed that resonance based nano sensors can be used for numerous sensing applications, for example sensing of small mass, with high reliability, high thermal stability in nuclear chamber, good semi conductive properties for fabricating semiconductors circuit. As far as mass detection is concerned, it relies on the fact that resonant frequency of the resonator is highly sensitive to its own mass as well as to the additional mass attached to it. Any change in the value of added mass on the resonator results in resonance frequency shift. The important concern of mass detection using resonator is measuring the deviation in resonance frequency caused by the addition of extra mass on resonator.

In an extensive study conducted by Lu and Czanderna[1], many applications of piezoelectric quartz crystal have been explored, followed by development of sensors based on the principle of piezoelectric resonators by Benes et al.,[2]. Micro-cantilever sensors were then studied by Thundat et al.,[3], and ultrasonic sensors were studied by Hauptman,[4] for process monitoring and performing chemical analysis. The mass sensitivity of such micro-sized mechanical resonators can be further enhanced by reducing their size from micro to nano level as explained earlier by Wenzel and White,[5]. Mechanical resonant immune specific biological

detector as reported by Ilic et al,[6] were followed by photo thermally actuated nano-mechanical resonators as developed by Lavrik and Datskos[7] and suggested that attached mass as of the order of the femtogram level can be easily detected by micro-sized silicon or silicon nitride cantilevers. At the same time, many researchers concluded that the requirement of high sensing performance can be achieved by nanotubes in various applications. Sensors based on the nanotubes rely on the principle of variation in resonance frequency due to addition of mass.

As boron nitride nanotubes are considered to have outstanding mechanical as well as physical properties with high aspect ratio and low-density nano material like CNTs, these properties have made BNNTs a suitable candidate for building nano devices of the next generation. BNNTs are not much explored as CNTs for various applications irrespective of the fact that both are structurally similar and in some cases BNNTs are superior to its counterpart CNTs as discussed in Chapter 1.

Li and Chou[8], reported that depending on the size of the CNT (diameter and length), fundamental frequencies of the order of gigahertz level can be achieved for cantilevered as well as bridged single-walled carbon nanotubes based nanomechanical resonators. The free vibrational behaviour of carbon nanotubes treated as solid, slender column were investigated by Sohlberg et al.,[9]. Li and Chou[10,11] provided a fast tool for calculating natural frequencies of CNT based resonators and developed a structural beam model for analysing the vibrational behaviour of SW-CNT. For exploring bio-sensing feature of CNTs, Chowdhury et al.,[12] examined the suitability of same as a bio sensor for detecting mass of biological entities by employing a continuum mechanics approach. Further investigations of SW-CNT were carried out by Sakhaee-Pour et al.,[13] based on atomistic finite element model. In continuation, vibrational behaviours of SW and MW-CNTs for different nano mass attached were explored by Georgantzinos and Anifantis[14], through finite element techniques using the spring - mass system. Later on, Boldrin et al.,[15], explored the suitability of boron nitride nanotube as mass sensor to detect mass of zeptogram level with the consideration of different boundary conditions and derived equations for obtaining sensitivity of the resonator.

Typically, research in the emerging field of nanotechnology has been conducted through experimental studies. However, computational as well as mathematical modelling techniques simplify and help in the development of nano devices and deliver a faster route to applications of

the technology. As stated by Ferrari "*Novel mathematical models are needed, in order to secure the full import of nanotechnology into oncology*".

Therefore, there is a dire need to explore computer simulation techniques, especially for nanotechnology because of the fact that nanomaterials and nano devices are found to be at an atomic or molecular level and fabricating and manipulating them at the atomic scale is not only difficult but also costly in terms of time and money both. At the same time, due to increased computing power along with enhancement in existing theoretical methodologies and use of finite element methods in recent years, the simulation capabilities have significantly increased.

In this chapter, various analytical methods used in the present study for benchmarking of the finite element (FE) models have been explained. Boron nitride nanotubes (BNNTs) can be modelled by using appropriate analytical methods for considering the effect of different boundary conditions and variation in attached mass on their vibrational behaviour. At the same time, for simulation purpose, two different finite element models, i.e. three dimensional space frame model and shell model for representing atomistic and continuum model respectively for SW-BNNT are developed in the present work.

The corresponding atomistic and continuum mechanics based analytical approach for theoretical modelling and simulation of the vibrational behaviour of BNNTs are used for validation of results obtained from FE space frame and shell models of BNNT. In order to analyse the vibrational behaviour of SW-BNNT based mass sensor, continuum mechanics based analytical model of single walled BNNT for two different boundary conditions, namely fixed-free and fixed-fixed, are developed in the current work. Using the same methodology, vibrational behaviour of multi walled BNNT based nano resonator is also analysed in this chapter.

3.2. Modeling and analysis of boron nitride nanotube using continuum mechanics approach

In this section, the use of continuum mechanics approach for nano-scale modelling is briefly described in contrast to bending vibration and modal analysis of a beam. Based on this, a mathematical model for two different configurations, namely fixed-free and fixed-fixed has been developed followed by continuum models of SW-BNNT.

3.2.1. Continuum mechanics approach for nano-scale modelling

Computational as well as mathematical models are important in all areas of nanotechnology in order to save time and money as spent for conducting experimental studies. Computational nano-mechanics can be treated as a feasible tool for providing and delivering substantial useful guidelines for subsequent molecular dynamic simulations and experimental studies. Therefore, using elementary mechanics and computational nano mechanics-based modelling techniques like continuum mechanics approach; the present research work specifically investigates the suitability of BNNT as mass sensor. Meanwhile, computations based on molecular dynamics (MD) simulations have certain limitations of achieving simulations for only small duration of time (few nanoseconds) and are possible for system size of the order of ~ 10^6 atoms as described by Qian et al[16], irrespective of substantial improvements in computational speed and storage availability in the recent years. Thus, an alternative approach is needed for simulating larger systems with longer times.

The continuum mechanics-based approach is considered as a vital approximation technique for analysing behaviour of material at nano-scale and Girifalco et al.,[17] stated that: "*From a physical point of view the discrete atom-atom model is not necessarily preferable to the continuum model. The discrete model assumes that each atom is the centre of a spherically symmetric electron distribution while the continuum model assumes that the electron distribution is uniform over the surface. Both of these assumptions are incorrect and a case can even be made that the continuum model is closer to reality than a set of discrete Lennard-Jones centres*."

C_{60} fullerence is the best example to understand the above, in which continuum distribution averages out the effect because of free rotation of molecules at higher temperatures, as further mentioned by Girifalco et al.,[17]. Qian et al.,[18] also suggested the accuracy of the approach based on continuum mechanics for the situation when "*C nuclei do not lie exactly in the centre of the electron distribution, as in the case for carbon nanotubes*." Thus, continuum mechanics approach is preferable for structures with high symmetry like nanotubes.

Further investigation about continuum mechanics-based approach carried out by Hodak and Girifalco[19] highlighted the ignorance of the chirality effect in this approach and characterisation of nanotubes is based only on their diameters. Later on, Leamy et al,[20], Arroya and Betytschko[21] and Zhang et al.,[22] suggested in their respective studies about the

proper incorporation of the effect of chirality by employing other refined continuum mechanics-based theories, typically through the elastic moduli in an indirect manner. The continuum mechanics approach has been successfully realised and employed by many researchers for different nano-systems and nanotubes Trivedi et. al. [23].

Based on above observations, following continuum model implemented for analysing dynamic behaviour of BNNT in the present work is shown in Fig. 3.1. where: D_n – Diameter of nitrogen atom, D_b - Diameter of brorn atom, t – total thickness of the nanotube.

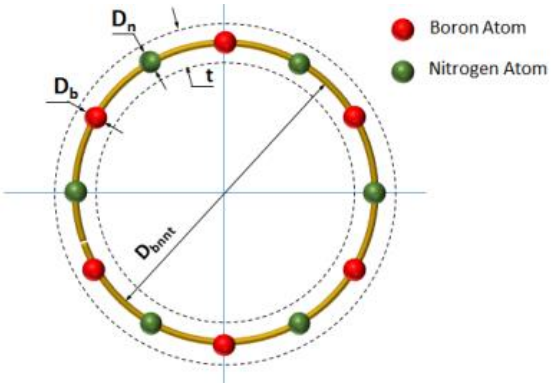

Fig. 3.1. Continuum model of boron nitride nanotube[23].

3.2.2. Flexural vibration of beam and equation of motion

Linear principles of nano-mechanical resonators considering the linear harmonic oscillator model were discussed in Chapter 1 with the assumption of a point mass attached with spring. However, in actual practice the distribution of mass and deformation properties takes place in a continuous manner as the actual mechanical systems are elastic in nature. Since, the beam is considered to be the most common and appropriate structure used for analysing flexural vibration mode of micro as well as nano-mechanical resonators, its modelling has been explained for two commonly employed boundary conditions (fixed-free and fixed-fixed). The analysis is based on the following assumptions:

- The dynamic motion is in the plane.
- Shear deformation of the beam is neglected.
- The effects of rotary inertia and axial forces are neglected.
- The section prior to and after deformation remains orthogonal to the neutral axis.

Newton's law is used to develop the equation of motion for beam vibrating in transverse direction, i.e., in *x*-*y* plane as shown in Fig. 3.2 (a). A small infinitesimal element of the beam of length *dx* is taken at a distance of *x*, with various forces acting on it as shown in Fig. 3.2 (b).

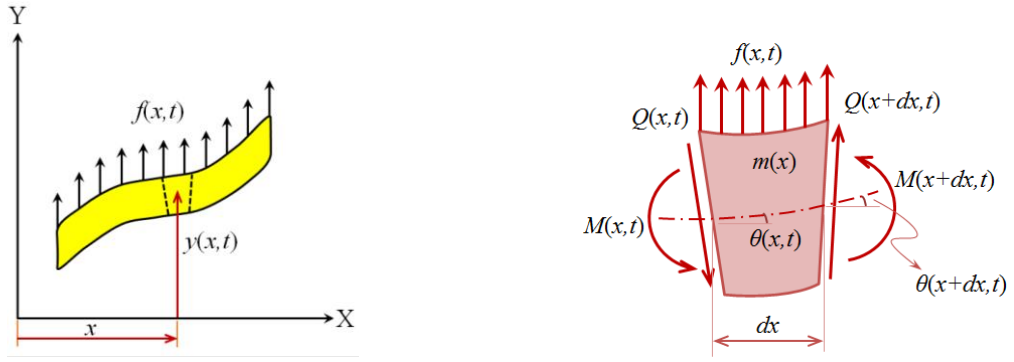

(a) (b)

Fig. 3.2. (a) Element of a beam in x-y plane and (b) forces on the element [24].

Taking force equilibrium in the *y* direction:

$$m(x)dx\frac{\partial^2 y(x,t)}{\partial t^2} = f(x,t) - Q\cos\theta + \left(Q + \frac{\partial Q}{\partial x}dx\right)\cos\left(\theta + \frac{\partial \theta}{\partial x}dx\right) \tag{3.1}$$

$$m(x)dx\frac{\partial^2 y(x,t)}{\partial t^2} = f(x,t) - \frac{\partial}{\partial x}(Q\cos\theta) \tag{3.2}$$

where, $m(x)$ represents the mass/unit length and $f(x, t)$ is distribution of force/unit length.

Taking moment equilibrium:

$$M(x,t) = \left(M(x,t) - \frac{\partial M(x,t)}{\partial x}\right)dx + f(x,t)dx\frac{dx}{2} + Q\cos\theta dx + Q\sin\theta\frac{\partial y}{\partial x}dx \tag{3.3}$$

for $\frac{\partial y}{\partial x} << 1, \cos\theta \sim 1, \sin\theta \sim \theta$, i.e., small displacement and considering the above assumptions following relation can be obtained: -

$$Q(x,t) = -\frac{\partial M(x,t)}{\partial x} \tag{3.4}$$

Applying the flexural theory for pure bending

$$M = EI\frac{\partial^2 y}{\partial x^2} \tag{3.5}$$

Thus, the equation of motion for beam can be obtained by combining Eq. (3.5) with Eq. (3.4) and Eq. (3.2) as:

$$\frac{\partial^2}{\partial x^2}\left(EI(x)\frac{\partial^2 y(x,t)}{\partial x^2}\right) + f(x,t) + m(x)\frac{\partial^2 y(x,t)}{\partial t^2} = 0 \tag{3.6}$$

In the absence of external forces, the equation becomes:

$$\frac{\partial^2}{\partial x^2}\left(EI(x)\frac{\partial^2 y(x,t)}{\partial x^2}\right) + m(x)\frac{\partial^2 y(x,t)}{\partial t^2} = 0 \tag{3.7}$$

Based on bending rigidity of nanotubes, two main regions were described by Witkamp et al.,[24] and accordingly nanotube is considered as a beam or a string. For nanotube to behave like a beam, it's bending rigidity should be greater than its tension otherwise nanotube can act as a string. Assuming small deformations, based on the Euler beam model as proposed by Gere and Timoshenko[25], the equation of motion for free vibration of a rod in the limit of small amplitude is governed by following simplified form of Eq. (3.7) as:

$$EI\frac{\partial^4 u}{\partial x^4} + \rho A\frac{\partial^2 u}{\partial t^2} = 0 \tag{3.8}$$

where, E and I represent Young's modulus and area moment of inertia, A is the cross-sectional area and ρ is the density of beam material.

On the basis of selected boundary condition for the beam and the position of the added mass along the length of the beam, the fundamental resonant frequency of the combined sensory system can be given as:

$$f_{fundamental} = \frac{1}{2\pi}\sqrt{\frac{k_{equiv.}}{m_{equiv.}}} \tag{3.9}$$

where, ($k_{equiv.}$) and ($m_{equiv.}$) are representing the equivalent stiffness and equivalent mass respectively of resonating beam including added mass as far as the first vibration mode is concerned.

3.2.3. Modal analysis of prismatic beam

Considering prismatic beam of uniform flexural rigidity along *x*-axis without external force, the Eq. (3.8) can be rewritten in the following form as:

$$\left.\begin{aligned} &\left(\frac{\partial^4 y(x,t)}{\partial x^4}\right)+\frac{1}{B^4}\frac{\partial^2 y(x,t)}{\partial t^2}=0 \\ &B^4=\frac{EI}{m} \end{aligned}\right\} \tag{3.10}$$

Separating Eq. (3.10) in time and space domains, by employing the concept of separation of variables, i.e., $y(x,t)=X(x).T(t)$ as:

$$\left.\begin{aligned} &\ddot{T}+\omega^2 T=0 \\ &X''''-\frac{\omega^2}{B^4}X=0 \end{aligned}\right\} \tag{3.11}$$

where, the over dot corresponds to time (t) derivative and prime denote space (x) derivative and the solution for the space domain representing characteristic normal mode for transverse vibration of the system is given as:

$$\left.\begin{aligned} X &= B_1\sin\lambda x+B_2\cos\lambda x+B_3\sinh\lambda x+B_4\cosh\lambda x \\ \lambda^4 B^4 &= \omega^2 \end{aligned}\right\} \tag{3.12}$$

B_1, B_2, B_3, and B_4 in Eq. (3.12) are constants and their values can be obtained by employing different boundary conditions as follows.

Case 1*: *Doubly clamped beam (both ends fixed)

For doubly clamped beam the boundary conditions are:

$$\left.\begin{aligned} &X\big|_{x=0}=0 \qquad \left.\frac{dX}{dx}\right|_{x=0}=0 \\ &X\big|_{x=L}=0 \qquad \left.\frac{dX}{dx}\right|_{x=L}=0 \end{aligned}\right\} \tag{3.13}$$

Using the first two boundary conditions in Eq. (3.12) results in $\left(B_3 = -B_1\ ,\ B_4 = -B_2\right)$, therefore

$$X = B_1\left(\sin\lambda x - \sinh\lambda x\right) + B_2\left(\cos\lambda x - \cosh\lambda x\right) \tag{3.14}$$

similarly, using the last two boundary conditions results in:

$$\left.\begin{aligned} B_1\left(\sin\lambda L - \sinh\lambda L\right) + B_2\left(\cos\lambda L - \cosh\lambda L\right) = 0 \\ B_1\left(\cos\lambda L - \cosh\lambda L\right) + B_2\left(-\sin\lambda L - \sinh\lambda L\right) = 0 \end{aligned}\right\} \tag{3.15}$$

In order to obtain non-zero solution for the constant B_1 and B_2, the determinant of Eq. (3.15) must be zero. This gives the following relation as:

$$\cos\lambda L.\cosh\lambda L = 1 \tag{3.16}$$

Infinite number of solutions of Eq. (3.16) is possible for (λL), and accordingly for doubly clamped beam, the first four roots are given as 4.730, 7.853, 10.996 and 14.137. Using $\lambda_i L \simeq \left(i + 1/2\right)\pi$, one may approximate higher roots also and determine the Eigen frequencies of the system as:

$$\omega_i = \frac{\lambda_i^2}{L^2}\sqrt{\frac{EI}{m}} \tag{3.17}$$

On substitution of eigen frequencies and the corresponding values of $k_i = \left(B_1/B_2\right)_i$ into Eq. (3.12), the normal vibration modes are obtained as:

$$\left.\begin{aligned} k_i = \left(\frac{B_1}{B_2}\right)_i = \frac{\left(\sin\lambda_i L - \sinh\lambda_i L\right)}{\left(\cos\lambda_i L - \cosh\lambda_i L\right)} \\ X_i(x) = k_i\left(\sin\lambda_i x - \sinh\lambda_i x\right) + \left(\cos\lambda_i x - \cosh\lambda_i x\right) \end{aligned}\right\} \tag{3.18}$$

k_i can be obtained by normalizing the i^{th} eigen mode as:

$$\int_0^L X_i^2 dx = 1 \tag{3.19}$$

Case 2: Clamp-free beam (one end fixed and the other is free)

For fixed-free (cantilever) beam, the boundary conditions are:

$$\left.\begin{array}{ll} X\big|_{x=0}=0 & \left.\dfrac{dX}{dx}\right|_{x=0}=0 \\ \left.\dfrac{d^2X}{dx^2}\right|_{x=L}=0 & \left.\dfrac{d^3X}{dx^3}\right|_{x=L}=0 \end{array}\right\} \tag{3.20}$$

On substitution of above boundary conditions into Eq. (3.12) and repeating the process of the previous case, results in:

$$\cos\lambda L.\cosh\lambda L=-1 \tag{3.21}$$

Infinite number of solutions of Eq. (3.21) are possible for (λL) and accordingly for fixed-free beam, the first four roots be given as 1.875, 4.694, 7.855 and 10.996. Using $\lambda_i L \simeq (i-1/2)\pi$, one may approximate higher roots also and determine the Eigen frequencies. On substitution of Eigen frequencies and the corresponding values of k_i into Eq. (3.12), the normal vibration modes are obtained as:

$$\left.\begin{array}{l} k_i=\left(\dfrac{B_1}{B_2}\right)_i=-\dfrac{(\sin\lambda_i L-\sinh\lambda_i L)}{(\cos\lambda_i L+\cosh\lambda_i L)} \\ X_i(x)=k_i(\sin\lambda_i x-\sinh\lambda_i x)+(\cos\lambda_i x-\cosh\lambda_i x) \end{array}\right\} \tag{3.22}$$

Therefore, the set of Eigen solutions can be obtained as $\{\omega_i, X_i(x)\}$, for i=1, 2, 3, 4…. n and the system solution may be expressed as:

$$y(x,t)=\sum_{i=1}^{\infty} X_i(x).\eta_i(t) \tag{3.23}$$

where, $\eta_i(t)$ is the projection of solutions along the i^{th} mode.

3.2.4. Modelling and analysis of single-walled boron nitride nanotubes based nanoresonator

A. Analysis for clamp-free configuration with mass at tip

A continuum mechanics approach based on Euler's-Bernoulli beam theory is used in the present work to calculate resonant frequency of SW-BNNT based nano-resonator. The resonant

frequency thus evaluated is influenced by the mass attached on the tip of SW-BNNT. The following wave equation governs the equation of motion of free vibration:

$$EI\frac{\partial^4 u(x,t)}{\partial x^4}+\rho A\frac{\partial^2 u(x,t)}{\partial t^2}=0 \tag{3.24}$$

where, $u(x, t)$ represents deflection of beam in transverse direction, E is Young's modulus, ρ represents density of beam material and I is the second moment of the cross-sectional area (A) of the beam. Therefore, the resonant frequency of SW-BNNT is given by:

$$f_{reso}=\frac{1}{2\pi}\sqrt{\frac{k_{equiv.}}{m_{equiv.}}} \tag{3.25}$$

where; $k_{equiv.}$ and $m_{equiv.}$ are equivalent stiffness and equivalent mass of complete sensory system (i.e., mass of BNNT and value of attached mass) respectively. The cantilever configuration as shown in Fig. 3.3 is considered for the analysis. The virtual force at the attached mass location is given to obtain unit deflection under it.

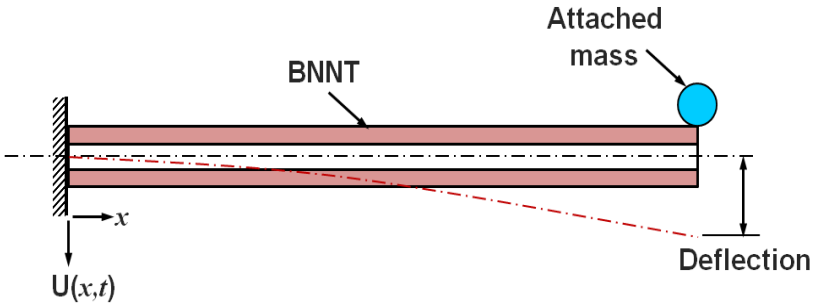

Fig. 3.3. Cantilever configuration of SW-BNNT based mass sensor with small mass attached at tip [23].

For SW-BNNT of cantilevered configuration, the equivalent stiffness is given by:

$$k_{equiv.\_CF}=\frac{3.E.I}{L^3} \tag{3.26}$$

and the deflection along the SW-BNNT length can be expressed as:

$$U(x)=\frac{x^2(3L-x)}{2L^3} \tag{3.27}$$

It is assumed for analysis that the amplitude of vibration is small enough for considering the resonance behaviour to be approximately harmonic i.e. $U(x, t) = U(x)e^{i.\omega.t}$, where '$\omega$' is the

frequency. The kinetic energy of the combined sensory system of SW-BNNT and attached mass (M) are obtained as:

$$\left.\begin{aligned} T &= \frac{\omega^2}{2}\int_0^L \rho.A.U^2(x).dx + \frac{\omega^2}{2}M.U^2(L) \\ &= \frac{\omega^2}{2}\left[\rho.A\left(\frac{33}{140}\right)L + M\right] = \frac{\omega^2}{2}m_{equiv.\_CF} \end{aligned}\right\} \tag{3.28}$$

where, $m_{equiv.\_CF}$ for clamp-free boundary condition is given by:

$$m_{equiv.\_CF} = \rho.A\left(\frac{33}{140}\right)L + M \tag{3.29}$$

Therefore, resonance frequency of the combined system can be obtained by using Eqs. (3.26) and (3.29) in Eq. (3.25) as:

$$f_{reso} = \frac{1}{2\pi}\sqrt{\frac{\frac{3.E.I}{L^3}}{\rho.A\left(\frac{33}{140}\right)L + M}} \tag{3.30}$$

$$f_{reso} = \frac{1}{2\pi}\frac{\alpha_{CF}^2.\beta_{CF}}{\sqrt{1+\Delta m}} \tag{3.31}$$

where,

$$\alpha_{CF}^2 = \sqrt{\frac{140}{11}},\ \beta_{CF} = \sqrt{\frac{E.I}{\rho.A.L^4}},\ \ \Delta m = \frac{M}{\rho.A.L}\mu_{CF}\ and\ \ \mu_{CF} = \frac{140}{33} \tag{3.32}$$

For a clamp-free SW-BNNT mass resonator, the fundamental resonance frequency with no mass attached at free end can simply be obtained by putting $\Delta m = 0$ in Eq. (3.31) as:

$$f_{0\_reso} = \frac{1}{2\pi}\alpha_{CF}^2.\beta_{CF} \tag{3.33}$$

From Eqs. (3.31) and (3.33) following relation can be established:

$$\frac{f_{reso}}{f_{0\_reso}} = \frac{1}{\sqrt{1+\Delta m}} \tag{3.34}$$

From Eq. (3.34), it can be seen that the resonance frequency of nano-resonator is sensitive to its mass. Thus, any variation in the value of attached mass is responsible for changes in the mass of resonator and ultimately results in frequency shift.

$$\Delta f = f_{0\_reso} - f_{reso} = f_{0\_reso} - \frac{f_{0\_reso}}{\sqrt{1+\Delta m}} \tag{3.35}$$

The resonance frequency shift is simply the difference of resonance frequencies with no attached mass and with attached mass on resonator.

On rearranging the terms of Eq. (3.35)

$$\Delta m = \frac{1}{\left(1-\frac{\Delta f}{f_{0\_reso}}\right)^2} - 1 \tag{3.36}$$

Using Taylor series, expanding Eq. (3.36) results in:

$$\Delta m = \sum\nolimits_j (j+1)\left(\frac{\Delta f}{f_{0\_reso}}\right),\ j = 1,2,3... \tag{3.37}$$

Linear approximation can be obtained by considering the first order term of Eq. (3.37) and results in:

$$\Delta m \approx 2\left(\frac{\Delta f}{f_{0\_reso}}\right) \tag{3.38}$$

And for keeping up to third order terms the cubic approximations is obtained as:

$$\Delta m \approx 2\left(\frac{\Delta f}{f_{0\_reso}}\right) + 3\left(\frac{\Delta f}{f_{0\_reso}}\right)^2 + 4\left(\frac{\Delta f}{f_{0\_reso}}\right)^3 \tag{3.39}$$

Thus, the value of the attached mass can be obtained from Eqs. (3.36) and (3.32) as:

$$M = \frac{\rho AL}{\mu_{CF}} \frac{\left(\alpha_{CF}^2 \beta_{CF}\right)^2}{\left(\alpha_{CF}^2 \beta_{CF} - 2\pi\Delta f\right)^2} - \frac{\rho AL}{\mu_{CF}} \tag{3.40}$$

Using the linear approximation, the value of the added mass can be obtained as:

$$M = \frac{\rho AL}{\mu_{CF}} \frac{2\pi\Delta f}{\alpha_{CF}^2 \beta_{CF}} \tag{3.41}$$

B. Analysis for clamp-clamped configuration with mass at mid-position

Consider a doubly clamped SW-BNNT with attached mass (M) at its centre as shown in Fig. 3.4. The equivalent stiffness for doubly clamped boundary condition is given as:

$$k_{equiv.\_CC} = \frac{192EI}{L^3} \tag{3.42}$$

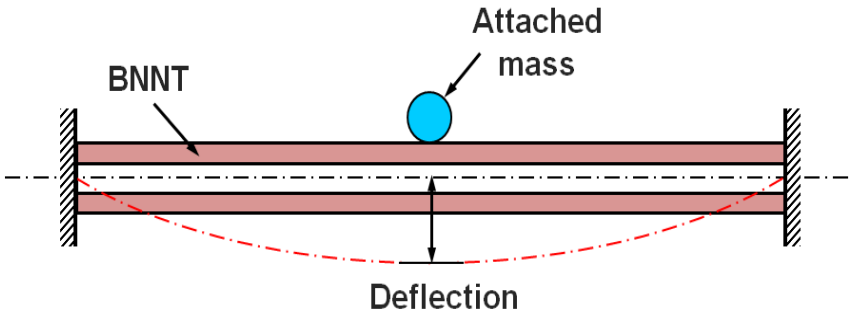

Fig. 3.4. Doubly clamped configuration of SW-BNNT with small mass attached at the mid-position.

In order to get a unit deflection under the attached mass, a virtual force is assumed to act at its position. The deflection of the SW-BNNT for doubly clamped condition is given as:

$$\left.\begin{aligned} U(x) &= \frac{32}{L^3}(1/2x^3 - 3/8x^2L) \ for\ x < L/2 \\ U(x) &= \frac{32}{L^3}(1/2x^3 - 3/8x^2L - (x - 1/2L)^3) \ for\ x \geq L/2 \end{aligned}\right\} \tag{3.43}$$

With the assumption of harmonic motion similar to the above case, the kinetic energy of the doubly clamped SW-BNNT is given by:

$$\left.\begin{aligned} T &= \frac{\omega^2}{2}\int_0^L \rho AU^2(x)dx + \frac{\omega^2}{2}MU^2(L) \\ &= \frac{\omega^2}{2}\left(\frac{13}{35}\rho AL + M\right) = \frac{\omega^2}{2}m_{equiv.\_CC} \end{aligned}\right\} \tag{3.44}$$

where, $m_{equiv._CC} = \frac{13}{35}\rho AL + M$ (3.45)

The resonance frequency can be obtained by using the relation: $f_{reso} = \frac{1}{2\pi}\left(\sqrt{\frac{k_{equiv._CC}}{m_{equiv._CC}}}\right)$ and substituting the relevant values from Eqs. (3.42) and (3.45) as:

$$f_{reso\_CC} = \frac{1}{2\pi}\sqrt{\frac{\frac{192EI}{L^3}}{\frac{13}{35}\rho AL + M}} = \frac{1}{2\pi}\frac{\alpha_{CC}^2.\beta_{CC}}{\sqrt{1+\Delta m}} \tag{3.46}$$

where,

$$\left.\begin{aligned} &\alpha_{CC}^2 = \sqrt{6720/13}, \qquad \beta_{CC} = \sqrt{EI/\rho AL^4} \\ &\Delta m = \frac{M}{\rho AL}.(\mu_{CC}) \qquad and\ \mu_{CC} = 35/13 \end{aligned}\right\} \tag{3.47}$$

The fundamental resonance frequency with no mass attached at the centre is simply obtained by putting $\Delta m = 0$ in Eq. (3.46) as:

$$f_{0\_reso} = \frac{1}{2\pi}\alpha_{CC}^2.\beta_{CC} \tag{3.48}$$

From Eqs. (3.46) and (3.48) following relation can be established:

$$f_{reso} = \frac{f_{0\_reso}}{\sqrt{1+\Delta m}} \tag{3.49}$$

From the above, it is evident that the parameter 'α' depends on the boundary conditions, whereas 'μ' depends upon the mass position on nano-resonator.

3.2.5. Development of finite element model for SW-BNNT using continuum mechanics approach

Continuum modelling technique has been used for the development of the finite element beam model. As, a beam model is a continuum approximation of actual atomistic model (i.e. space-frame model) of BNNT, chirality cannot be introduced in such models. However, proper

benchmarking of beam model is essentially required to realise the same in actual practice as compared to corresponding actual space frame model of BNNTs. At the same time, modelling of SW-BNNT using a space frame modelling technique is very difficult for sizes required for experimentation purposes. On the contrary the continuum model, if benchmarked properly, can solve the modelling problem of experimental size of SW-BNNTs. For analysis purposes, the SW-BNNT is considered to be as a solid and continuous thin walled hollow cylindrical tube in shell model.

Effective continuum properties at the elementary level can be employed successfully in the beam model. Molecular mechanics based model as proposed by Li and Chou[26] is used for benchmarking of different BNNT samples (as shown in Table 3.1). In the present work, the same are analysed for two different boundary conditions. Further, the effect of addition of mass on resonance frequency of SW-BNNT has been investigated by varying the value of attached mass ranging from 10^{-8} to 10^{-2} fg. As the mass landing position influences the resonance behaviour of SW-BNNT, the same has also been analysed by altering the position of attached mass on SW-BNNT.

Table 3.1: Dimensions of SW-BNNT model under study.

SW-BNNT case	**Diameter (nm)**	**Length (nm)**	**Boundary Condition**
1	0.8	6.00	Clamp-free & Clamp-clamped
2	0.8	8.00	Clamp-free & Clamp-clamped
3	0.8	10.0	Clamp-free & Clamp-clamped
4	1.0	6.00	Clamp-clamped
5	1.2	6.00	Clamp-clamp

3.3. Modeling and analysis of SW-BNNT using hybrid modeling appraoch

This section deals with the development of three-dimensional atomistic models of both, armchair and zigzag SW-BNNT using hybrid, i.e., molecular structural mechanics-based methodology. Further, this helps in investigation of the effect of chirality (as the continuum mechanics

approach is not capable of doing so) and atomic vacancy defects as normally found in BNNTs. The presence of defects is considered as one of the vibration generation sources in nanotubes. As far as space frame structures at macroscopic level are concerned, material data handbook is available for obtaining material and element sectional properties of common materials used for engineering purposes. Similar data handbook for nanoscopic materials like BNNTs is not available and hence information about B-N bonds and BNNT properties are missing. The hybrid modelling approach can be successfully applied to nanoscopic materials which act as a connection between structural mechanics and molecular mechanics in order to obtain equivalent sectional properties of boron-nitrogen bonds in BNNT structures. At the same time, it can be anticipated that a potential relationship exists between the BNNT deformations and frame like structure of BNNTs. Li and Chou[27] have successfully applied this approach for analysing CNT and the same was subsequently used by Bodily and Sun[28].

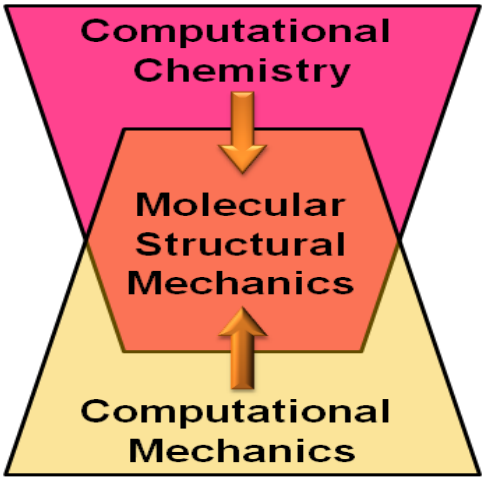

Fig. 3.5. Representation of molecular structural mechanics as a link between computational chemistry and computational mechanics.

Molecular structural mechanics based modelling approach thus provides an intermediate link between computational chemistry (study of system behaviour at atomic level) and computational mechanics as depicted in Fig. 3.5.

3.3.1. Structural mechanics

In BNNT, boron and nitrogen atoms are bonded together by strong covalent B-N bonds, making them very strong similar to other known nano-materials. These bonds have characteristic length

as well as bond angles in three-dimensional space. When nanotube is subjected to external forces, the displacements of the individual atoms in the nanotube are constrained by these bonds and the deformation of the nanotube is caused by the bond interactions.

The beam element corresponds to the B-N bond of SW-BNNT subjected to axial tensile load, pure bending moment and torsion is represented in Fig. 3.6.

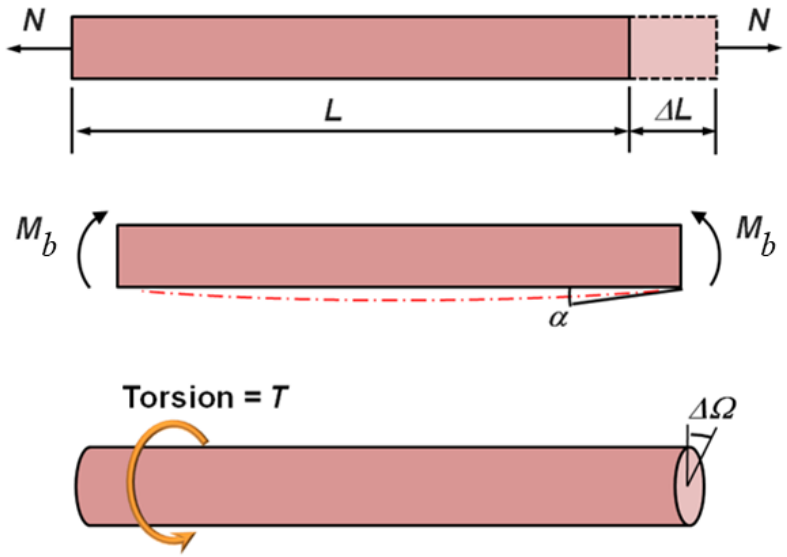

Fig. 3.6. Beam element in structural mechanics approach representing pure tension, pure bending and pure torsion respectively.

B-N bond can be treated as a beam element for connecting boron and nitrogen atoms respectively, whereas boron and nitrogen atoms themselves are considered as joints, which connects various beam elements at a point called nodal point. Using these assumptions, a BNNT can be simulated as a structure similar to space frame one. The elemental total strain energy of the system is the sum of strain energy caused by the application of the tensile force (N) in the beam's axial direction, moment (M_b) and due to torsion (T_b). These strain energies are given by following set of equations:

$$\varepsilon_{tension} = \frac{1}{2}\int_0^L \frac{N^2}{EA}dL = \frac{1}{2}\frac{N^2 L}{EA} = \frac{1}{2}\frac{EA}{L}\left(\Delta L\right)^2 \tag{3.50}$$

$$\varepsilon_{bending} = \frac{1}{2}\int_0^L \frac{M_b{}^2}{EI}dL = \frac{2EI}{L}\alpha^2 = \frac{1}{2}\frac{EI}{L}\left(2\alpha\right)^2 \tag{3.51}$$

$$\varepsilon_{torsion} = \frac{1}{2}\int_0^L \frac{T^2}{GJ} dL = \frac{1}{2}\frac{T^2 L}{GJ} = \frac{1}{2}\frac{GJ}{L}\left(\Delta\Omega\right)^2 \tag{3.52}$$

where; E and G are Young's modulus and shear modulus of beam element, L is length of the beam element having I as moment of inertia and J as polar moment of inertia for beam cross-sectional area A. ΔL, α and $\Delta\Omega$ represent stretching due to tension, rotational angle at the ends of the beam element due to moment and relative rotation between the ends due to torsion respectively.

Based on conventional structural mechanics approach, the elemental total strain energy is thus given by:

$$\varepsilon_{total} = \Sigma\varepsilon_{tension} + \Sigma\varepsilon_{bending} + \Sigma\varepsilon_{torsion} \tag{3.53}$$

3.3.2. Molecular mechanics

In molecular mechanics approach, a BNNT is considered as a large molecule consisting of boron and nitrogen atoms, which are strongly bonded. The bonding mechanism in a BNNT system is similar to that of hexagonal boron nitride (h-BN) sheet, since a BNNT can be thought of as a rolled-up section of such sheet.

The atomic nuclei can be treated as a material point at the atomistic level and the movement of BNNTs are considered to be regulated by a force field generated due to interactions between electron and nucleus and (or) nucleus and nucleus. The force field generated within the BNNT can be expressed in steric potential energy terms. Li and Chou[27] suggested that the generalized relation for total steric potential energy for CNT consists of bonded and non-bonded interaction terms excluding the term related to electrostatic interaction, i.e., Columbic term. As far as BNNT is concerned, Born-Oppenheimer approximation included such electrostatic term for evaluating total energy and this can be expressed in terms of functions of nuclear coordinates. Based on this approximation interaction within a system due to bond stretching, variation in bond angle and inversion can be modelled by molecular mechanics as explained by Odegard et al.,[29]. This motivates us to use following mathematical model for the assemblies of boron and nitrogen atoms in the SW-BNNT system.

$$E_{total} = E_{bs} + E_{av} + E_{at} + E_{inv} + E_{vdW} + E_{es} \tag{3.54}$$

All energy terms depicted in Eq. (3.54) consist of bonded (first four terms) and non- bonded terms (last two terms) as explained by Chowdhury et al.,[30] and given as:

$$\left.\begin{aligned} E_{bs} &= \frac{1}{2}k_1(r-r_o)^2 \\ &= \textit{associated energy with bond stretching} \end{aligned}\right\} \tag{3.54a}$$

$$\left.\begin{aligned} E_{av} &= \frac{1}{2}k_2\left(C_0 + C_1\cos\theta + C_2\cos 2\theta\right) \\ &= \textit{associated energy with angle variation} \end{aligned}\right\} \tag{3.54b}$$

where,

$$C_0 = C_2\left(2\cos^2\theta_0\right);\ C_1 = -4C_2\cos\theta_0 \textit{ and } C_2 = \frac{1}{4\sin^2\theta} \tag{3.54c}$$

$$\left.\begin{aligned} E_{at} &= k_3\left(1\pm\cos\eta\phi\right) \\ &= \textit{associated energy with angle torsion} \end{aligned}\right\} \tag{3.54d}$$

$$\left.\begin{aligned} E_{inv} &= k_4\left[1\pm\cos\left(\eta\chi-\chi_0\right)\right] \\ &= \textit{associated energy for inversion terms} \end{aligned}\right\} \tag{3.54e}$$

$$\left.\begin{aligned} E_{vdW} &= D\left[\left(\frac{r^*}{r}\right)^{12} - \left(\frac{r^*}{r}\right)^{6}\right] \\ &= \textit{non bonded van der Walls interaction} \end{aligned}\right\} \tag{3.54f}$$

$$\left.\begin{aligned} E_{es} &= \frac{q_i q_j}{\varepsilon\tau_{ij}} \\ &= \textit{non-bonded interaction energy consisting of electrostatics} \end{aligned}\right\} \tag{3.54g}$$

The non-bonded interaction energy as given by Eq. (3.54g) is associated with Columbic term and unlike CNTs, it is significant in BNNTs. Using 'Q_{Eq}. i.e., charge equilibrium algorithm', the atomic charges for boron and nitrogen are assigned as defined by Rappe and Goddard[31]. The representation of a B-N bond in molecular mechanics is shown in Fig. 3.7 and various inter-atomic interactions are represented in Fig. 3.8.

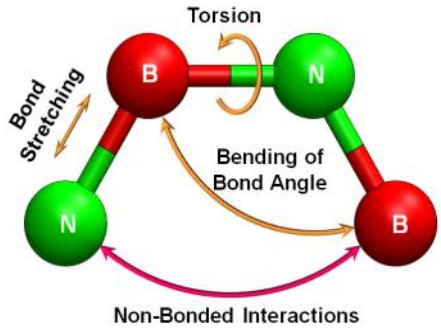

Fig. 3.7. Representation of B-N bonding in molecular mechanics approach [31].

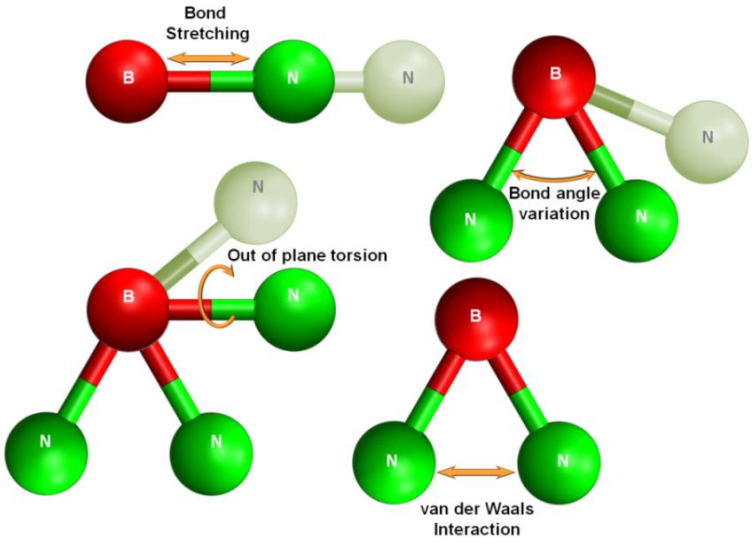

Fig. 3.8. Various inter-atomic interactions in molecular mechanics approach [31].

In the above described energy terms, k_1, k_2, k_3, k_4 represent force constants, θ_0 is regular bond angle, r^* is van der Waals length, D represents van der Waals depth, q_i and q_j represent total charges of boron and nitrogen atoms respectively, ε is dielectric constant and τ_{ij} is the distance between B and N atoms. The values of the variables described in Eq. (3.54) can be obtained from Rappe et al.,[31]. For systems containing covalent bonds, only three terms of Eq. (3.54) are responsible for contributing the total steric potential energy. Under the assumption of small deformation for harmonic approximation, the potential energies due to stretching, bending and torsion are sufficient to describe the total steric potential energy. Thus, Eq. (3.54) can be rewritten as:

$$E_{total} = E_{bs} + E_{av} + E_{at} \tag{3.55}$$

and all three energy terms are described as:

$$E_{bs} = \frac{1}{2} k_1 \left(r - r_o \right)^2 \tag{3.56}$$

$$E_{av} = \frac{1}{2} k_2 \left(\theta - \theta_0 \right)^2 \tag{3.57}$$

$$E_{at} = \frac{1}{2} k_3 \left(\phi - \phi_0 \right)^2 \tag{3.58}$$

where, the terms (r-r_o), (θ-θ_o) and (ϕ-ϕ_o) represent the increment in bond stretching, change in bond angle and the change in angle due to bond twisting, respectively.

The comparison between the various terms used in structural mechanics and their equivalent terms in molecular mechanics are shown in Table 3.2.

Table 3.2: Comparison of structural and molecular mechanics terms.

Structural Mechanics	**Molecular Mechanics**
Joint	Atom
Beam	Bond
Beam Tension	Bond Stretching
Beam Bending	Bond Bending
Beam Torsion	Bond Torsion

3.3.3. Hybrid modelling

BNNT properties have been mainly investigated theoretically by employing tight-binding as clarified by Sanchez-Portal and Hernandez[32] and using first-principle methods as discussed by Wirtz and Rubio[33]. Irrespective of the fact that these methods usually provide accurate results, they are still not suitable for analysing complex structures requiring time consuming calculations. The molecular dynamics simulation approach has been employed by many researchers. Geometry of BNNTs and its thermal behaviour was investigated in optimized manner by Moon and Hwang,[34] using the Tersoff-like potential.

Although, there has been significant development in computing-power, the molecular dynamics simulation approach is still considered to be very time consuming and not appropriate for studying static properties. The force field method is thus considered as the most effective way for studying mechanical properties of nanotubes. Large numbers of molecular force fields have been developed for computational chemistry of materials. Molecular structural mechanics approach using AMBER (Assisted Model Building with Energy Refinement) molecular force field of Cornwell et al.,[35] for studying CNTs has been proposed. The same approach has been used again for studying BNNTs. Since, parameters for boron and nitrogen are available in DREIDING and UFF (Universal Force Fields) amongst all other force fields, Rappe et al.,[36] employed DREIDING force field with minor modifications to investigate BNNTs. At the same time, DREIDING force field is well defined for any pair of atoms and it is not necessary to differentiate the bending stiffness between the three-body angles of B-N-B and N-B-N. Thus, the simplicity of DREIDING force field offers a suitable basis for the use of hybrid modelling approach for investigating the dynamic behaviour of SW-BNNT in the present work.

This modelling technique combines the features of both structural as well as molecular mechanics approaches as discussed above. On the basis of Born–Oppenheimer approximation, energy can be expressed in terms of nuclear coordinates. Based on this approximation, a simple platform provided for modelling the interactions within a system with regards to bond elongation, bond angle variation and inversion in bond using molecular mechanics. One of its forms required to model single molecules or assemblies of atoms as described above in Eq. (3.54) consists of bonded (first four terms) and non-bonded terms (last two terms).

The present analysis is concerned about BNNT, which has two elements B and N different from most common CNT. Different atoms have different charges which lead to different angle bending force constants. Due to rolling of the h-BN sheet into a single cylindrical tube to form BNNTs, the electron-electron repulsion force decreases because of relaxation of anions and cations from their ideal atomic positions. This results in a buckled surface of BNNT, in which boron atoms tend to retain the sp^2 bonding with 120°, whereas the nitrogen atoms tends to an admixture of sp^3 hybridization as discussed by Blase et al.,[37]; Baumeier et al.,[38] and Zhang et al.,[39,40]. The consideration of the inversion term in calculating total energy of the system for BNNT is debatable, because the buckling of BNNTs results in larger value of out of

plane angles in BNNT than its counterpart CNT. This inversion term is essential to be incorporated in the force field for achieving desired geometry as suggested by Jiang and Guo,[41]. Molecular structural mechanics is thus a blend of the two approaches as discussed above. Therefore, it helps in establishing the relation between the element sectional parameters related to the stiffness of structural mechanics and the various force constants as used in molecular mechanics approach and such relationship are described in Fig. 3.9. For the convenience, a symmetrical rod like section is considered for B-N bonds, which are treated as beam for which $I_x=I_y=I$ and only three stiffness parameters, i.e., *EA*, *EI* and *GJ* need to be determined. Further, it is assumed that the change in bond length due to stretching is ΔL and is equivalent to $(r\text{-}r_o)$, change in bond rotation angle (2α) is equivalent to change $(\theta\text{-}\theta_o)$ in the bond angle and $\Delta\Omega$ is equivalent to $(\phi\text{-}\phi_o)$.

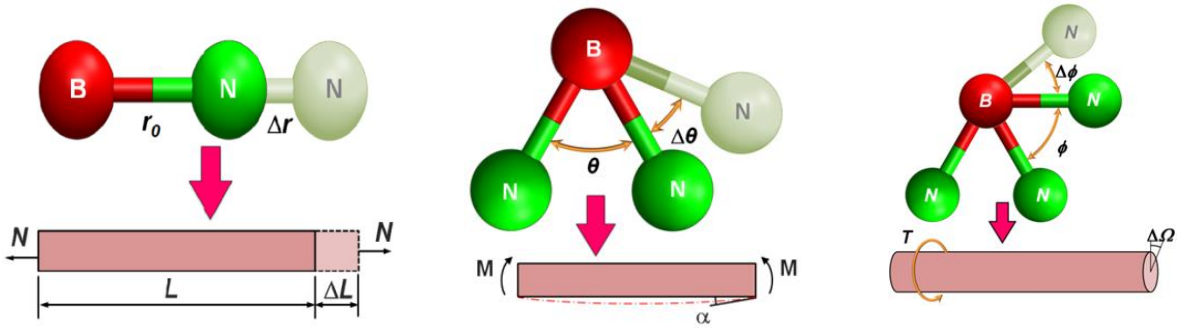

(a) (b) (c)

Fig. 3.9. Equivalent representation of molecular and structural mechanics deformation (a) Bond stretching (b) Bond angle and (c) Out of plane torsion.

Since, the potential energy in the two above approaches is independent of each other, energy equivalence of the stored energy of the two approaches reveals that:

$$\frac{EA}{L}=k_1;\quad \frac{EI}{L}=k_2\quad and\ \frac{GJ}{L}=k_3 \tag{3.59}$$

and accordingly the elastic properties of the beam element are evaluated as:

$$d=4\sqrt{\frac{k_2}{k_1}};\quad E=\frac{k_1^{\,2}L}{4\pi k_2}\quad and\ G=\frac{k_1^{\,2}k_3L}{8\pi k_2^{\,2}} \tag{3.60}$$

where; *d*, *E*, *L* and *G* represent the diameter, modulus of elasticity, length and shear modulus of the beam element respectively. Since BNNT is considered as a space frame structure in the present analysis, the beam element length is taken equal to the distance of the covalent bond

between B-N atoms in the h-BN sheet. Many literatures explained the use of molecular structural mechanics for studying dynamic properties of CNTs and only few literatures suggest the use of same approach for analysing dynamic behaviour of BNNTs. This is because of the fact that BNNT behaves in a more differentiated manner as there are two different types of atoms, i.e., boron and nitrogen, in BNNTs. This nature of BNNT increases the complexity in establishing the mass matrix.

For simulating a SW-BNNT as an equivalent space frame-like structure, the fundamental frequency of the nanotube can be obtained by solving the following equation of motion for free vibration as:

$$[M]\{y''\}+[K]\{y\}=\{0\} \tag{3.61}$$

where [*M*] represents a global mass matrix and is assembled from the elemental mass matrix as $[M]=\sum_{e=1}^{e=n}[M]^e$ and [*K*] is the global stiffness matrix assembled as $[K]=\sum_{e=1}^{e=n}[K]^e$, *n* = number of equivalent B-N beams in space frame structure of BNNT. The vectors representing nodal displacement and acceleration are represented by $\{y\}$ and $\{y''\}$ respectively.

Mass of electron being very less as compared to that of nucleus can thus be neglected and the mass of boron / nitrogen nucleus in the space frame-like structure of BNNT can be assumed to be concentrated at the centre of the respective atoms. This complete BNNT system behaves like a lumped system and the global mass matrix of this lumped system is represented by a diagonal matrix and can be recognized by assigning the mass of boron atom (m_{Boron}= 1.828 × 10^{-6} kg) / nitrogen atom ($m_{Nitrogen}$= 2.326 × 10^{-6} kg) to the corresponding diagonal elements in the matrix. Also, the coefficients in the mass matrix corresponding to bending and torsional rotation, i.e., $\frac{2}{3}m_i r_i^2$ (*i*=Boron, Nitrogen) are neglected and only the coefficients related to translational displacements have been considered in the present work because of very small radius of the atomic nucleus. Thus, the elemental stiffness matrix $[K]^e$ of the equivalent B-N beam is represented by:

$$[K]^e=\begin{bmatrix}[k_{ii}] & [k_{ij}]\\ [k_{ij}] & [k_{jj}]\end{bmatrix} \tag{3.62}$$

where; the sub-matrices of above Eq. (3.62), represent stiffness coefficients related to the cross-sectional parameters of the equivalent beam element representing B-N bond (*i-j*) and values of same have been taken from Li and Chou[42].

The fundamental frequencies (*f*) and mode shapes are then easily obtained by Eigen-solutions as:

$$\left([K]-\omega^2[M]\right)\{y_p\}=0 \tag{3.63}$$

where, 'y_p' represents the translational displacement vector of atoms corresponding to primary coordinates and 'ω' is the angular frequency ($2\pi f$).

To model the space frame structure of SW-BNNT, the elastic beam properties are applied to an elastic beam element and the mass properties to the point masses, which correspond to mass of boron and nitrogen atoms, assumed to act at the ends of the beam element. The properties of beam element are calculated using the values of the constants given in Table 3.3 and using Eq. (3.60). The cross-section diameter, the modulus of elasticity and shear modulus of the beam element are taken as 0.1647 nm, 4.21 TPa and 0.49 TPa, respectively.

Table 3.3: Properties of beam element for BNNT.

Property	**Numerical value**
$\boldsymbol{k_1}$	620 nN/nm
$\boldsymbol{k_2}$	1.05 nN-nm
$\boldsymbol{k_3}$	2.47 nN-nm
$\boldsymbol{L}$	0.145 nm

3.3.4. Development of 3-d atomistic finite element model of SW-BNNT using molecular structural mechanics approach

In any finite element model, the sectional modulus properties must be entered into the FE code at the elemental level. As mentioned earlier, the elemental properties of B-N bonds and their material properties at the elementary level are not known. Therefore, the molecular structural mechanics approach is used to get these stiffness parameters associated with B-N bonds. The

whole geometrical concept of creating a space frame model is described in Fig. 3.10 at the elemental level.

In the present work, achiral structure of BNNT (namely armchair and zigzag) have been investigated. The BNNTs are modelled as a space-frame like structure as depicted in Fig. 3.10. In the 3-D atomistic finite element space frame like model of SW-BNNT, each boron and nitrogen atom behaves like a node and a boron-nitrogen bond is represented by a beam element. The characteristic B-N bond length ($a_{B\text{-}N}$ =0.145 nm) also representing the length of beam element has been used for the development of a space frame model of BNNT as shown in Fig. 3.10.

Further, the molecular structural mechanics concept has been used as discussed above to incorporate the properties of the beam element as described in Table 3.3.

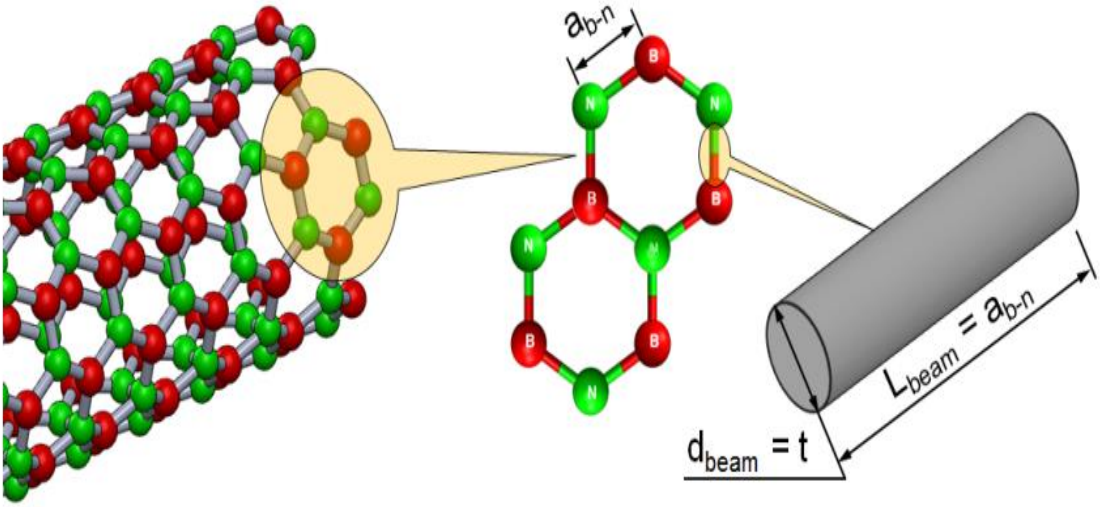

Fig. 3.10. Space form structure of SW-BNNT showing beam element connectivity and its geometric dimensions.

In order to model any structural form of BNNT (i.e. armchair, zigzag or chiral form), a finite element package, *ABAQUS*, is used in the present work, in which the coordinates of different nodes correspond to boron and nitrogen atoms are required.

With the help of nanotube co-ordinates generating software, i.e. Nanotube Modeler, these coordinates can be determined easily and used in *ABAQUS* by importing the same. A typical tool bar window of such nanotube coordinates generating software is shown in Fig. 3.11.

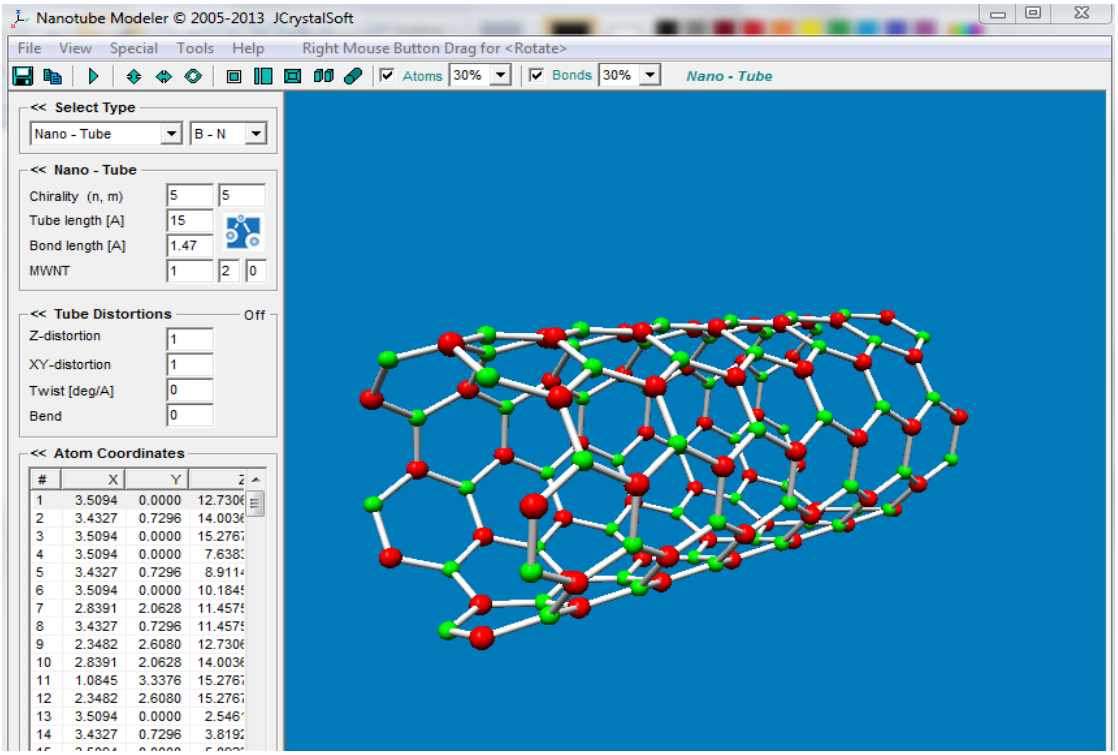

Fig. 3.11. Nanotube Modeler tool bar window.

Nanotube Modeler is capable of generating the coordinates of specific forms of BNNT with the variation in input parameters like type, length of the nanotube, bond length, bending of nanotube in order to model curved nanotubes, chirality and number of walls in order to model MWNT etc.

Although, BNNTs are hollow cylindrical tubes having hemispherical caps at both ends, but in the present analysis the caps are not considered and it is assumed that BNNTs are open at both ends. Various coordinate points corresponding to boron and nitrogen atoms are connected precisely in *ABAQUS* to get beam elements after importing the same to generate particular BNNT structure for analysis.

This method facilitates to construct any form of straight as well as wavy BNNT. From the preceding sections, it has been identified that excitation frequency are mainly affected by size (i.e. length and/or diameter) of the tube and boundary conditions. For the considered boundary conditions, it has been observed that the BNNT system excites at different frequencies due to variation in equivalent stiffness values for the two cases.

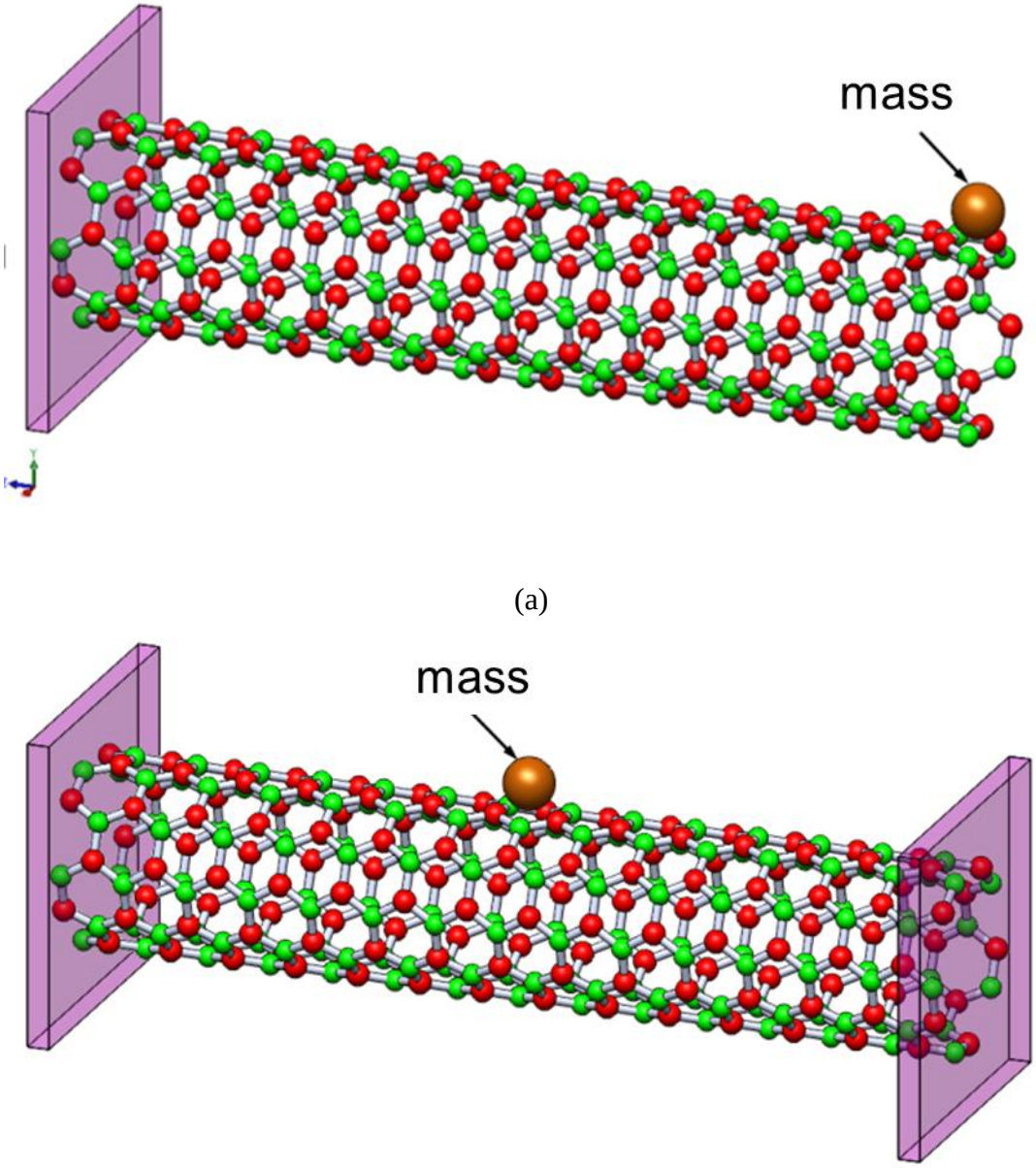

(a)

(b)

Fig. 3.12. Hybrid model of SW-BNNT with attached mass (a) at tip of cantilever and (b) at centre of bridge configuration.

Figure 3.12 represents the molecular structural mechanics based model of the arm chair form of SW-BNNT with a mass attached on it for two different boundary conditions. Further, change in length also alters the stiffness of the BNNT, thus changing the resonance frequency shift. Addition of small mass also affects the resonance frequency of BNNT as discussed in the previous sections. All these parameters are considered as sources of vibration in BNNTs for analysing dynamic behaviour of SW-BNNT based nanoresonator in present work.

3.4. Dynamic analysis of defects present in single-walled boron nitride nanotube

The presence of defects in nanotubes can be one of the vibration generating sources apart from parametric excitations as discussed in *Chapter 1*. The dynamic behaviour of defective BNNTs can be precisely investigated by atomistic finite element model based on molecular structural mechanics. In this modelling approach, the atomic vacancy defectsare created by removing the corresponding atom(s), which is not possible in continuum mechanics-based approach. However, continuum mechanics approach is more convenient for investigating the effect of pin-hole defects on the dynamic behaviour of BNNT and such defects have also been considered in present work.

In this chapter, the vibrational behaviour of a SWBNNT is investigated considering atomic vacancy defects (single atom vacancies like boron atom or nitrogen atom vacancy and di-atomic vacancies corresponds to vacancy of one boron and adjacent one nitrogen atom) in context of their applicability as mass sensors. The cantilevered armchair (5, 5) and zigzag (10, 0) form of SW-BNNT with different vacancy defects has been modelled considering it as a space frame structure with three dimensional elements and point masses in such a way that the proximity of the model with the actual atomic structure of nanotube can be significantly retained. The finite element simulation approach is used to analyse the effect of vacancy defects like single atom vacancies (V_B – boron vacancy or V_N – nitrogen vacancy) and di-vacancies ($V_{B\text{-}N}$). Also, the resonant frequency shift due to different vacancy defects for different positions along the length with mass attached at the tip has been analysed.

Further, to elaborate the influence of atomic vacancy defect on resonant frequency, present work has also considered the effect of removal of one complete hexagonal ring consisting of six atoms (in equal proportion of boron and nitrogen atoms). The effect of multiple six atoms vacancy defect on resonance behaviour has been analysed for (14, 0) zigzag configuration of SW-BNNT with varying aspect ratios. Using present atomistic finite element based simulation approach; different atomic structures of BNNTs with various vacancy defects and different boundary conditions can be simulated efficaciously. The present resonant frequency-based analysis of defective SW-BNNTs is useful to develop the algorithm for the detection of the added mass at the tip of the nanotube as well as identification of the type of vacancy defect and its position along the length of the nanotube.

3.4.1 Atomic vacancy defects in SW-BNNT

It has been observed that BNNTs contain certain defects of nature similar to that of CNTs. Atomic vacancies arise in BNNTs when boron or nitrogen atoms are missing and such defects are called single atom vacancies. At the same time, absence of boron and adjacent nitrogen atom results in formation of di-atomic vacancy defect in BNNTs. Such atomic vacancies arise during electron irradiation while synthesizing the BNNTs. The extension of such vacancy defects in continuous manner further leads to the dislocation line as explained by Lee et al.,[42] and Zobelli et al.,[43].

For deep understandings of atomic vacancy defects, Zobelli et al.,[43] employed high-resolution electron microscopy (HREM) technique and density function theory (DFT) based calculation for investigating the structure of defective BNNTs and its formation energies. Further, it has been observed that defective BNNTs also possess remarkable properties like better magnetic properties and enhanced adsorption of chemical spices like H, O, CO, H_2, H_2O, and NH_3 as discussed by Wei et al.,[44].

The reactivity of defective BNNT was observed to be higher near the defective sides as compared to perfect one due to formation of vacancies and frustrated B-B and N-N bonds along with the local strain caused by pentagonal and heptagonal pairs in the case of Stone Wales defects. Zhao and Ding[45] clarified that better adsorption property of defective BNNTs are suitable for detection of various gases and molecules having mass of the order of zeptogram level and ideal for hydrogen storage in safe manner.

It was also mentioned that the atomic vacancy defects formed under electron irradiation in BNNTs are primarily BN di-vacancies. The properties of BNNTs with di-vacancies were explored in their study and surface reactivity was estimated toward various adsorbents through density functional theory calculations. This motivated to further explore the defective BNNTs through vibrational aspects for identifying the nature of various defects to explore suitability of defective BNNTs in nano-electronics.

The fabrication of single layer of hexagonal-boron nitride (h-BN) sheet was successfully achieved by Jin et al.,[46] through controlled energetic electron irradiation method. The atomic vacancy defects of triangular shape were resolved in h-BN sheet using transmission electron microscopy (TEM) of high resolution with corrected aberration and exit-wave reconstruction.

Fig. 3.13 displays the HREM images of a bundle of BNNTs showing the sign of vacancy defects such as single atom vacancies (V_B or V_N) and BN di-vacancy (V_{B-N}) for zigzag (14, 0) form of SW-BNNT [Zobelli et al.,43].

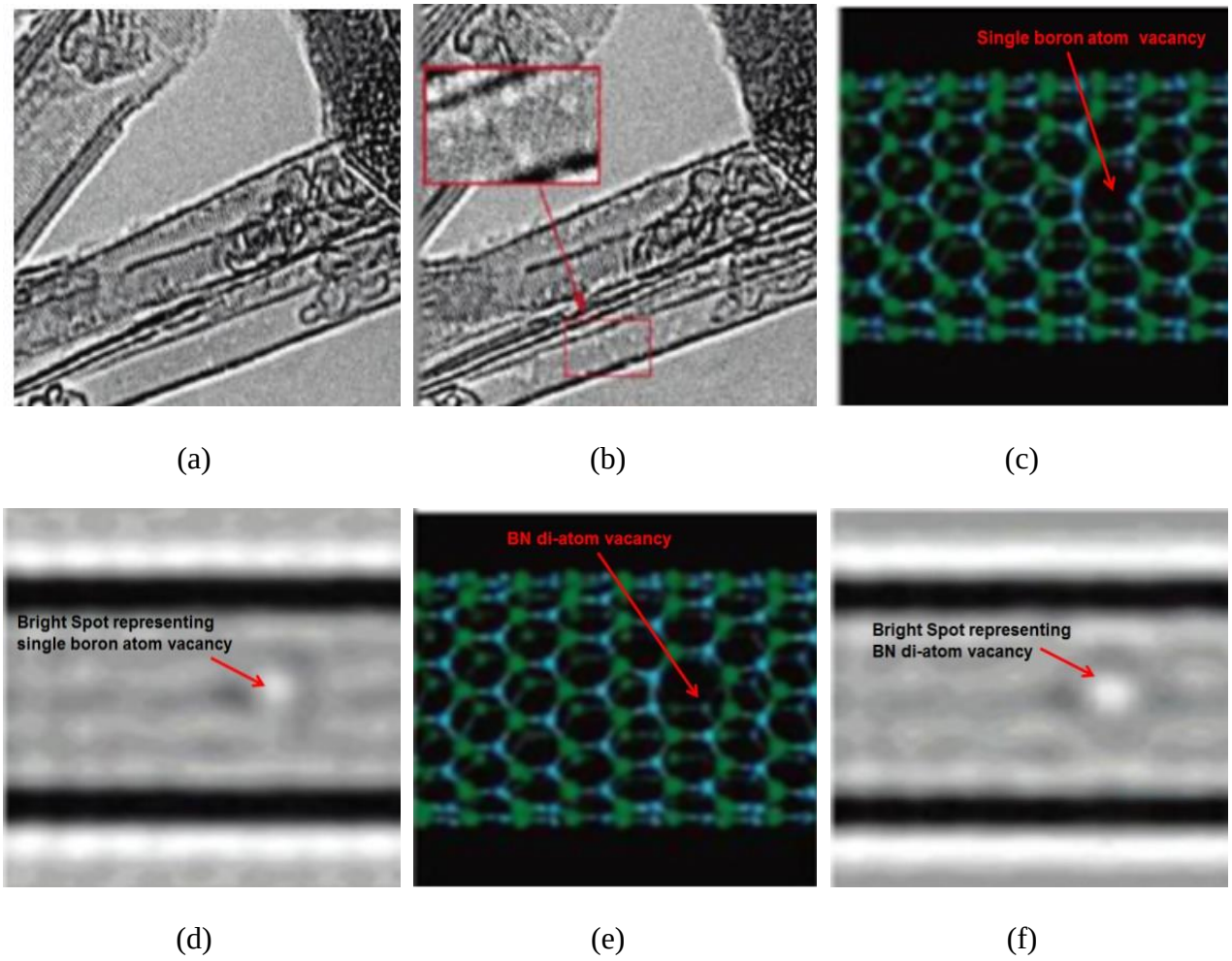

Fig. 3.13 (a) HREM images of a bundle of BN nanotubes for irradiation times of t = 0 s and t = 20 s. (b) Appearance of bright spots in HRTM image representing vacancy defect signature (c, d) Relaxed structures of single boron vacancy and its corresponding HREM simulated images of (14, 0) SW-BNNT (e, f) Relaxed structures of B-N di-vacancy and its corresponding HREM simulated images for a (14, 0) SW-BNNT [Zobelli et al.,43].

Fig. 3.14 represents reconstructed and simulated phase image of the vacancy prone area in which the dark region is representing missing atom in h-BN sheet. Such missing atom was assigned single boron atom vacancy (V_B) by Jin et al., (2009) and no nitrogen atom vacancy was observed.

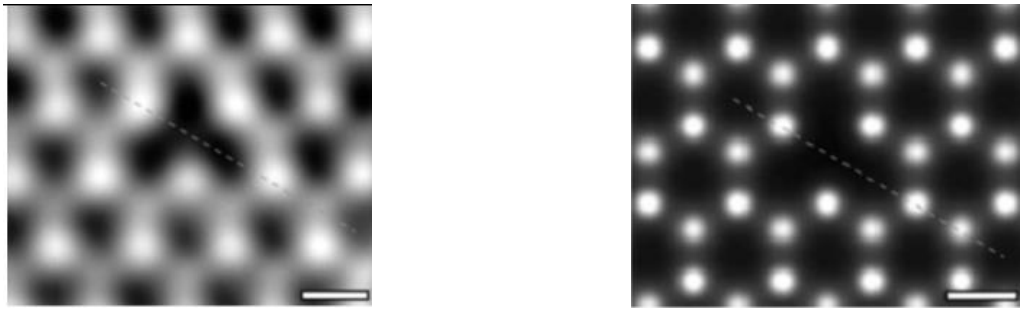

(a) (b)

Fig. 3.14. The phase images of a single boron atom vacancy (V_B) in h-BN layer at scale of 0.2 nm (a) reconstructed exit wave of a region and (b) simulated image [Jin et al.,46].

3.4.2 Effect of atomic vacancy defects on dynamics of SW-BNNT

A single atom vacancy defect corresponds to the removal of one atom (either boron or nitrogen atom) and three bonds associated with it, whereas di-vacancy defect refers to the removal of one boron and one adjoining nitrogen atom with seven associated bonds. These defects can be located along the length of BNNT at different positions and the number of such defects can vary. All such possibilities have been explored in the present work to analyse BNNT based system in a more realistic way.

Charlier[47] demonstrated the existence of various defects in CNTs. It has also been observed that similar to CNTs, experimental growth of BNNTs has resulted in various types of defects, such as atomic vacancies, foreign atom substitutions, and Stone-Wales (S-W) defects were described[48-51]. They experimentally found that vacancies and extended topological defects in the BNNTs can be formed by electron irradiation. Formation of S-W defects in BNNTs are due to application of large strain. Electronic structure modifications of BNNTs due to a single atom missing, di-atom vacancies, and S-W defects have been studied extensively Moradian and Azadi[52].

3.4.2.1 Development of finite element model for defective SW-BNNT using hybrid modelling approach

In any finite element model, the sectional modulus properties must be entered into the FE code at the elemental level. As mentioned earlier, the elemental properties of B-N bonds and their

material properties at the elementary level are not known. Therefore, hybrid modelling (i.e. molecular structural mechanics) approach is used to get these stiffness parameters associated with B-N bonds. The whole geometrical concept of creating a space frame model has been demonstrated above.

In the present work, two different BNNT structures (namely armchair and zigzag) with missing single boron/nitrogen atom or one BN bond have been investigated. The modelling of the defect is performed during the creation of the FE mesh where the necessary modifications in the nanotube lattice structure are made. The hybrid modelling approach has the ability to consider vacancy defects at multiple positions in the space frame model of SW-BNNT after necessary modifications in the nanotube lattice. After constructing the space frame structure, to model the non-reconstructed single atom-vacancy and di atom-vacancy defects, boron/nitrogen atom(s) and associated bonds are removed from the nanotube structure.

In the 3-D atomistic finite element space frame like model of SW-BNNT, each boron and nitrogen atom behaves like a node and a boron-nitrogen bond is represented by a beam element. The characteristic B-N bond length ($a_{B\text{-}N}$=0.145 nm) also representing the length of beam element has been used for the development of space frame model of BNNT as described above. Finally, the concept of hybrid approach is applied to incorporate the properties of beam element in the similar way as discussed in Table 3.4.

The defective SW-BNNT has been modelled using molecular structural mechanics approach as described above with the help of Nanotube Modeller and *ABAQUS* software. The vacancy defects have been created during modelling stage by removing atom(s) and associated beam elements as depicted in Fig. 3.15. The molecular structural mechanics based models of armchair SW-BNNT containing various atomic vacancy defects (V_B, V_N and $V_{B\text{-}N}$). In the structural model of defective BNNT, the nitrogen atoms nearer to the boron atom vacancy have one dangling bond and such atoms are connected by two adjoining boron atoms farther from the vacancy.

Similarly, the boron atoms nearer to the nitrogen atom vacancy have one dangling bond and such atoms are connected by two adjoining nitrogen atoms farther from the vacancy. The principle of operation of nanoresonator based on defective SW-BNNT rely on the fact that existence of vacancy defect(s) in SW-BNNT and its location influences the structural stiffness of

system which is responsible for the variation in resonance frequency. At the same time added mass at the free end of cantilevered SW-BNNT also changes its frequency.

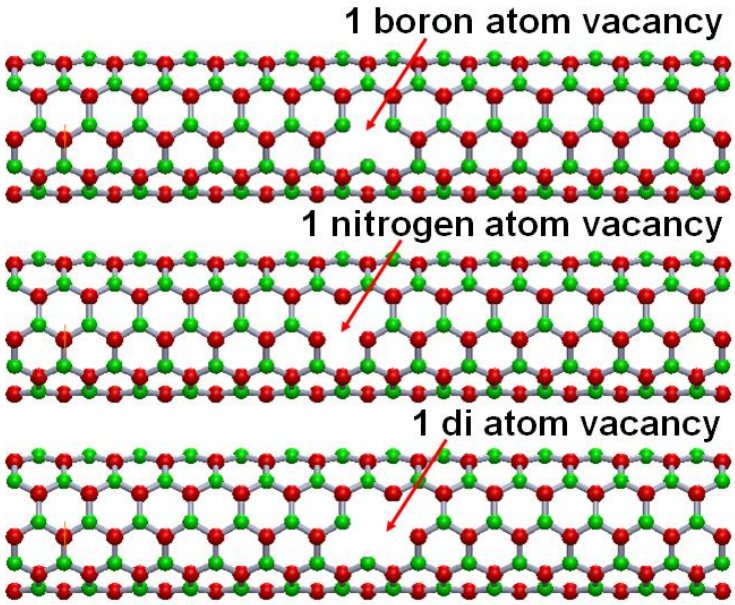

Fig. 3.15. Partial representation of different atomic vacancy defects in SW- BNNT.

Thus, such variation in resonance frequency due to the existence of vacancy defect along the tube length is helpful for identifying the types of defect (single or di-vacancy) and their locations which further extends in the development of an algorithm for defective SW-BNNT based sensory system.

The resonant frequency of defective SW-BNNT due to the presence of nitrogen vacancy (V_N) is slightly more than that of boron vacancy (V_B), because of a small mass difference between two atoms. Thus, the present work mainly is focused on the effect of boron atom vacancy on the resonance behaviour of SW-BNNT. At the same time Jin et al., (2009) also explained that it is easy to remove boron atom from BNNT.

Further, the present work also analyses the effect of increase in the number of missing atoms and varying aspect ratios (11, 13, 15, 17 and 19) on resonance frequency of BNNT. For this six atoms vacancy (i.e., removal of one complete hexagonal ring consisting of 3 boron and 3 nitrogen atoms) is created at a number of locations in the molecular structural mechanics model of zigzag (14, 0) BNNT.

In order to validate the developed model of SW-BNNT, present simulation results are compared with previously published data. For this, two different types of defects (type I and type II, representing removal of 3 and 12 pairs of BN di-vacancies respectively in BNNT structure) have been considered for zigzag (19, 0) and armchair (11, 11) BNNTs of cantilevered configuration. The resonance frequency analysis is performed for varying aspect ratios (AR=10, 15 and 20) and number of vacancy defects (1, 3, 5 and 7 defects). The effect of number of both types of defects as well as their location on resonance frequency of BNNT is investigated. The non-dimensional location (x/L_{bnnt}) of vacancy along the length of BNNT has been taken as 0.1, 0.3, 0.5, 0.7 and 0.9 from fixed end. The types of vacancy defects as considered in the present work for simulating the resonance behaviour of defective SW-BNNT are shown in Fig. 3..

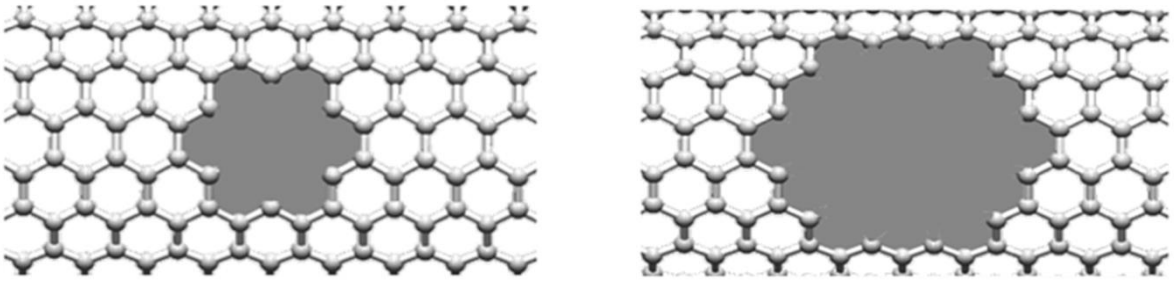

(a) (b)

Fig. 3.16. Types of vacancy defects (a) 3 pairs of BN di-vacancy and (b) 12 pairs of BN di-vacancy.

The atomistic model of BNNT is developed in such a manner that B-N bond representing beam element and all elastic properties as described above is applied on beam elements because of the fact that these are load carrying elements in the BNNT structure.

3.5 Results and discussion

3.5.1 Effect of single and di-atomic vacancy defect on SW-BNNT based mass sensor

Analysis of two different chiral forms of SW-BNNT (armchair and zigzag) with defects in the form of single and di-atom vacancies are performed by employing a hybrid approach as discussed above. The clamp-free BNNT is modelled by considering it as a space frame like structure similar to three dimensional beams and point masses. The position of atomic vacancies along the length of BNNT is varied for investigating the effect of location of the defect on

resonance frequency.The elastic beam properties are applied to B-N bond representing an elastic beam element and the mass properties to the nodes corresponding to boron and nitrogen atom.

Present work analyses three dimensional atomistic FE models of defective SW-BNNT of two different forms, viz., armchair (5, 5) and zigzag (10, 0) of aspect ratio 5 with single boron atom and di-atom vacancies, for investigating their effect on the dynamic behaviour of SW-BNNT. The position of atomic vacancy has been varied (i.e., at 25%, 50% and 90% of length from fixed end) in order to investigate the effect of location of defect along the length on the resonance behaviour of SW-BNNT. Further defective BNNTs have been analysed in such a way that the same can be used as nanomechanical resonator for detecting small mass of the order of femtogram level. For this,a small mass (varying from 10^{-20} to 10^{-25}kg) is attached at the tip of cantilevered SW-BNNT.

The variation in resonance frequency shift of (5, 5) SW-BNNT with one containing one boron atom vacancy has been plotted in Fig. 3.17. This clearly shows that as the position of defect moves toward free end there is substantial drop in frequency shift due to increase in resonance frequency and becomes negative at position of vacancy between 75% to 100% (value corresponding to position of defect at 90% of length from fixed end is shown in Fig. 3.17). This is because of the fact that stiffness variation becomes higher as position of atomic vacancy moves towards free end. This causes higher value of resonance frequency and approaches towards the value of the resonance frequency of defect free BNNT. Further, it becomes negative for vacancy position beyond 75% of length from fixed end because structural stiffness is of less significance near free end.

This clearly suggests that the exciting frequency of defective nanotube is more than that of a perfect one near the free end. The same phenomenon is observed for all the values of attached mass at the free end of cantilevered defective (5, 5) SW-BNNT.

In order to investigate the influence of di-atomic vacancy (i.e., removal of 1 BN-bond) on the dynamic behaviour of SW-BNNT, the variation in resonance frequency shift containing BN (di-atoms) vacancy with varying mass for three different positions of defect is plotted as shown in Fig. 3.18.

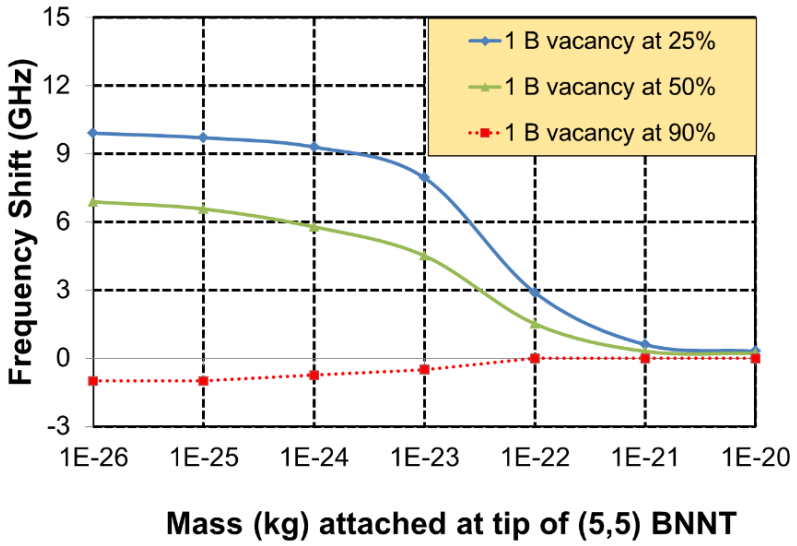

Fig. 3.17. Variation in resonance frequency shift of defective BNNT having 1 boron atom vacancy for three different positions from perfect (5, 5) SW-BNNT.

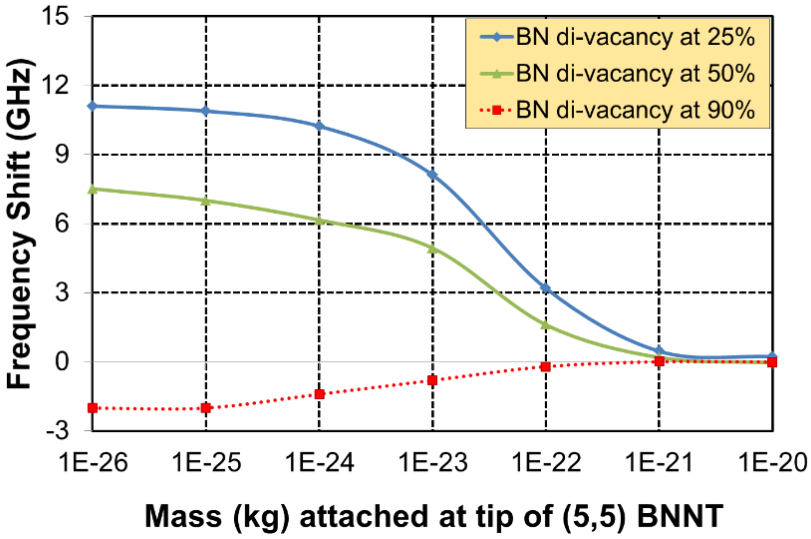

Fig. 3.18. Variation in resonance frequency shift of defective BNNT having BN (di-atom) vacancy for three different positions from perfect (5, 5) SW-BNNT.

It is observed that the influence of atomic vacancy is greatest when these are located near the fixed end of cantilevered BNNT. At the same time, it is also observed that the effect of vacancy defect is not significant beyond the value of attached mass of 10^{-20} kg.

For analysing the effect of the number of missing atoms in the SW-BNNT, the frequency shifts of single and di-atomic vacancies are compared as shown in Fig. 3.19. This clearly shows the resonance frequency shift corresponding to di-atomic vacancy is higher as compared to single boron atom vacancy for position of vacancy nearer to fixed end and this difference goes on decreasing as the position of vacancy moves towards free end.

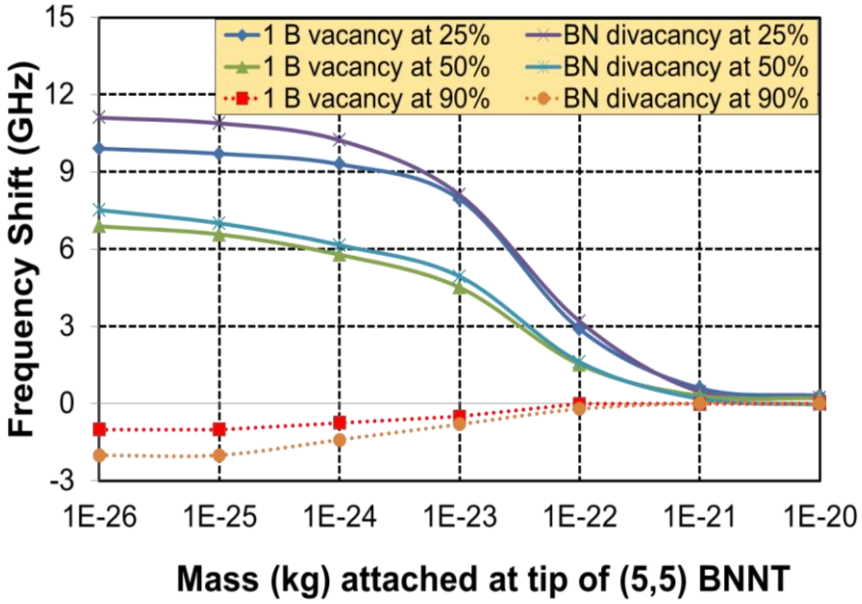

Fig. 3.19. Comparison of variation in frequency shift having single boron atom and BN di-vacancy at three different positions for (5, 5) BNNT.

Further, the present work also analyses the effect of chirality on defective BNNT by considering a zigzag (10, 0) BNNT with missing atoms. Fig. 3.20 represents a comparison of resonance frequency shifts of defective (10, 0) SW-BNNT between single boron atom vacancy and one BN (di-atoms) vacancy. The similar trend has been observed as seen for (5, 5) BNNT.

For zigzag configuration, it has been observed that there is no significant difference between resonance frequencies corresponding to single or di-atoms vacancy. This is because of the fact that structural stiffness is more significant in zigzag (10, 0) BNNT unlike an armchair form of BNNT (5, 5), in which it is less significant. Thus, for zigzag BNNT, mass as well as stiffness both contributes in the variation of frequency. The two forms of defective BNNTs as discussed above have been compared for single boron atom vacancy for three different locations of defect as shown in the bar chart (Fig. 3.21).

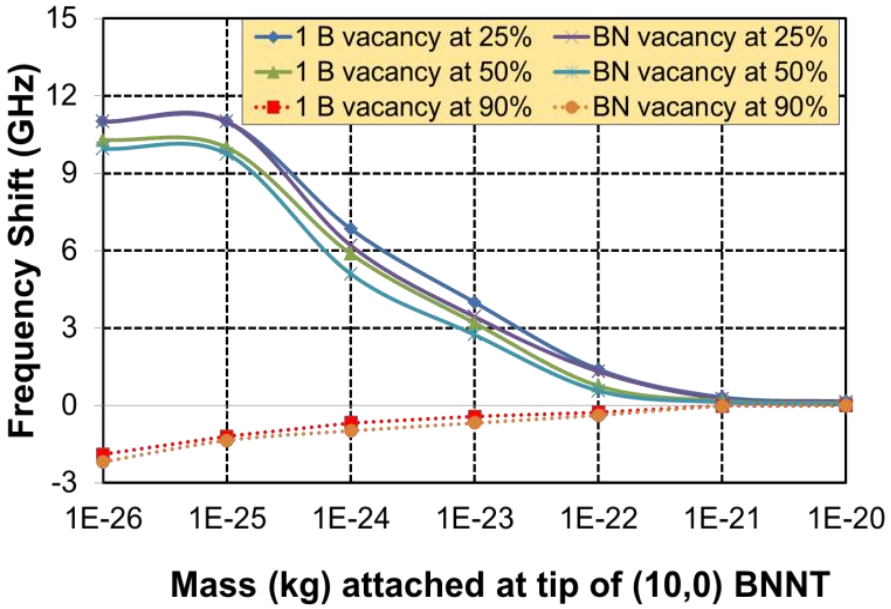

Fig. 3.20. Comparison of variation in frequency shift from perfect (10, 0) SW-BNNT having 1 (B atom) and 2 atoms (BN) vacancy at three different positions along the length.

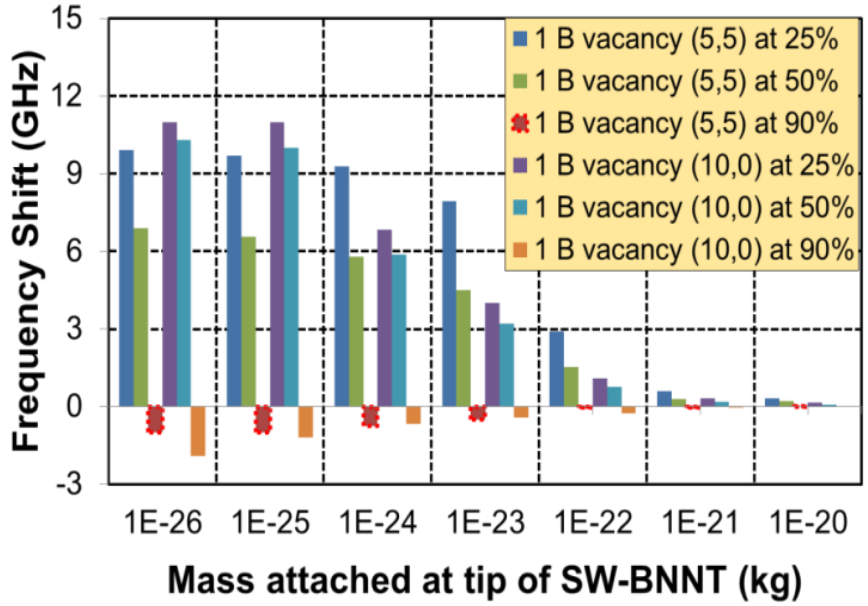

Fig. 3.21. Comparison of variation in frequency shift of (5, 5) and (10, 0) SW-BNNT having 1B atom vacancy at three different positions along the length.

In both forms of BNNT, it is observed that negative shift in resonance frequency arises for the position of vacancy near the free end. The value of this negative resonance frequency shift goes on decreasing with increasing value of mass attached at the free end and becomes

positive for mass beyond 10^{-22} kg. The negative resonance frequency shift indicates that the exciting frequency of defective BNNT is higher than that of pristine BNNT near free end.

3.5.2 Effect of number of atomic vacancies on SW-BNNT based mass sensor

In order to investigate the effect of increasing number of missing atoms (more than two atoms), present work also analyses the effect of six atom vacancy defect (i.e., removal of 3 pairs of BN bonds) for varying aspect ratio as well as varying number of such six atom vacancy on the dynamic behaviour of zigzag (14, 0) SW-BNNT.

Fig. 3.22 shows variation of the resonance frequency of defective zigzag (14, 0) SW-BNNT with varying aspect ratios and number of defects. It is observed that the resonance frequency decreases with increase in aspect ratio of BNNT, thus, suggesting the suitability of smaller size of BNNT in sensing applications.

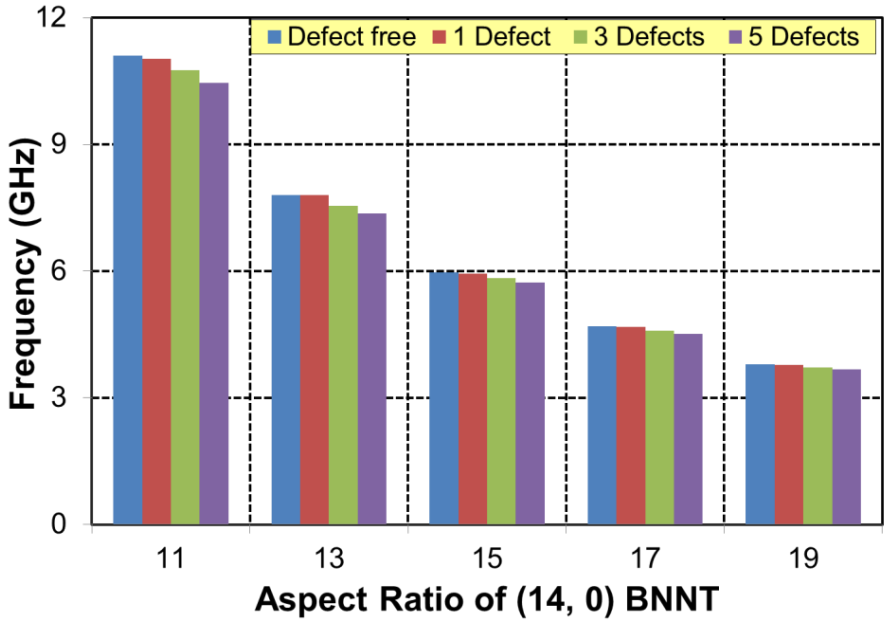

Fig. 3.22. Effect of aspect ratio on resonance frequency of (14, 0) SW-BNNT with varying number of 6 atom vacancy.

At the same time, it is also observed that increasing the number of defects along length of BNNT results in reduction of the resonance frequency. This is because increasing the number of defects causes the mass of BNNT to decrease resulting in increased frequency, but at the same time the structural stiffness goes on decreasing resulting in decrease in frequency. The overall

effect of reduction in resonance frequency with increasing number of defects suggests that the domination of stiffness is more than the mass of the system for a zigzag form of BNNT.

Further, it has been observed that the number of six atom vacancy defect for particular aspect ratio influences the resonance frequency. For 1 defect, the shift in frequency is very low and as the number of six atom vacancy defect increases; there is a substantial drop in frequency due to further reduction in structural stiffness of defective BNNT resulting in more frequent shift as depicted in Fig. 3.23.

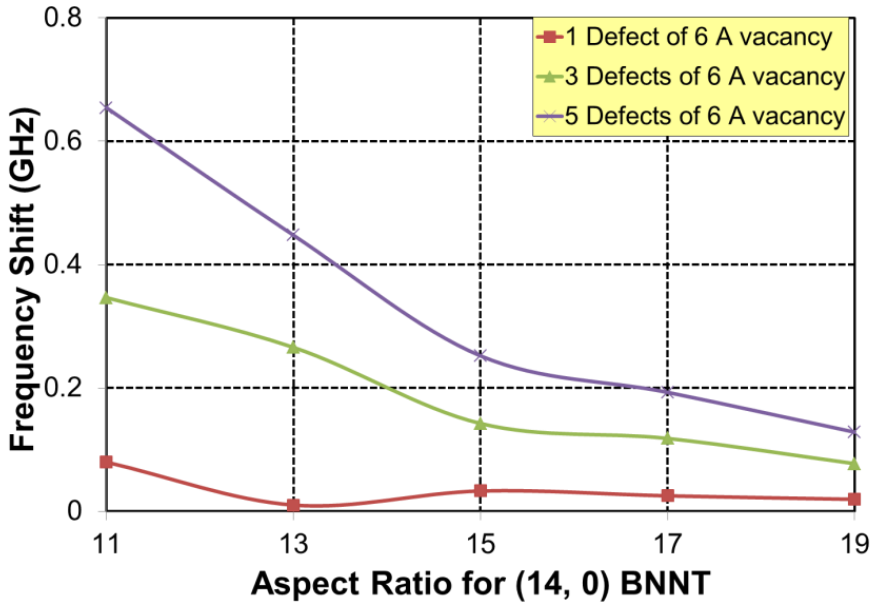

Fig. 3.23. Effect of aspect ratio on resonance frequency shift of defective (14, 0) SW-BNNT with perfect one at varying number of 6 atom vacancy.

The resonance frequency shift in defective (14, 0) BNNT with perfect one has been plotted in Fig. 3.23 for different aspect ratios. Simulation results reveal that resonance frequency shift is higher for more number of six atom vacancies and its value continuously decreases with increase in aspect ratio. However, this is not true for smaller aspect ratios having 1 defect of six atom vacancy, in which both mass and structural stiffness are equally dominating. It is found that for aspect ratio of 13, the shift is less as compared to higher value of aspect ratios. This indicates that the structural stiffness is less dominating then mass and due to presence of a defect (i.e., removal of six atoms) frequency increases and thus causes smaller shifts in frequency with defect free BNNT.

The present simulation approach as discussed is helpful for performing resonance frequency based analysis of BNNT in quantified manner. This helps in identifying the amount of mass added at the tip of cantilevered BNNT as well as the type of vacancy defect, whether single/di-atomic or six atom vacancy and location of vacancy along the length of BNNT.

From the obtained simulation results, it has been observed that the resonance frequency of BNNT is significantly affected by the types of vacancy defects as well as their position when varying mass is attached at the tip of cantilevered BNNT. Present work also analyses the shift in resonance frequency due to presence of vacancy in BNNT with defect free BNNT. It can be concluded that the resonance frequency shift continuously decreases as the position of vacancy moves towards the free end of BNNT. Finally, it has been observed that the resonance frequency shift becomes negative for the position of vacancy defect nearer to free end.

The simulation results of developed 3D atomistic FE model of defective BNNT have been compared with continuum mechanics based analytical results as discussed above. The trend of resonance frequency as obtained through simulation for different aspect ratio (L/D= 11, 13, 15, 17 and 19) for (14, 0) zigzag BNNT is following the same pattern as obtained analytically using the continuum mechanics approach as shown in Fig. 3.24.

The difference in values obtained by two approaches is attributed to the fact that chirality effect has been ignored in the continuum mechanics based analytical approach as it is not possible to incorporate the same. On the contrary, the present work has incorporated the chirality in developed molecular structural mechanics based model of SW-BNNT. The decreasing trend of resonance frequency with increase in aspect ratio is due to increase in mass of BNNT.

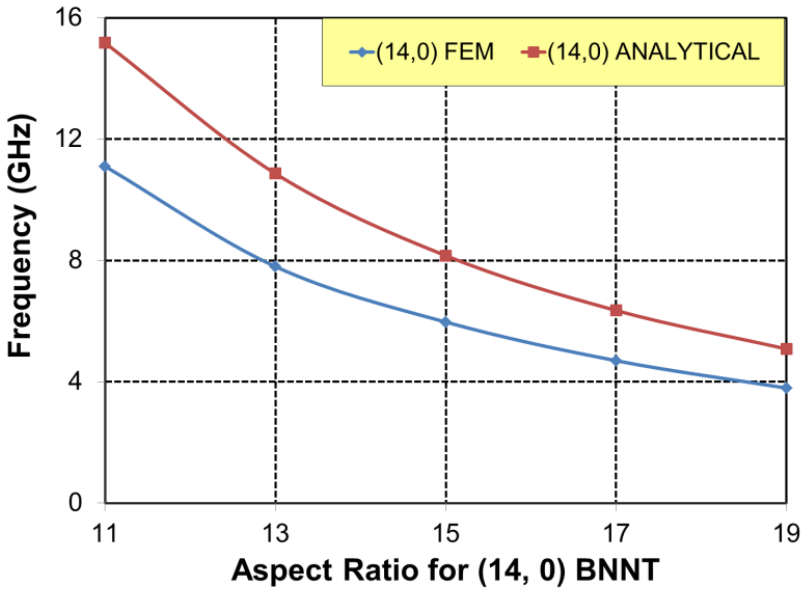

Fig. 3.24. Comparison of simulated and continuum mechanics based analytical frequency of (14, 0) zigzag SW-BNNT for different aspect ratios.

In order to validate the developed 3D atomistic model of BNNT, elastic modulus and density of BNNT has been considered as 1.18 TPa and 2180 kg/m^3, respectively in continuum mechanics based analytical approach. In order to maintain the equilibrium, the BNNT wall thickness should be less than the diameter of an atom. With this assumption, Vodenitcharova and Zhang (2003) used wall thickness as 43.4% of the theoretical diameter of a carbon atom (~0.142 nm) for SW-CNT. Since, the present work analyses SW-BNNT and both boron and nitrogen atoms are present at the side wall of actual BNNT, thickness of the continuum wall of BNNT should be smaller than the average diameter of boron and nitrogen atoms. The thickness of continuum wall has been taken as 0.064 nm (i.e., 43.4 % of the average value of the diameter of boron atom (~0.145 nm) and nitrogen atom (~0.150 nm) in order to maintain the equilibrium between two approaches. As a matter of fact, the stresses are transmitted through a continuous wall area in continuum mechanics model when it is subjected to an external load, but factually, only a few atoms (boron and nitrogen) are responsible for the transfer of such stresses in an actual BNNT.

The obtained analytical results for different aspect ratios are compared with the FE simulation results and close proximity has been found between the two approaches.

3.5.3 Effect of number of missing bn pairs on SW-BNNT based mass sensor

In order to investigate the effect of a number of missing BN pairs in BNNT, present work also analyses the influence of increasing number of missing BN bonds in SW-BNNT on its resonance behaviour. The impact of number of different types of vacancy defect (designated as type I and type II in the present work) and their positions along the length of cantilevered SW-BNNT of armchair (11, 11) and zigzag (19, 0) form have been investigated by considering the normalized frequency of SW-BNNTs. The location of defects has also been varied from fixed end of BNNT (i.e. 10%, 30%, 50%, 70% and 90% of the total length from fixed end). The resonance frequency based analysis has been performed for varying aspect ratios (AR=10, 15 and 20) of defective SW-BNNT. The simulated normalized frequency results of (11, 11) and (19, 0) BNNT with different vacancy defects for various aspect ratios are plotted against number of defects as shown in Fig. 3.25.

For type I defects in armchair (11, 11) BNNT, small variations in the normalized frequency have been observed up to three numbers of defect for aspect ratio of 15 and 20 as compared to 10, beyond this such variation is found to be significant and continuously increases as the number of defects exceeds three as shown in Fig. 3.25 (a). This is due to reduction in structural stiffness of BNNT with increasing number of defects in the case of armchair form. At the same time, it has also been observed that reduction in frequency is higher for aspect ratio of 10, i.e., for smaller BNNT. A similar trend has also been observed for type II defect in the armchair form of BNNT as depicted in Fig. 3.25 (b).

However, normalized frequency of the zigzag (19, 0) BNNT with type I defect increases with increase in the number of defects. This variation is higher for smaller size of BNNT, i.e., for aspect ratio of 10, as can be seen in Fig. 3.25 (a). This clearly suggests that mass is dominating over stiffness in the case of smaller size BNNTs thus making them suitable for sensing mass of the order of femtogram level. For type II defects, zigzag BNNT (19, 0) follows almost a similar trend as that of armchair BNNT (11, 11) beyond three defects as shown in Fig. 3.25 (b) but with larger reduction in frequency.

Thus, based on above, it can be concluded that the normalized frequency of armchair (11, 11) BNNT decreases with an increase in the number of defects of type I and type II. On the contrary, normalized frequency of zigzag (19, 0) BNNT increases with increase in the number of

type I defectsand decreases with increase in the number of type II defects in the same way as that of armchair BNNT for all considered aspect ratios.

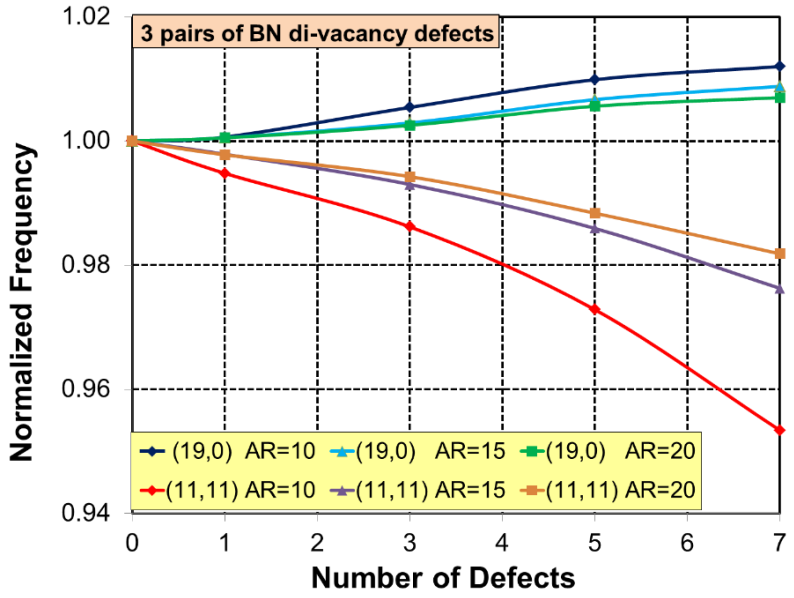

(a)

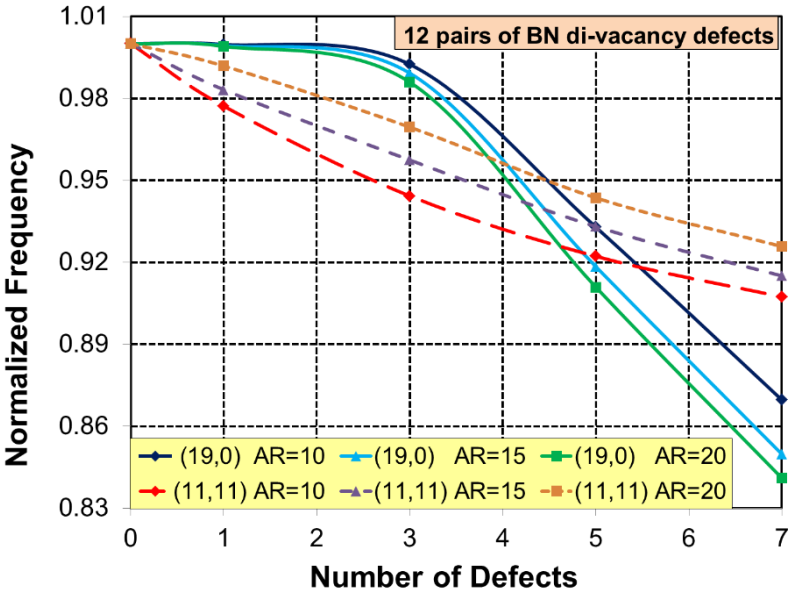

(b)

Fig. 3.25. Normalized frequency of (11, 11) and (19, 0) SW-BNNTs with a number of defects for (a) type I representing 3 pairs of BN di-vacancy and (b) type II defects representing 12 pairs of BN di-vacancy.

It has already been mentioned that location of defect also influences the resonance frequency of BNNT. In order to investigate the effect of the position of the defect on resonance frequency, the location of both types of defect has been varied in terms of percentage of the total length (i.e., 10, 30, 50, 70 and 90% from fixed end) of BNNT. Based on analysis performed for (11, 11) and (19, 0) SW-BNNT of different aspect ratios, it has been observed that as the position of defect moves from fixed end and approaches towards the free end of BNNT, its frequency increases for both types of defects considered. This happens because of large variations in structural stiffness of BNNT due to presence of defect and variation in its location. For the location of the defect nearer to fixed end, the frequency of BNNT containing type II defect is lower as compared to type I defect for all aspect ratios due to larger loss in structural stiffness.

As the position of defect in BNNT moves towards the free end its frequency increases.It has been observed that such increase in frequency is higher for BNNT containing type II defect. This is due to more gain in stiffness, thus lowering the difference in frequencies between the two types of defects. Further, it has been noticed for armchair (11, 11) BNNT that both types of defects behave in the same way when defect lies between 50% and 70% of BNNT's length for all aspect ratios.

The frequencies of both types of defects are same when defect is located at a distance of 55% of length from fixed end for aspect ratio of 10 as shown in Fig. 3.26 (a). On the contrary, for zigzag (19, 0) BNNT the range of defect position for which both types of defects behaves almost in similar fashion is observed as 40 to 70% for aspect ratio of 10 as shown in Fig. 3.26 (b). This indicates that the influence of types of defect on the resonance frequency is more significant in armchair BNNT. For higher aspect ratios, such equality in frequencies of both types of defects is observed when the defect position is shifted towards free end, i.e., at the defect location of 60% for (11, 11) and 50% for (19, 0) BNNT for aspect ratio of 15 as shown in Fig. 3.26 (c) and (d), respectively. For the location of the defect beyond 70% of length towards the free end, the frequency corresponding to type II defect is higher than that of type I defect due to the fact that in this zone reduction in mass is more dominating than stiffness for type II defect. For zigzag (19, 0) BNNT, influences of types of defect and their position differ from armchair (11, 11) BNNT. In zigzag BNNT, both types of defects show an almost similar effect on frequency for a wider range of location of defects (30% to 70% of length of BNNT) as depicted in Fig. 3.26 (b), (d) and (f).

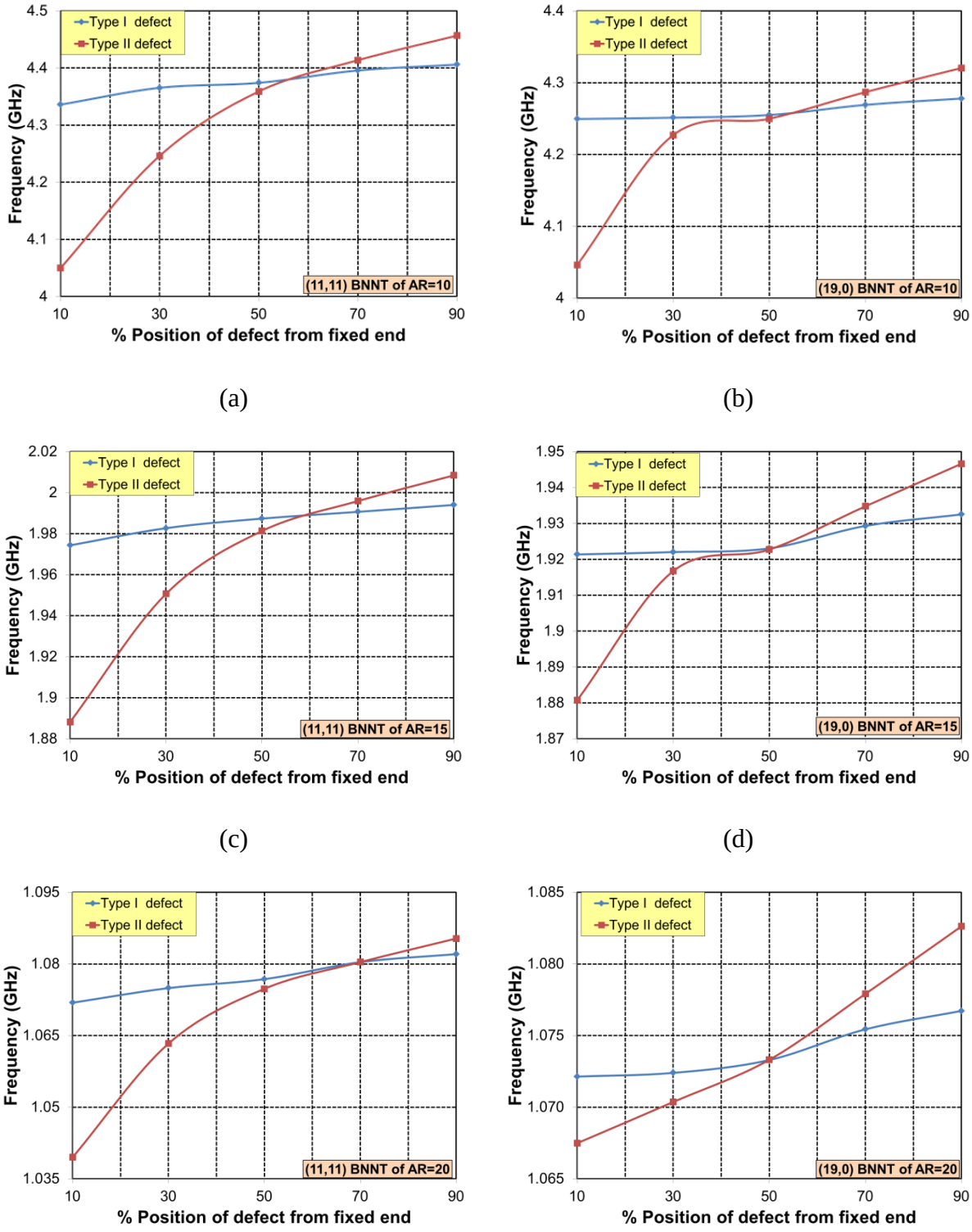

Fig. 3.26. Effect of defect position on frequency of SW-BNNT for different aspect ratios.

The frequencies for both types of defects are almost identical when defect is located at 50% (i.e., at centre) of length of BNNT, thus, it can be concluded that effect of types of defect does not influence the resonance behaviour of BNNT when its location is nearer to or at the centre. Fig. 3.27 clearly explains the comparison of frequency with different types of defect in both forms of BNNTs for varying positions of defect.

For both forms of BNNTs, it has been observed that influence of type II defect on frequency is more significant as compared to type I defect at positions near to fixed end for all aspect ratios as clearly shown in Fig. 3.27. A lower value of frequency has been observed for zigzag (19, 0) BNNT as compared to armchair (11, 11) BNNT for aspect ratio of 10 and 15 for the type I defect. This difference in frequency goes on decreasing with increasing length of BNNT.

In order to validate the molecular structural mechanics based 3D atomistic finite element models of type I and type II defective SW-BNNT, the simulation results have been compared with previously published molecular dynamics results using Tersoff-Brenner potential of Hirai et al.,[55] and continuum mechanics based results of Joshi et al.,[53,54]. Although, both the works are related to CNT, but it has already been mentioned that BNNTs are behaving in the similar way and also contain certain defects like CNT.

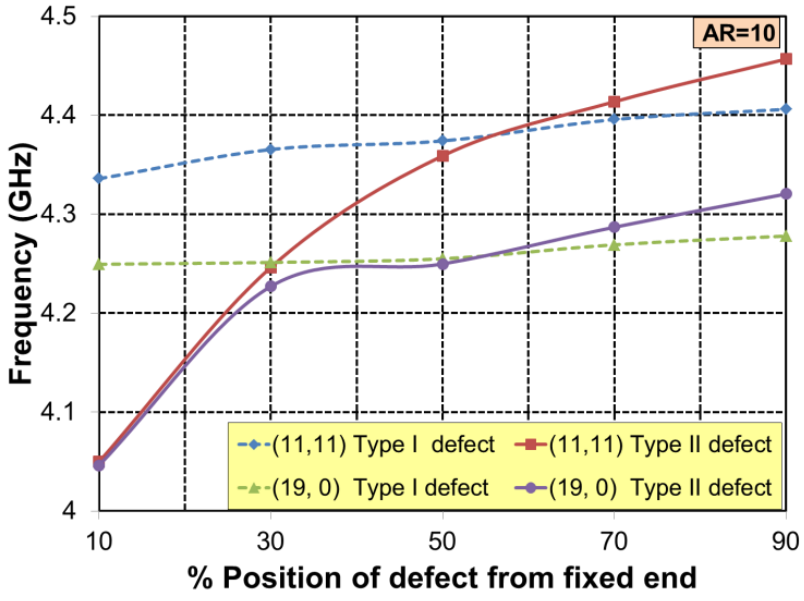

(a)

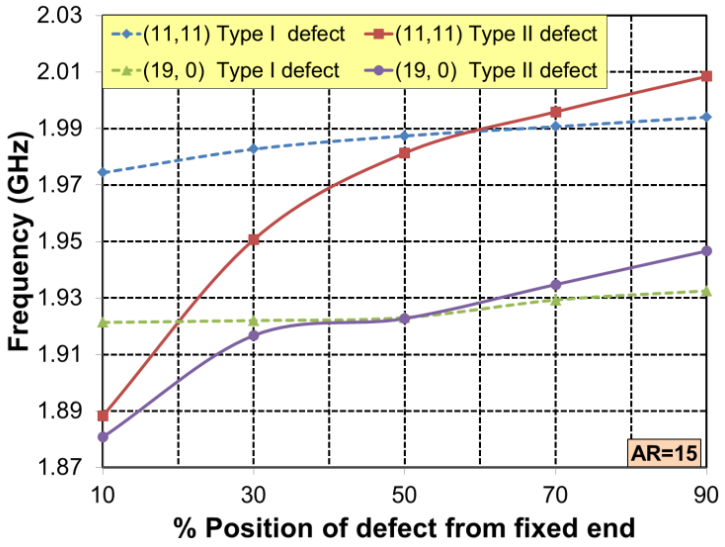

(b)

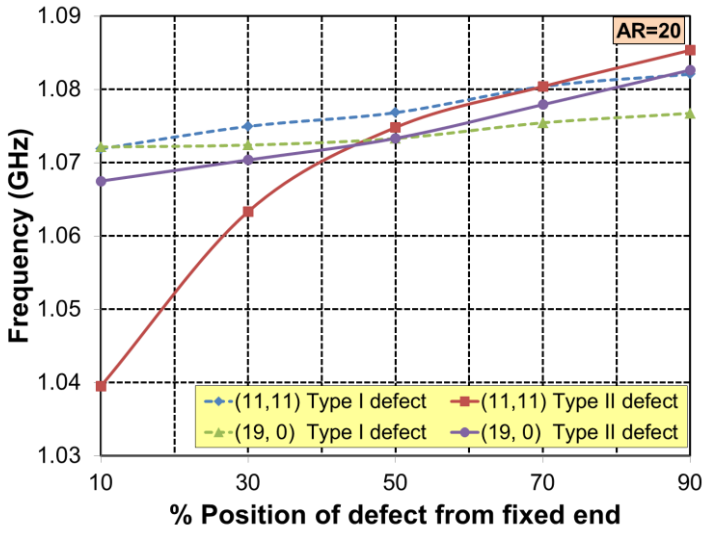

(c)

Fig. 3.27. Comparison of frequency of armchair (11, 11) and zigzag (19, 0) nanotubes with position of type I and type II defects for aspect ratio (a) AR=10, (b) AR=15 and (c) AR=20.

The present molecular structural mechanics based simulation results of cantilevered armchair (11, 11) BNNT are compared with continuum mechanics based results of Joshi et al.[53,54] as shown in Fig. 3.28 and similarity in trends is observed. The deviation in results is mainly due to incorporation of chirality in the present work which was not considered in continuum mechanics-based results of Joshi et al.,[53,54] and also due to slight differences in material properties of CNT and BNNT.

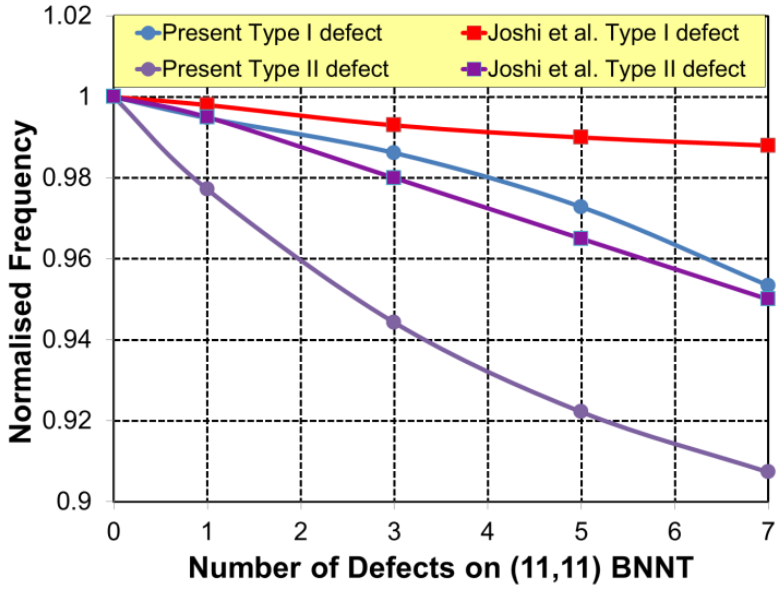

Fig. 3.28. Result validation of present approach with continuum approach of Joshi et al.,[53,54] for (11, 11) BNNT.

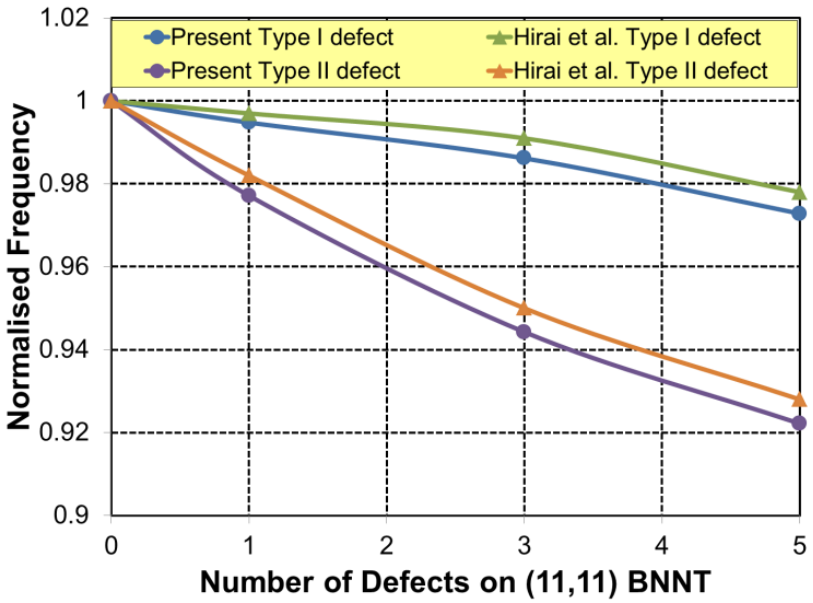

Fig. 3.29. Result validation of present approach with molecular dynamics approach of Hirai et al.,[55] armchair BNNT.

Present simulation is achieved in such a way that proximity of the actual atomic structure of BNNT can be significantly retained, thus giving more accurate results as compared to continuum mechanics approach.

Furthermore, the present simulation results are compared with molecular dynamics based results for (10, 10) SW-CNT as obtained by Hirai et al.,[55] for different types of vacancy defects and are found to be in close proximity as depicted in Fig. 3.29, thus validating the developed 3D atomistic finite element model of defective SW-BNNT. The small deviation in the results of both approaches is due to variation in type and diameters of SWNTs.

The comparison of present normalized frequency with Joshi et al.,[53,54] and Hirai et al.,[55] is shown in Fig. 3.30 for diameter of 15±0.1 nm. A close proximity has been observed with molecular dynamic simulation results of Hirai et al.,[55] as compared to continuum mechanics based results of Joshi et al.,[53,54] suggesting the exactness of the present model in order to retain the actual atomic structure of BNNT.

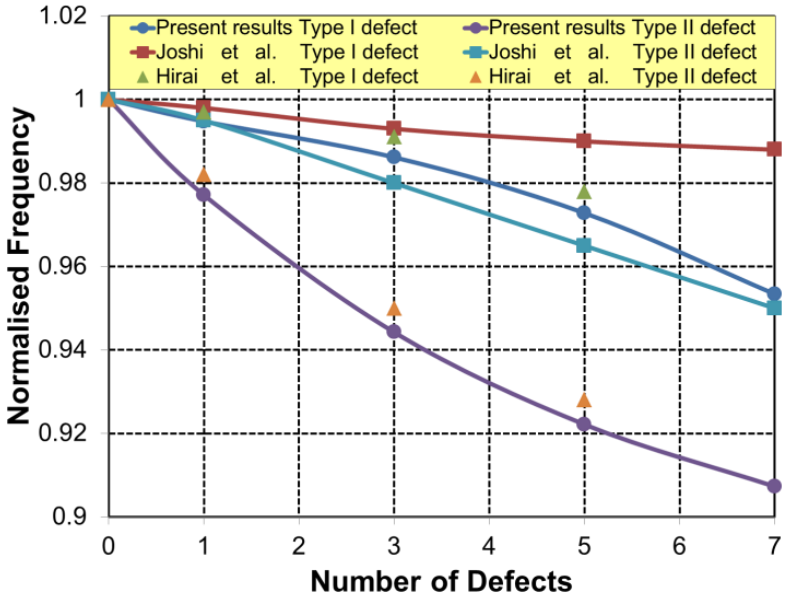

Fig. 3.30. Comparison of present simulation results of BNNT with Joshi et al.,[53,54] and Hirai et al.,[55] for diameter 1.5±0.1 nm.

3.6 Conclusions

In this chapter atomistic finite element simulation approach is found to be effective for performing the resonant frequency-based analysis of a defective SW-BNNT based nano-mechanical mass sensor. The obtained simulation results due to attached mass considering different types of vacancy defect (V_B, 1 V_{BN}, 3 pairs of V_{BN} and 12 pairs of V_{BN}) and their

positions along the length of the SW-BNNT are suitable to develop an algorithm for the detection of the attached mass, to identify the type of vacancy defect and its position.

- The present atomistic finite element approach is validated with continuum mechanics based analytical approach for resonant frequency based analysis and are found to be in excellent agreement. A mass sensitivity of 10^{-25} kg using SW-BNNT based nano mechanical mass sensor is observed. The enhancement in mass sensitivity of defective SW-BNNT based mass sensor is possible by using smaller size of BNNT.
- Substantial drop in frequency shift is observed when the position of defect moves toward the free end. This is due to increase in resonance frequency and finally shift becomes negative at vacancy position nearer to free end. This indicates that the excitation frequency of defective BNNT is larger near the free end as compared to pristine one.
- Resonant frequency due to presence of di-vacancy (removal of 1 pair of B-N bond) is larger as compared to the presence of single atom vacancy (removal of either boron or nitrogen atom) for all the considered positions of the defect along the length of nanotube. The difference in frequencies due to presence of V_{BN} and V_B decreases as the position of vacancy moves from fixed end to the free end of the cantilevered configuration of SW-BNNT. In the middle portion of the nanotube, the difference in resonant frequencies due to single atom vacancies (V_B and V_N) is significant for the value of attached mass greater than 10^{-23} kg.
- For both armchair and zigzag BNNTs, it is observed that influence of type II defect on the resonance frequency is more significant as compared to type I defect for positions nearer to fixed end irrespective of aspect ratios.
- The present simulation approach as discussed above is helpful for performing resonance frequency based analysis of BNNT in a quantified manner. This helps in identifying the amount of mass added at the tip of cantilevered BNNT, the type of vacancy defect, whether single/di-atomic or six atom vacancy and location of vacancy along the length of BNNT.
- It is observed that the shift in resonant frequency is relatively large for variation in length of BNNT from 20 nm to 40 nm, whereas it is small for larger lengths.

REFERENCES

[1] Lu, C. and Czanderna W., Applications of Piezoelectric Quartz Crystal, 1984, Elsevier, New York.

[2] Benes, E., Groschl, M., Burger, W., and Schmid, M., Sensors based on piezoelectric resonators, Sensors & Actuators A: Physical, vol. 48, 1995, pp. 1-21.

[3] Thundat, T., Oden, P. I. and Warmack, R. J., Microcantilever sensors, Microscale Thermophysics Engineering, vol. 1, 1997, pp. 185-199.

[4] Hauptmann P., Lucklum, R., Puttmer, A., and Henning, B., Ultrasonic sensors for process monitoring and chemical analysis: state-of-the-art and trends, Sensors and Actuators A, vol. 67, 1998, pp. 32- 48.

[5] Wenzel S. W. and White R. M., Analytic comparison of the sensitivities of bulk-wave, surface-wave, and flexural plate-wave ultrasonic gravimetric sensors, Applied Physics Letters, vol. 54, 1989, pp. 1976- 1978.

[6] Ilic, B., Czaplewski, D., Craighead, H. G., Neuzil, P., Campagnolo, C. and Batt, C., Mechanical resonant immunospecific biological detector, Applied Physics Letters, vol. 77, 2000, pp. 450-452.

[7] Lavrik, N. V. and Datskos, P. G., Femtogram mass detection using photothermally actuated nanomechanical resonators, Applied Physics Letters, vol. 82, 2003, pp. 2697-2699.

[8] Li, C. and Chou, T.W., A structural mechanics approach for the analysis of carbon nanotubes. International Journal of Solids and Structures, vol. 40, 2003a, pp. 2487–2499.

[9] Sohlberg, K., Sumpter, B.G., Tuzun, R.E. and Noid, D.W., Continuum methods of mechanics as a simplified approach to structural engineering of nanostructures, Nanotechnology, vol. 9, 1998, pp. 30-36.

[10] Li, C. and Chou, T.W., A structural mechanics approach for the analysis of carbon nanotubes. International Journal of Solids and Structures, vol. 40, 2003a, pp. 2487–2499.

[11] Li, C. and Chou, T.W., Vibrational behaviors of multiwalled-carbon nanotube based nanomechanical resonators, Applied Physics Letters, vol. 84, 2003c, pp. 121-123.

[12] Chowdhury R., Adhikari S. and Mitchell J., Vibrating carbon nanotube based bio-sensors, Physica E: Low-dimensional Systems and Nanostructures, vol. 42, (2), 2009, pp. 104-109.

[13] Sakhaee-Pour, A., Ahmadian, M.T. and Vafai, A., Vibrational analysis of single-walled carbon nanotubes using beam element, Thin-Walled Structures, vol. 47, 2009, pp. 646–652.

[14] Georgantzinos, S.K. and Anifantis N.K., Carbon nanotube-based resonant nanomechanical sensors: A computational investigation of their behavior, Physica E: Low Dimensional Systemsand Nanostructures, vol. 42, 2010, pp. 1795–1801.

[15] Boldrin, L., Scarpa, F., Chowdhury, R. and Adhikari, S., Effective mechanical properties of hexagonal boron nitride nanosheets, Nanotechnology, vol. 22, 2011, pp. 505702.

[16] Qian, D., Wagner, G. J., Liu, W. K., Yu, M. F. and Ruoff, R. S., Mechanics of carbon nanotubes, Applied Mechanics Reviews, vol. 55, 2002, pp. 495-533.

[17] Girifalco, L.A., Hodak, M. and Lee, R.S., Carbon nanotubes, buckyballs, ropes and a universal graphitic potential, Physical Review B, vol. 62, 2000, pp. 13104-13110.

[18] Qian, D., Liu, W.K., Subramoney, S. and Ruoff, R.S., Effect of inter-layer potential on mechanical deformation of multiwalled carbon nanotubes, Journal of Nanoscience & Nanotechnology, vol. 3, 2003, pp.185-191.

[19] Hodak, M. and Girifalco, L.A., Fullerenes inside carbon nanotubes and multi-walled carbon nanotubes: Optimum and maximum size, Chemical Physics Letters, vol. 350, 2001, pp. 405-411.

[20] Leamy, M.J., Bulk dynamic response modeling of carbon nanotubes using an intrinsic finite element formulation incorporating interatomic potentials, International Journal of Solids and Structures, vol. 44, 2007, pp. 884-894.

[21] Arroyo, M. and Belytschko, T., Finite crystal elasticity of carbon nanotubes based on exponential Cauchy-Born rule, Physical Reviews B, vol. 69, 2004, pp. 115415.

[22] Zhang, P., Huang, Y., Geubelle, P.H., Klein, P.A. and Hwang, K.C., The elastic modulus of single-walled carbon nanotubes: a continuum analysis incorporating interatomic potentials, International Journal of Solids and Structures, vol. 39, 2002, pp. 3893-3906.

[23] S. Trivedi, S. C. Sharma, and S. P. Harsha, “Single walled-boron nitride nanotubes based nanoresonator for sensing of acetone molecules,” Nano, vol. 9, no. 8, p. 1450086, Dec. 2014, doi: 10.1142/S1793292014500866.

[24] Witkamp, B., Poot Me. and Herre S.J., Bending-Mode Vibration of a suspended Nanotube resonator, Nano Letters, vol.6, (12), 2006, pp. 2904-2908.

[25] Gere, J.M. and Timoshenko, S.P, Mechanics of Materials (fifth edition). Brooke/Cole, 2000.

[26] Li C. and Chou T.W., Atomistic modeling of carbon nanotube-based mechanical sensors, Journal of Intelligent Materials System and Structures, vol. 17, 2006, pp 247-254.

[27] Li, C. and Chou, T., Static and Dynamic Properties of Single-Walled Boron Nitride Nanotubes, Journal of Nanoscience and Nanotechnology, vol. 6, 2006, pp. 54-60.

[28] Bodily, B. H. and Sun, C.T., Structural and equivalent continuum properties of single-walled carbon nanotubes, International Journal of Materials and Product Technology, vol. 18, 2003, pp. 381-397.

[29] Odegard, G. M., Gates, T. S., Nicholson, L. M., and Wise, K. E., Equivalent continuum modeling of nano-structured materials, Composites Science and Technology, vol. 62, (14), 2002, pp. 1869–1880.

[30] Chowdhury R., Adhikari S. and Mitchell J., Vibrating carbon nanotube based bio-sensors, Physica E: Low-dimensional Systems and Nanostructures, vol. 42, (2), 2009, pp. 104-109.

[31] Rappe, A.K. and Goddard W.A., Charge Equilibration for Molecular Dynamics Simulations, Journal of Physical Chemistry, vol. 95, 1991, pp. 3358.

[32] Sánchez-Portal, D. and Hernández, E., Vibrational properties of single-wall nanotubes and monolayers of hexagonal BN, Physical Review B, vol. 66, 2002, pp. 235415.

[33] Wirtz, L., Rubio, A., Concha R.A. de la and Loiseau, A., Ab initio calculations of the lattice dynamics of boron nitride nanotubes, Physical Review B, vol. 68, 2003, pp. 045425.

[34] Moon, W. and Hwang, H., Molecular mechanics of structural properties of boron nitride nanotubes, Physica E: Low-Dimensional Systems and Nanostructures, vol. 23, 2004, pp. 26-30.

[35] Cornwell, C.F. and Wille, L.T., Elastic properties of single-walled carbon nanotubes in compression, Solid State Communications, vol. 101, 1997, pp. 555-558.

[36] Rappe, A.K., Casewit, C.J., Colwell, K.S. Goddard, W.A. and Skiff, W.M., UFF, a Full Periodic Table Force Field for Molecular Mechanics and Molecular Dynamics Simulations, Journal of American Chemical Society, vol. 114, 1992, pp. 10024.

[37] Blase, X., Rubio, A. Louie. S. and Cohen, M.L., Stability and Band Gap Constancy of Boron Nitride Nanotubes, Europhysics Letters, vol. 28, 1994, pp. 335.

[38] Baumeier, B., Krüger, P. and Pollmann, J., Structural, elastic, and electronic properties of SiC, BN, and BeO nanotubes, Physical Review B, vol. 76, 2007, pp. 085407.

[39] Zhang, Z.H., Guo, W.L. and Dai, Y.T., Freestanding (3, 0) boron nitride nanotube: Expected to be stable well over room temperature. Applied Physics Letters, vol. 93, 2008, pp. 223108.

[40] Zhang, Z.H., Guo, W.L. and Dai, Y.T., Stability and electronic properties of small boron nitride nanotubes, Journal of Applied Physics, vol. 105, 2009, pp. 084312.

[41] Jiang, L and Guo, W., A molecular mechanics study on size-dependent elastic properties of single-walled boron nitride nanotubes, Journal of the Mechanics and Physics of Solids, vol. 59, 2011, pp. 1204–1213.

[42] Lee, R.S., Gavillet, J., Chapelle, M.L., Loiseau, A., Cochon, J.L., Pigache, D., Thibault, J. and Willaime, F., Catalyst-free synthesis of boron nitride single-wall nanotubes with a preferred zigzag configuration, Physical Review B, vol. 64, 2001, pp. 121405.

[43] Zobelli, A., Ewels, C.P., Gloter, A., Seifert, G., Stephan, O., Csillag, S. and Colliex, C., Defective structure of BN nanotubes: from single vacancies to dislocation lines, Nano Letters, vol. 6 (9), 2006, pp. 1955–1960.

[44] Wei, A, Wu, X, Yang, J. L. and Zeng, X. C., Adsorption and Surface Reactivity on Single-Walled Boron Nitride Nanotubes Containing Stone-Wales Defects, Journal of Physical Chemistry C, vol.111, 2007, pp. 14105-14112.

[45] Zhao, J.X. and Ding, Y.H., The effects of O_2 and H_2O adsorbates on field-emission properties of an (8, 0) boron nitride nanotube: a density functional theory study, Nanotechnology, vol. 20, No. 8, 2009, pp. 85704.

[46] Jin, C., Lin, F., Suenaga, K. and Iilima, S., Fabrication of a freestanding boron nitride single layer and its defect assignments, Physical Review Letters, vol. 102, 2009, pp. 195505.

[47] Charlier, J.C., Defects in Carbon Nanotubes. Accounts of Chemical Research, vol. 35, 2002, pp. 1063–1069.

[48] Sainsbury, T., Ikuno, T., Okawa, D., Pacile, D., Frechet, J.M.J. and Zettl, A., Self-Assembly of Gold Nanoparticles at the Surface of Amine- and Thiol-Functionalized Boron Nitride Nanotubes, Journal of Physical Chemistry C, vol. 111, 2007, pp. 12992–12999.

[49] Schmidt, T.M., Baierle, R.J., Piquini, P. and Fazzio, A., Theoretical study of native defects in BN nanotubes, Physical Review B, vol. 67, 2003, pp. 113407–113410.

[50] Piquini, P., Baierle, R.J., Schmidt, T.M. and Fazzio, A., Formation energy of native defects in BN nanotubes: An ab initio study, Nanotechnology, vol. 16, 2005, pp. 827–831.

[51] Miyamoto, Y., Rubio, A., Berber, S., Yoon, M. and Tomanek, D., Spectroscopic characterization of Stone-Wales defects in nanotubes, Physical Review B, vol. 69, 2004, pp. 121413–121416.

[52] Moradian, R. and Azadi, S., Magnetism in defected single-walled boron nitride nanotubes, Europhysics Letters, vol. 83, 2008, pp. 17007–17011.

[53] Joshi, A.Y., Sharma, S.C. and Harsha, S.P., The Effect of Pinhole Defect on Dynamic Characteristics of Single Walled Carbon Nanotube Based Mass Sensors, Journal of Computational and Theoretical Nanoscience, vol. 8, 2011, pp. 776.

[54] Joshi, A.Y., Sharma, S.C. and S.P. Harsha, The effect of pinhole defect on vibrational characteristics of single walled carbon nanotube, Physica E, vol. 43, 2011, pp. 1040–1045.

[55] Hirai Y. and Nishimaki S., Molecular Dynamics Studies on Mechanical Properties of Carbon Nano Tubes with Pinhole Defects, Japanese Journal of Applied Physics, 42, 2003, pp. 4120 - 4123.

CHAPTER 4

Non-Linear Vibrational Analysis of Curvy Single-Walled Boron Nitride Nanotube Using Different Response Tools

4.1 Introduction

Boron nitride nanotubes (BNNTs) have similar mechanical properties as carbon nanotubes with the added benefits of biosafety, bio-sensing applications and biocompatibility. Biocompatibility refers to the ability of a material to perform with an appropriate host response in a specific application. BNNTs have been shown to be non-toxic and non-immunogenic, meaning they do not produce an adverse immune response in the body[1-3]. While more research is needed to fully understand the biocompatibility and bio safety of BNNTs, these initial findings suggest that they have potential for use in a variety of biomedical applications, such as drug delivery and tissue engineering. It is important to note, however, that the biocompatibility, bio-sensing applications and bio safety of BNNTs can depend on a number of factors, including the size, shape, and surface properties of the nanotubes, as well as the specific application and the host environment[4-6].

BNNTs have better high-temperature thermal and electrical stability than CNTs. BNNTs' outstanding qualities make them ideal for biomedicine, NEMS, sensor systems, and composites[7]. The special features of BNNT like its homogenous structure; delivers strength with less weight, more toughness and durability. These features make its prominent use as composite structure’s fibers, hydrogen storage, nanodevices, high frequency microchemical oscillators. BNNTs have shown no long-lasting damage to the atomic structure while experiencing nonlinear deformations or warping. It has shown remarkable thermal conductivity. Exceptional sensitivity for inertial mass sensing is provided by Very high frequency (VHF) nano electrochemical systems (NEMS). It was found that the SWBNNT provides the best mass resolution which relates to 30 xenon atoms[8,9].

Tuzun et al. considered BNNT as a solid cylinder beam and discovered its free vibrational behavior. The Eigen values of BNNT free vibration were found by using Euler-Bernoulli beam theory. An elasticity solution of thin-walled cylinder was suggested by Mahan for Vibration

analysis[10-11]. At Atomic scale interactions, the atomistic approaches are more established than the continuum-based methods. Wu *et al.* studied and found the sensitivity of BNNT mass sensor in their investigation and reported the use of multiwall Boron Nitride nanotubes (MWBNNT's) as a mass sensor. They can be utilized for sensing and spotting of chiral molecules[12].
BNNTs aren't always perfect atomic structure. Vacancy defect like Boron and nitrogen single atom vacancies, boron-nitrogen di-vacancies, and extended line vacancies makes BNNT defective. Panchal et al. analysed the defective atomic structures of SWBNNTs for prospective mass-based sensor systems[13,14].

Wavy nanotube atomic structure (not straight) impacts mechanical properties. The existence of waviness in atomic structures impacts the mechanical characteristics of SWBNNTs by impacting the B-N bonds; the presence of waviness changes the twisting and stretching stresses of the B-N bonds, eventually modifying the stiffness in the region of waviness in the atomic structure[15]. The stiffness changes with the SW-BNNTs atomic structure. Varying SWBNNT stiffness influences its natural frequency. Thus, it's important to examine the effect of different forms of atomic waviness when analysing the natural frequencies of SWBNNTs for applications dependent on natural frequency variation (mass-based sensors systems). Researchers have only investigated sinusoidal wavy nanotube (CNTs and BNNTs) atomic structure [16,17].

The present study is also focused on studying the effects of various types of nonlinearity (i.e., mid-plane stretching and waviness) on the vibrational behaviour of doubly clamped SW- BNNT. Similar to SW-CNT, it is quite obvious that the SW-BNNT also have a wavy shape and such waviness indicates the existence of geometric nonlinearity and acts as a quadratic restoring force. Another type of nonlinearity is demonstrated in terms of a cubic restoring force that arises due to stretching of mid-plane when doubly clamped SW- BNNT vibrates.

A nonlinear mathematical model for analysing the wavy nature of SW- BNNT is developed and the dynamic responses are analysed using various tools like time series, phase space, Poincare section and Fast Fourier Transforms. Nanotubes are considered to have great impact on various nano-electromechanical (NEMS) applications like charge detection devices and oscillators as discussed by Pelesko and Bernstein. Therefore, there is a need to understand their dynamic behaviour in order to design future devices based on nanotubes[18].

In most of the previous studies, nanotubes were considered as perfectly straight beams / cylindrical shells, but due to process-induced waviness during manufacturing processes, these small nano-structures (nanotubes) contain a definite curvature along their length (Fig. 4.) as reported by Qian et al., and Joshi et al., also reported that a wavy CNT with and without attached mass shows periodic and different nonlinear behaviours. Therefore, a continuum mechanics based finite element model of wavy SW- BNNT for both cantilever and bridged configurations is proposed to investigate the effect of surface deviation like waviness on resonance frequency[19,21].

Saurabh Kumar et al. examined the vibrational properties of single-walled boron nitride nanotubes (SWBNNT) with surface deviation as waviness along its axis and confirmed their viability as nanomechanical sensors. The bridged and cantilevered configurations were taken into consideration and their resonant frequencies were calculated[22,23]. Jiger et al. conducted a study in which Continuum modelling based analytical and finite element method (FEM) simulation approaches were used to estimate the natural frequencies of various modes of vibration of SWBNNTs with different types of wavy curvatures including sinusoidal, elliptical, and parabolic waviness.

The observed results implied that regardless of the kind of waviness, natural frequencies rise as the degree of curvature (e/l) increases[24]. Unnati A. Joshi et al. investigated the impact of wavy carbon nanotubes on mechanical characteristics such as elasticity and strength aspects for nanocomposites. It was implicated that waviness greatly lowers the effective reinforcement of the nanocomposites; it was demonstrated that the waviness can greatly impair the stiffening effect of the nanotubes[25].

Anand Y. Joshi et al studied the nonlinear vibrational behavior of mass sensors based on single-walled carbon nanotubes and examined an analytical model of a bridged CNT with surface variations. The connected mass and the geometrical distortion of the CNT are the major causes of the system's excitation. Instability and chaos in the dynamic reaction were found. It was evident that the surface deviations and attached mass affect the regions of periodic, subharmonic, and chaotic behaviour. Frequency spectra and Poincare maps were used to explain and illustrate the variety of system behaviour[26].

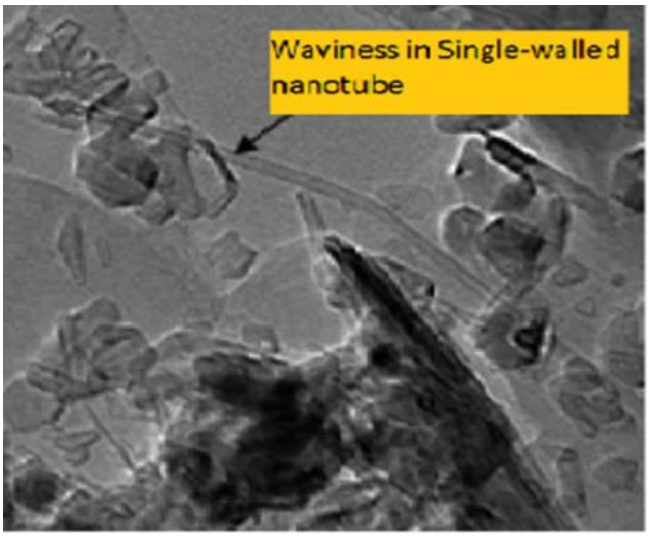

Fig. 4.1. Transmission electron microscope (TEM) image of a nanotube indicating the waviness [J. Ning et al., 27].

4.1.1. Development of finite element model for wavy SW-BNNT using continuum mechanics approach

In order to investigate the effect of waviness, continuum mechanics-based model of cylindrical shape with small thickness have been developed in the present work. The value of mass attached at the tip of cantilevered configuration and at its mid position for bridged boundary condition has been varied so that the same can be used as a mass sensor. The analysis has been performed for three different lengths (L=20, L=40 and L=60 nm) of wavy SW-BNNT having small thickness. The thickness of SW-BNNT is taken in such a way that proper equilibrium between proposed model and actual atomistic model of SW-BNNT can be maintained as discussed earlier.

4.1.2. Nonlinear mathematical model of wavy SW-BNNT based mass sensor

Similar to macroscopic structures, the actual deformation is nonlinear in nanostructures like nanotubes. Zhongping et al., suggested that large amplitude of oscillation results in nonlinear vibrations in nano-scale systems. Thus, for accurate assessment of nanostructure properties, inclusion of nonlinearity in the analysis provides more realistic results[28].

The effects of various sources of nonlinearity (i.e. mid-plane stretching and waviness) on the vibrational behaviour of doubly clamped SW-BNNT is studied. To account for the effect of

different nonlinearities as discussed above, a nonlinear mathematical model is proposed in the present work for doubly clamped wavy SW- BNNT with additional mass attached at the centre.

A wavy SW- BNNT clamped at both ends having additional mass attached at the centre for behaving as a mass sensor is considered as shown in Fig. 4.2.

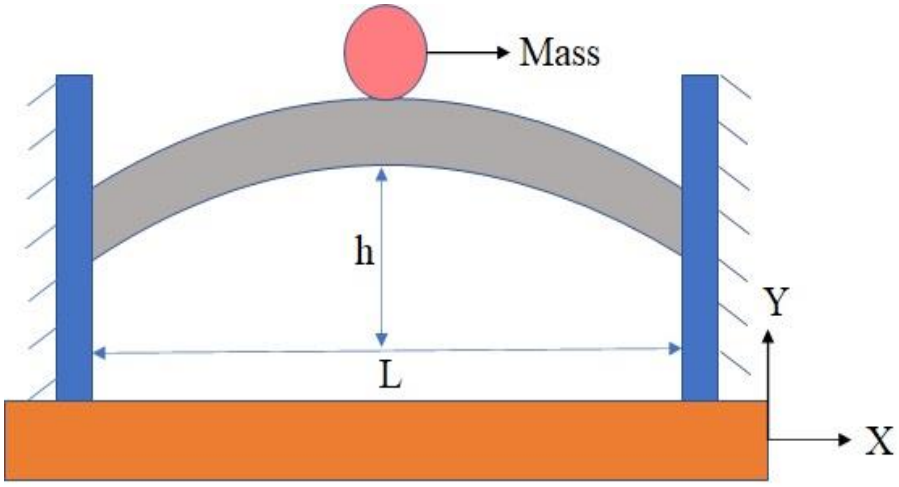

Fig. 4.2. Schematics of a doubly clamped wavy SW- BNNT based mass sensor with waviness factor ($w= h/L_{SW\text{-}BNNT}$)

Energy approach has been used to derive the equation of motion of mass sensor based on wavy SW- BNNT. The kinetic energy of the combined sensory system (SW-BNNT and attached mass) is:

$$E_{KE} = \frac{1}{2}\left[\rho_{bnnt} A \int_0^L \left(\frac{\partial u}{\partial t}\right)^2 dx\right] + \frac{1}{2} m_{added} \left(\frac{\partial u}{\partial t}\right)^2 \tag{4.1}$$

The two terms in the above equation represent energy due to mass of SW-BNNT and attached mass respectively as explained by Gaziantep and Pakdimerlli, [29].

Similarly, the potential energy of the system can be obtained as:

$$E_{PE} = \left.\begin{aligned} &\frac{1}{2}\left[E_{bnnt} A \int_0^L \left(\frac{\partial w}{\partial x} + \frac{1}{2}\left(\frac{\partial u}{\partial x}\right)^2 + \frac{\partial Z}{\partial x}\frac{\partial u}{\partial x}\right)^2 dx\right] \\ &+ \frac{1}{2}\left[E_{bnnt} I_{bnnt} \int_0^L \left(\frac{\partial^2 u}{\partial x^2}\right)^2 dx\right] + \frac{1}{2}\int_0^L k_{elastic} u^2 dx \end{aligned}\right\} \tag{4.2}$$

The three terms of Eq. (4.2) represent energy due to the mid-plane stretching of SW-BNNT, bending of SW- BNNT and energy due to elastic ground support respectively. Using the Lagrangian, $L_G = E_{KE} - E_{PE}$ and the applying the Hamiltonian principle as:

$$\delta \int_{t_1}^{t_2} L_G .dt = 0 \tag{4.3}$$

Coupled equations of motion as obtained are:

$$\left.\begin{aligned} & E_{bnnt} I_{bnnt} \frac{\partial^4 u}{\partial x^4} + \rho_{bnnt} A \frac{\partial^2 u}{\partial t^2} + m_{added} \frac{\partial^2 u}{\partial t^2} \\ & \qquad = E_{bnnt} A \frac{\partial}{\partial x}\left[\left(\frac{\partial w}{\partial x} + \frac{1}{2}\left(\frac{\partial u}{\partial x}\right)^2 + \frac{\partial Z}{\partial x}\frac{\partial u}{\partial x}\right) \times \left(\frac{\partial Z}{\partial x} + \frac{\partial u}{\partial x}\right)\right] \\ & E_{bnnt} A \frac{\partial}{\partial x}\left(\frac{\partial u}{\partial x} + \frac{1}{2}\left(\frac{\partial w}{\partial x}\right)^2\right) = 0 \end{aligned}\right\} \tag{4.4}$$

In order to eliminate the longitudinal displacement, it is assumed that both ends of SW-SW-BNNT are firmly clamped and their movement is totally restricted. Integration of the second equation of 4.4. results in,

$$\left.\begin{aligned} & E_{bnnt} I_{bnnt} \frac{\partial^4 u}{\partial x^4} + \rho_{bnnt} A \frac{\partial^2 u}{\partial t^2} + m_{added} \frac{\partial^2 u}{\partial t^2} \\ & = F.cos(\omega t) + \frac{E_{bnnt} A}{L_{bnnt}} \int_0^{L_{bnnt}} \left[\frac{\partial Z}{\partial x}\frac{\partial u}{\partial x} + \frac{1}{2}\left(\frac{\partial u}{\partial x}\right)^2\right].dx \times \left(\frac{\partial^2 u}{\partial x^2} + \frac{\partial^2 Z}{\partial x^2}\right) \end{aligned}\right\} \tag{4.5}$$

Separating the variables with consideration of the first vibration mode,

$$v(x,t) = \eta(x).\theta(t) \tag{4.6}$$

Applying a simple approximation for the first vibration mode shape as:

$$\eta(x) = 0.816\left(1 - \cos\left(\frac{2\pi x}{L_{bnnt}}\right)\right) \tag{4.7}$$

It is assumed that wavy SW-BNNT is having a half sinusoidal wave shape with centre amplitude (h) as shown in Fig. 4.6, thus giving curvature shape as:

$$\Psi = h.\sin\left(\frac{\pi x}{L_{bnnt}}\right) \qquad (h=0 \text{ results in straight SW-BNNT}) \tag{4.8}$$

Upon Substitution of Eqs 4.7 and 4.8 in Eq. 4.5 gives;

$$\left.\begin{aligned}
&-0.816\frac{16\pi^4}{L_{bnnt}^{\ 4}}E_{bnnt}I_{bnnt}.cos\left(\frac{2\pi x}{L_{bnnt}}\right)\theta \\
&+0.816\left[\rho_{bnnt}A\left(1-cos\left(\frac{2\pi x}{L_{bnnt}}\right)\right)+m_{added}\left(1-cos\left(\frac{2\pi x}{L_{bnnt}}\right)\right)\right]\ddot{\theta} \\
&=F\cos(\omega t)+\frac{E_{bnnt}A}{L_{bnnt}}\left[\int_0^{L_{bnnt}}\left[\begin{aligned}&-0.816h\frac{\pi}{L_{bnnt}}\cos\left(\frac{\pi x}{L_{bnnt}}\right)\left(\frac{2\pi}{L_{bnnt}}\sin\left(\frac{2\pi x}{L_{bnnt}}\right)\right)\theta\\&+\frac{1}{2}\left(0.816\frac{2\pi}{L_{bnnt}}\sin\left(\frac{2\pi x}{L_{bnnt}}\right)\right)\theta\end{aligned}\right]^2 dx\right] \\
&\times\left(0.816\frac{4\pi^2}{L_{bnnt}^2}cos\left(\frac{2\pi x}{L_{bnnt}}\right)\theta-h\left(\frac{\pi}{L_{bnnt}}\right)^2\sin\left(\frac{\pi x}{L_{bnnt}}\right)\right)
\end{aligned}\right\} \tag{4.9}$$

Integrating and combining similar terms,

$$\left.\begin{aligned}
&-0.816\frac{16\pi^4}{L_{bnnt}^{\ 4}}E_{bnnt}I_{bnnt}.cos\left(\frac{2\pi x}{L_{bnnt}}\right)\theta+0.816\left(1-cos\left(\frac{2\pi x}{L_{bnnt}}\right)\right)\left[\rho_{bnnt}A+m_{added}\right]\ddot{\theta} \\
&=F\cos(\omega t)+7.11\left(\frac{\pi^3hE_{bnnt}A}{L_{bnnt}^4}\right)\theta^2\cos\left(\frac{2\pi x}{L_{bnnt}}\right)-2.176\left(\frac{h^2\pi^3E_{bnnt}A}{L_{bnnt}^4}\right)\theta\sin\left(\frac{\pi x}{L_{bnnt}}\right) \\
&+2.176\left(\frac{\pi^4E_{bnnt}A}{L_{bnnt}^4}\right)\theta^3\cos\left(\frac{2\pi x}{L_{bnnt}}\right)-0.66\left(\frac{h\pi^4E_{bnnt}A}{L_{bnnt}^4}\right)\theta^2
\end{aligned}\right\} \tag{4.10}$$

Since, Eq. (4.10) describes the oscillation of the first mode of vibration in space and time domain, *the Galerkin approach* can be used to obtain the solution of such an equation. Applying this method by multiplying Eq. (4.10) with first vibration mode shape, i.e., Eq. (4.7) and integrating between limits of $x=0$ to $x=L_{SW\text{-}BNNT}$ gives:

$$(1+M)\ddot{\theta}+\alpha_w\theta+\beta_w\theta^2+\varepsilon_w\theta^3=0.816\frac{F}{\rho_{bnnt}AL_{bnnt}^2}\cos(\omega t) \tag{4.11}$$

where,

$$\left.\begin{aligned} \alpha_w &= \left(5.33\frac{E_{bnnt}I_{bnnt}\pi^4}{\rho_{bnnt}AL_{bnnt}^4}+4.74\frac{h^2\pi^2E_{bnnt}}{\rho_{bnnt}L_{bnnt}^4}\right)=\omega_0{}^2; \\ \beta_w &= 4.352\frac{\pi^3hE_{bnnt}}{\rho_{bnnt}L_{bnnt}^4}; \quad \varepsilon_{bnnt}=0.89\frac{E_{bnnt}\pi^4}{\rho_{bnnt}L_{bnnt}^4} \quad and \;\; M=\frac{m_{added}}{2\rho_{bnnt}AL_{bnnt}} \end{aligned}\right\} \tag{4.12}$$

Equation (4.11) is a second order nonhomogeneous nonlinear differential equation, in which square and cubic terms represent quadratic and cubic nonlinearities associated with stiffness terms. It is worth mentioning here that coefficient 'α_w' is independent of the sign of curved SW-BNNT as 'h' is squared, and this represents the square of first fundamental natural frequency of SW-BNNT.

Quadratic nonlinearity arises due to surface waviness (h) as indicated by coefficient 'β_w'. The sign of a quadratic term depends on curvature of SW-BNNT, it is positive for upward curvature i.e. (+h) and negative for downward curvature (-h).

The coefficient 'ε_w' corresponds to stretching of the middle plane of SW-BNNT when it is allowed to vibrate and is responsible for cubic nonlinearity.

It is a requirement to scale down all the terms of nonlinear nonhomogeneous differential equations to nanoscale level. The normalization (scaling) is essential for identifying the degree of nonlinearity in the system. For this, a characteristic length (r) of nanometre level and time ($1/\omega_0$) or the oscillation period for space and time domain respectively is selected and Eq. (4.11) is scaled down by incorporating new dimensionless displacement (θ`) and time ($t$`) respectively as:

$$\left.\begin{aligned} \theta` &= \theta/r \\ t` &= t\omega_0 \end{aligned}\right\} \tag{4.13}$$

Thus, normalized or scaled down equation of motion can be obtained as:

$$(1+M)\ddot{\theta}+\theta+\frac{\beta_w r}{\alpha_w}\theta^2+\frac{\varepsilon_w r^2}{\alpha_w}\theta^3=\frac{f_w}{r\alpha_w}\cos(\omega t) \tag{4.14}$$

where;

$$f_w = 0.816\frac{F}{\rho_{bnnt}AL_{bnnt}^2} \tag{4.15}$$

'*F*' in the above equation represents the physical force applied on the SW-BNNT, '*r*' is the scaling parameter or the characteristic length and 'θ' represents the transverse displacement of the SW-BNNT. The entire equation represents the solution in time domain.

Quality factor (*Q*), the ratio of the energy stored to the energy lost per cycle in the oscillator due to damping is an important parameter for characterizing oscillators. The damping coefficient (ζ) is related to the quality factor as:

$$\zeta = 1/2Q \tag{4.16}$$

Damping coefficient must be added to the equation of motion in order to make the equation more realistic for nanotubes as:

$$(1+M)\ddot{\theta} + 2\zeta\dot{\theta} + \theta + \frac{\beta_w r}{\alpha_w}\theta^2 + \frac{\varepsilon_w r^2}{\alpha_w}\theta^3 = \frac{f}{r\alpha_w}\cos(\omega t) \tag{4.17}$$

The coefficients of the nonlinear terms as described above are functions of many parameters.

4.2 Result and discussion

4.2.1 Nonlinear dynamic analysis of wavy SW-BNNT based mass sensor

It has already been mentioned that nanotubes are not perfectly straight in actual practice and contain surface waviness resulting in wavy shape. Equation of motion developed for non-linear model of doubly clamped wavy SW-BNNT as given by Eq. (4.17) comprises of two nonlinear terms. It has a quadratic nonlinear term arising due to the wavy shape of the SW-BNNT and a cubic nonlinear term resulting from the mid-plane stretching. Also, it is found that if the amplitude of its waviness, *'h'*, is taken equal to zero; the problem becomes that of a straight SW-BNNT.

These nonlinear terms have been plotted in Fig. 4. for varying values of diameters of wavy SW-BNNT. The quadratic nonlinearity varies widely over the range of diameter (0.5 to 3 nm). From Fig. 4. (a), it is clear that for a specific waviness factor (say 0.06) the quadratic coefficient corresponding to 0.5 nm diameter is about 0.3 indicating relatively "weak nonlinearity" and its value increases continuously with an increase in diameter of SW-BNNT and

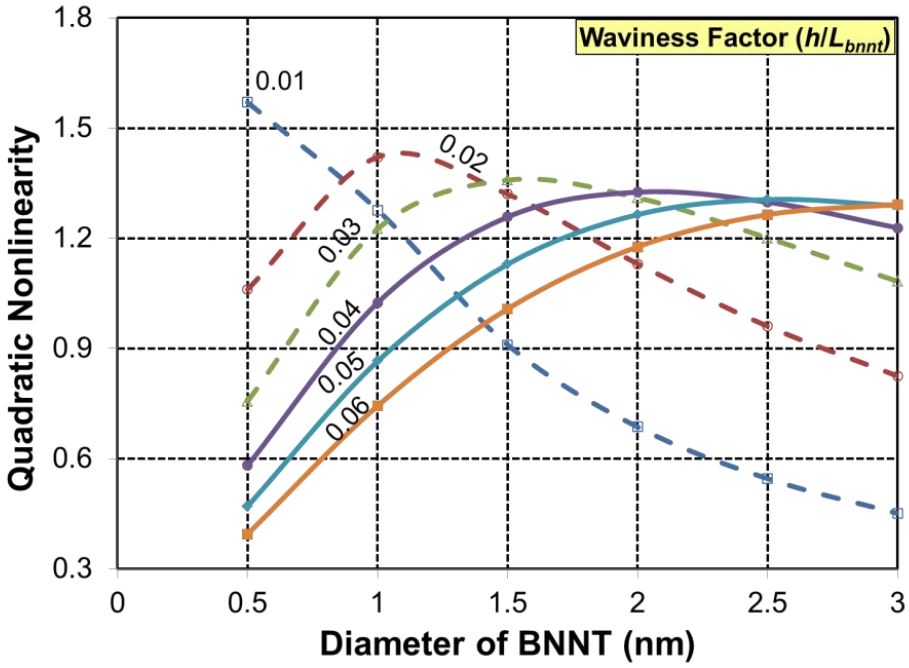

(a)

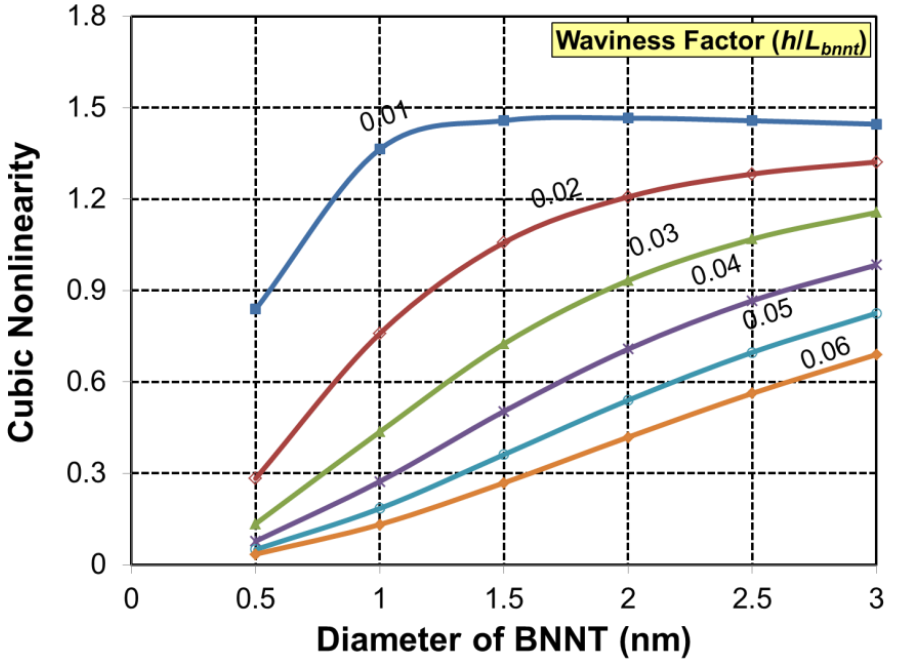

(b)

Fig. 4.3. Variation in degree of nonlinearity with the outer diameter of SW-BNNT for different waviness factors (a) Quadratic nonlinearity and (b) Cubic nonlinearity.

attains a value of 1.3 at a diameter of 3 nm indicating moderate nonlinearity. As far as strong quadratic nonlinearity is concerned, it is observed that at lower waviness factor (0.01), its value is about 1.6 corresponding to 0.5 nm diameter of SW-BNNT. The cubic nonlinearity behaves in a different manner than quadratic one. For small diameter range of SW-BNNT (say 0.5 to 1.0 nm) and for small waviness factor (0.01), the cubic nonlinear coefficient varies from 0.8 to 1.4 and beyond this range; it remains almost constant as shown in Fig. 4. (b). This is true for smaller values of waviness factor.

The cubic nonlinearity originates from internal sources, i.e., due to stretching of mid-plane. Unlike quadratic nonlinearity, it is less affected by external changes in geometry. These observed results thus confirm the effect of the quadratic nonlinearity that appears in the equation of motion as a result of geometric nonlinearity (curvature).

It is observed that the cubic nonlinearity decreases as the waviness factor for a specific diameter increases. On the contrary, the quadratic nonlinearity increases with increase in waviness factor up to a certain limit beyond which it starts declining, thus following a parabolic path as shown in Fig. 4..

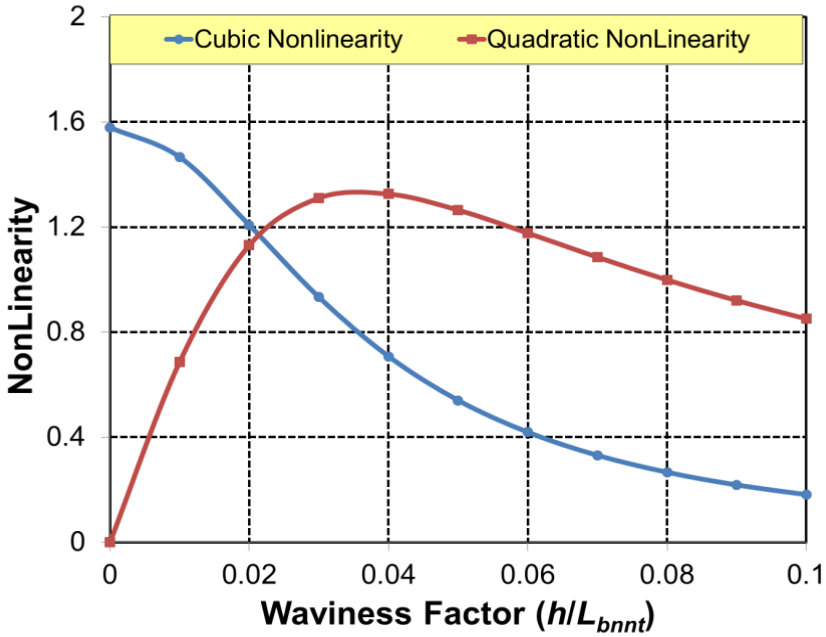

Fig. 4.4. Nonlinearity as a function of the SW-BNNT waviness for 60 nm length and 2.0 nm diameter.

4.2.2. Dynamic responses of wavy SW-BNNT

Various response tools can be applied to investigate the nonlinear dynamic behaviour of the system. For studying the dynamics of doubly-clamped wavy SW-BNNT, the response tools used in the present work are described briefly as follows:

4.2.2.1 Time series

Time series technique for identifying the system response relies on the fact that various data points taken over considered time interval may comprise of internal structures like autocorrelation or trends that should be accounted for. The time series is a representation of sequence of variable values in an ordered manner spread out in equal time intervals.

4.2.2.2. Phase space

Phase plane analysis is considered to be the most appropriate technique for investigating the responses of nonlinear dynamic systems as no analytical solution exists for studying the behaviour of a nonlinear system. Phase plane analysis is a graphical tool used to study second-order systems by examining the useful features of trajectories of motion after generating the same in regard to various initial conditions. Thus, it helps in obtaining useful information about the stability of dynamic systems. The advantage of this technique is that system behaviour can be visualized from different initial conditions only and there is no need to solve nonlinear equations analytically.

4.2.2.3. Poincaré section

Poincaré map is the intersection of a periodic orbit in the state space of a continuous dynamical system with a certain lower-dimensional subspace known as the Poincaré section, transversal to the flow of the system. So, the Poincaré sections are considered to be an appropriate tool for studying any dynamic system theoretically and mostly employed for systems exhibiting periodic or quasi-periodic behaviour in nature.

4.2.2.4. Fast Fourier Transforms

Frequency domain signals are preferable than corresponding time domain signals because they not only help in visualizing the individual frequency components within the signal, but also

provide useful information about any distortion effects or spurious frequency components. Fourier transform technique is used to convert time domain signals into frequency domain. The Fast Fourier Transform (FFT) resolves a time domain signal in the form of a waveform into its corresponding sinusoidal component. The FFT takes time-domain data in the form of a block and returns the frequency spectrum of same. The FFT does not provide a continuous frequency spectrum and it returns the data in discrete form as it is a digital implementation of the Fourier transform.

Thus, the frequency content of the time domain waveform is resolved into a finite number of frequency lines. The frequency spectrums are computed with the help of sample time domain waveform input through FFT. If for an arbitrary signal of sampling frequency (f_s) over an acquisition time (T) the samples acquired are (N) then acquisition time is given by: $T = \frac{N}{f_s}$. For FFT, the spectrum computed from the sampled signal has a frequency resolution defined as '*df*'. Thus, the frequency resolution can be obtained as: $df = \frac{1}{T} = \frac{f_s}{N}$.

The frequency resolution is determined solely by the acquisition time. The frequency resolution improves as the acquisition time increases.

Considering the nonlinear model of the wavy SW-BNNT rigidly clamped at both ends as discussed above, the dynamic characteristics of wavy SW-BNNT with varying waviness are assessed on the basis of tools like time series, phase portrait, Poincaré maps and Fast Fourier Transform (FFT). The following parameters of SW-BNNT are considered as: outer diameter 2.0 nm, Young's modulus 1180 GPa and density 2180 kg/m^3.

The dynamic responses of a vibrating wavy SW-BNNT based nano-resonator is observed by numerical integration method. Primary resonance mode of vibration is assumed for excitation of the system. The dynamic behaviour is studied using the tools for different lengths (20, 40, and 60 nm) and varying waviness factors (0.1 to 0.6). The additional mass of 10^{-22} kg at the centre of doubly clamped wavy SW-BNNT is attached for obtaining above responses.

The time and frequency based dynamic responses of wavy SW-BNNT for a length of 20 nm with varying waviness ($h/L_{SW\text{-}BNNT}$=0.1, to 0.6) is shown in Fig. 4.5 to Fig. 4.10, respectively.

The multiple orbits in phase space diagram with multiple peaks of excitation in corresponding FFTs for lower values of waviness (0.1 to 0.2) represents the periodic nature and followed by quasi-periodic nature for waviness value up to 0.4 as the frequency of multiple peaks of excitation reduces, chaotic behaviour is then observed for higher values of waviness. Poincaré maps also confirm the type of responses for system corresponding to different waviness by representing multiple dots.

Fig. 4.11 to Fig. 4.16 displays the responses of wavy SW-BNNT fixed at both ends for a length of 40 nm corresponding to different waviness (0.1 to 0.6), respectively. From response diagrams, it has been observed that for 40 nm long wavy SW-BNNT the system responses for lower values of waviness are changing from periodic to quasi-periodic and with the increase in waviness the system starts to behave in irregular manner.

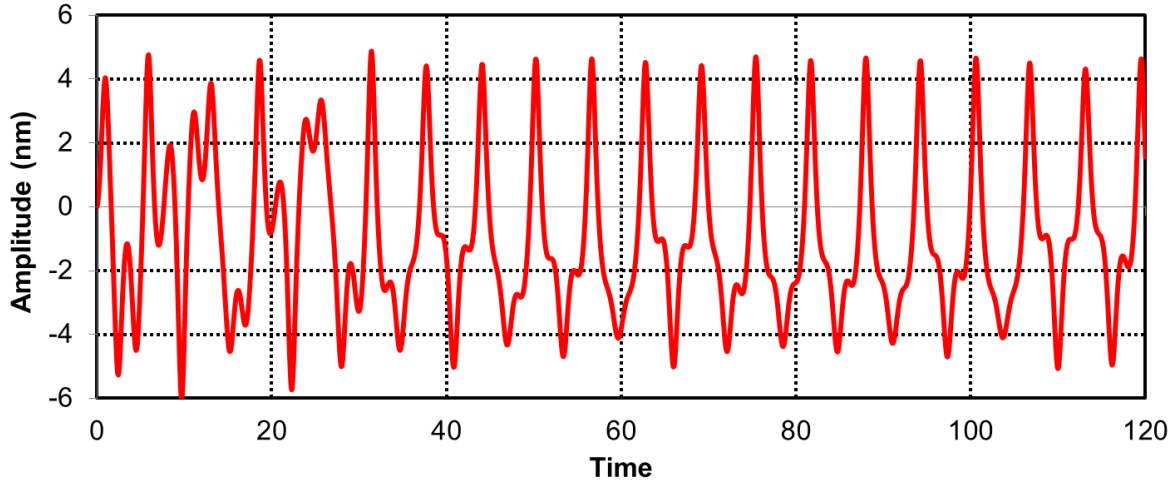

(a)

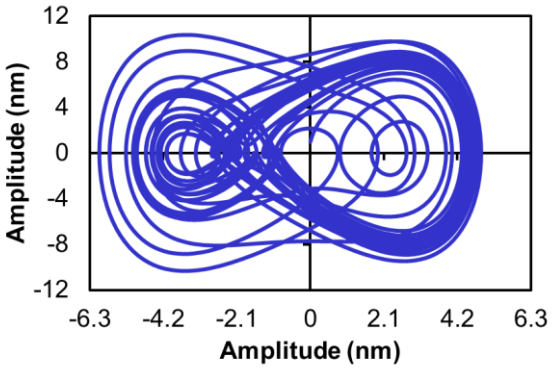

(b)

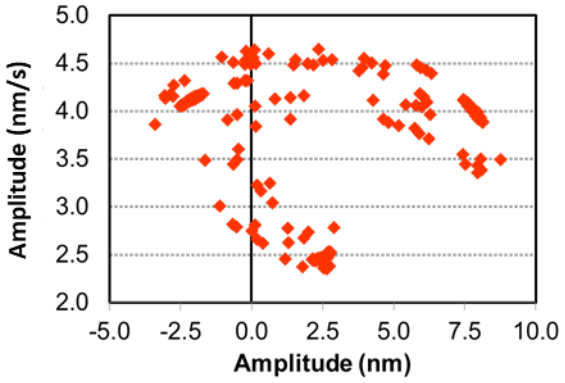

(c)

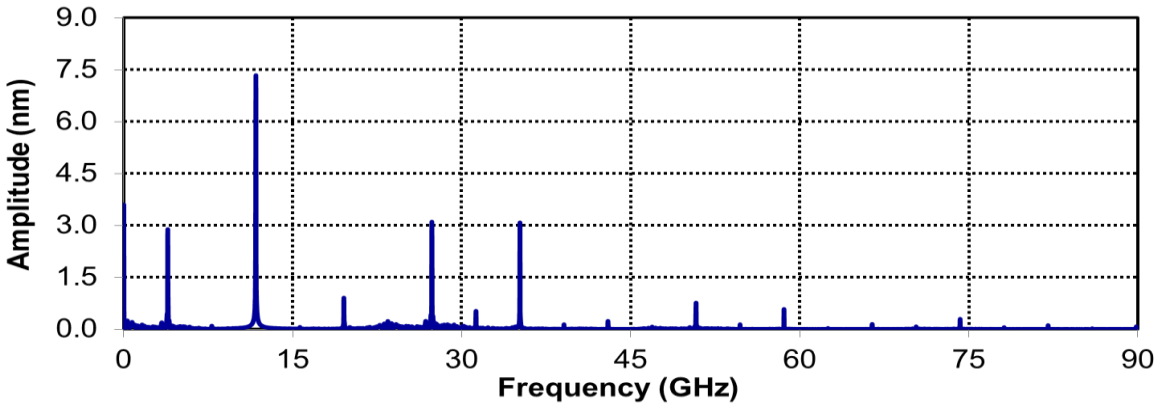

(d)

Fig. 4.5. Dynamic responses: (a) Time series (b) Phase plane (c) Poincare section and (d) Fast Fourier Transform for L=20nm waviness 0.1.

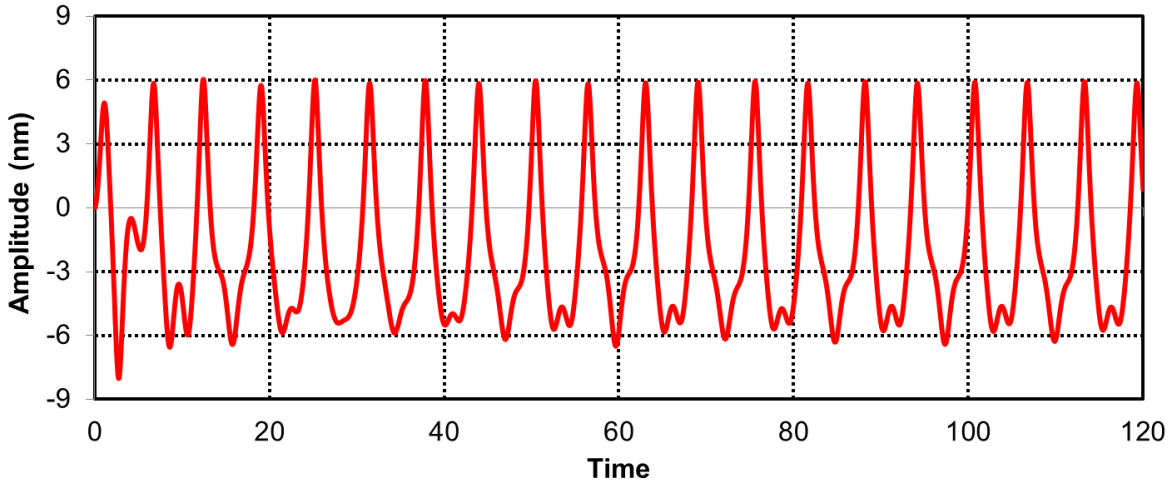

(a)

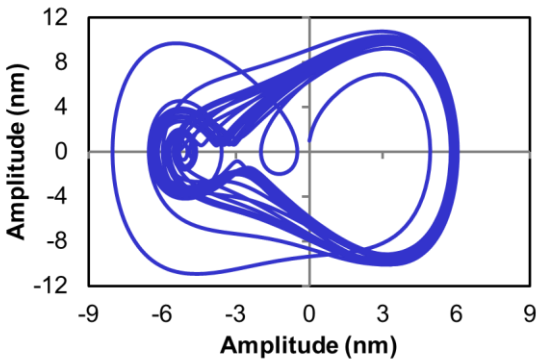

(b)

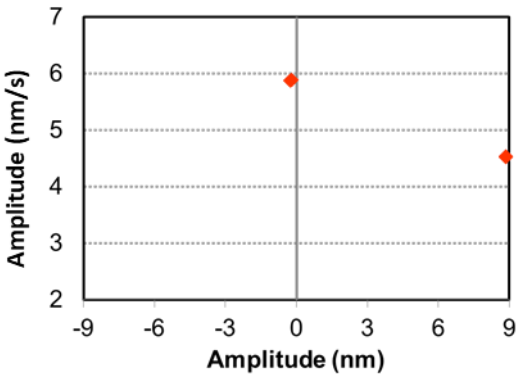

(c)

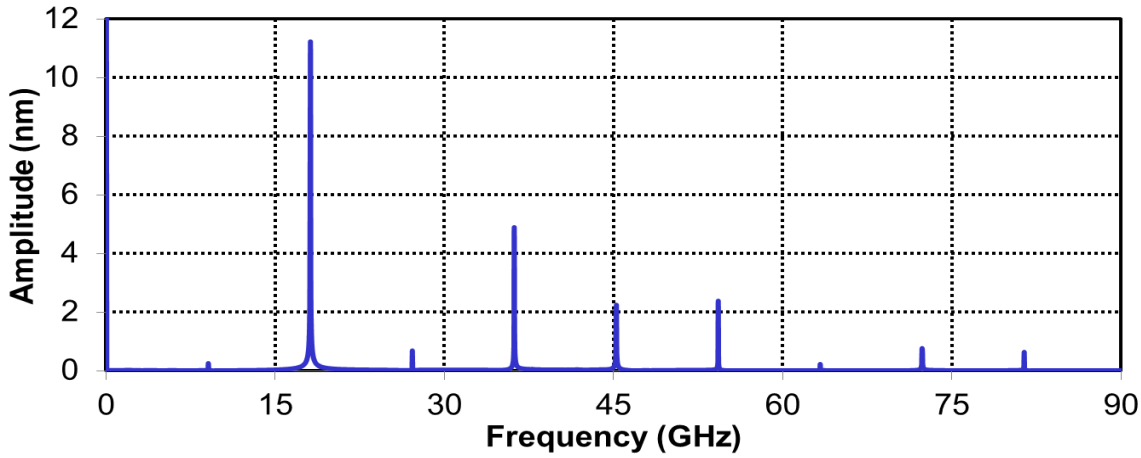

(d)

Fig. 4.6. Dynamic responses: (a) Time series (b) Phase plane (c) Poincare section and (d) Fast Fourier Transform for L=20nm waviness 0.2.

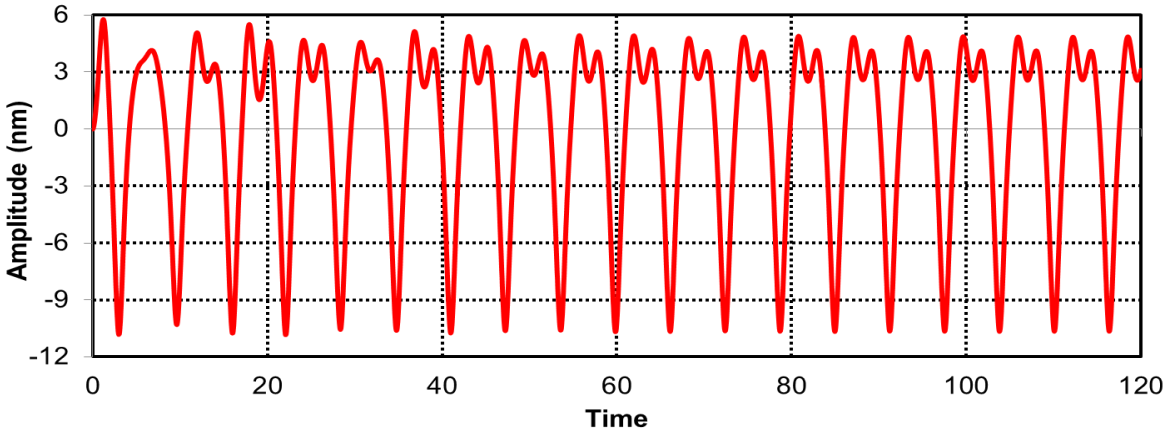

(a)

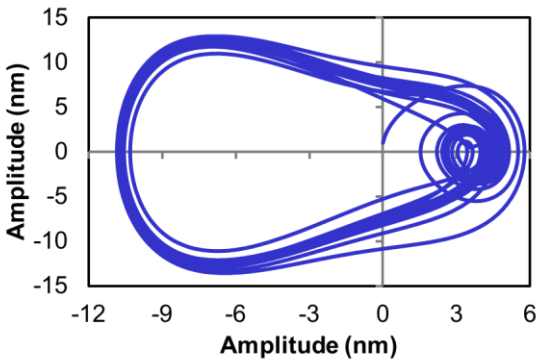

(b)

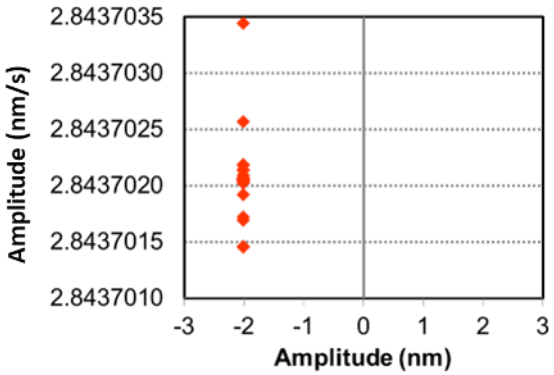

(c)

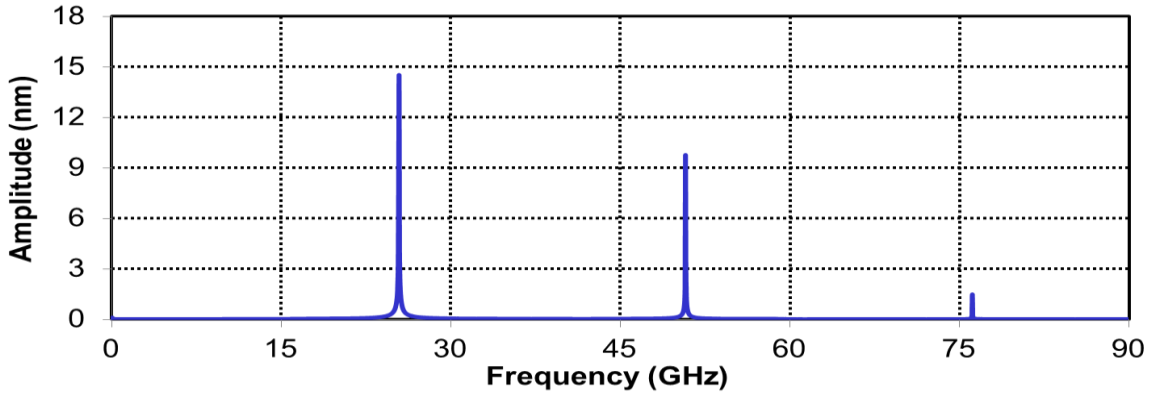

(d)

Fig. 4.7. Dynamic responses: (a) Time series (b) Phase plane (c) Poincare section and (d) Fast Fourier Transform for L=20nm waviness 0.3.

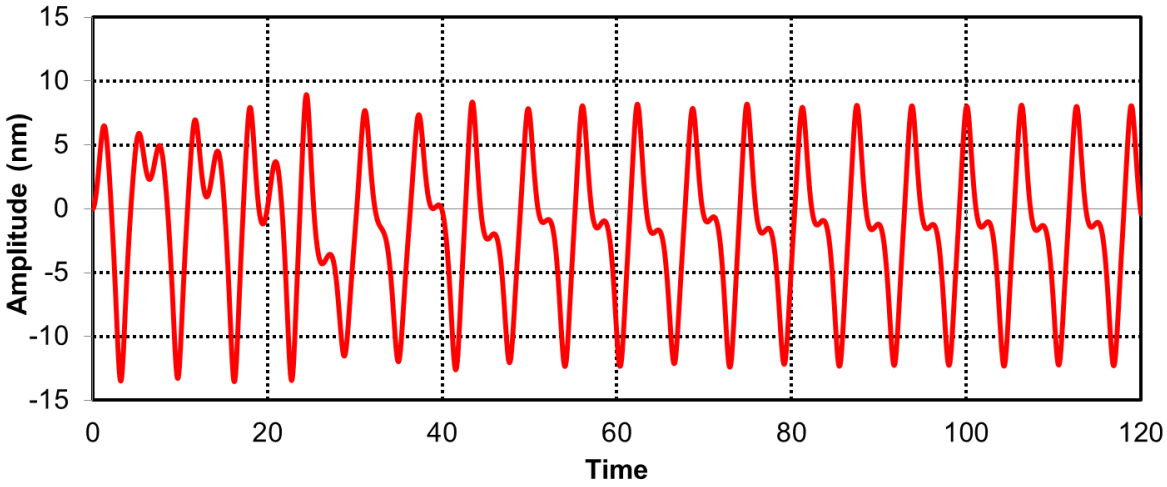

(a)

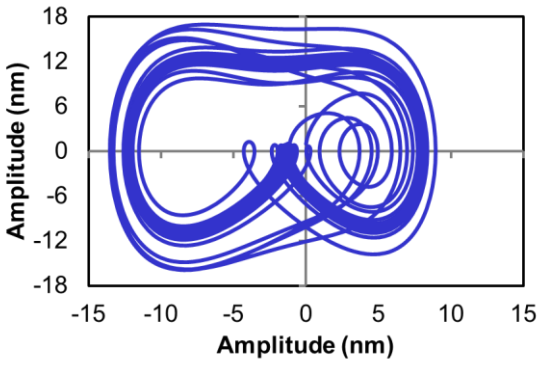

(b)

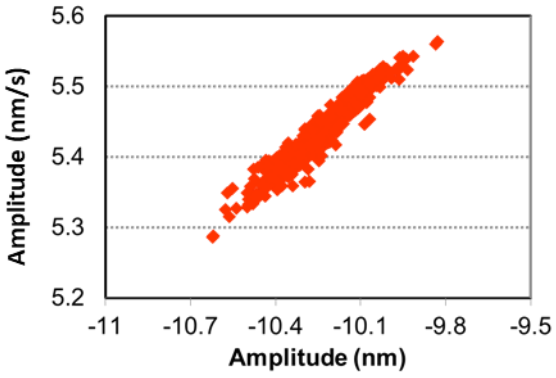

(c)

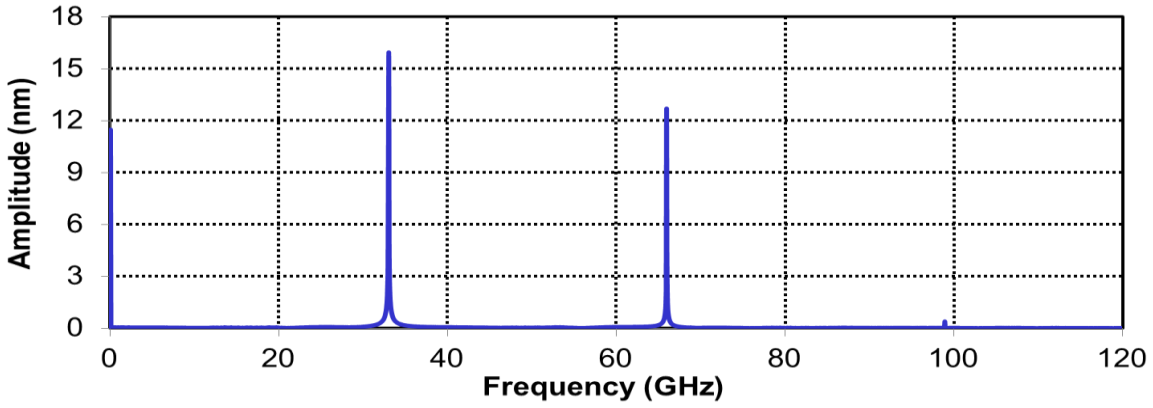

(d)

Fig. 4.8. Dynamic responses: (a) Time series (b) Phase plane (c) Poincare section and (d) Fast Fourier Transform for L=20nm waviness 0.4.

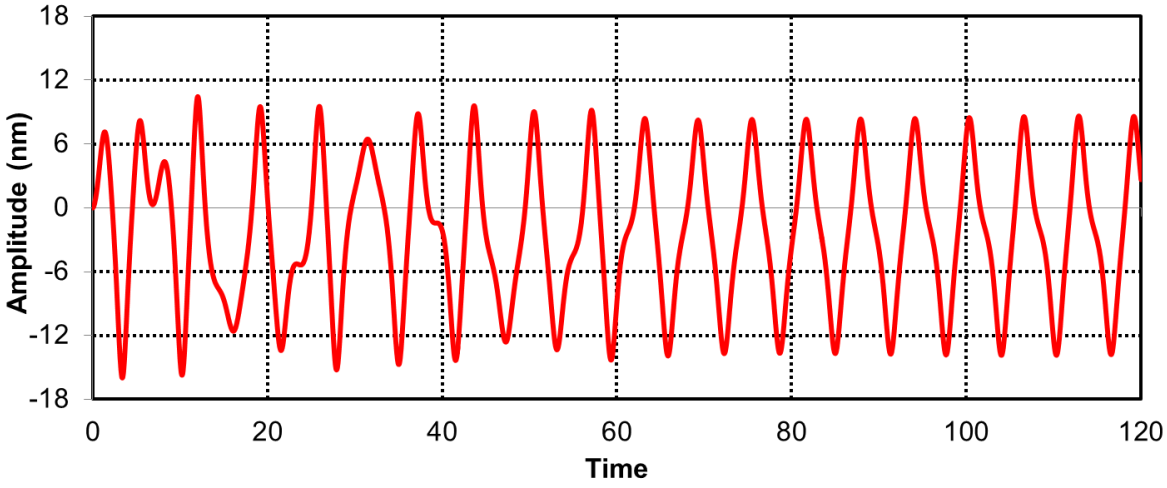

(a)

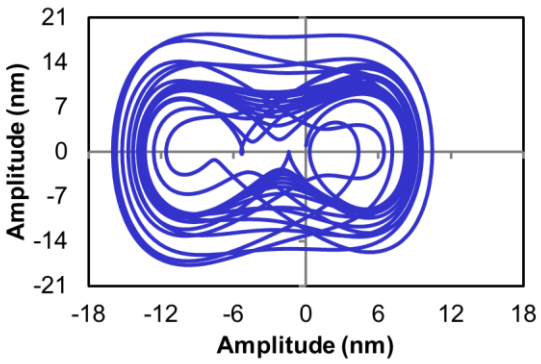

(b)

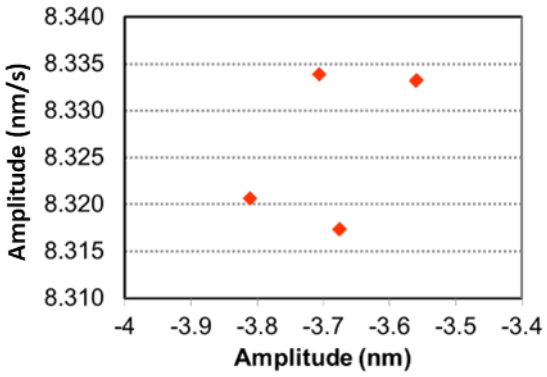

(c)

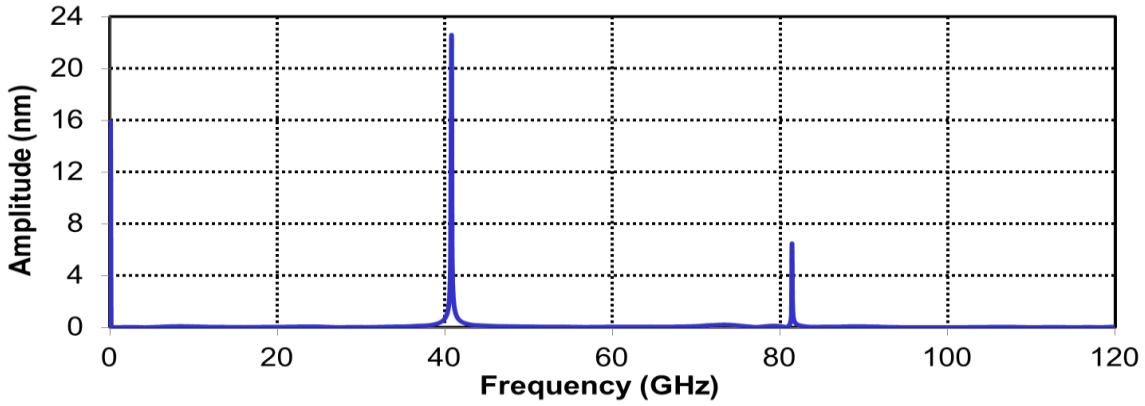

(d)

Fig. 4.9. Dynamic responses: (a) Time series (b) Phase plane (c) Poincare section and (d) Fast Fourier Transform for L=20nm waviness 0.5.

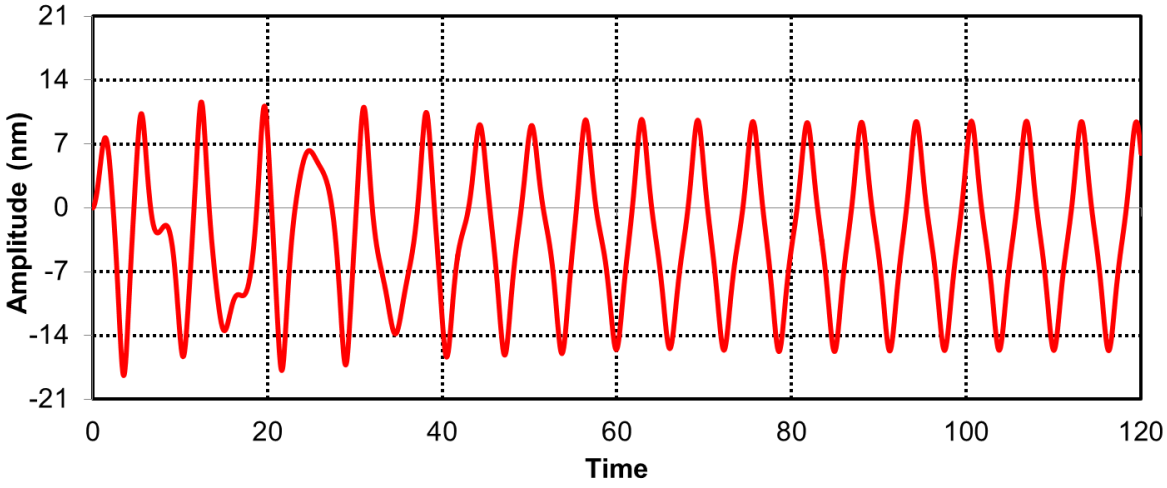

(a)

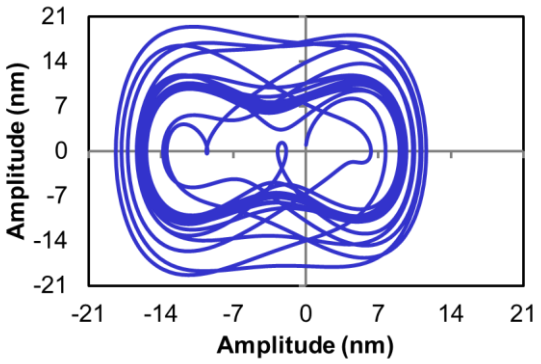

(b)

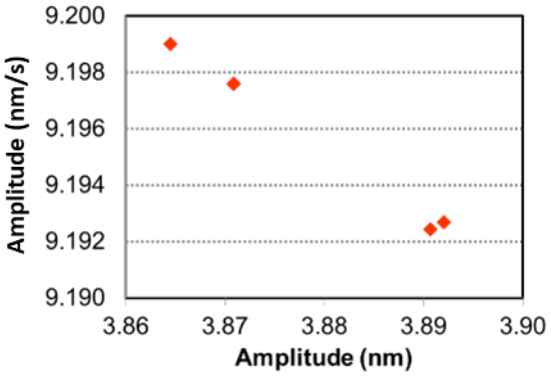

(c)

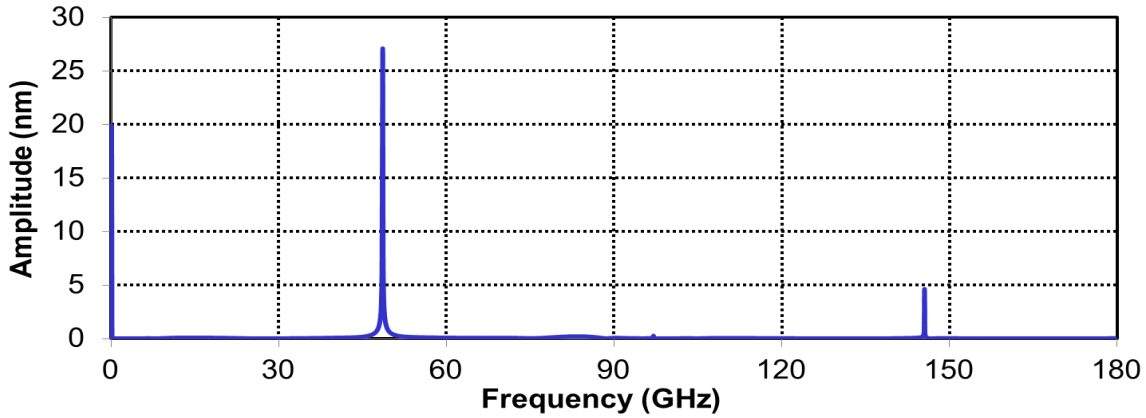

(d)

Fig. 4.10. Dynamic responses: (a) Time series (b) Phase plane (c) Poincare section and (d) Fast Fourier Transform for L=20nm waviness 0.6

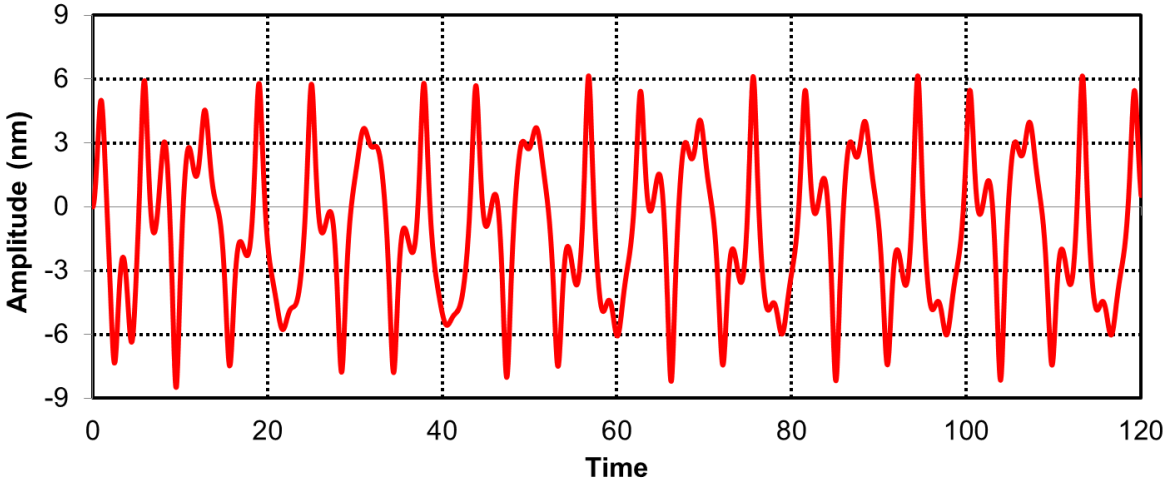

(a)

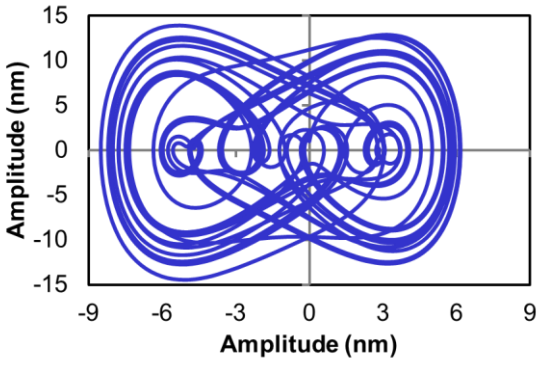

(b)

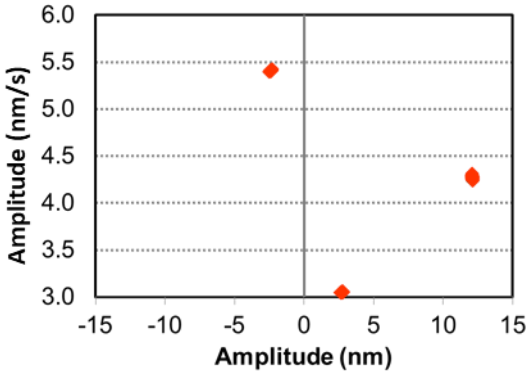

(c)

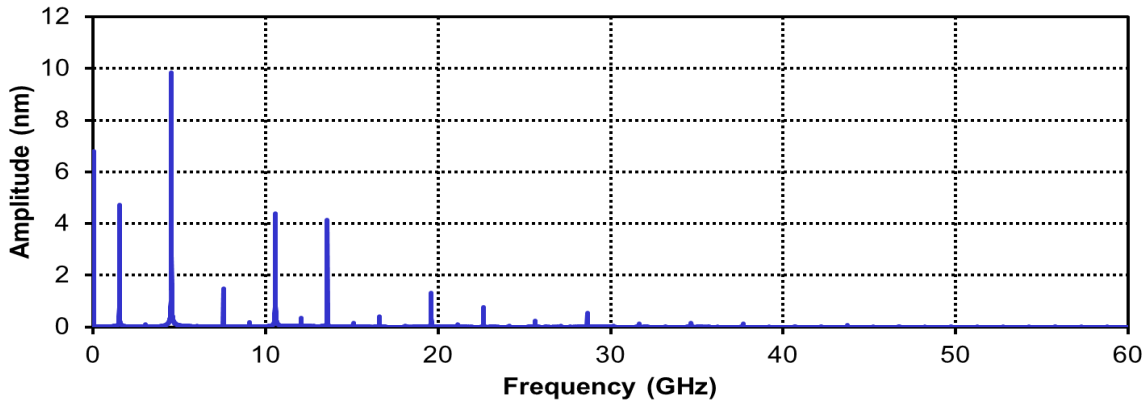

(d)

Fig. 4.11. Dynamic responses: (a) Time series (b) Phase plane (c) Poincare section and (d) Fast Fourier Transform for L=40nm waviness 0.1.

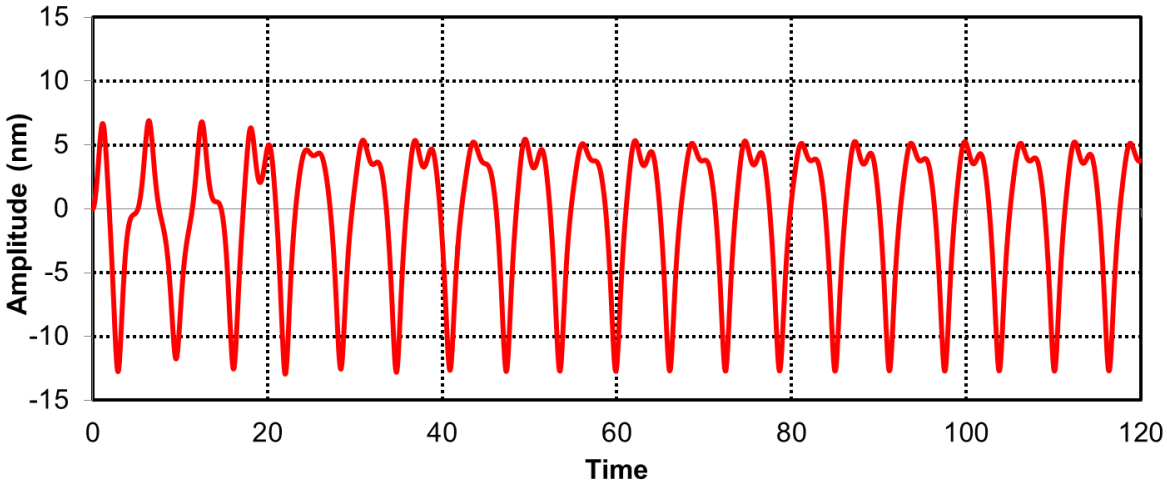

(a)

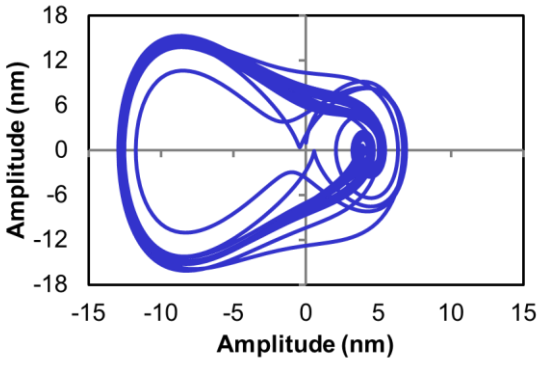

(b)

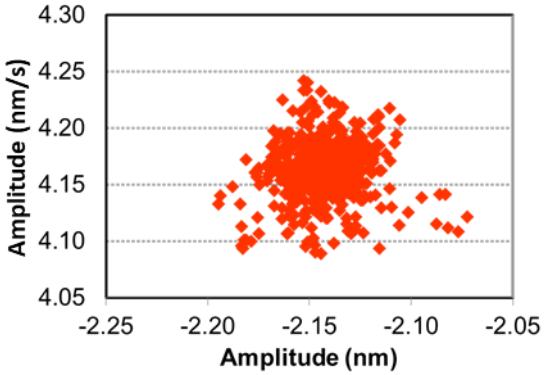

(c)

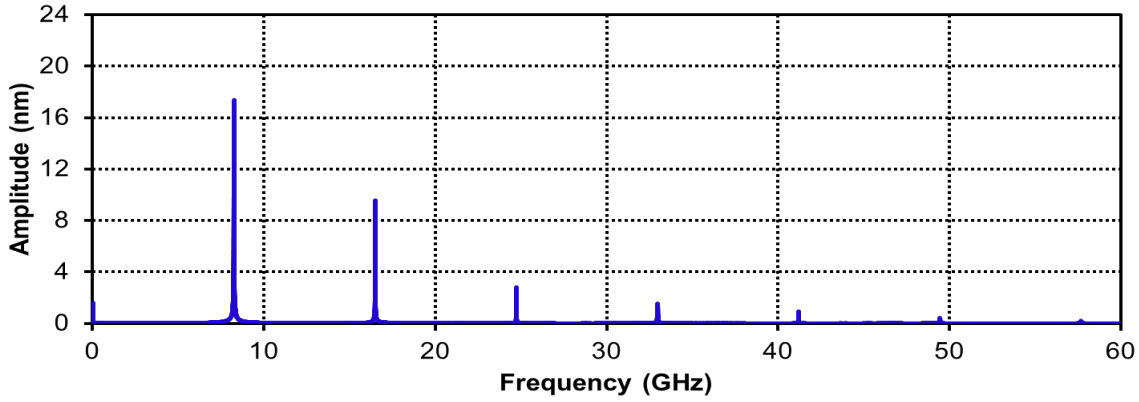

(d)

Fig. 4.12. Dynamic responses: (a) Time series (b) Phase plane (c) Poincare section and (d) Fast Fourier Transform for L=40nm waviness 0.2.

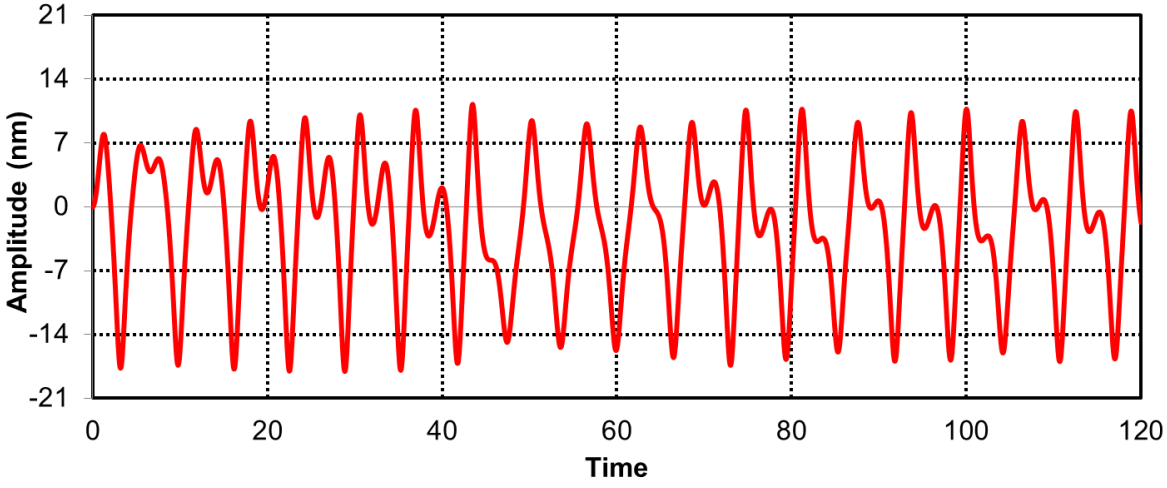

(a)

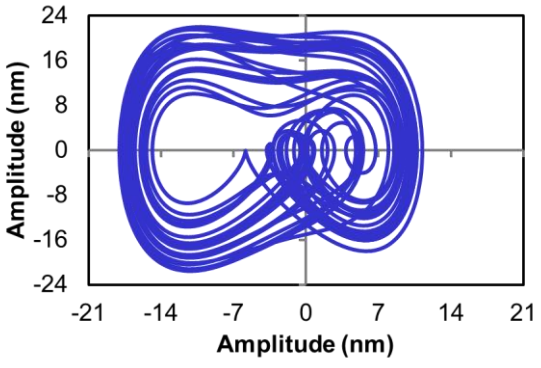

(b)

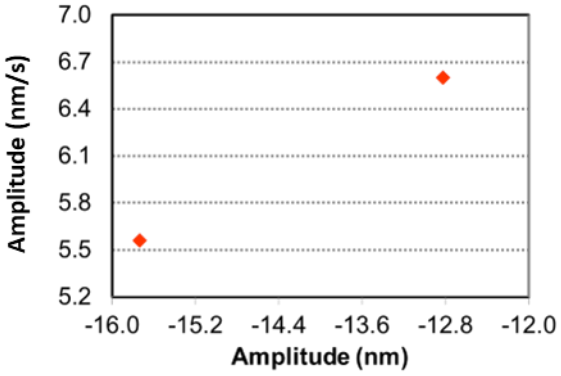

(c)

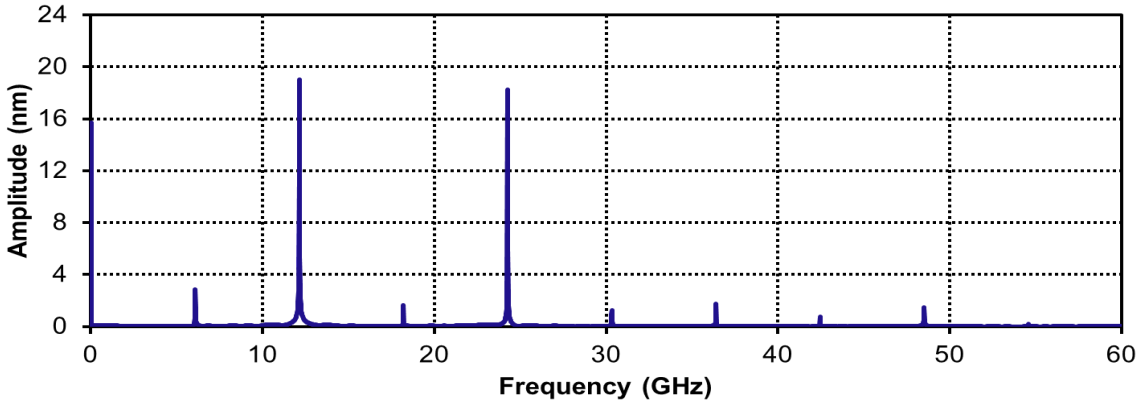

(d)

Fig. 4.13. Dynamic responses: (a) Time series (b) Phase plane (c) Poincare section and (d) Fast Fourier Transform for L=40nm waviness 0.3.

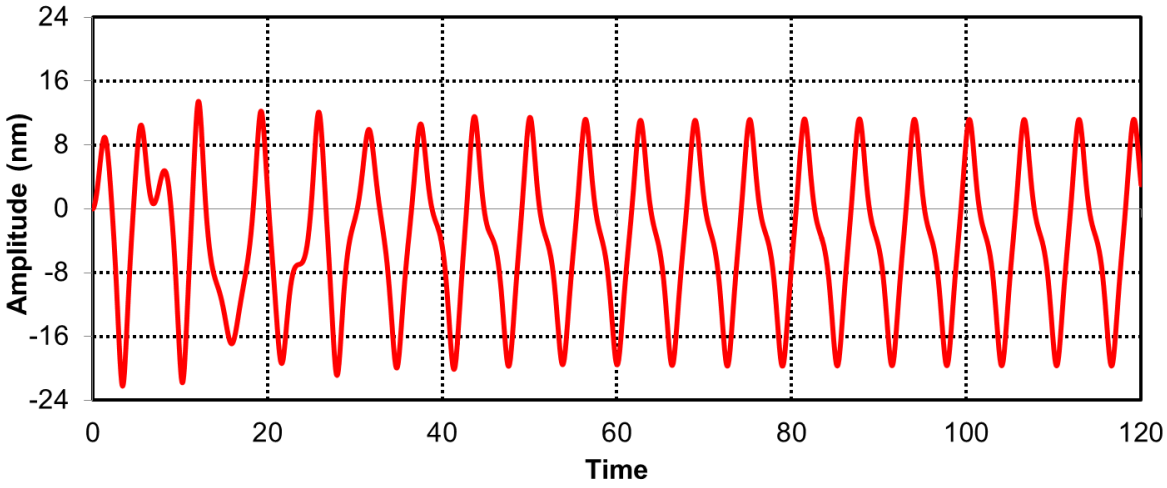

(a)

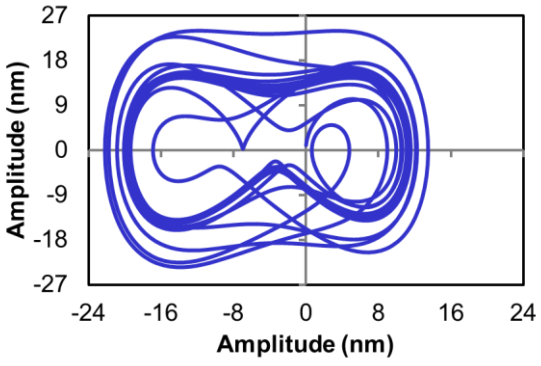

(b)

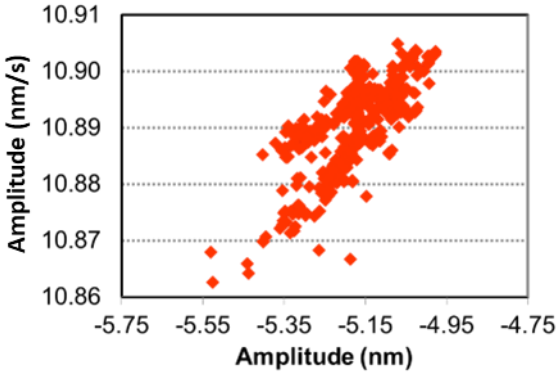

(c)

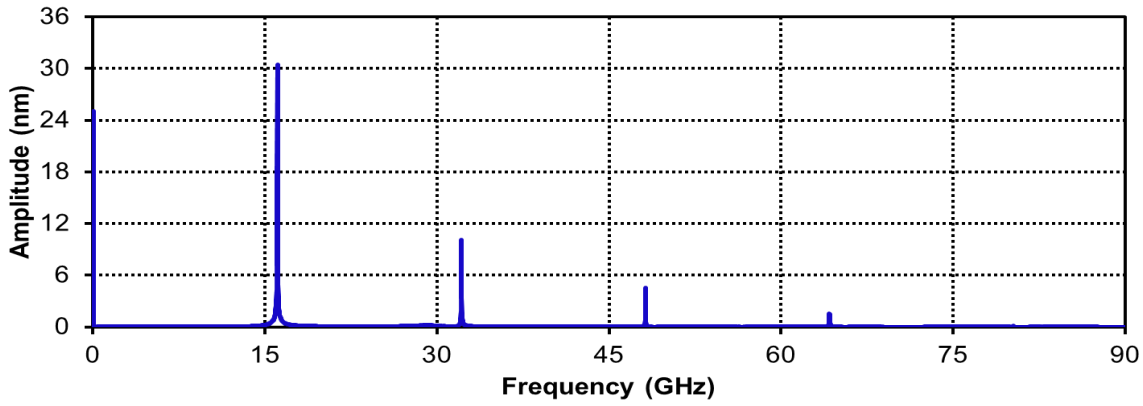

(d)

Fig. 4.14. Dynamic responses: (a) Time series (b) Phase plane (c) Poincare section and (d) Fast Fourier Transform for L=40nm waviness 0.4.

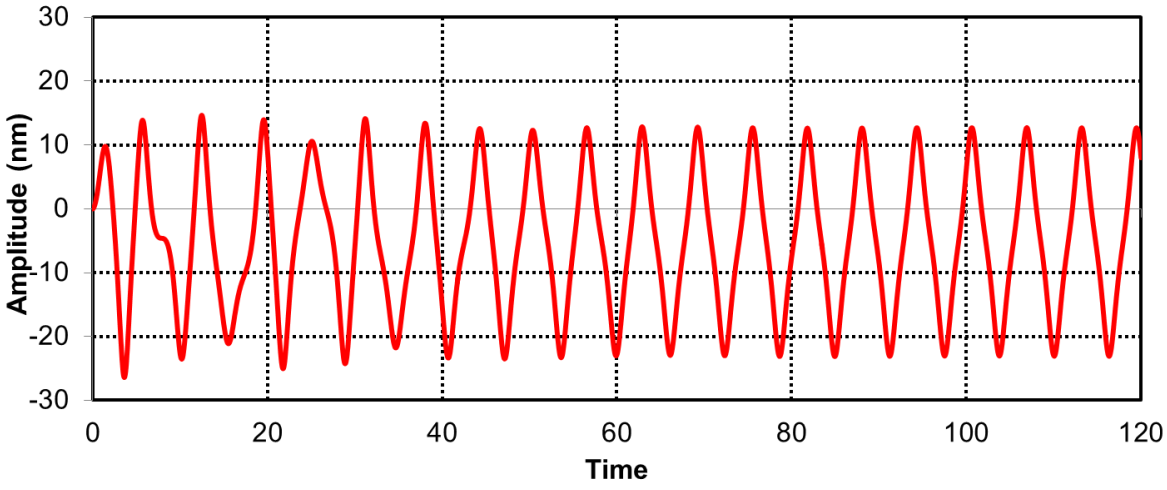

(a)

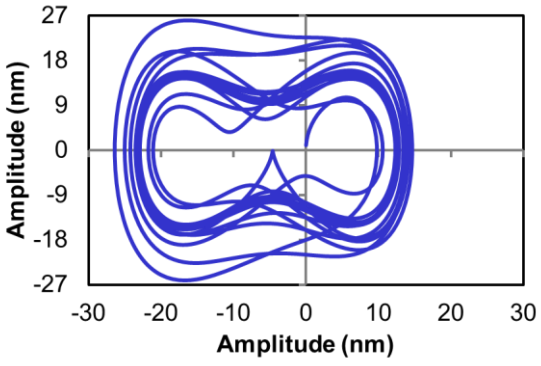

(b)

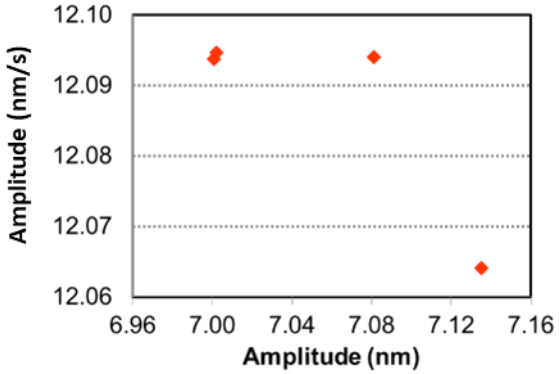

(c)

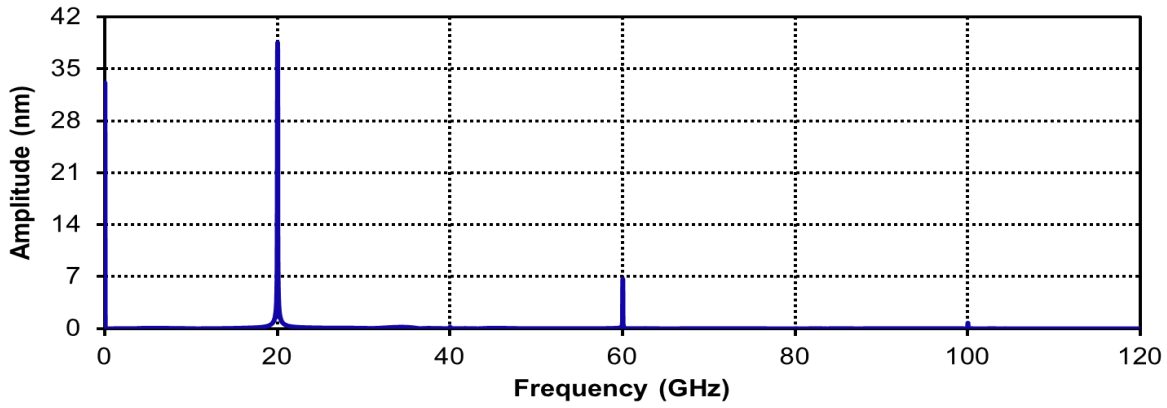

(d)

Fig. 4.15. Dynamic responses: (a) Time series (b) Phase plane (c) Poincare section and (d) Fast Fourier Transform for L=40nm waviness 0.5.

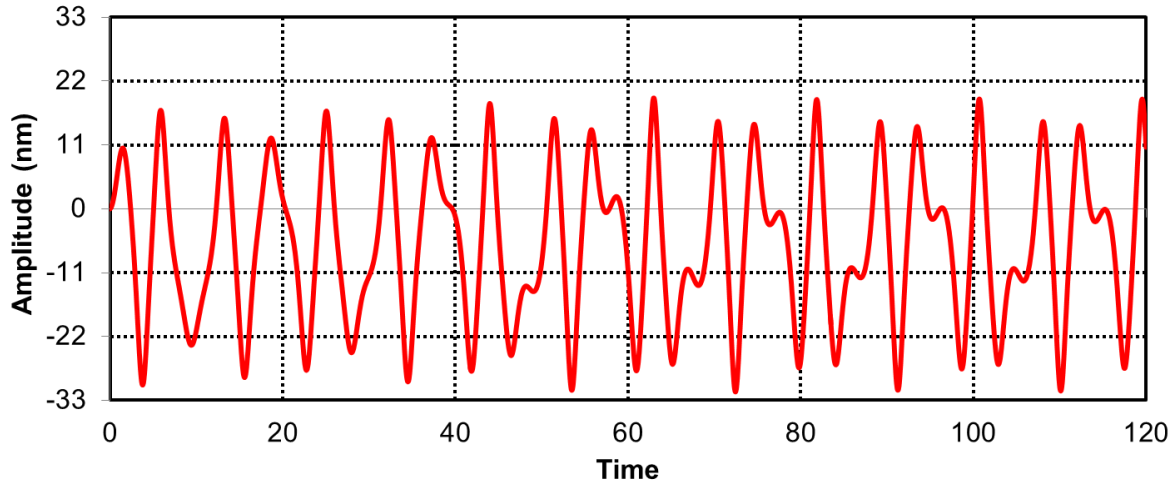

(a)

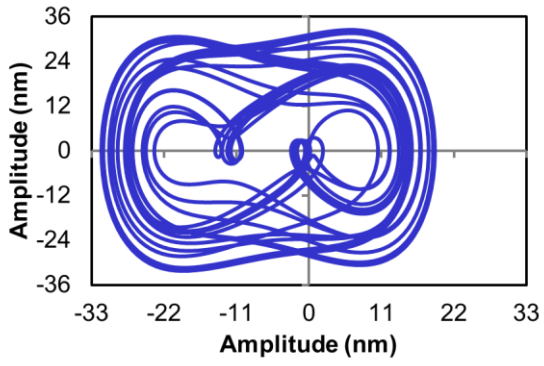

(b)

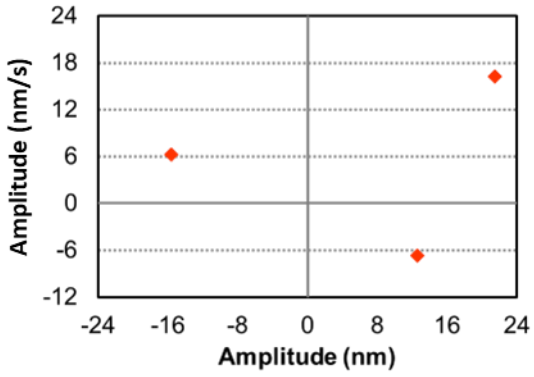

(c)

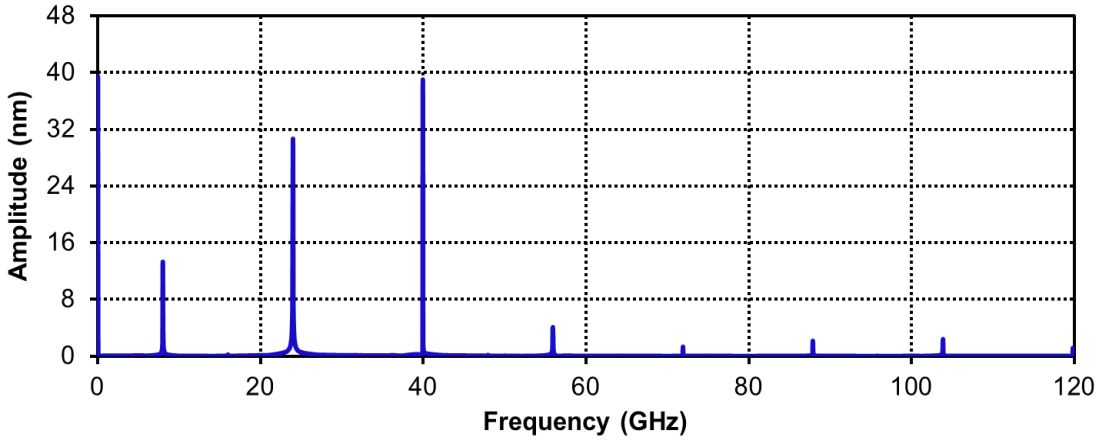

(d)

Fig. 4.16. Dynamic responses: (a) Time series (b) Phase plane (c) Poincare section and (d) Fast Fourier Transform for L=40nm waviness 0.6.

The dynamic responses have been observed for higher length (i.e. $L_{SW\text{-}BNNT}$= 60nm) also. The time domain responses are showing some irregular spikes with regular beat like structure with increasing wave amplitude as shown in Fig. 4.17 to Fig. 4.22, respectively. This shows that motion is of quasi-periodic nature. The similar trend of motion can be seen in phase plots with multiple loops and some dense points in Poincare maps. FFTs are showing clear peak of excitations at different frequencies.

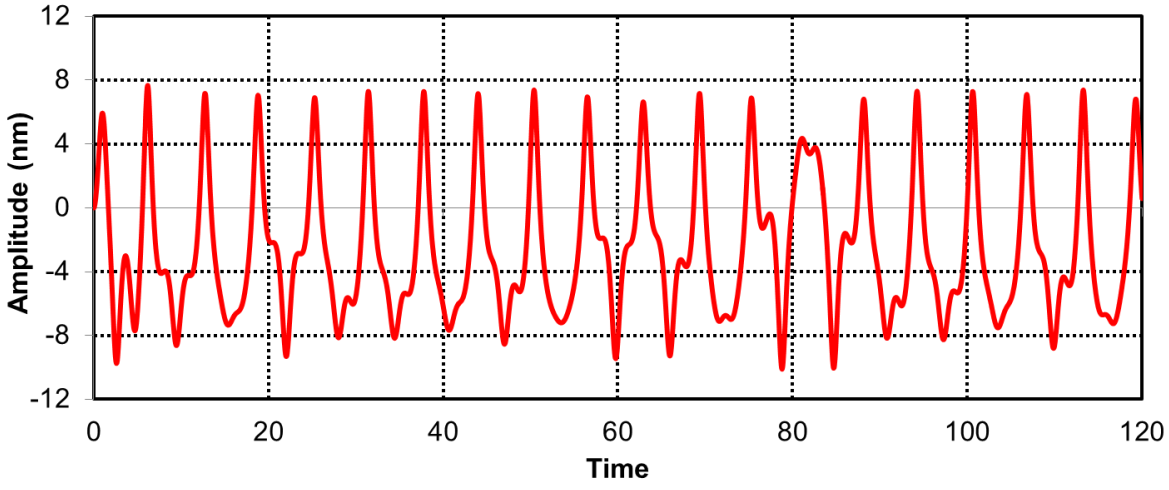

(a)

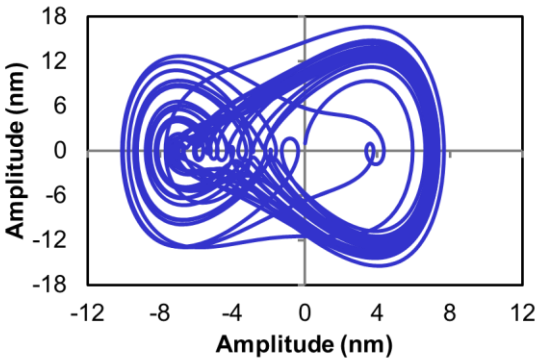

(b)

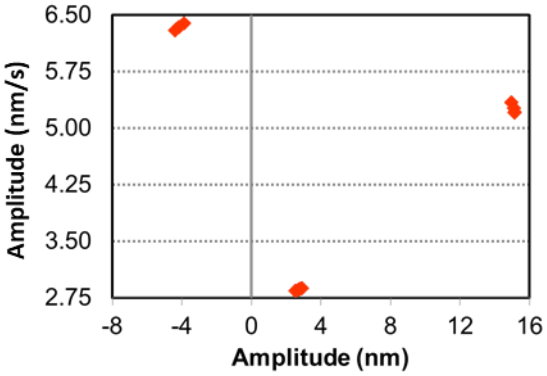

(c)

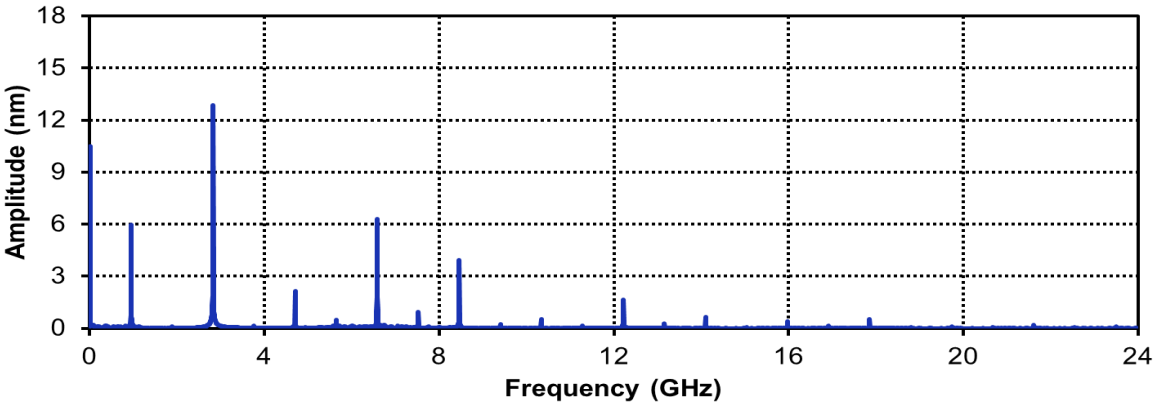

(d)

Fig. 4.17. Dynamic responses: (a) Time series (b) Phase plane (c) Poincare section and (d) Fast Fourier Transform for L=60nm waviness 0.1.

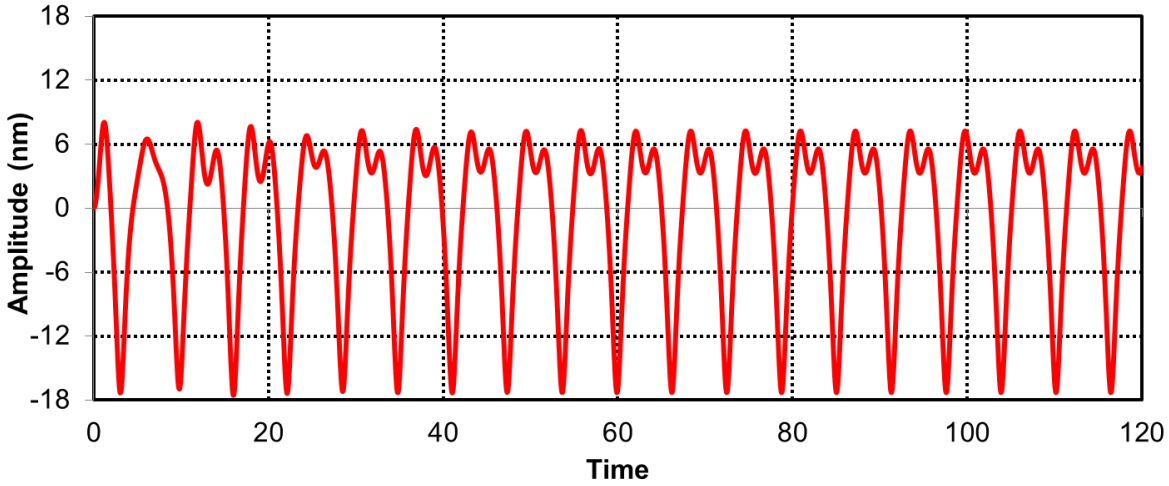

(a)

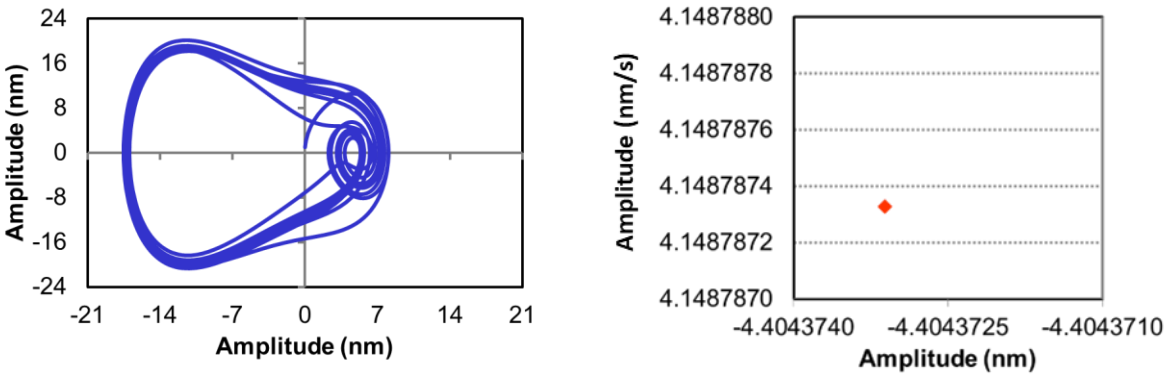

(b) (c)

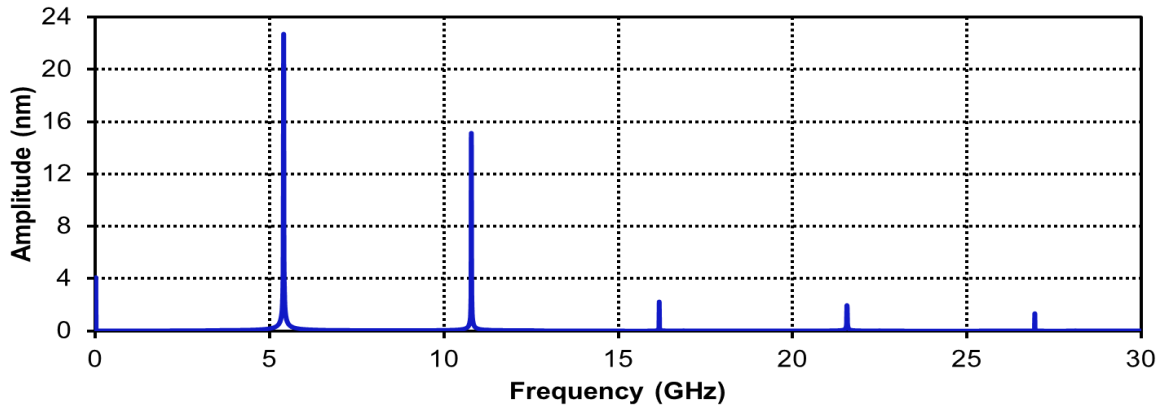

(d)

Fig. 4.18. Dynamic responses: (a) Time series (b) Phase plane (c) Poincare section and (d) Fast Fourier Transform for L=60nm waviness 0.2.

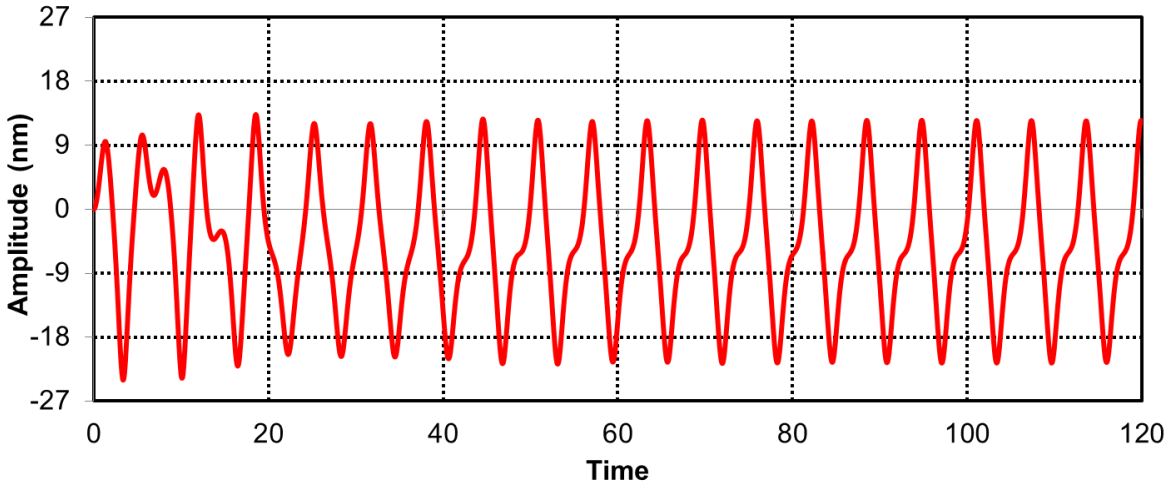

(a)

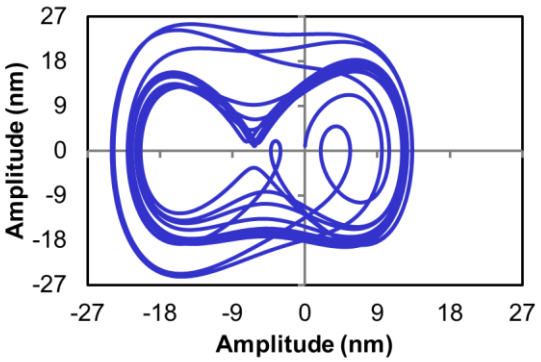

(b)

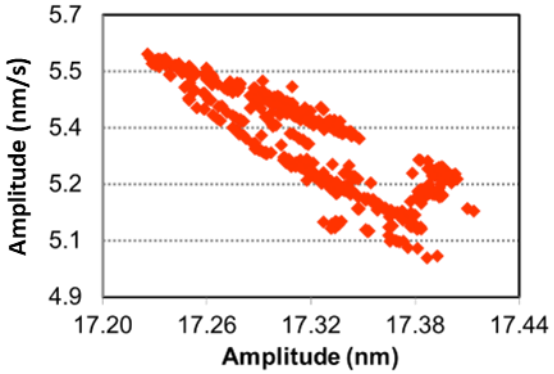

(c)

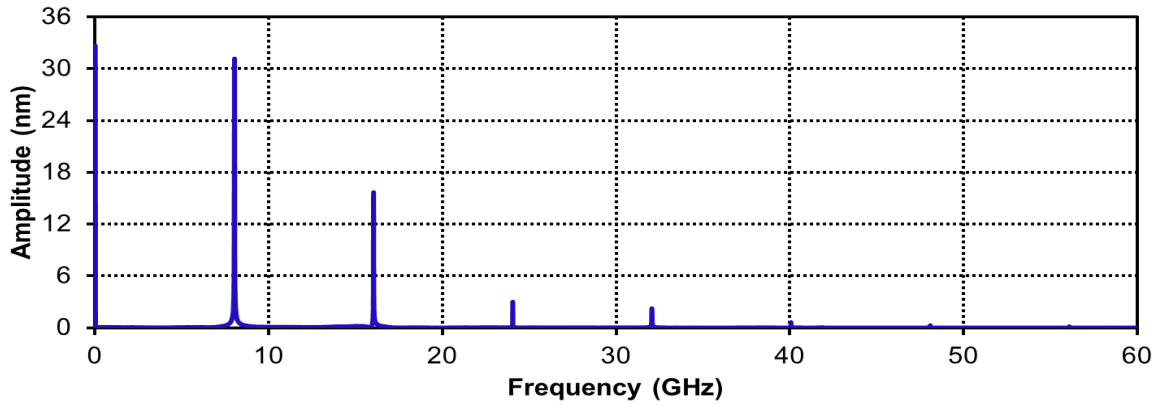

(d)

Fig. 4.19. Dynamic responses: (a) Time series (b) Phase plane (c) Poincare section and (d) Fast Fourier Transform for L=60nm waviness 0.3

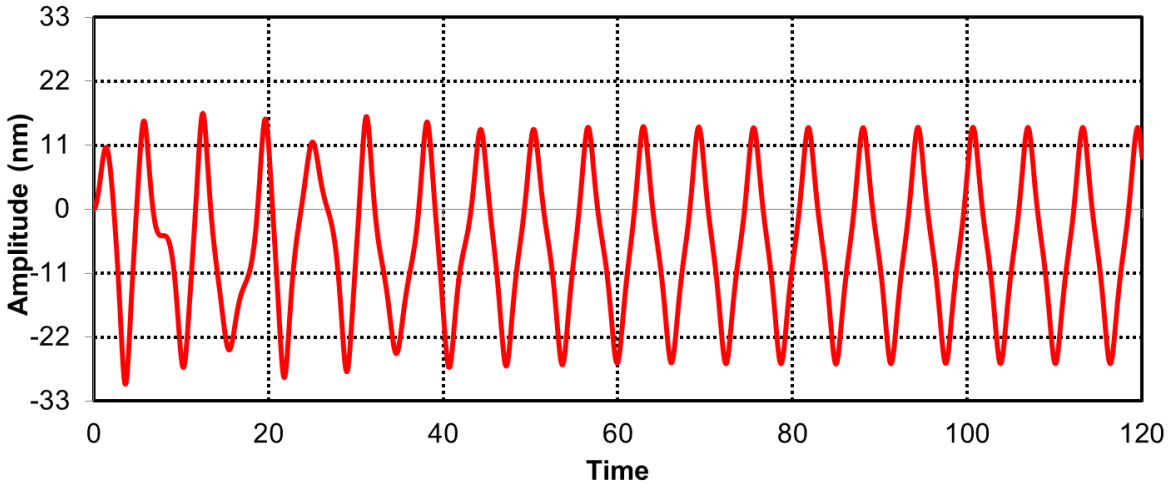

(a)

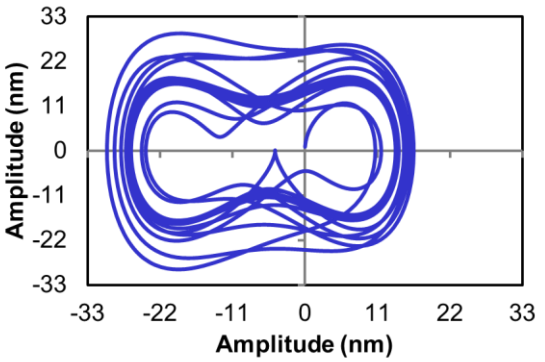

(b)

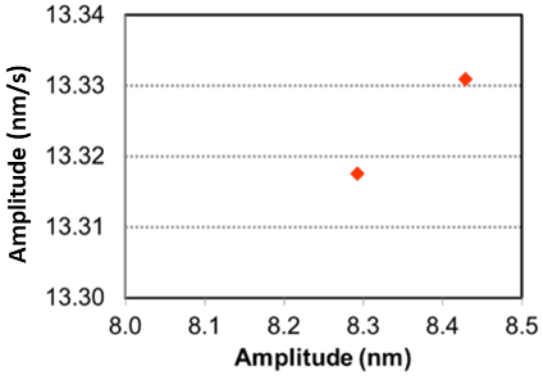

(c)

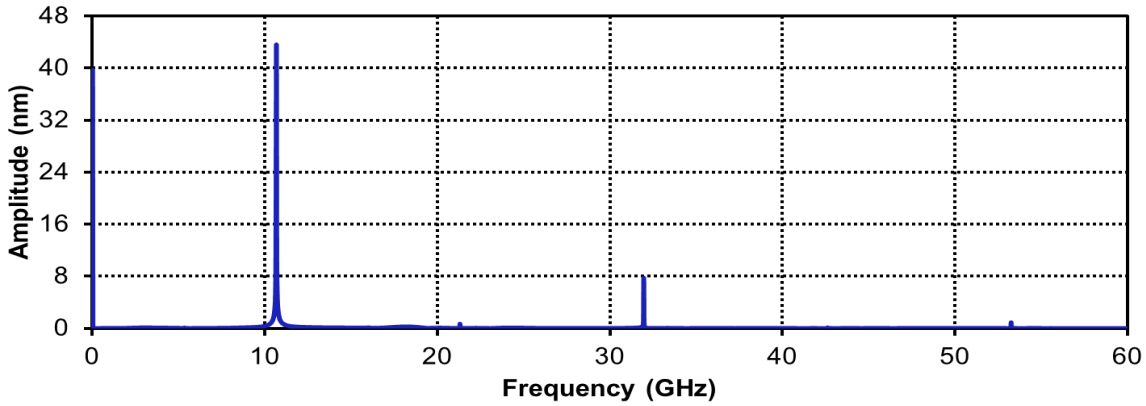

(d)

Fig. 4.20. Dynamic responses: (a) Time series (b) Phase plane (c) Poincare section and (d) Fast Fourier Transform for L=60nm waviness 0.4.

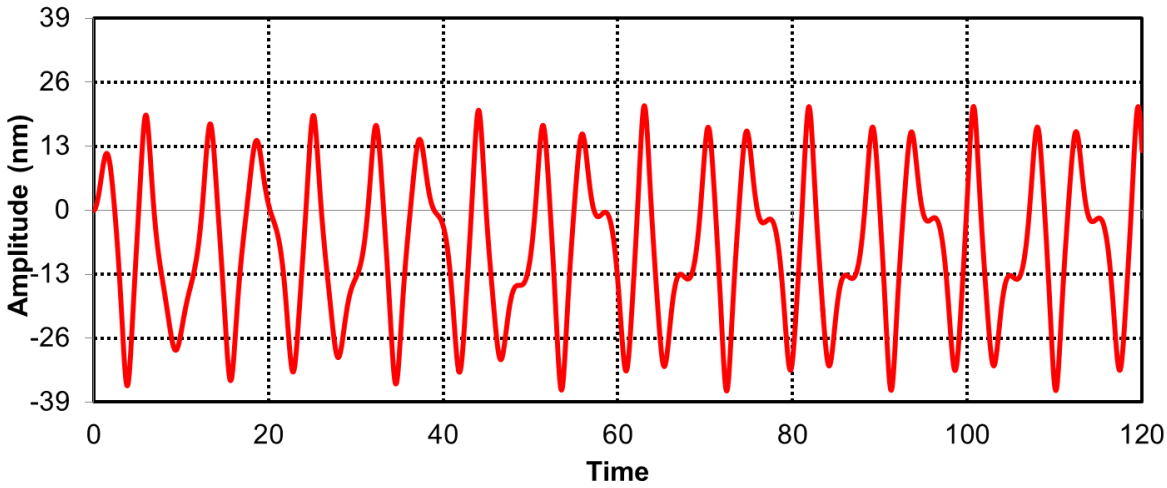

(a)

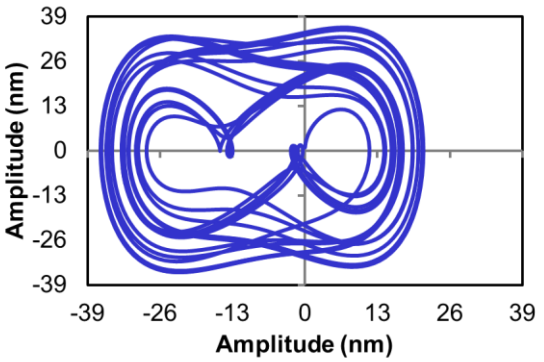

(b)

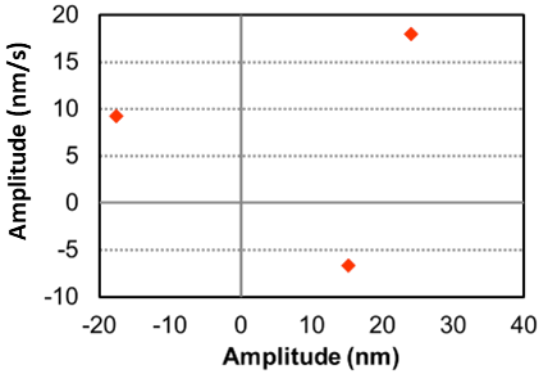

(c)

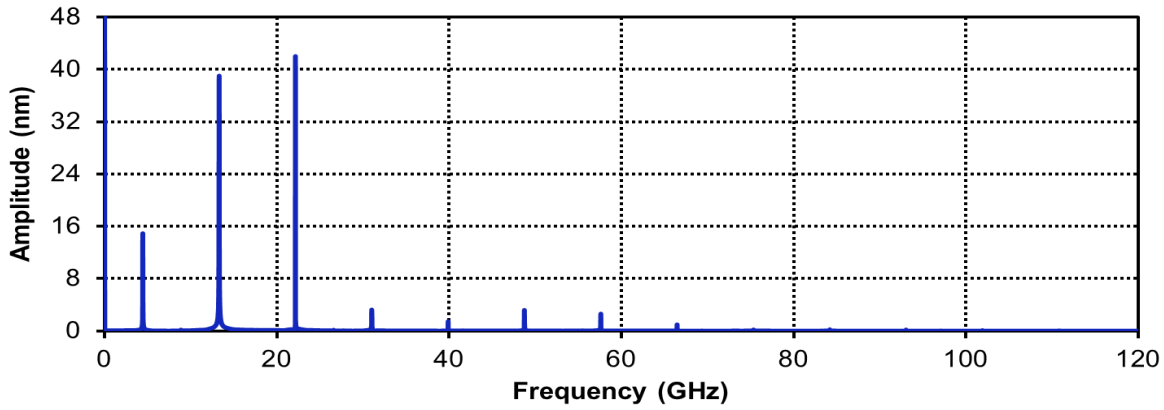

(d)

Fig. 4.21. Dynamic responses: (a) Time series (b) Phase plane (c) Poincare section and (d) Fast Fourier Transform for L=60nm waviness 0.5.

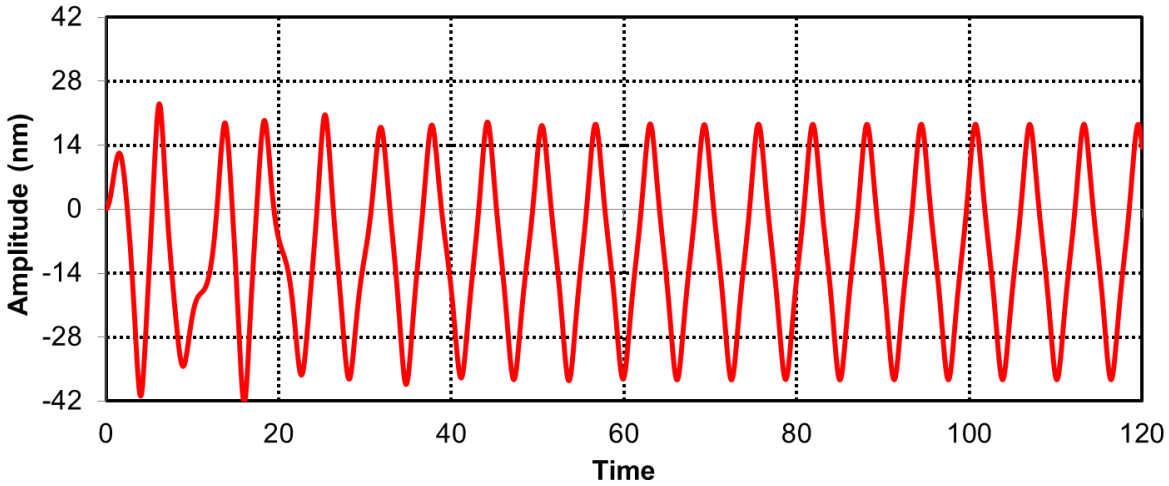

(a)

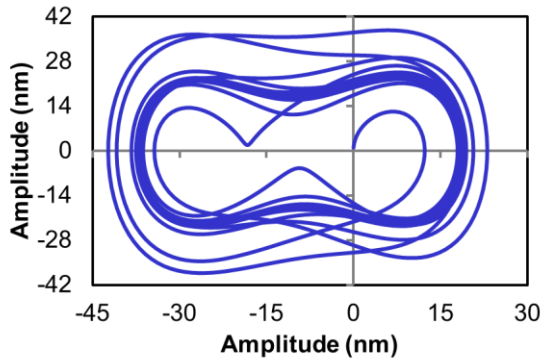

(b)

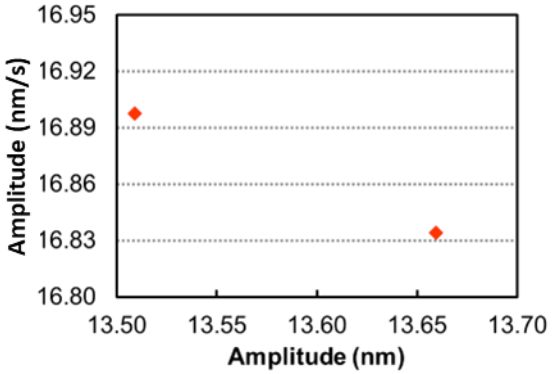

(c)

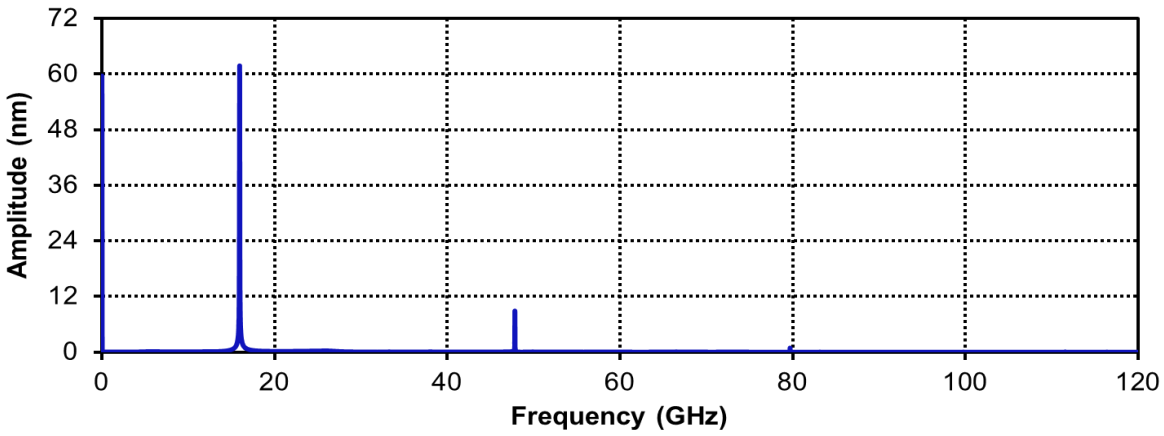

(d)

Fig. 4.22. Dynamic responses: (a) Time series (b) Phase plane (c) Poincare section and (d) Fast Fourier Transform for L=60nm waviness 0.6

4.3. Conclusions

In this chapter 3D atomistic finite element simulation approach is found to be effective for performing the resonant frequency-based analysis of a defective SW-BNNT based nano-mechanical mass sensor. The obtained simulation results due to surface deviation like waviness in SW-BNNT are suitable to develop an algorithm for analysis the effect of waviness present in SW-BNNTs.

- It can be concluded that surface deviation like waviness in SW-BNNT enhances the resonance frequency of SW-BNNT.
- As compared to straight SW-BNNT, the amplitude of oscillation of a wavy SW-BNNT

for a given length reduces and the system behaves initially as chaotic followed by quasi-periodic. Further, It is observed that there is a substantial and abrupt change in the value of amplitude for a wavy SW-BNNT beyond the length of 40 nm.

- It has also been observed that the cubic nonlinearity decreases as the waviness factor for a specific diameter increases. On the contrary, the quadratic nonlinearity increases with increase in waviness factor up to a certain limit, beyond this it starts declining thus following a parabolic path.
- The multiple orbits in phase space diagram with multiple peaks of excitation in corresponding FFTs for lower values of waviness (0.1 to 0.2) represent the periodic nature followed by quasi-periodic for waviness value up to 0.4 as the frequency of multiple peaks of excitation reduces and irregular behaviour is then observed for higher values of waviness.
- It has been observed that for 40 nm long wavy SW-BNNT the system responses for lower values of waviness are changing from periodic to quasi-periodic and with the increase in waviness the system starts to behave in a chaotic manner. Similar types of responses have also been observed for higher length.
- It is observed that the shift in resonant frequency is relatively large for variation in length of SW-BNNT from 20 nm to 40 nm, whereas it is small for larger lengths.

REFERENCES

[1.] S. Iijima, “Helical microtubules of graphitic carbon,” *Nature*, vol. 354, no. 6348, Nov. 1991, pp. 56–58.

[2.] S. Trivedi, S. C. Sharma, and S. P. Harsha, "Single walled-boron nitridenanotubes based nanoresonator for sensing of acetone molecules," *NANO, WorldScientific Publisher*, vol. 9, No. 8, 2014, pp. 1450086).

[3.] S. Trivedi, S. Kumar, Satish C. Sharma, and S. P. Harsha, "Biosensing applicationof multiwall boron nitride nanotube-based nanoresonator for detecting various viruses," *IETNanobiotechnology, IEEE*, vol. 9, No. 5, 2015, pp. 259-263.

[4.] N. G. Chopra and A. Zettl, “Measurement of the elastic modulus of a multi-wall boron nitride nanotube,” *Solid State Commun.*, vol. 105, no. 5, 1998, pp. 297–300.

[5.] N. G. Chopra *et al.*, “Boron Nitride Nanotubes,” *Science (80-.).*, vol. 269, no. 5226, 1995, pp. 966–967.

[6.] R. Chowdhury and S. Adhikari, “Boron-Nitride Nanotubes as Zeptogram-Scale Bionanosensors: Theoretical Investigations,” *IEEE Trans. Nanotechnol.*, vol. 10, no. 4, pp. 659–667.

[7.] E. T. Thostenson, Z. Ren, and T.-W. Chou, “Advances in the science and technology of carbon nanotubes and their composites: a review,” *Compos. Sci. Technol.*, vol. 61, no. 13, 2001, pp. 1899–1912.

[8.] E. T. Thostenson and T.-W. Chou, “Aligned multi-walled carbon nanotube-reinforced composites: processing and mechanical characterization,” *J. Phys. D. Appl. Phys.*, vol. 35, no. 16, 2002, pp. L77–L80.

[9.] E. T. Thostenson and T.-W. Chou, “On the elastic properties of carbon nanotube-based composites: modelling and characterization,” *J. Phys. D. Appl. Phys.*, vol. 36, no. 5, 2003, pp. 573–582.

[10.] R. E. Tuzun, D. W. Noid, B. G. Sumpter, and R. C. Merkle, “Dynamics of fluid flow inside carbon nanotubes,” *Nanotechnology*, vol. 7, no. 3, 1996, pp. 241–246.

[11.] G. D. Mahan, “Oscillations of a thin hollow cylinder: Carbon nanotubes,” *Phys. Rev. B*, vol. 65, no. 23, 2002, p. 235402.

[12.] W. Wu, M. Palaniapan, and W.-K. Wong, “Multiwall carbon nanotube resonator for ultra-sensitive mass detection,” *Electron. Lett.*, vol. 44, no. 18, 2008, p. 1060.

[13.] M. B. Panchal, S. H. Upadhyay, and S. P. Harsha, “Vibrational characteristics of defective single walled BN nanotube based nanomechanical mass sensors: single atom vacancies and divacancies,” *Sensors Actuators A Phys.*, vol. 197, 2013, pp. 111–121.

[14.] M. Brcic, M. Canadija, and J. Brnic, “Influence of Waviness and Vacancy Defects on Carbon Nanotubes Properties,” *Procedia Eng.*, vol. 100, 2015, pp. 213–219.

[15.] I. Y. Stein and B. L. Wardle, “Influence of waviness on the elastic properties of aligned carbon nanotube polymer matrix nanocomposites,” *57th AIAA/ASCE/AHS/ASC Struct. Struct. Dyn. Mater. Conf.* , 2015, pp. 0–9.

[16.] S. Kumar, S. H. Upadhyay, and A. Kumar, “Continuum Solid Modeling Based Finite Element Method Simulation Approach for Wavy Single Walled Boron Nitride Nanotube Based Resonant Nano Mechanical Sensors,” *J. Comput. Theor. Nanosci.*, vol. 12, no. 8, 2015, pp. 1841–1846.

[17.] F. Fisher, “Fiber waviness in nanotube-reinforced polymer composites—I: Modulus predictions using effective nanotube properties,” *Compos. Sci. Technol.*, vol. 63, no. 11, 2003, pp. 1689–1703.

[18.] J. A. Pelesko and D. H. Bernstein, *Modeling MEMS and NEMS*. CRC Press, 2002, pp.202-213.

[19.] A. Y. Joshi, S. C. Sharma, and S. P. Harsha, “The Effect of Pinhole Defect on Dynamic Characteristics of Single Walled Carbon Nanotube Based Mass Sensors,” *J. Comput. Theor. Nanosci.*, vol. 8, no. 4, 2011, pp. 776–782.

[20.] A. Joshi, B. Aashish, S. C. Sharma, and S. Harsha, “Vibratory Analysis of a Doubly Clamped Wavy Single Walled Carbon Nanotube based Nano Mechanical Sensors,” Int. J. Eng. Sci. Technol., vol. 2, no. 2010, pp. 263-275.

[21.] A. Y. Joshi, S. C. Sharma, and S. P. Harsha, “Dynamic Analysis of a Clamped Wavy Single Walled Carbon Nanotube Based Nanomechanical Sensors,” J. Nanotechnol. Eng. Med., vol. 1, no. 3, 2010, pp. 327-363.

[22.] A. Y. Joshi, A. Bhatnagar, S. P. Harsha, and S. C. Sharma, “Vibration Response Analysis of Doubly Clamped Single Walled Wavy Carbon Nanotube Based Nanomechanical Sensors,” J. Nanotechnol. Eng. Med., vol. 1, no. 3, 2010, pp. 613-625.

[23.] S. Kumar, S. H. Upadhyay, and A. Kumar, “Continuum Solid Modeling Based Finite Element Method Simulation Approach for Wavy Single Walled Boron Nitride Nanotube

Based Resonant Nano Mechanical Sensors," *J. Comput. Theor. Nanosci.*, vol. 12, no. 8, 2015, pp. 1841–1846.

[24.] R. Article, J. A. Desai, and M. B. Panchal, "Vibrational characterization of wavy atomic structures of single walled boron nitride nanotubes," 2019, pp. 2235-2247.

[25.] U. A. Joshi, S. C. Sharma, and S. P. Harsha, "Effect of waviness on the mechanical properties of carbon nanotube based composites," Phys. E Low-Dimensional Syst. Nanostructures, vol. 43, no. 8, 2011, pp. 1453–1460.

[26.] A. Y. Joshi, S. C. Sharma, and S. P. Harsha, "Chaotic response analysis of single-walled carbon nanotube due to surface deviations," Nano, vol. 7, no. 2, 2012, pp. 1–10.

[27.] J. Ning, J. Zhang, Y. Pan, and J. Guo, "Fabrication and mechanical properties of SiO2 matrix composites reinforced by carbon nanotube," *Mater. Sci. Eng. A*, vol. 357, no. 1–2, 2003, pp. 392–396.

[28.] Zhongping B., Mukherjee S., Roman M. and Aubry N., Nonlinear vibrations of beams, strings, plates, and membranes without initial tension, Journal of Applied Mechanics, vol. 71. 2004, pp. 551-559.

[29.] Gaziantep, H. and Pakdimerlli, M., Two-to-one internal resonances in a shallow curved beam resting on an elastic foundation, Acta Mechanica, vol. 185, 2006, pp. 245-260.

CHAPTER 5

Thermoatomic Analysis of Monovacancy Defected Single-Walled Boron Nitride Nanotube Under Quasi-Static Strain: Insights from Molecular Dynamics

5.1 Introduction

Boron nitride nanotube (BNNT) has similar lattice structures that of carbon nanotube (CNT) with multifunctional features [1]. BNNTs can be obtained by rolling up 2D hexagonal BN sheets (h-BNNS), also known as "white graphene" [2]. BNNTs have a strong anti-oxidation ability and structural stability [3], high thermal and electrical conductivity and remarkable mechanical characteristics at room temperature [4,5]. Experimental and theoretical studies showed that h-BNNs and BNNTs are constant band gap materials (5.5 eV) [6,7], which provides more chemical stability to BNNTs than the CNTs regardless of the tube chirality and morphology [3]. The extraordinary and multifunctional qualities of the BNNTs, attract enormous attention as a nanofiller for nanocomposites material that can replace CNTs [8–10]. BNNTs and BNNS are less explored compared to CNTs and graphene due to the dearth of successful experiments performed on BNNTs and h-BNNS.

Recent development in fabrication of BNNTs has led their use in biosensing systems, radiation shielding, strong insulators, transistors, optoelectronics, and hydrogen storage applications [11–17]. However, well-established methods of CNTs and graphene fabrication does not fit for the h-BN based nanostructures fabrication, due to possibilities of defects, especially for the bulk fabrication of single-walled BNNTs (SW-BNNTs) and remains a challenge [19– 23]. The available experimental methods for fabrication of SW-BNNTs such as arc discharge , laser ablation, and chemical vapor deposition (CVD) have intrinsic limits of the fabrication and purification procedures [18,19]. The investigations on the mechanics of BNNTs and h-BNNS by experiments primarily focused on Young's modulus measurements, which is found to be dependent on the type of fabrication method. Falin et al. [20] and Suryavanshi et al. [21] studied the Young's modulus of SW-BNNTs with varying lengths and diameters. They

reported the experimental values of Young's modulus ranges from 0.505–1.031 TPa. The low strength was mainly attributed to the inherent topological defects such as atomic vacancies, anti-sites, doping, and Stone-Wales [1,22,23]. Among all, vacancy defect is one of the typical type of defects found in BNNTs [24].

Molecular dynamics (MD) simulation is widely used as an atomistic modeling tool for characterization of nanomaterials and nanocomposites [5,25,26]. Griesel et al. [27] investigated the influence of vacancies in (6, 0) BNNTs on its Young's modulus using MD simulations. Their research revealed that the Young's modulus of BNNTs decreases from 1.2 to 0.7 TPa as the number of vacancy defects increases. Krishnan et al. [28] studied the effect of chirality on the Young's modulus of SW-BNNTs under uniaxial and torsion loadings using MD simulations. They showed that the elastic and shear modulus of BNNTs are affected by their chirality. Furthermore, Zigzag type BNNTs has showed the highest Young's modulus. Li and Chou [33] investigated the static and dynamic elastic moduli of SW-BNNTs using a molecular structural mechanics technique.

Previous studies reported the effect of temperature variation on mechanical properties of h-BNNS [29–31]. Li et al. [31] showed that the Young's modulus of h-BNNS is highly sensitive to temperature by simulating MD models with Tersoff potential. They reported that the Young's modulus and fracture strength of pristine h-BNNS decreases with the increase in the temperature. Strain hardening process was observed during the tensile strain and its shows that the large strain rate ($\geq 10^{10}$ s^{-1}) increases the fracture strength. Li et al. [32] performed MD simulations to investigate the mechanical and thermal properties of CNTs and BNNTs under the axial compressions. They evaluated the Young's modulus, critical bucking strain, maximum stress, and thermal conductivities for (10, 0) CNTs and (10, 0) BNNTs with various diameters and length-diameter ratios. Their investigation shows that the thermal conductivity of BN nanostructures is higher than that of their carbon analogs at low temperatures. To the best of our knowledge, the elastic properties of SW-BNNTs with single point defects or monovacancy defect at different temperatures is yet to be studied in detail. In this work, the effect of temperature on elastic properties of atomistic model of monovacancy defected zigzag SW-BNNTs were studied using extended version of Tersoff potential. The uniaxial tensile and torsional quasi-static strain in monovacancy defected SW-BNNTs were applied to calculate

Young's modulus, Poisson's ratio, and shear modulus. The thermoatomic models were used to understand the bond formation, stretching and breaking phenomenon in monovacancy defected SW-BNNTs during equilibration and deformation at different temperatures.

5.2 Computational details and models

MD simulation were performed on the large scale atomic/molecular massively parallel simulator (LAMMPS) package, developed by Sandia National Laboratories, USA [25,33]. LAMMPS package allows an insight study of interatomic interactions of distinct atoms/molecules using newtonian mechanics and a temporal integration technique. This complements traditional experiments by providing cheaper and quicker simulations. MD simulations provide an advantage in access to dynamical aspects of the molecular system, such as time-dependent responses to perturbations, transport coefficients, thermo-mechanical properties, rheological properties, and spectra.

The extended Tersoff potential for boron nitride (BN-ExTeP) [34] with an optimized parameters defined by Los et al. [45] is used to describe the interactions between the boron and nitrogen atoms of SW-BNNTs for application in large scale atomistic simulations. The BN-ExTeP potential, with its precise parameters, has the ability to accurately match the experimental results with density functional theory calculations and also ensured the computational efficiency for large-scale atomic systems. This extension of Tersoff describes the low energy of B, N, and BN structures and yields quantitatively correct trends in the bonding as a function of coordinates. The bond order added in BN-ExTeP potential improves the dependence of bonding on the chemical environment, leads to an accurate description of point defects in hexagonal BN (h-BN)[35].

The systematic steps followed in MD simulations are described in Fig. 5.1. Which shows the required steps for performing MD simulation on SW-BNNT in presence of defects at different positions and temperature conditions. Fig. 5.1 comprises initial SW-BNNT generation to post processing work including visualization and loop mechanism. Initial atomistic position of SW-BNNT structures were acquired using the software Nanotube Modeler© (version 1.8.0, ©JCrystalSoft) [36]. The SW-BNNTS were modelled with zig-zig type (5, 0) chirality, 1.47 nm of bond length, and 5 nm of tube length.

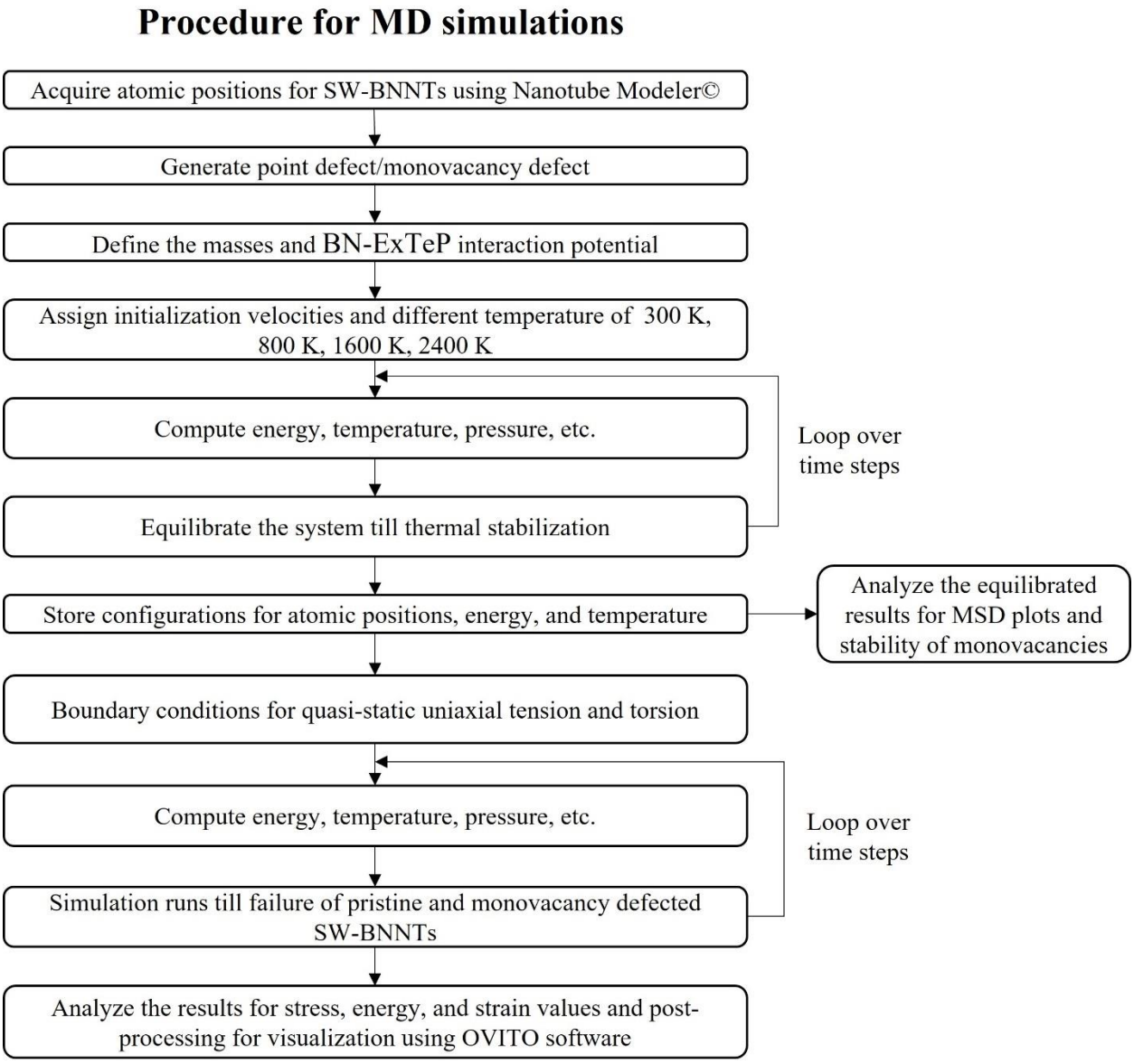

Fig. 5.1. Systematic steps to perform MD simulations for SW-BNNTs.

The zig-zag type (5, 0) SW-BNNT structure can be considered as hollow cylinder and the mean effective diameter, D_m is calculated using following relation:

$$D_m = \frac{\alpha_{n-m} \cdot \sqrt{3 \cdot (n^2 + n \cdot m + m^2)}}{\pi} \quad (5.1)$$

where n and m are chiral, and α_{n-m} is the equilibrium B–N covalent bond length, which usually considered equal to 0.145 nm [37]. The effective wall thickness of SW-BNNT is ~3.4 Å. The cross-sectional area of SW-BNNTs were calculated as, $A_{cs} = \pi(D_o^2 - D_i^2)/4$, where D_o (= D_m+ t/2)

and D_i (=D_m- t/2) are outer and inner diameter of SW-BNNT [36,38]. The initial atomic configurations of SW-BNNT systems with aspect ratio of 5 and total length (L) of 5 nm, as shown in the Fig. 5.2(a). The boron monovacancies in the pristine SW-BNNTs were introduced by removing boron atoms. The concentration of monovacancy (ρ) is defined using following relation to understand the incorporated defects:

$$\rho = \frac{number\ of\ removing\ atoms}{total\ atoms\ in\ a\ pristine\ SW-BNNT} \times 100 \quad (5.2)$$

The SW-BNNT with boron vacancies were modelled for three different cases (see **Fig. 5.2 (a)**): (i) case 1 modeled for pristine SW-BNNT with no defect, (ii) case 2 modeled for monovacancy defect at 3L/4 length of nanotube with ρ = 0.2% and (iii) case 3 modeled for monovacancy defect at L/4 and 3L/4 length of nanotube with ρ = 0.4%.

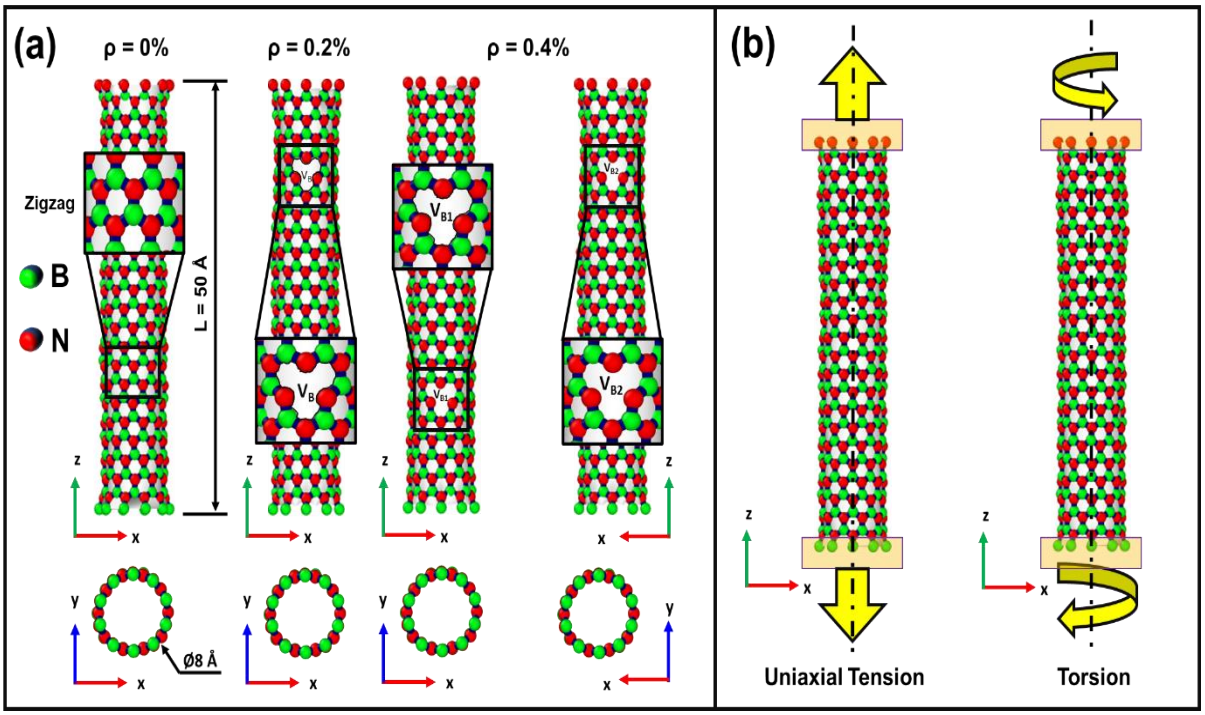

Fig. 5.2. Initial atomic configuration of SW-BNNTs model used for MD simulations: (a) case 1 for pristine SW-BNNT with no defect with ρ = 0%, case 2 for monovacancy defect at 3L/4 length of nanotube with ρ = 0.2%. case 3 for monovacancy defect at L/4 and 3L/4 length of nanotube with ρ = 0.4%. Here, pristine SW-BNNT case is comprised of total 460 atoms in the system. (b) quasi-static straining conditions for uniaxial tension and torsion at different temperature ranges from 300 K to 2400 K.

The SW-BNNT systems were pre-equilibrated at different temperature of analysis (300 K, 800 K, 1600 K and 2400 K). The particle motion was initialized using the velocity Verlet method to integrate Newton's classical equations of motion. To equilibrate the SW-BNNT at different temperature, the simulations were run in the constant volume and temperature ensemble (NVT) with a time step of 0.5 fs for total duration of 2 ns. This step performed time integration on Nose-Hoover style non-Hamiltonian equation of motion and updates the position and velocity for atoms at each timestep [26,39].

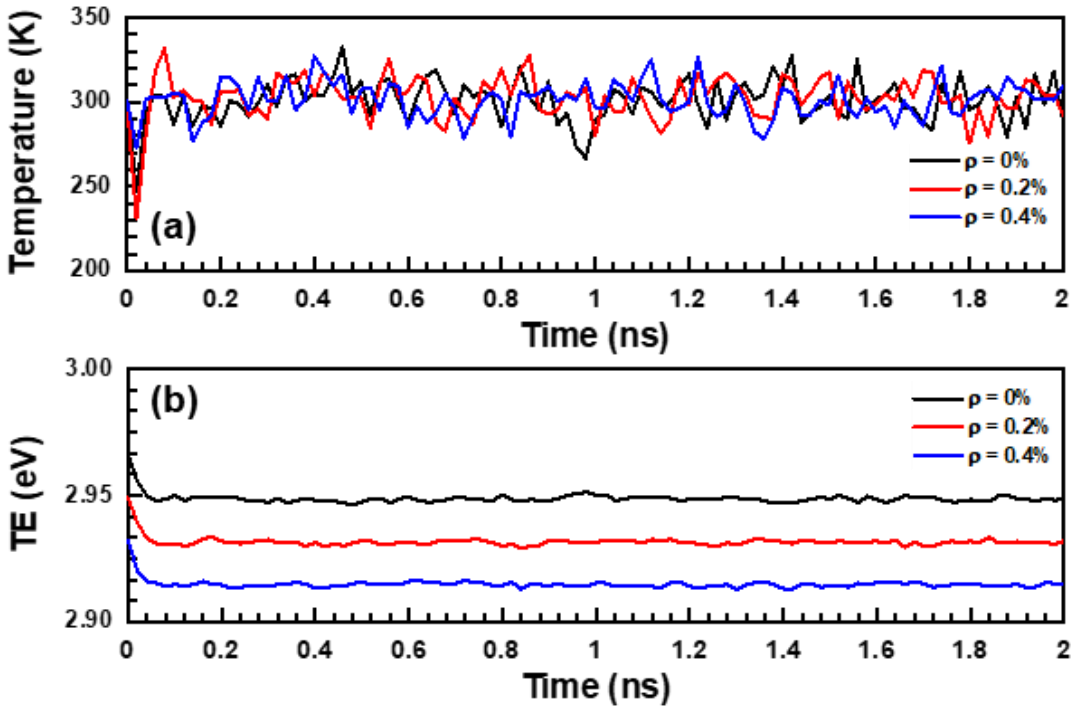

Fig. 5.3. (a) Temperature and **(b)** total energy plots during equilibration of SW-BNNT system for different cases of defects at 300 K. Note that the SW-BNNT systems were considered to reach equilibrium condition when the slope of temperature and TE profiles are zero for at least 1 ns under NVT ensemble.

The equilibration results for temperature and total energy (TE) at 300 K are shown in Fig. 5.3. The equilibration was observed for the activation of the given interatomic potential. During the equilibration at 300 K, the SW-BNNT systems were considered as equilibrated when the slope of temperature and TE profiles are zero for at least 1 ns under NVT ensemble, see Fig. 5.3

(a and b). Similarly, SW-BNNT systems were equilibrated at 800 K, 1600 K and 2400 K. To observe the effect of random collisions at different temperature, the mean-square displacement (MSD) was calculated for the displacements of the SW-BNNTs atoms.

To investigate the elastic properties of SW-BNNT at different temperature, the following two different quasi-static stain conditions were considered (see Fig. 5.2(b)): the uniaxial tension for axial Young's modulus (E_1) and major Poisson's ratio (ν_{12}), and constant torsional loading for longitudinal shear modulus (G_{12}). These elastic constants were evaluated on (5, 0) SW-BNNTs modeled using the continuum-based elasticity theory [24]. Under the deformation condition, the potential energy (PE) of the structure was calculated as the summation of interatomic interaction of neighbouring atoms, which is equal to the strain energy density of the assumed continuum structure. This technique has been extensively used by many researchers for similar structures including SW-BNNTs such as graphene, CNTs, and h-BNNS [40,41], and moreover, they also validated their observation and results with those obtained by different methods.

The strained conditions were applied at extreme ends of the SW-BNNT, as shown in Fig. 5.2. To better understand the failure mechanics of defective SW-BNNT models, the stress–strain curve was determined throughout their deformation under uniaxial tension, and torsion. During deformation of SW-BNNT models, constant pressure and temperature NPT ensemble was applied to reduce the effect of interatomic fluctuations before failure. The independent conformational simulation runs were conducted four time for each case to confirm the reliability and integrity of results. The different temperature conditioned maintained using Nose-Hoover thermostat [42]. Obtained stress-strain curves from the simulations were used to estimate the various elastic moduli.

For uniaxial tension loading, incremental displacements along the axial direction were applied on both ends of SW-BNNT models at a constant strain of 0.05 Å/ps. Elastic constants of a SW-BNNT was calculated from the initial slope of the stress-strain curve and deformation energy density-elastic constant relation. The axial stress (σ_{axial}) was calculated at the cross-sectional area of the SW-BNNT models as follows:

$$\sigma_{axial} = \frac{1}{AL}\left(\frac{dE_1}{d\bar{\varepsilon}_{11}}\right). \tag{5.3}$$

Where ε is the axial strain during loading. The strain energy density (U) of a SW-BNNTs can be expressed as follows:

$$U = \frac{1}{2} E_1 \bar{\varepsilon}_{11}^2. \tag{5.4}$$

Here, the strain energy density is the stored strain energy, $\bar{\varepsilon}_{11}$ = ΔL/L is the axial strain of SW-BNNTs, and ΔL is the change of a SW-BNNT length.

The modelling concept of molecular structures for SW-BNNT as "stick-spiral" system was used to estimate the ν_{12} using basic relation between axial strain $\bar{\varepsilon}_{11}$and circumferential strain $\bar{\varepsilon}_{22}$ [43,44]; as follows:

$$\nu_{12} = -\frac{\bar{\varepsilon}_{22}}{\bar{\varepsilon}_{11}}. \tag{5.5}$$

For torsional loading, twisting moment applied to both ends of SW-BNNT models at a constant relative rotation of 0.81°/ps. The strain energy density in this case can be expressed as follows:

$$U = \frac{G_{12}\phi^2 J}{2L}. \tag{5.6}$$

Where ϕ is the angle of twist and J is the polar moment of inertia, which is given as:

$$J = \frac{\pi(D_o^4 - D_i^4)}{32}. \tag{5.7}$$

5.3 Result and discussion

5.3.1 Thermal stability of SW-BNNTs models

The atoms of SW-BNNTs in its molecular structure changes the direction of motion and locations significantly under different temperature conditions. The atoms of SW-BNNTs in its molecular structure changes the direction of motion and location significantly under different temperature conditions. Thus, the atoms have extreme interaction with each other, which can affect their atomic positions during equilibration at every timestep [39]. Hence, the path of atoms was irregular and random. The trajectories of SW-BNNTs atoms were difficult to track in real-time. Therefore, mean-square displacement (MSD) is used to calculate the displacement of the atoms in the system.

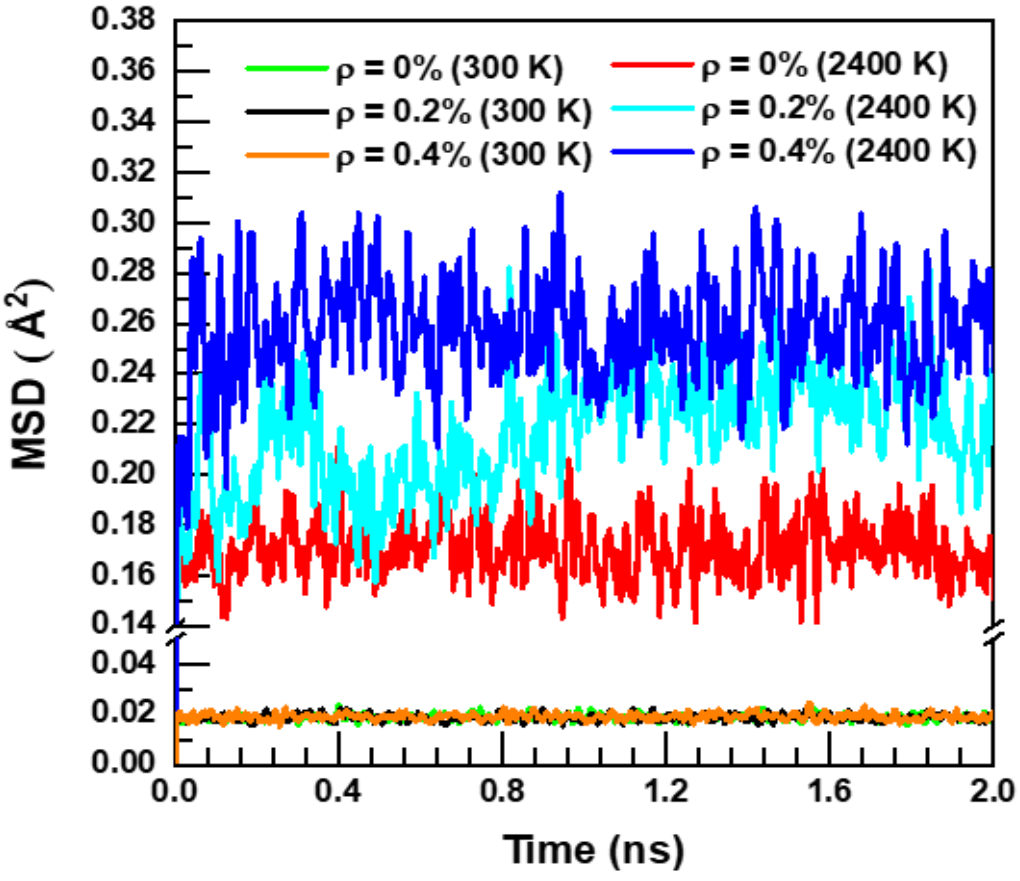

Fig. 5.4. Average Mean Square Displacement for the system at different temperature with different type of defect.

The MSD is computed using vector position of atoms at any instant of time and can be given as [45]:

$$MSD(t) = r_i(t)^2 = \{r_i(t) - r_i(0)\}^2. \tag{5.8}$$

where $r_i(0)$ and $r_i(t)$ are the vector displacement of an atom *i* at time t = 0 and t = t, respectively. More correctly, the average MSD ($\overline{MSD}$) for the bulk of atoms at N number of atomic sites in the system is given as [46]:

$$\overline{MSD}(t) = \sum_{i=1}^{n} \frac{\{r_i(t) - r_i(0)\}^2}{N}. \tag{5.9}$$

The obtained MSD plots with respect to time for the different cases of vacancy concentration at 300 K and 2400 K temperature are shown in Fig. 5.4. For all cases of vacancy concentration, the average MSD values were higher for systems at 2400 K as compared to systems at 300 K, which confirms the increased collision and randomness of the system at high temperature. Case 3 with ρ = 0.4% at 2400 K depicts average MSD value of 0.265 $Å^2$ exhibited 32.45 % increase compared to the average MSD value of 0.179 $Å^2$ for case 1 with ρ = 0.4% while Case 2 with ρ = 0.2% showed an intermediate average MSD value of 0.214 $Å^2$. These increase in average MSD values was occurred due to structural disorder in SW-BNNT across monovacancy defects.

Fig. 5.5 (a and b) illustrates the atomistic arrangement across the monovacancy defect with a missing boron atom at equilibration temperature of 300 K. Due to lower average MSD values, atoms across defective site were stable and bonded with same neighbouring atoms as before the equilibration at 300 K (refer Fig. 5.2).

However, at 2400 K, atomic arrangement across V_B (vacancy of boron atom) defect formed as a pentagon ring and nonagon ring to bring stability in the structure at high average MSD values (see Fig. 5.5 (c and d)). Where in, atom N_1 formed N-N bond with atom N_2 and N_2 forms N-N bond with N_3 to fill the vacancy space with a new pentagon (N_1, N_2, B_3, N_5, B_4) and a nonagon (N_2, B_4, N_6, B_5, N_7, B_2, N_4, B_1, N_3). Similar results were found in Case 3 with ρ = 0.4%, as shown in Fig. 5.5 (e and f).

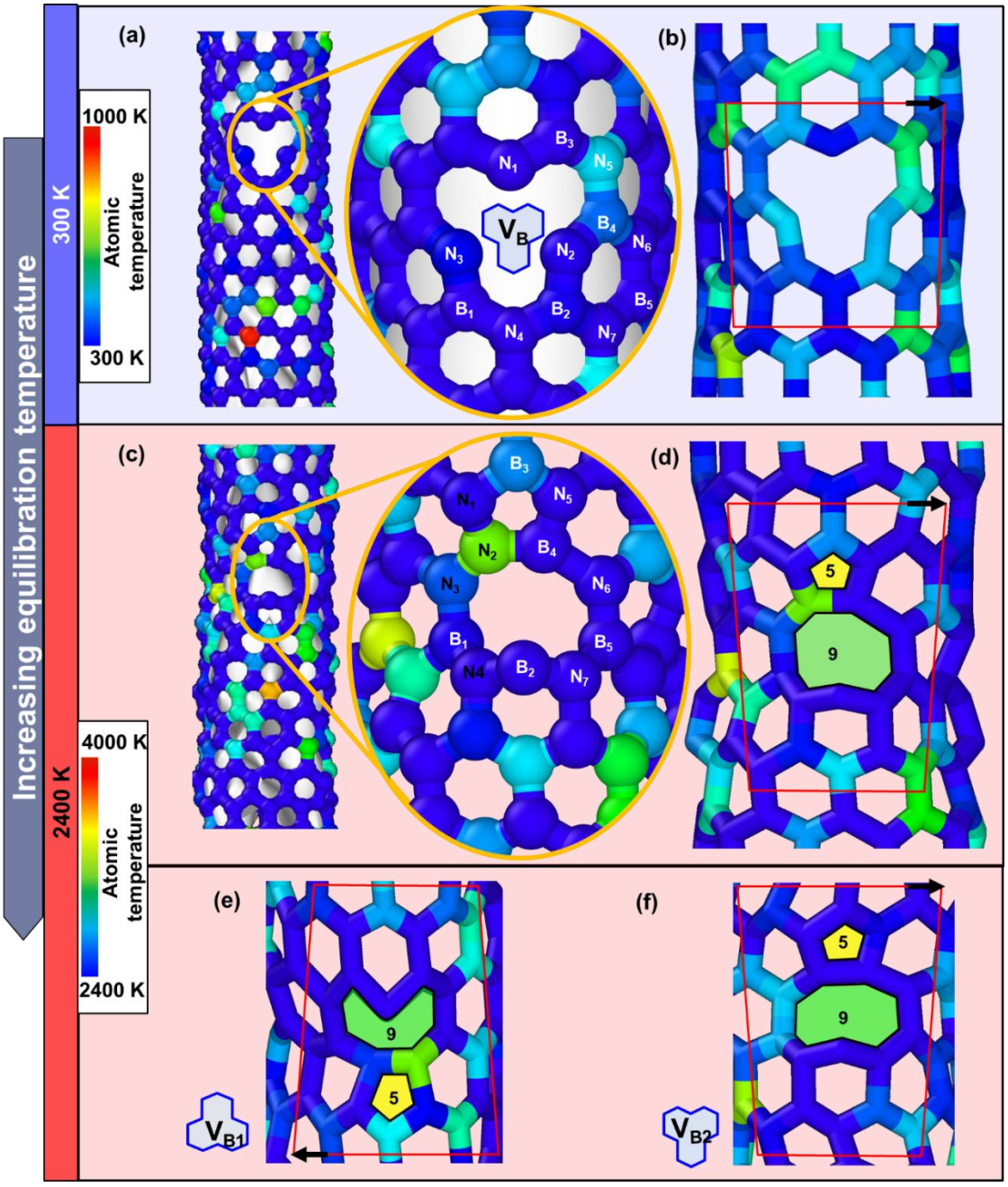

Fig. 5.5. Atomic arrangement across monovacancy defects in BNNT after equilibration: (a-b) and (c-d) for case 2 with ρ = 0.2% at 300 K and at 2400 K, respectively; (e) and (f) for defect V_{B1} and V_{B2} of case 3 with ρ = 0.4% at 2400 K, respectively. The pentagon (ring 1) and nonagon (ring 2) defective rings forming 5|9 defects are highlighted by yellow and green colours, respectively. The direction of the burgers vector and circuit or loop are shown by black arrow and red colour, respectively, which define the translational vector of atomic arrangement after equilibration [49].

The derivative of the MSD determined the diffusivity of the atoms and used to estimate the dynamic properties of a system [47]. However, it is observed that the slopes of MSD curves were nearly equal to zero after 0.2 ns for all cases, including systems at 2400 K temperature, which means the diffusion coefficient (i.e. slope of MSD/6) is also equal to zero [48]. This revealed that, at high temperature, the atoms position of SW-BNNTs condition were at stable state without observing random Brownian motion of atoms during simulation.

5.3.2 Effect of temperature on pristine and monovacancy defected SW-BNNTs under strained environment

We performed MD simulations to atomistically analyse the behaviour of pristine and monovacancy defected zig-zag h-BN structure of (5, 0) SW-BNNTs at different temperature under uniaxial tensile and torsional strain. Particularly, the effects of temperature on isotropic elastic properties of SWBBNT models were studied.

5.3.2.1 Atomistic behaviour under uniaxial tensile strain

The SW-BNNT models were stretched to apply the uniaxial tensile straining at different temperature. During simulation, the thermoatomic snapshots for all cases of pristine and monovacancy defected SW-BNNT models were captured to understand the facture in detail at different strain, as shown in Fig. 5.6. It was observed from Fig. 5.6(a) that the tensile straining of h-BN structure in SW-BNNTs has increased the atomic stresses that eventually started the fracture across B-N bonds and continued till ultimate fracture. Here, h-BN structures of pristine SW-BNNTs have shown structural stability at high strain, obviously, due to perfect hexagonal crystallography and thermal stability state at 300 K (see Fig. 5.5). During deformation at 300 K, the pristine SW-BNNT have showed higher strain till the initiation of fracture than that of monovacancy defected SW-BNNTs (see Fig. 5.6 a, c, and e). This revealed that the perfect h-BN structure of pristine SW-BNNT has high yielding compared to monovacancy defected SW-BNNTs before fracture. In case of monovacancy defect at 2400K, the atomic density at 5|9 defected polygons (refer Fig. 5.5d-f) reduces the cross-sectional strength of nanotube. The large polygons across monovacancy defected SW-BNNTs were propagated to form new polygons under tensile straining, as shown in Fig. 5.6d-f. These new polygons further reduced cross-sectional strength and therefore early fracture occurred in monovacancy defected SW-BNNTs as

compared to pristine. The stress-strain curve of pristine and monovacancy defected SW-BNNTs were obtained based on the data extracted from uniaxial tensile simulations at different temperature conditions. Fig. 5.7a shows the stress-strain curves of all cases at different temperature for uniaxial tensile strain. It can be observed that at a same axial strain value, stresses are higher in case of low temperature with no defect than that in high temperature with monovacancy defects. In case of pristine SW-BNNT, with an increase in temperature from 300 K to 2400 K the axial stress decreased by 39.02% from 166.3 GPa to 101.4 GPa and the axial strain decreased by 46.15% from 0.52 to 0.28. Whereas, in case of monovacancy defect of ρ = 0.2% and 0.4%, axial stress decreased up to 60.04 GPa (at 2400 K) and 52.28 GPa (at 2400 K) with the strain range of 0.16–0.31 and 0.14–0.28, respectively, as depicted from Fig. 5.7b and c. During uniaxial tensile straining in case of pristine SW-BNNT at 300 K temperature, the yielding and strain hardening effect was observed from the stress-strain curve (refer Fig. 5.7a). The plot depicts strain hardening effect with an increase in deformation in the SW-BNNTs structure at constant stress. The hexagonal structure of the SW-BNNTs stretched along the direction of tensile strain and the bond length increased compared to the initial configuration (refer insert of Fig. 5.6a). At high temperatures, strain hardening was not observed due to the high vibrational mobility and kinetic energies of atoms, which led to bond failure under strain and decreased the tensile strength of the nanotube structure [50]. Furthermore, there was no such observation found in case of monovacancy defected SW-BNNTs due to early failures at weaker cross-section across defective sites (see Fig. 5.6c-f).

Table 5.1. Elastic constant of pristine and monovacancy defected SW-BNNTs at different temperature.

ρ (%)	**Isotropic elastic constant values at different temperature**											
	E (TPa)				**ν**				**G**			
	300 K	**800 K**	**1600 K**	**2400 K**	**300 K**	**800 K**	**1600 K**	**2400 K**	**300 K**	**800 K**	**1600 K**	**2400 K**
0	1.097	1.040	0.961	0.860	0.231	0.225	0.208	0.182	1.015	0.850	0.718	0.649
0.2	0.987	0.910	0.798	0.734	0.194	0.186	0.167	0.149	0.981	0.793	0.674	0.582
0.4	0.802	0.763	0.672	0.629	0.163	0.158	0.141	0.125	0.946	0.745	0.629	0.461

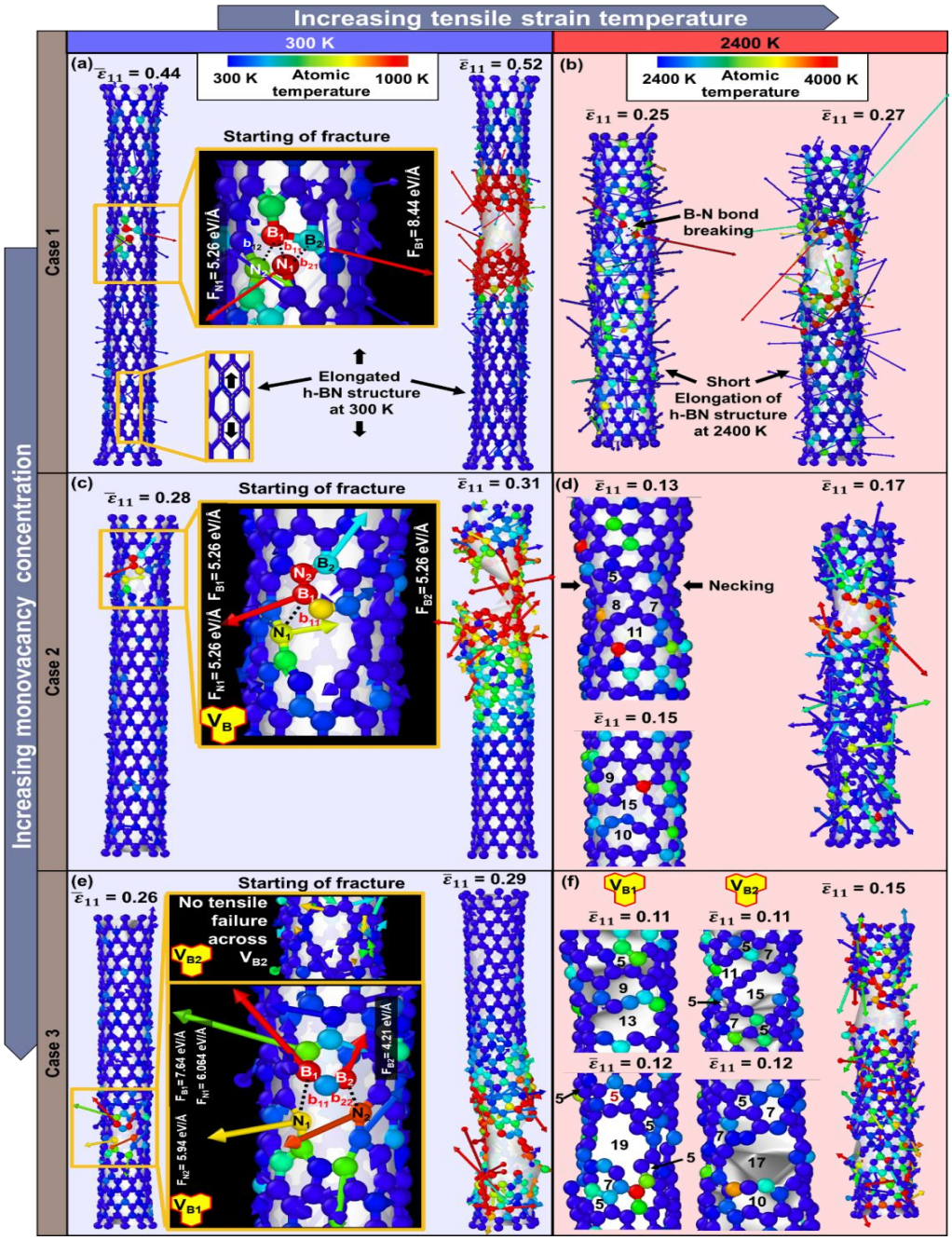

Fig. 5.6. Thermoatomic snapshots during uniaxial tensile straining of pristine and monovacancy defected SW-BNNT models at 300 K and 2400 K temperatures. (a-b) for pristine SW-BNNT, (c-d), and (e-f) for case 2 and 3 monovacancy defected SW-BNNTs respectively. Here, breaking of a B-N bond (b_{BN}) is shown in doted black line and colours of atoms, bonds, and atomic force ($F_{B\ or\ N}$) arrows on atoms are as per the atomic temperature scale of respective cases.

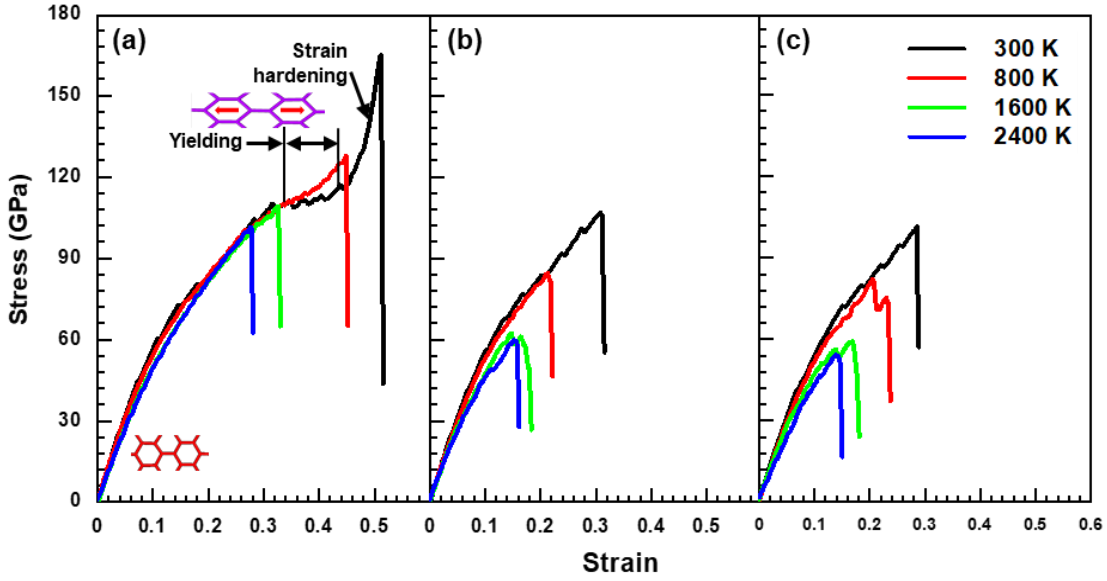

Fig. 5.7. Stress–strain curves for uniaxial tensile straining of pristine and monovacancy defected (5, 0) SW-BNNTs at different temperatures: (a) case1 pristine SW-BNNTs, here, insert shows yielding and strain hardening in perfect h-BN structure, (b) case 2 and (c) case 3 monovacancy defected SW-BNNTs.

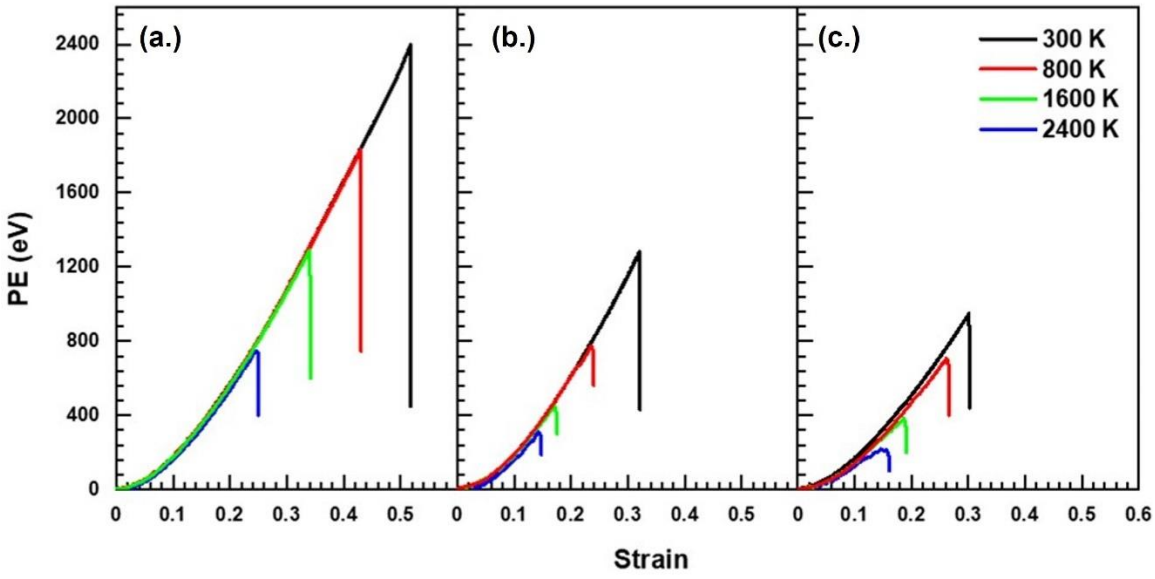

Fig. 5.8. Energy–strain curves for uniaxial tensile straining of pristine and monovacancy defected (5, 0) SW-BNNTs at different temperatures: (a) case 1 pristine SW-BNNTs, (b) case 2 and (c) case 3 monovacancy defected SW-BNNTs.

The potential energy was also calculated during the deformation from initial state to final facture state under uniaxial tensile strain. The variation of potential energy of SW-BNNT models under uniaxial tensile strain is shown in Fig. 5.8. It was found that the increased temperature and monovacancy defects under strain condition decreased the stored potential energy before fracture. This attributed to the fact that the early bond breaking started at high temperature releases the stored energy during deformation of monovacancy defected SW-BNNTs. The observed higher stored energy and strain for the pristine SW-BNNTs results in higher Young's modulus and Poisson ratio compared to monovacancy defected SW-BNNTs at all temperature conditions, as listed in Table 5.1. The energy-strain and stress-strain curves shown in Fig. 5.7 and 5.8 were found to be in good agreement with those obtained for pristine SW-BNNTs in the MD study by Choyal et al [24]. Furthermore, Wei et al [51] have reported the similar trend of energy-strain curves for (10,0) single-walled CNTs.

5.3.2.2 Atomistic behaviour under torsional strain condition

In addition to torsional straining, we performed MD simulations on pristine and monovacancy defected SW-BNNTs till fractured at different temperatures. To better visualize the effect of torsional strain on the mechanical behaviour, thermoatomic snapshots of SW-BNNTs at 300 K and 2400 K are shown in Fig. 5.9. It shows that at 300 K temperature, flattening or stretching effect in h-BN rings observed at approximate twist angles of 90°.

The flattering of h-BN rings in zig-zag SW-BNNTs leads to initialization of fracture, as shown in Fig. 5.9a. Due to the propagation of localized failure of h-BN bonds in the respective case of monovacancy defect at 300 K and 2400K leads to ultimate fracture, as observed from snapshots at different twist angle in Fig. 5.9(a-f). Further it has been observed that the monovacancy defected SW-BNNTs requires smaller angular twist for the complete fracture compared to the pristine SW-BNNTs. Fig. 5.10 illustrates the changes of the PE with the angle of twist during torsional strain. The changes of PE of all cases shows almost same trends, where the early failures occurred due to reduced strength of nanotubes at high temperatures [52]. It is observed that at a same angle of twist, the monovacancy defected cases store less PE than pristine SW-BNNTs due to easy twisting of large polygons at weak cross-sections of defective sites [53] (see Fig. 5.9c for monovacancy) than twisting of h-BN pristine (see Fig. 5.9a for

pristine). It can also be observed that the stored energy before fracture is higher in case of low temperature than that in high temperature under torsional strain. In case of pristine SW-BNNT, with an increase in temperature from 300 K to 2400 K the change in PE decreased by 70.72 % from 1286 eV to 379.46 eV and the twisting angle decreased by 54.99% from 328º to 146º. Whereas, in case of monovacancy defect of $\rho = 0.2\%$ and 0.4% at 2400 K, the maximum change in PE values decreased up to 1102 eV and 926 eV, respectively, as depicted from Fig. 5.10b and c. The observed higher potential energy and twisting for the pristine SW-BNNTs results in higher shear modulus compared to monovacancy defected SW-BNNTs at all temperature conditions, as listed in Table 5.1. The observed twisting deformation mechanics are in good agreement with study by Wernik and Meguid [41].

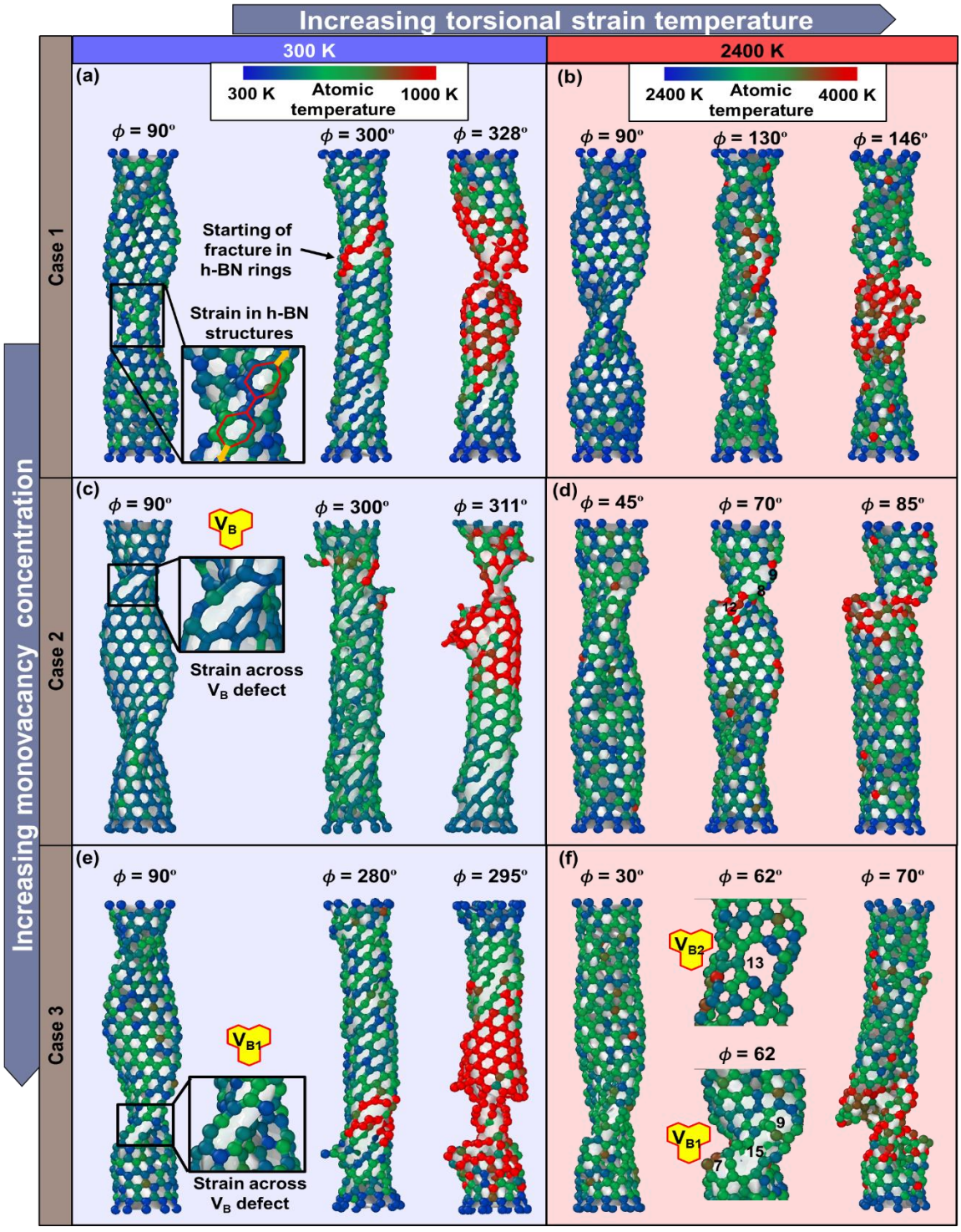

Fig. 5.9. Thermoatomic snapshots during torsional straining of pristine and monovacancy defected SW-BNNT models at 300 K and 2400 K temperatures. (a-b) case 1 for pristine SW-BNNT, (c-d) case 2, and (e-f) case 3 for monovacancy defected SW-BNNTs. Here, bonds are coloured as per the atomic temperature scale.

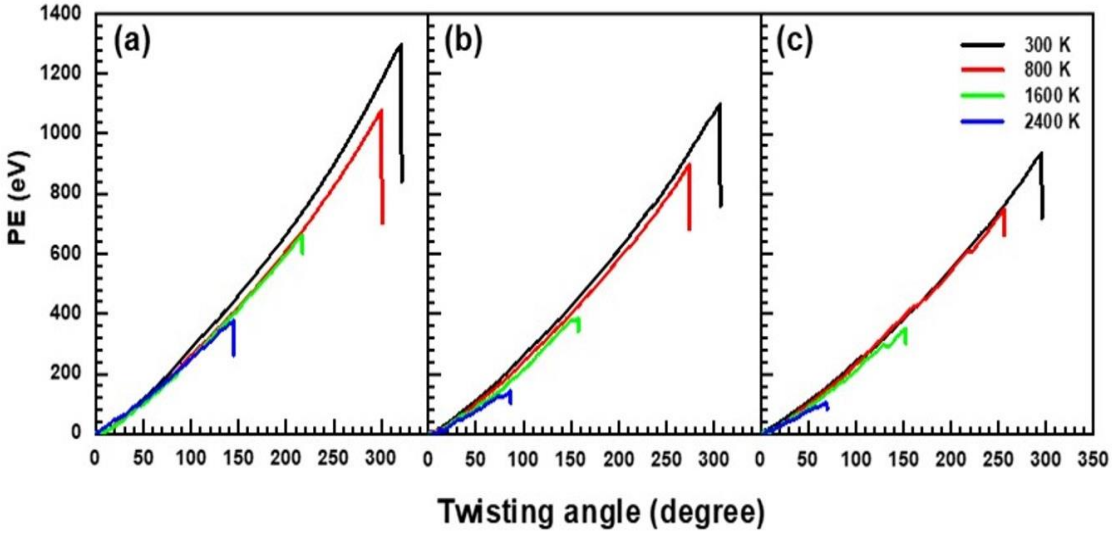

Fig. 5.10. Energy–twist angle curves for torsional straining of pristine and monovacancy defected (5, 0) SW-BNNTs at different temperatures: (a) case 1 pristine SW-BNNTs, (b) case 2 and (c) case 3 for monovacancy defected SW-BNNTs.

5.4 Conclusion

In this chapter, the effects of different temperatures on the structural and elastic properties of atomistic model of monovacancy defected SW-BNNTs were investigated by using MD simulation. An advance extended Tersoff potential was successfully used to describe the interactions between the boron and nitrogen atoms of SW-BNNTs. The mean square displacement revealed the structural stability of monovacancy defected SW-BNNT structures during equilibration up to 2400 K temperature. At higher temperature, the shape of monovacancy defected site converted into new polygenic defected sites to maintain the stability of structure. The monovacancy defected SW-BNNTs showed reduction in thermal stability and mechanical performance at high temperature. For uniaxial tensile straining, the pristine SW-BNNTs showed 39.02% and 46.15% decrease in axial stress and strain on increasing the temperature from 300 K to 2400 K, which further decreased with the monovacancy defects. Similarly, for torsional straining, the pristine SW-BNNTs showed 70.72 % and 54.99% decrease in change in stored PE and twisting angle on increasing the temperature from 300 K to 2400 K, whereas further reduction in change in PE was observed in the monovacancy defected SW-BNNTs. The Young's modulus, Poisson's ratio, and shear modulus of monovacancy defected SW-BNNTs were

decreased on increasing the monovacancy concentration and temperature under the uniaxial tensile and torsional quasi-static strain environment. Outcomes of this study may be useful to accelerate the in-depth studies of the next generation BNNT based nanocomposites with high temperature applications, such as heat shields, space exploration, aircraft bodies, sensors, automobile parts, and actuator systems.

REFERENCES

[1] J.H. Kim, T.V. Pham, J.H. Hwang, C.S. Kim, M.J. Kim, Boron nitride nanotubes: synthesis and applications, Nano Converg. 5 (2018) 17.

[2] D. Golberg, Y. Bando, C.C. Tang, C.Y. Zhi, Boron Nitride Nanotubes, Adv. Mater. 19 (2007) 2413–2432.

[3] Y. Chen, J. Zou, S.J. Campbell, G. Le Caer, Boron nitride nanotubes: Pronounced resistance to oxidation, Appl. Phys. Lett. 84 (2004) 2430–2432.

[4] N.G. Chopra, A. Zettl, Measurement of the elastic modulus of a multi-wall boron nitride nanotube, Solid State Commun. 105 (1998) 297–300.

[5] V.K. Choyal, V. Choyal, S. Nevhal, A. Bergaley, S.I. Kundalwal, Effect of aspects ratio on Young's modulus of boron nitride nanotubes: A molecular dynamics study, Mater. Today Proc. 26 (2020) 1–4.

[6] X. Blase, A. Rubio, S.G. Louie, M.L. Cohen, Quasiparticle band structure of bulk hexagonal boron nitride and related systems, Phys. Rev. B. 51 (1995) 6868–6875.

[7] X. Blase, A. Rubio, S.G. Louie, M.L. Cohen, Stability and Band Gap Constancy of Boron Nitride Nanotubes, Europhys. Lett. 28 (1994) 335–340.

[8] A. Owhal, A. Pingale, S. Belgamwar, Developing sustainable Zn-MWCNTs composite coatings using electrochemical co-deposition method: Tribological and surface wetting behavior, Adv. Mater. Process. Technol. (2022) 1–14.

[9] A.D. Pingale, A. Owhal, S.U. Belgamwar, J.S. Rathore, Electro-codeposition and properties of Cu–Ni-MWCNTs composite coatings, Trans. IMF. 99 (2021) 126–132.

[10] C.Y. Zhi, Y. Bando, C.C. Tang, Q. Huang, D. Golberg, Boron nitride nanotubes: functionalization and composites, J. Mater. Chem. 18 (2008) 3900.

[11] S. Trivedi, S. Kumar, S.C. Sharma, S.P. Harsha, Biosensing application of multiwall boron nitride nanotube-based nanoresonator for detecting various viruses, IET

Nanobiotechnology. 9 (2015) 259–263.

[12] J.H. Kang, G. Sauti, C. Park, V.I. Yamakov, K.E. Wise, S.E. Lowther, C.C. Fay, S.A. Thibeault, R.G. Bryant, Multifunctional Electroactive Nanocomposites Based on Piezoelectric Boron Nitride Nanotubes, ACS Nano. 9 (2015) 11942–11950.

[13] D. Golberg, Y. Bando, P. Dorozhkin, Z.-C. Dong, Synthesis, Analysis, and Electrical Property Measurements of Compound Nanotubes in the B-C-N Ceramic System, MRS Bull. 29 (2004) 38–42.

[14] N.P. Bansal, J.B. Hurst, S.R. Choi, Boron Nitride Nanotubes-Reinforced Glass Composites, J. Am. Ceram. Soc. 89 (2006) 388–390.

[15] M.R. Mananghaya, Titanium-decorated boron nitride nanotubes for hydrogen storage: a multiscale theoretical investigation, Nanoscale. 11 (2019) 16052–16062.

[16] W. Meng, Y. Huang, Y. Fu, Z. Wang, C. Zhi, Polymer composites of boron nitride nanotubes and nanosheets, J. Mater. Chem. C. 2 (2014) 10049–10061.

[17] S. Ye, C. Cheng, X. Chen, X. Chen, J. Shao, J. Zhang, H. Hu, H. Tian, X. Li, L. Ma, W. Jia, High-performance piezoelectric nanogenerator based on microstructured P(VDF-TrFE)/BNNTs composite for energy harvesting and radiation protection in space, Nano Energy. 60 (2019) 701–714.

[18] C. Zhi, Y. Bando, C. Tang, D. Golberg, Boron nitride nanotubes, Mater. Sci. Eng. R Reports. 70 (2010) 92–111.

[19] J.H. Kim, H. Cho, T.V. Pham, J.H. Hwang, S. Ahn, S.G. Jang, H. Lee, C. Park, C.S. Kim, M.J. Kim, Dual growth mode of boron nitride nanotubes in high temperature pressure laser ablation, Sci. Rep. 9 (2019) 15674.

[20] A. Falin, Q. Cai, E.J.G. Santos, D. Scullion, D. Qian, R. Zhang, Z. Yang, S. Huang, K. Watanabe, T. Taniguchi, M.R. Barnett, Y. Chen, R.S. Ruoff, L.H. Li, Mechanical properties of atomically thin boron nitride and the role of interlayer interactions, Nat. Commun. 8 (2017) 15815.

[21] A.P. Suryavanshi, M.-F. Yu, J. Wen, C. Tang, Y. Bando, Elastic modulus and resonance behavior of boron nitride nanotubes, Appl. Phys. Lett. 84 (2004) 2527–2529.

[22] T.M. Schmidt, R.J. Baierle, P. Piquini, A. Fazzio, Theoretical study of native defects in BN nanotubes, Phys. Rev. B. 67 (2003) 113407.

[23] J. Song, H. Jiang, J. Wu, Y. Huang, K.-C. Hwang, Stone–Wales transformation in boron

nitride nanotubes, Scr. Mater. 57 (2007) 571–574.

[24] V. Choyal, V.K. Choyal, S.I. Kundalwal, Effect of atom vacancies on elastic and electronic properties of transversely isotropic boron nitride nanotubes: A comprehensive computational study, Comput. Mater. Sci. 156 (2019) 332–345.

[25] A.B. Shinde, A. Owhal, A. Sharma, P. Ranjan, T. Roy, R. Balasubramaniam, Comparative analysis of mechanical properties for mono and poly-crystalline copper under nanoindentation – Insights from molecular dynamics simulations, Mater. Chem. Phys. 277 (2022) 125559.

[26] D.P. Ranjan, M.A. Owhal, D. Chakrabarti, D.S. Belgamwar, T. Roy, D.R. Balasubramaniam, Fundamental Insights of Mechanical Polishing on Polycrystalline Cu Through Molecular Dynamics Simulations, SSRN Electron. J. (2022).

[27] M. Griebel, J. Hamaekers, F. Heber, A molecular dynamics study on the impact of defects and functionalization on the Young modulus of boron–nitride nanotubes, Comput. Mater. Sci. 45 (2009) 1097–1103.

[28] N.M. Anoop Krishnan, D. Ghosh, Chirality dependent elastic properties of single-walled boron nitride nanotubes under uniaxial and torsional loading, J. Appl. Phys. 115 (2014) 064303.

[29] M. Mirnezhad, R. Ansari, A. Shahabodini, Temperature Effect on Young's Modulus of Boron Nitride Sheets, J. Therm. Stress. 36 (2013) 152–159.

[30] X. Liu, C. Li, J. Eckert, K.G. Prashanth, O. Renk, L. Teng, Y. Liu, R. Bao, J. Tao, T. Shen, J. Yi, Microstructure evolution and mechanical properties of carbon nanotubes reinforced Al matrix composites, Mater. Charact. 133 (2017) 122–132.

[31] N. Li, N. Ding, S. Qu, L. Liu, W. Guo, C.-M.L. Wu, Mechanical properties and failure behavior of hexagonal boron nitride sheets with nano-cracks, Comput. Mater. Sci. 140 (2017) 356–366.

[32] T. Li, Z. Tang, Z. Huang, J. Yu, A comparison between the mechanical and thermal properties of single-walled carbon nanotubes and boron nitride nanotubes, Phys. E Low-Dimensional Syst. Nanostructures. 85 (2017) 137–142.

[33] J. Tersoff, Modeling solid-state chemistry: Interatomic potentials for multicomponent systems, Phys. Rev. B. 39 (1989) 5566–5568.

[34] J.H. Los, J.M.H. Kroes, K. Albe, R.M. Gordillo, M.I. Katsnelson, A. Fasolino, Extended

Tersoff potential for boron nitride: Energetics and elastic properties of pristine and defective h-BN, Phys. Rev. B. 96 (2017) 184108.

[35] K. Albe, Computersimulationen zu Struktur und Wachstum von Bornitrid, Technische Universität Dresden, 1998.

[36] N.A. Sakharova, J.M. Antunes, A.F.G. Pereira, B.M. Chaparro, J. V. Fernandes, On the Determination of Elastic Properties of Single-Walled Boron Nitride Nanotubes by Numerical Simulation, Materials (Basel). 14 (2021) 3183.

[37] M. Menon, D. Srivastava, Structure of boron nitride nanotubes: tube closing versus chirality, Chem. Phys. Lett. 307 (1999) 407–412.

[38] V. Verma, V.K. Jindal, K. Dharamvir, Elastic moduli of a boron nitride nanotube, Nanotechnology. 18 (2007) 435711.

[39] A. Owhal, D. Gautam, S.U. Belgamwar, V.K.P. Rao, Atomistic approach to analyse transportation of water nanodroplet through a vibrating nanochannel: scope in bio-NEMS applications, Mol. Simul. (2022) 1–8.

[40] L. Bian, M. Gao, Nanomechanics model for properties of carbon nanotubes under a thermal environment, Acta Mech. 229 (2018) 4521–4538.

[41] J.M. Wernik, S.A. Meguid, Atomistic-based continuum modeling of the nonlinear behavior of carbon nanotubes, Acta Mech. 212 (2010) 167–179.

[42] A. Khaitan, A. Owhal, S.U. Belgamwar, R. Raman Mishra, S. Goel, T. Roy, Designing porous electrode structures for supercapacitors using quenched MD simulations, Mater. Today Proc. (2022).

[43] T. Chang, H. Gao, Size-dependent elastic properties of a single-walled carbon nanotube via a molecular mechanics model, J. Mech. Phys. Solids. 51 (2003) 1059–1074.

[44] J.R. Xiao, B.A. Gama, J.W. Gillespie, An analytical molecular structural mechanics model for the mechanical properties of carbon nanotubes, Int. J. Solids Struct. 42 (2005) 3075–3092.

[45] C.Y. Won, N.R. Aluru, Structure and Dynamics of Water Confined in a Boron Nitride Nanotube, J. Phys. Chem. C. 112 (2008) 1812–1818.

[46] X. Bian, C. Kim, G.E. Karniadakis, 111 years of Brownian motion, Soft Matter. 12 (2016) 6331–6346.

[47] Z. Li, L. Hong, On the Knudsen transport of gases in nanochannels, J. Chem. Phys. 127

(2007) 074706.

[48] K. Zhang, F. Wang, Y. Lu, Molecular dynamics simulation of continuous nanoflow transport through the uneven wettability channel, AIP Adv. 8 (2018) 015111.

[49] O. V. Yazyev, S.G. Louie, Topological defects in graphene: Dislocations and grain boundaries, Phys. Rev. B. 81 (2010) 195420.

[50] C. Zhang, Y. Song, H. Zhang, B. Lv, J. Qiao, N. Yu, Y. Zhang, J. Di, Q. Li, Mechanical properties of carbon nanotube fibers at extreme temperatures, Nanoscale. 11 (2019) 4585–4590.

[51] C. Wei, K. Cho, D. Srivastava, Tensile strength of carbon nanotubes under realistic temperature and strain rate, Phys. Rev. B. 67 (2003) 115407.

[52] V. Choyal, S.I. Kundalwal, Transversely isotropic elastic properties of multi-walled boron nitride nanotubes under a thermal environment, Nanotechnology. 31 (2020) 395707.

[53] D.A. Damasceno, C.R. Miranda, The role of topological defects on the mechanical properties of single-walled carbon nanotubes, Philos. Mag. 102 (2022) 210–227.

CHAPTER 6

Conclusions, Application and Scope for Future Work

Sources of vibration in BNNTs are due to the parametric excitations and due to presence of defects have been discussed. The mass sensing ability of SW-BNNT has been investigated through resonance frequency-based analysis. Two different approaches, viz., hybrid modelling approach through ABAQUS and ANSYS software and atomistic modelling through LAMMPS software, have been employed for modelling of BNNT based mass sensors. The following conclusions are drawn from the present study:

6.1. Effect of defect on dynamics of BNNT and its applications

An atomistic finite element model consisting of beam elements and concentrated masses is employed to study the vibration characteristics of SW-BNNTs with defects behaving as mass sensors. An Atomistic simulation approach is used to find the natural frequencies of defective BNNTs containing atomic vacancy, pinhole and waviness and their effect on the vibration characteristics.

- Substantial drop in frequency shift is observed when the position of defect moves toward free end and finally shift becomes negative at vacancy position nearer to free end.
- Resonant frequency due to presence of di-vacancy (removal of 1 pair of B-N bond) is larger as compared to the presence of single atom vacancy (removal of either boron or nitrogen atom) for all the considered positions of the defect along the length of nanotube.
- The influence of Type II defect on resonance frequency is more significant as compared to Type I defect at positions near the fixed end, irrespective of aspect ratios for both armchair and zigzag BNNTs.
- The resonance frequency-based analysis of BNNT helps in identifying the amount of mass added at the tip of cantilevered BNNT, the type of vacancy defect and its location along the length of BNNT.
- Using the higher modes of vibration, the amount and location of the mass on the BNNT can be identified.

6.1.1. Potential applications

Boron nitride nanotubes (BNNTs) can be employed as sensors even in the presence of defects. Defects in BNNTs can alter their electronic and surface properties, making them sensitive to various analytes and suitable for sensing applications. Here are some potential applications of defect containing BNNTs as sensors:

• Gas Sensing: Defects in BNNTs can significantly impact their gas sensing capabilities. The presence of defects alters the electronic structure and surface reactivity of BNNTs, enabling them to selectively adsorb and detect gas molecules. By functionalizing or engineering defects in BNNTs, their sensitivity and selectivity towards specific gases can be enhanced. Defect-rich BNNTs have been explored for the detection of gases, including toxic gases, volatile organic compounds (VOCs), and environmental pollutants.

• Biosensing: Defect-containing BNNTs can be utilized as biosensors for detecting biomolecules, such as proteins, DNA, or viruses. The presence of defects can provide active sites for biomolecular interactions, leading to enhanced sensitivity and specificity. Functionalizing defect-rich BNNTs with biomolecules or utilizing defect-induced surface modifications enables the detection and quantification of biomarkers, facilitating applications in medical diagnostics, biochemistry, and biotechnology.

6.2. Effect of waviness on dynamics of BNNT and its applications

Surface deviations like waviness influences the dynamic behaviour of BNNT. The same has been revealed through present analysis.

- The shift in resonant frequency is relatively large for variation in length of BNNT from 20 nm to 40 nm as compared to larger lengths.
- The resonance frequency of wavy BNNT is higher as compared to straight one for higher values of mass. The difference in their resonance frequency almost disappears as the value of attached mass reaches 10^{-5} fg or less.
- It has been observed that the cubic nonlinearity decreases as the waviness factor for specific diameter increases, while the quadratic nonlinearity increases with increase in waviness factor up to a certain limit. Beyond this, it starts declining thus following a parabolic path.
- The multiple orbits in phase space diagram with multiple peaks of excitation in corresponding FFTs represent the periodic nature for lower values of waviness (0.1 to 0.2); quasi-periodic

nature for waviness values up to 0.4 as the frequency of multiple peaks of excitation reduces and irregular behaviour is observed for higher values of waviness.

• It has been observed that for 40 nm long wavy BNNT the system responses for lower values of waviness changes from periodic to quasi-periodic and with the increase in waviness the system starts to behave in a chaotic manner. Similar types of responses have also been observed for higher length (i.e., L_{bnnt}= 60nm).

6.2.1. Major applications

• Optical Sensing: Defects in BNNTs can induce localized electronic states and modify their optical properties. This characteristic can be exploited for optical sensing applications. Defect-engineered BNNTs have been explored for their tunable photoluminescence and absorption properties, enabling their application as optical sensors for detecting and quantifying analytes based on changes in fluorescence or absorption spectra.

The presence of defects in BNNTs can introduce new sensing mechanisms and enhance the sensitivity and selectivity of BNNT-based sensors. Through the deliberate control and engineering of defects, BNNTs can be tailored for specific sensing applications, opening up opportunities for advanced sensing technologies in various fields.

6.3. Effect of defect on thermo-mechanical dynamics of BNNT and its applications

Defects and temperature conditions affects the structural and elastic properties of SW-BNNT. The same has been revealed through present analysis.

• The mean square displacement revealed the structural stability of monovacancy-defected SWBNNT structures during equilibration up to 2400 K temperature.

• At higher temperature, the shape of monovacancy-defected site converted into new polygenic defected sites to maintain the stability of structure. The monovacancy-defected SWBNNTs showed reduction in thermal stability and mechanical performance at high temperature.

• For uniaxial tensile straining, the pristine SWBNNTs showed 39.02% and 46.15% decrease in axial stress and strain on increasing the temperature from 300 K to 2400 K, which further decreased with the monovacancy defects.

• For torsional straining, the pristine SWBNNTs showed 70.72% and 54.99% decrease in change in stored PE and twisting angle on increasing the temperature from 300 K to 2400 K,

whereas further reduction in change in PE was observed in the monovacancy defected SWBNNTs.

• The Young's modulus, Poisson's ratio, and shear modulus of monovacancy-defected SWBNNTs were decreased on increasing the monovacancy concentration and temperature under the uniaxial tensile and torsional quasi-static strain environment.

6.3.1. Potential applications

• Strain and Pressure Sensing: Defects in BNNTs can influence their mechanical properties and response to strain or pressure. The presence of defects alters the nanotube's structural integrity, resulting in changes in its electrical conductivity or mechanical response when subjected to strain or pressure. Defect-containing BNNTs have been explored as strain or pressure sensors, where the electrical or mechanical changes induced by the applied strain or pressure can be measured, enabling applications in structural health monitoring, wearable electronics, and smart materials.

• Chemical Sensing: Defect-rich BNNTs can exhibit enhanced sensitivity to various chemical species, enabling their application as chemical sensors. The presence of defects modifies the electronic structure and reactivity of BNNTs, facilitating the adsorption and detection of specific chemical analytes. By functionalizing or engineering defects, the selectivity and sensitivity of BNNT-based chemical sensors can be further improved, enabling applications in environmental monitoring, industrial process control, and quality assurance.

6.4. Future scopes

• Laboratory tests need to be conducted on SW-BNNT mass sensors in order to establish the regimes for an unstable and chaotic response.

• The effect of multiple types of defects on vibration response of the BNNT-based system can be considered.

• Laboratory tests are required for effective utilization of BNNTs based resonator for sensing viruses, and acetone molecules as bio-medical sensors.

• Outcomes of molecular scale thermos-mechanical study can be used to accelerate the in-depth studies of the next generation BNNT based nanocomposites with high-temperature applications, such as heat shields, space exploration, aircraft bodies, sensors, automobile parts, and actuator systems.

List of Publications

International Journal: 03

1. **Harsh Sharma**, Ayush Qwhal, Sharad Shrivastava, Jitendra S. Rathore, "Thermoatomic analysis of monovacancy defected single-walled boron nitride nanotube under quasi-static strain: Insights from molecular dynamics'' Material Chemistry and Physics. (**SCI, SCOPUS** indexing, **IF 5.0, Q1**),2022. (DOI: 10.1016/j.matchemphys.2022.1270200)
2. **Harsh Sharma,** Sharad Shrivastava, Jitendra S. Rathore, Sandesh Trivedi, "Nonlinear Vibration Analysis of Curvy Single Walled Boron Nitride Nanotube Using Mathematical Modelling for Dynamic Responses'' Journal of Modern Physics B (**SCI, SCOPUS** indexing, **IF 1.4, Q2**),2023. (Accepted)
3. **Harsh Sharma,** Sharad Shrivastava, Jitendra S. Rathore, Sandesh Trivedi, "Dynamic Analysis of Curvy Single Walled Boron Nitride Nanotube Using Mathematical Modelling under influence of vacancy defects '' International Journal of Non-Linear Mechanics(SCI, SCOPUS indexing, **IF 3.33, Q2**),2023. (Under Review)

International Scopus Index Proceedings: 03

1. **Harsh Sharma,** Sharad Shrivastava, Jitendra S. Rathore, Sandesh Trivedi, "Dynamic analysis of boron nitride nanotube using different boundary conditions under influence of vacancy defect: Insights from finite element method'' Material Today Proceeding (ESCI, SCOPUS indexing), 2022. (10.1016/j.matpr.2023.01.291)
2. **Harsh Sharma,** Sharad Shrivastava, Jitendra S. Rathore, Sandesh Trivedi, "Hybrid Approach for Dynamic Analysis of Single-Walled Boron Nitride Nanotube (SW-BNNT) in Presence of Vacancy Defect.'' Material Today Proceeding (ESCI, SCOPUS indexing),2021.(DOI: 10.1016/j.matpr.2021.07.287)
3. **Harsh Sharma,** Sharad Shrivastava, Jitendra S. Rathore, Sandesh Trivedi, "Atomistic Modelling and Dynamic Analysis of Boron Nitride Nanotube in the Presence of Pinhole Defect'' Material Today Proceeding (ESCI, SCOPUS indexing),2019.(DOI: 10.1016/j.matpr.2019.12.294

Brief biography of the Candidate

Harsh Sharma joined Birla Institute of Technology and Science, Pilani, Pilani Campus, Rajasthan, India in Jan 2019 with broad expertise in material & nano biosensors, structural design, atomic and FEM based Modelling. He completed a B.Tech. degree in Mechanical engineering from Swami Keshvanand Institute of Technology, Jaipur, India in 2016, and an M.Tech. degree in Production Engineering from the Government College, Ajmer, India in 2018. His research activities focused on the modeling of nano biosensors, dynamic analysis of BNNTs, development of nanotube-based mass sensors, dynamics of defects present in nanotubes, atomistic modeling, and finite element simulation of various nanotubes-based sensors.

Brief biography of the Supervisor

Prof. Sharad Shrivastava holds a Ph.D. degree from BITS-Pilani, Pilani Campus, India and a master's degree from Indian Institute of Technology (IIT) Kharagpur. His Ph.D. was in the field of application of non-destructive testing in Biomedical engineering. He has more than 18 years of teaching and research experience. He is presently Associate Professor, Mechanical Engineering Department, BITS-Pilani, Pilani Campus, India. He has more than 20 research publications in the field of Materials, Non-destructive techniques, coating technology and Biomedical engineering. He is member of a number of professional societies and has delivered number of invited lectures both in India and abroad. He has successfully handled a sponsored project (73lakhs) from GAIL India Limited on condition monitoring on underground pipelines.

His area of research is on

- Biomedical engineering, biomaterials for flame retardant applications, coatings by thermal spray HVOF process, hybrid composite materials, fracture mechanics, non-destructive testing,
- Specializes in non-destructive testing techniques mainly acoustic emission and acousto-ultrasonic technique, biomaterials
- Involved in teaching and research of subjects related to NDT, materials,fracture mechanics and theory of elasticity and plasticity, mechanics of solids

He has 15+ years teaching expertise on Non-destructive testing, composite materials, biomedical engineering, thermal spray coatings,fracture mechanics, mechanics of materials. He has supervised several Ph.D., master and undergraduate students for thesis and project work.

Prof. Sharad Shrivastava has served as Principal Investigator and Co-Principal Investigatorin many projects based on Biomedical engineering, biomaterials for flame retardant applications, coatings by thermal spray HVOF process, hybrid composite materials, fracture mechanics, non-destructive testing.

Brief biography of the Co-Supervisor

Prof. Jitendra Singh Rathore received his B.E. degree in Mechanical Engineering from M.B.M. Engineering College, Jodhpur (Rajasthan) in 2000, M.Tech. degree in Machine Design Engineering from Indian Institute of Technology (IIT), Roorkee in 2005, and Ph.D. from Birla Institute of Technology and Science (BITS), Pilani in 2014. His Ph.D. research was on "Investigations on the Dynamics and Design of Uniflagellated Nanoswimmers using Resistive Force Theory". After working for four years in Indian Ordnance Factories Organization, he joined the Mechanical Engineering Department, BITS, Pilani, India, in December 2006. Currently, He is a faculty in Mechanical Engineering Department, BITS, Pilani for over 17 years and serving as an Associate Professor. He has more than 30 international and national publications. His area of research includes.

- Nanorobotics and low Reynolds number hydrodynamics
- Human skin tribology and biomaterials
- Carbon nanotube (CNT) reinforced metal matrix composites.

He has 18+ years teaching expertise on Theory of Elasticity and Plasticity, Advance Mechanics of Solids, Thermodynamics, Mechanisms and Machines, Fluid Mechanics and Mechanics of Materials. He has supervised several Ph.D., Master and Undergraduate students for thesis and project work.